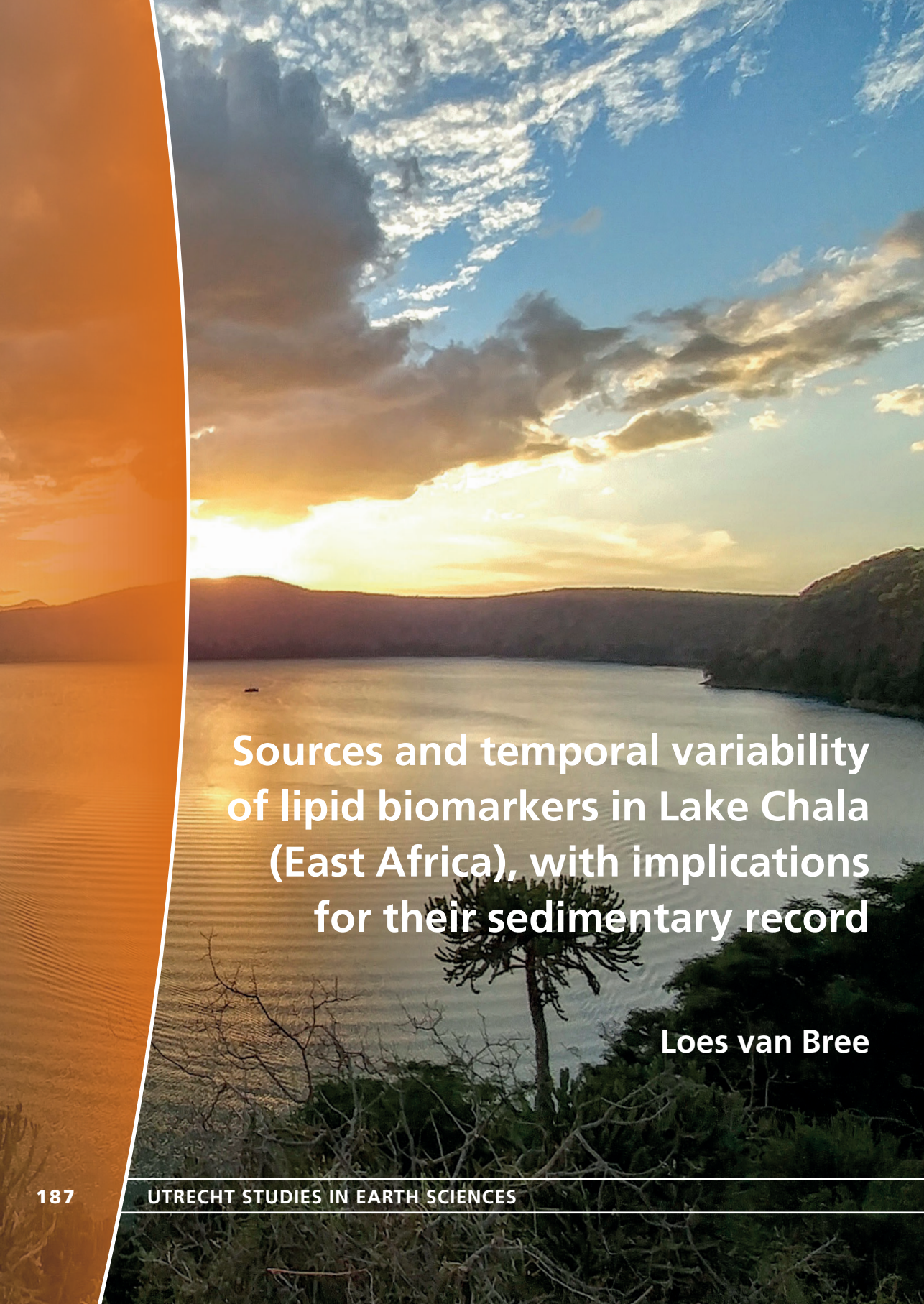

Sources and temporal variability of lipid biomarkers in Lake Chala (East Africa), with implications for their sedimentary record

Loes van Bree

187 UTRECHT STUDIES IN EARTH SCIENCES

Sources and temporal variability of lipid biomarkers in Lake Chala (East Africa), with implications for their sedimentary record

Loes van Bree

Utrecht Studies in Earth Sciences
No. 187

Promotoren:
Prof. dr. J.S. Sinninghe Damsté
Prof. dr. D. Verschuren
Prof. dr. S. Schouten

Copromotor:
Dr. F. Peterse

Sources and temporal variability of lipid biomarkers in Lake Chala (East Africa), with implications for their sedimentary record

Herkomst en temporele variatie van lipide biomarkers in het Chala-meer (Oost-Afrika), en implicaties voor hun registratie in het sedimentarchief

(met een samenvatting in het Nederlands)

Proefschrift

ter verkrijging van de graad van doctor aan de Universiteit Utrecht
op gezag van de rector magnificus, prof. dr. H.R.B.M. Kummeling,
ingevolge het besluit van het college voor promoties in het openbaar te verdedigen op
vrijdag 7 juni 2019 des middags te 2.30 uur

door

Louise Gerarda Johanna van Bree

geboren op 20 juni 1987 te Heemskerk

ISBN 978-90-6266-542-6
ISSN 2211-4335

USES No. 187

Author contact: LoesvanBree@gmail.com

Cover: Panoramic view of Lake Chala (Kenya/Tanzania) during the ICDP DeepCHALLA coring expedition in November 2016. Photo by Nicolas Waldmann, design by Margot Stoete.

Printed in the Netherlands by Ipskamp.

This thesis was accomplished with funding from the Netherlands Earth System Science Centre (NESSC), which is financially supported by the Ministry of Education, Culture and Science (OCW) of the Netherlands.

Fantastic piece of work
- Reviewer 2

Sunset at Lake Chala.
Photo credit: N. Waldmann

Contents

Perfect view of Mt. Kilimanjaro towering over Lake Chala, August 2014.
Photo credit: F. Peterse

General summary (in English)

Human-induced climate change is expected to cause large societal and economical disruptions in the centuries to come. To understand how the climate system will react to increasing atmospheric CO_2 levels and associated changes, it is important to study natural climate changes and their effects that have occurred in the past. Paleoclimate reconstructions provide critical knowledge for validation, testing and improvement of the climate models that are needed to accurately predict future climate changes. Records of past climate change need to be reconstructed by so-called proxies, as instrumental records only go back a few decades to centuries. Most studies have focused on exploring marine archives, but understanding continental climate changes is crucial as this is where future societal and economic impacts will be highest. Lake sediments are among the best archives of past continental climate change, especially in tropical areas where other archives (such as ice cores) are often lacking. Lakes are sensitive to environmental changes, both within the lake and in its catchment area, and sediments accumulate at the bottom of the lake usually at a relatively high rate. Lakes with a lack of oxygen in the bottom water are especially valuable for paleoclimate studies, as these conditions can produce finely laminated sediments, enabling the study of the sediments on a decadal or even annual scale. These sediment layers usually contain remains of microorganisms, pollen, spores, soil and dust, which can provide information on the conditions at the time of deposition. One way of extracting paleoclimate information from these lake sediments is by looking at lipid biomarkers. These 'molecular fossils' are produced by organisms both on land and in the lake itself and can be linked by their specific structure and / or their stable-isotopic composition to a known biological source or certain process. Many of these lipids are well preserved over time and can be found in records spanning many millions of years. The occurrence and variation with depth – and thus over time – of numerous biomarkers in the sedimentary record can therefore reveal aspects of past environmental conditions enabling the reconstruction of paleoclimate changes.

This thesis focuses on Lake Chala, a tropical East African crater lake at the border of Kenya and Tanzania, as its sediments contain a long and continuous, finely layered paleoenvironmental record spanning at least two glacial-interglacial cycles. Furthermore, the permanently anoxic lower water column of Lake Chala enables excellent preservation of organic material in the sediments. Lake Chala is thus the key site for unraveling continental paleoclimate history near the equator. Sediment cores spanning the last 25 thousand years were collected previously in the CHALLACEA project, and more recently, approximately 250 thousand years of lake sediments were recovered during the ICDP (International Continental Scientific Drilling Program) DeepCHALLA expedition in 2016. The paleoclimate record contained in the sediments will enhance our understanding of tropical (paleo)climate and ecosystem dynamics. However, to ensure the reliability of the climate records based on biomarker proxies, we need a thorough understanding of the occurrence and production of these biomarkers in the modern system.

The main objectives of this study are all geared towards the understanding, validation and expansion of the biomarker 'toolbox' that can be used in paleoclimate reconstructions. First, I want to identify and trace the occurrence of a large variety of lipid biomarkers in Lake Chala, and link them to their possible source organism(s). Many lipids found in lake sediments have an unknown biological origin or even a molecular structure that is not yet fully resolved. It is therefore important to further characterize these lipids and to identify their biological sources. Second, I want to link the occurrence, abundance and distribution of these biomarkers to various physical processes that are

influenced by climatic parameters (such as water column oxygen content, temperature, mixing and stratification) in the water column over short (seasonal to inter-annual) timescales. And third, as we now know the source organisms of the studied biomarkers, and how they are influenced by climatic parameters, I study selected biomarkers captured in Lake Chala's sediments to understand the climate variability over the past 25 thousand years. To achieve these objectives, I studied biomarkers in suspended particulate matter (SPM) that was collected monthly over a 17-month period at various water depths in Lake Chala, in settling particles collected monthly in a sediment trap over a period of 53 months, in the 25-kyr sedimentary record, and in vegetation, litter and soil from the surroundings of Lake Chala. Furthermore, additional data to have a better understanding of our biomarker record was collected. These other datasets include for example bacterial and archaeal 16S rRNA records, microscopic phytoplankton biomass estimates, and physical and chemical water column conditions such as temperature, pH, oxygen and carbon content collected during extensive monitoring of the water column.

Tracing phytoplankton biomarkers

The large majority of the biomarkers found in the water column of Lake Chala are produced aquatically. Generally, phytoplankton biomarkers are produced in the top part of the water column, where oxygen and light is available. Their abundance is higher during times of water column mixing, when nutrients from the deeper water layers are mixed upwards and become available for the phytoplankton. Most of the biomarkers found in Lake Chala show a large range of variation without systematic annual recurrences, although the mixing and stratification regime seems an important driver for biomarker variability over time. The irregularity in the presence of biomarkers in settling particles captured over 53 months indicates that modest but unique changes in water-column conditions are required to initiate the large inter-annual variations in the aquatic productivity of Lake Chala.

The main group of phytoplankton found in Lake Chala are diatoms, and the sediments of Lake Chala are full of their microscopic silica remains. The compounds loliolide and isololiolide are often used as diatom biomarkers. Indeed, in the suspended and settling particles, these biomarkers match with the trends seen in microscopic diatom biomass and can therefore be safely used in sedimentary reconstructions of these microorganisms. Chlorophytes (green algae) are also an important constituent of the phytoplankton assemblage in Lake Chala. Chlorophytes are the likely source of *n*-alk-1-enes (with carbon chain lengths of $C_{23:1}$, $C_{25:1}$ and $C_{27:1}$) and mid-chain *n*-alkanes (C_{21} and C_{23}). The occurrence and distribution of the long-chain *n*-alk-1-enes in the 25 kyr sediment record of Lake Chala shows that these green algal lipids become more prevalent during and after the glacial-to-Holocene transition. The relative abundance of $C_{27:1}$ *n*-alk-1-enes varies over the sedimentary record with a periodicity of ~2.3 kyr. This suggests that the production of specific *n*-alk-1-enes by chlorophytes might be linked to variations in monsoon intensity, and as the specific periodicity suggests, might be (in)directly forced by solar radiation. The $C_{19:1}$ *n*-alkene is most likely of cyanobacterial origin, based on a very distinguished seasonal trend compared to other biomarkers. Interestingly, this biomarker is generally highest in the short dry interval between the two main rain seasons, when shallow water column mixing is superimposed on a longer period of water column stratification. More research is needed to not only uncover the precise cyanobacterial origin of $C_{19:1}$ *n*-alkenes, but also to see if the occurrence of this biomarker in sedimentary records could for example help identify these specific water column conditions.

At times of high primary productivity, the stable-carbon isotopic composition of the phytoplankton biomarkers becomes ^{13}C depleted. In general, organisms preferably incorporate as

little of the 'heavy' carbon (^{13}C) as possible. During times of high primary productivity, a relatively large proportion of light carbon (^{12}C) is normally already used by other organisms and therefore no longer available. The other organisms therefore will have to incorporate more ^{13}C. However, this is not what we see in the modern-day Lake Chala. The ^{13}C depleted phytoplankton biomarkers during high primary productivity indicate that contrary to normal processes, other processes must occur in the water column of Lake Chala: chemically-enhanced diffusion and chemically-enhanced fractionation. These processes occur due to the high pH of the surface water of Lake Chala. This can have a large influence on the carbon isotopic signal of the sedimentary record, but these processes are not often considered or identified in paleoclimate studies. These processes should thus be taken into consideration when interpreting $\delta^{13}C$ records of aquatic biomarkers. This is not only important in Lake Chala, but also in other high pH lakes.

Aquatic sources of terrestrial biomarkers

The C_{28} fatty acid is a compound that is thought to have a terrestrial higher plant source, as it is abundantly present in the waxy layer of leaves. It is therefore often used as plant-wax biomarker in paleoenvironmental reconstructions. But, interestingly, the seasonal trends and $\delta^{13}C$ values of the C_{28} fatty acid record in the water column of Lake Chala indicate that it is not of terrestrial origin but is actually produced aquatically. Its seasonal distribution indicates that a green algal source is most likely, possibly of the species *Tetraedron minimum*. When studying the plant-wax record of lake sediments, and especially East African lake settings, one should be aware that the C_{28} fatty acid is likely produced in the water column and is not a plant-wax biomarker.

Some members of another class of biomarkers also indicate an unexpected source. *Des*-A-triterpenoids are degradation products of non-hopanoid pentacyclic triterpenoids that are often found in plant waxes. And in most cases, such as *des*-A-lupane, these biomarkers are indeed of terrestrial origin. The occurrence and $\delta^{13}C$ signature of *des*-A-lupane was studied in the sedimentary record of Lake Chala. Usually, plant waxes studied in sediments (such as long-chain *n*-alkanes) are of a mixed C_3/C_4 vegetation origin. Plant waxes of these two vegetation types have a different carbon isotopic composition, as C_3 and C_4 plants follow a different isotopic fractionation pathway during photosynthesis. It turns out that *des*-A-lupane in Lake Chala sediments can be used as a novel and independent proxy for the stable carbon isotopic composition of local terrestrial C_3 plants, that is not influenced by the mixed C_3/C_4 vegetation input into the sediments. But, not all *des*-A-triterpenoids have a terrestrial source as one would expect. *Des*-A-arborene isomers are degradation products of isoarborinol, which is often regarded as a terrestrial biomarker. However, the occurrence, trends and $\delta^{13}C$ signatures of *des*-A-arborenes in the 25-kyr sediment record indicate that isoarborinol must have had an aquatic microbial source in Lake Chala. Molecular mechanics calculations indicate that the transformations of the large suite of *des*-A-arborene isomers are microbially mediated. The occurrence of *des*-A-arborenes, both in modern and ancient tropical lake settings, seems typical for crater lakes with permanently anoxic bottom waters and sediments like Lake Chala. In those settings degradation products of isoarborinol are likely to have an aquatic microbial source.

Paleoclimate proxies for temperature, rainfall and stratification

An increasing number of climate proxies are based on glycerol dialkyl glycerol tetraethers (GDGTs), even though the biological sources of most of these GDGTs are not well constrained. Isoprenoid GDGTs (isoGDGTs) are membrane lipids of the archaea, and are for example used to reconstruct past temperatures and precipitation. In the modern-day Lake Chala they are mainly found in the

deep anoxic water column. Branched GDGTs are bacterial membrane lipids. The abundance of specific brGDGTs relative to the isoGDGT crenarchaeol is often used to assess the terrestrial contribution to sediments. In lakes, this so-called Branched and Isoprenoid Tetraether (BIT) index has been used as an indirect proxy for rainfall and subsequent runoff into the lake, on the premise that archaeal isoGDGTs are mainly produced within the lake, while soil bacterial brGDGTs are washed in with rainfall. But, the interpretation of BIT index records in lake settings is no longer straightforward since both isoGDGTs and brGDGTs are produced in the water column. In Lake Chala, conditions of strong water-column stratification where anoxic conditions are very shallow appear to play a key role in the production of isoGDGTs. This strong stratification leads to the suppression of a Thaumarchaeotal bloom, therefore results in low isoGDGT concentrations, and thus in high BIT index values. During these periods of strong stratification, the concentration of isoGDGT-0 is high. This isoGDGT-0 is produced by other archaea than Thaumarchaea, so that the resulting high isoGDGT-0 over crenarchaeol ratio is also useful in recognizing periods with strong water column stratification. In addition, the relative proportion of an isomer of crenarchaeol seems indicative of prolonged periods of strong stratified conditions. This study reveals that the 25-kyr BIT record of Lake Chala should be interpreted as a record of upper water column stratification, which is associated with wetter and less windy climate conditions, and thus indirectly reflects past variation in hydroclimate conditions. This study therefore helps understanding why the BIT index works so well in this lake, even though there is not a direct link between rainfall and the GDGTs. The distribution of specific isoGDGTs produced by Thaumarchaea is also related to temperature, expressed as the TEX_{86} proxy. This paleothermometer does not seem to work well in lake settings, as archaea other than Thaumarchaea contribute to the isoGDGTs incorporated into the proxy. This is especially evident at times of strong stratification. The three isoGDGT-based stratification proxies can therefore identify periods in time that are not suitable for TEX_{86} paleothermometry, but also identify periods where these paleotemperature reconstructions are likely usable.

BrGDGTs are increasingly used in paleotemperature reconstructions, although it is unclear which (group of) bacteria produce these lipids. Moreover, a mechanistic understanding of brGDGT production in lakes and the link with temperature and other environmental conditions is still lacking. In the water column of Lake Chala, the concentration and distribution of brGDGTs greatly varies over time. It is now also clear that almost all brGDGTs found in the water column have an aquatic origin. The brGDGT record of the water column is compared to the bacterial 16S rRNA gene abundance of the same samples. It is unlikely that Acidobacteria, the only known group of bacteria to produce building blocks of brGDGTs, are the main producers of brGDGTs in the water column of Lake Chala. And it turns out more difficult than expected to link the bacterial genes to the bacterial biomarkers and to assign a probable biomarker source. In addition, the modern-day brGDGT fluxes and distributions in Lake Chala cannot directly be linked to water column conditions. Although on seasonal to interannual timescales the variability of reconstructed temperature does not correspond to the actual temperature, the overall brGDGT signature in settling particles does correspond to mean annual air temperature. This suggests that brGDGTs can probably still be used as paleothermometer in the time-integrated archive of lake sediments.

Main conclusions

In summary, this thesis emphasizes the importance of extensive studies of the modern-day lake system prior to interpretation of climate-proxy records based on the occurrence and distribution of lipid biomarkers in its sediments. The biomarkers in the modern lake system show a much more complicated picture than usually is expected, and this thesis highlights in various ways the

importance of studying modern systems for paleoclimate research. Firstly, certain biomarkers are shown to have a different origin than generally presumed (such as the C_{28} fatty acid, and *des*-A-arborenes). Secondly, this thesis describes significant steps in tying established and new biomarkers (such as the $C_{19:1}$ *n*-alkene, and long-chain *n*-alk-1-enes) to their possible microbial sources. Thirdly, the ^{13}C-depleted aquatic biomarkers found in Lake Chala and its sediments can be explained by physical fractionation processes associated with high pH, a common condition in East African lakes. These findings are not only important for the quality and impact of paleoenvironmental reconstructions based on biomarker $\delta^{13}C$ values in the sediment record of Lake Chala, but for all (East African) lakes. Finally, this thesis highlights that monitoring programs need to run for many more years (>5) to fully characterize the relation between environmental conditions and the temporal patterns of the studied biomarkers, as well as to reveal the drivers and underlying patterns forcing the lake's microbial community. Although this is practically challenging and costly to implement, it is crucial in order to improve our understanding of paleoenvironmental reconstructions based on lake sediments.

A perfect view of Mt Kilimanjaro on the way from Taveta town to Lake Chala during the dry season in August 2014.
Photo credit: F. Peterse

Algemene samenvatting (in het Nederlands)

De door de mens veroorzaakte klimaatverandering zal de komende eeuwen grote maatschappelijke en economische verstoringen veroorzaken. Om te begrijpen hoe het klimaatsysteem zal reageren op de stijgende CO_2-niveaus in de atmosfeer en de oceaan is het bestuderen van natuurlijke klimaatveranderingen in het verleden essentieel. Reconstructies van het klimaat van vroeger (paleoklimaat) dragen bij aan het valideren, testen en verbeteren van de klimaatmodellen die nodig zijn om toekomstige klimaatveranderingen nauwkeurig te kunnen voorspellen. Aangezien instrumentele meetgegevens maximaal enkele eeuwen teruggaan, moeten we het paleoklimaat reconstrueren met zogenoemde proxy's. Het begrijpen van continentale klimaatveranderingen is cruciaal omdat hier de gevolgen voor de mens het grootst zullen zijn. Meersedimenten behoren tot de beste archieven van het continentale paleoklimaat, vooral in tropische gebieden waar andere archieven (zoals ijskernen) vaak ontbreken. Meren zijn gevoelig voor veranderingen in hun omgeving, zowel in het meer zelf als in het stroomgebied. Op de bodem van een meer stapelen sedimenten zich laag voor laag op. Deze sedimentlagen bevatten onder andere resten van micro-organismen, pollen, sporen, bodem en stof, die informatie kunnen verschaffen over de omstandigheden op het moment van afzetting. Eén manier om paleoklimaatinformatie uit deze meersedimenten te ontsluiten is door te kijken naar lipide biomarkers. Deze 'moleculaire fossielen' worden geproduceerd door organismen, zowel op het land als in het meer zelf, en kunnen door hun specifieke structuur of hun stabiele-isotoopsamenstelling worden gekoppeld aan hun biologische oorsprong of een bepaald proces. Veel van deze lipiden blijven goed bewaard in sedimenten, en kunnen dan ook gebruikt worden om zelfs hele oude sedimentarchieven te onderzoeken. De aanwezigheid van deze biomarkers en hun variatie met diepte - en dus in tijd - in de sedimentlagen kan daarom aspecten van de vroegere leefomgeving blootleggen die paleoklimaatreconstructies mogelijk maken.

Dit proefschrift concentreert zich op het Chala-meer, een klein doch diep tropisch Oost-Afrikaans kratermeer gelegen op de grens tussen Kenia en Tanzania. De sedimenten in dit meer bestaan uit dunne laagjes die in opeenvolgende seizoenen zijn afgezet en uitstekend bewaard zijn gebleven door de zuurstofloze omstandigheden in het bodemwater en het sediment. Nadat er sedimentkernen van de afgelopen 25 duizend jaar werden verzameld in het CHALLACEA-project, zijn er zeer recent sedimentkernen van de afgelopen 250 duizend jaar verkregen tijdens de ICDP (International Continental Scientific Drilling Program) DeepCHALLA expeditie. De paleoklimaatreconstructies die hierdoor mogelijk zijn, zullen ons inzicht in de tropische klimaats- en ecosysteemdynamiek over lange tijdschalen vergroten. Om de betrouwbaarheid van de klimaatreconstructies op basis van biomarkerproxy's te vergroten hebben we wel grondig inzicht nodig in de aanwezigheid en de productie van deze biomarkers in het moderne systeem.

De vragen die tijdens dit onderzoek worden gesteld, zijn allemaal gericht op het begrijpen, valideren en uitbreiden van de 'biomarker gereedschapskist' die gebruikt wordt voor paleoklimaatreconstructies. Ten eerste heb ik de grote verscheidenheid aan biomarkers in het Chala-meer vastgesteld en de biomarkers gekoppeld aan de organismen die deze markers produceren. Veel lipiden die in meersedimenten worden gevonden hebben een onbekende biologische oorsprong of moleculaire structuur. Het is daarom belangrijk om deze lipiden verder te karakteriseren en hun biologische bronnen te identificeren. Ten tweede wilde ik de aanwezigheid, hoeveelheid en de verspreiding van deze biomarkers koppelen aan verschillende fysische processen in de waterkolom.

En ten derde, nadat de bronorganismen van de bestudeerde biomarkers waren bepaald en hun dynamiek met klimatologische parameters was vastgesteld, heb ik op basis van de geselecteerde biomarkers in de sedimenten van het Chala-meer de klimaatvariabiliteit in de afgelopen 25 duizend jaar zo goed mogelijk gereconstrueerd. Om deze doelstellingen te bereiken, bestudeerde ik biomarkers in: gesuspendeerde deeltjes (SPM) die maandelijks verzameld werden over een periode van 17 maanden op verschillende waterdieptes in het Chala-meer; neerdwarrelende deeltjes die maandelijks gevangen werden in een sedimentval gedurende een periode van 53 maanden; de sedimentkern van de afgelopen 25 duizend jaar; en vegetatie en bodems uit de omgeving van het Chala-meer. Bovendien werden aanvullende gegevens verzameld om de aanwezigheid van biomarkers te kunnen duiden. Deze toegevoegde datasets zijn onder andere verzameld tijdens uitgebreide maandelijkse monitoring van de waterkolom, en omvatten bijvoorbeeld metingen van bacterieel en archaeaal DNA, fytoplankton biomassaschattingen, en fysische en chemische waterkolomomstandigheden.

Primaire productie

De overgrote meerderheid van de biomarkers aanwezig in de waterkolom van het Chala-meer wordt aquatisch geproduceerd. Over het algemeen leeft fytoplankton in het bovenste deel van de waterkolom, waar zuurstof en licht beschikbaar zijn. Hun hoeveelheid is groter in tijden van waterkolom-menging, wanneer voedingsstoffen uit de diepere waterlagen naar boven komen en beschikbaar komen voor het fytoplankton. Het meng- en stratificatieregime is dus erg belangrijk voor de groei van fytoplankton. De afwisseling van de soorten van fytoplankton door het jaar heen kun je goed zien door de fytoplanktonbiomarkers te bestuderen. Maar tussen de verschillende jaren zijn er weinig systematisch terugkerende patronen te ontdekken, ondanks een redelijk regelmatig meng- en stratificatieregime. De onregelmatigheid in de aanwezigheid van biomarkers in bijna 4,5 jaar lang verzamelde sedimenterende deeltjes geeft aan dat onopvallende maar belangrijke veranderingen in waterkolomcondities optreden die grote jaarlijkse schommelingen in de aquatische productiviteit van het Chala-meer veroorzaken.

De belangrijkste groep van fytoplankton in het Chala-meer zijn diatomeeën (kiezelwieren), en de sedimenten van het Chala-meer zitten dan ook vol met hun silicaresten. De lipiden loliolide en isololiolide worden vaak gebruikt als diatomeeënbiomarkers, en zoals verwacht komen de trends van deze biomarkers in de gesuspendeerde en sedimenterende deeltjes overeen met de biomassa-trends van de diatomeeën. Chlorofyten (groenalgen) zijn ook een belangrijk deel van de fytoplanktonsamenstelling in het Chala-meer. Chlorofyten zijn de meest waarschijnlijke bron van *n*-alk-1-enen (met ketenlengten van C_{23}, C_{25} en C_{27}) en middellange *n*-alkanen (C_{21} en C_{23}). De aanwezigheid en de variatie van de *n*-alk-1-enen in de sedimentkern laten zien dat deze groenalgen gestaag toenemen tijdens en na de overgang van de ijstijd naar het Holoceen. De relatieve hoeveelheid van $C_{27:1}$ *n*-alk-1-een in het sediment varieert met een periodiciteit van ongeveer 2300 jaar. Dit suggereert dat de productie van specifieke *n*-alk-1-enen door chlorofyten kan worden gekoppeld aan variaties in moessonintensiteit, en zoals de specifieke periodiciteit suggereert, mogelijk (in)direct wordt geforceerd door periodieke variaties in de instraling van de zon. In tegenstelling tot de langere *n*-alk-1-enen heeft de kortere $C_{19:1}$ *n*-alkeen geen chlorofyten maar een cyanobacteriële oorsprong. Interessant is dat deze biomarker over het algemeen het hoogst is in het korte droge interval tussen de twee belangrijkste regenseizoenen, wanneer er ondiepe menging plaatsvindt in de gestratificeerde waterkolom. Meer onderzoek is nodig om niet alleen de exacte cyanobacteriële oorsprong van de $C_{19:1}$ *n*-alkenen bloot te leggen, maar ook om te

zien of de aanwezigheid van deze biomarker in sedimentaire archieven bijvoorbeeld kan helpen bij het identificeren en reconstrueren van deze specifieke waterkolomomstandigheden.

In tijden van hoge primaire productiviteit wordt de stabiele-koolstofisotopensamenstelling van de biomarkers van fytoplankton verarmd aan ^{13}C. Organismen nemen bij voorkeur zo weinig mogelijk van de 'zware' koolstof (^{13}C) op. Maar in tijden van hoge primaire productiviteit wordt een relatief groot deel van lichte koolstof (^{12}C) al door andere organismen gebruikt en is daarom niet langer beschikbaar. De organismen zullen daarom meer ^{13}C moeten opnemen. Dit is echter niet wat we zien in het Chala-meer. De fytoplanktonbiomarkers bevatten juist relatief weinig ^{13}C tijdens hoge primaire productiviteit. Dat geeft aan dat in tegenstelling tot normale processen, andere processen plaatsvinden in de waterkolom van het Chala-meer: chemisch verhoogde diffusie en chemisch versterkte fractionering. Deze processen vinden plaats door de hoge pH van het oppervlaktewater, en kunnen een grote invloed hebben op het koolstofisotopensignaal dat uiteindelijk wordt bewaard in de sedimenten. Toch wordt er in paleoklimaatstudies aan het bestaan van deze processen niet vaak gedacht. Deze processen moeten dus wel in overweging worden genomen bij de interpretatie van de $\delta^{13}C$-historie van aquatische biomarkers. Dit is niet alleen belangrijk in het Chala-meer, maar ook in andere meren met een hoge pH.

Aquatische herkomst van terrestrische biomarkers

Van het C_{28}-vetzuur wordt vaak aangenomen dat het afkomstig is van hogere planten, omdat het overvloedig aanwezig is in de waslaag van bladeren. Het wordt daarom vaak gebruikt als plantwasbiomarker bij paleomilieureconstructies. Interessant genoeg geven de seizoentrends en $\delta^{13}C$-waarden van het C_{28}-vetzuur in de waterkolom van het Chala-meer aan dat het niet van terrestrische oorsprong is, maar daarentegen aquatisch wordt geproduceerd. De seizoentrends wijzen erop dat de waarschijnlijkste bron een groenalg is, mogelijk *Tetraedron minimum*. Bij het bestuderen van plantenwassen in meersedimenten, en met name in Oost-Afrikaanse meren, moet men er zich dus van bewust zijn dat het C_{28}-vetzuur waarschijnlijk in de waterkolom wordt geproduceerd en daarom onbruikbaar is als biomarker voor planten.

Naast deze onverwachte aquatische bron van het C_{28}-vetzuur, laten sommige andere biomarkers ook een andere biologische oorsprong zien dan verwacht. *Des*-A-triterpenoïden zijn afbraakproducten van niet-hopanoïde pentacyclische triterpenoïden die ook vaak worden aangetroffen in plantenwassen. En in de meeste gevallen, zoals bij *des*-A-lupaan, zijn deze biomarkers inderdaad van terrestrische origine. Bovendien blijkt dat *des*-A-lupaan in de sedimenten van het Chala-meer gebruikt kan worden als een nieuwe en onafhankelijke proxy voor de stabiele-koolstofisotopensamenstelling van lokale terrestrische C_3-planten. Maar, zoals gezegd, niet alle *des*-A-triterpenoïden hebben een terrestrische bron, zoals *des*-A-arborenen (afbraakproducten van isoarborinol). De aanwezigheid, trends en $\delta^{13}C$-waarden van deze *des*-A-arborenen in de sedimentkern geven aan dat isoarborinol een microbiële bron in het water van het Chala-meer moet hebben gehad. Moleculaire-mechanicaberekeningen bevestigen bovendien dat de transformatie van de verschillende *des*-A-arborenen microbieel gemedieerd zijn. Het voorkomen van *des*-A-arborenen, zowel in hedendaagse als oude tropische meren, lijkt kenmerkend voor kratermeren zoals het Chala-meer, met permanente zuurstofloze bodemwater- en sedimentcondities. In dit soort meren hebben de degradatieproducten van isoarborinol zeer waarschijnlijk een microbiële bron in het water.

Proxy's voor temperatuur, regenval en stratificatie

Een toenemend aantal klimaatproxy's is gebaseerd op glycerol dialkyl glycerol tetraethers (GDGTs), hoewel de biologische oorsprong van de meeste van deze GDGTs niet bekend is. Isoprenoïde GDGTs (isoGDGTs) zijn archaeale membraanlipiden die bijvoorbeeld gebruikt worden om temperatuur en neerslag te reconstrueren. In het hedendaagse Chala-meer worden deze lipiden vooral aangetroffen in de diepe, anoxische waterkolom. Vertakte GDGTs (brGDGTs) zijn bacteriële membraanlipiden. De verhouding van verschillende brGDGTs ten opzichte van een specifieke isoGDGT (crenarchaeol) wordt vaak gebruikt om de relatieve terrestrische bijdrage aan sedimenten in te schatten. In meren is deze vertakte en isoprenoïde tetraether (BIT)-index vaak gebruikt als een indirecte regenvalindicator, met de aanname dat de archaeale isoGDGTs hoofdzakelijk in het meer worden geproduceerd, terwijl bodembacteriële brGDGTs tijdens regenbuien van het land in het meer worden gespoeld. Toch is de interpretatie van de BIT-index in meren niet zo eenvoudig, omdat zowel isoGDGTs als brGDGTs in de waterkolom worden geproduceerd. In het Chala-meer lijken de condities van sterke stratificatie waarbij de zuurstofloosheid in het water erg ondiep reikt een sleutelrol te spelen in de productie van isoGDGTs. Deze sterke stratificatie leidt tot de onderdrukking van een bloei van Thaumarchaeota, wat resulteert in lage isoGDGT-concentraties en dus in hoge BIT-indexwaarden. Tijdens deze perioden van sterke stratificatie is de concentratie van isoGDGT-o hoog. Deze biomarker wordt geproduceerd door andere archaea dan Thaumarchaea, waardoor hoge concentraties van isoGDGT-o ten opzichte van crenarchaeol wijzen op perioden met een sterke waterkolomstratificatie. Bovendien lijkt het relatieve aandeel van een isomeer van crenarchaeol indicatief voor langdurige perioden van sterke stratificatie. Deze studie geeft dus aan dat de BIT-waarden in de sedimenten van het Chala-meer moeten worden geïnterpreteerd als documentatie van sterke stratificatie. Deze sterke stratificatie wordt geassocieerd met nattere en minder winderige omstandigheden, en zo weerspiegelt de BIT-index dus indirect de variatie in paleoprecipitatie. Mijn studie helpt daarom te begrijpen waarom de BIT-index zo goed werkt in dit meer, ook al is er geen direct verband tussen regenval en de GDGTs.

De verdeling van specifieke isoGDGTs geproduceerd door Thaumarchaea houdt ook verband met de watertemperatuur, uitgedrukt als de TEX_{86}-proxy. Deze paleothermometer lijkt niet goed te werken in het meer, niet alleen omdat Thaumarchaea bijdragen aan de isoGDGTs in het sediment, maar ook andere archaea die geen relatie hebben met de productie van specifieke isoGDGTs en temperatuur. Dit is vooral evident in tijden van sterke stratificatie. De drie isoGDGT-stratificatie-proxy's kunnen daarom perioden identificeren die niet geschikt zijn voor de TEX_{86}-temperatuurreconstructies, maar identificeren ook perioden waarin deze paleotemperatuurreconstructies waarschijnlijk wel bruikbaar zijn. Ook brGDGTs worden steeds vaker gebruikt in temperatuurreconstructies, hoewel het onduidelijk is welke bacteriële groep(en) deze lipiden produceren. Bovendien ontbreekt nog een mechanistisch inzicht in de productie van brGDGT in meren en milieuomstandigheden zoals temperatuur. In de waterkolom van het Chala-meer varieert de concentratie en verdeling van brGDGTs sterk in de tijd. Het is nu ook duidelijk dat bijna alle brGDGTs in de waterkolom van aquatische oorsprong zijn. Het is onwaarschijnlijk dat Acidobacteria, de enige bekende groep bacteriën die bouwstenen van brGDGTs produceert, belangrijke producenten zijn van brGDGTs in de waterkolom van het Chala-meer. En het blijkt moeilijker dan verwacht om specifieke bacteriën (geïdentificeerd door hun DNA) te koppelen aan de bacteriële biomarkers en een waarschijnlijke biomarkerbron toe te wijzen. Bovendien kunnen de variaties in de brGDGTs in het Chala-meer niet rechtstreeks worden gekoppeld aan de omstandigheden in de waterkolom. Hoewel de brGDGTs niet de seizoensmatige temperatuurtrends reconstrueren, corresponderen de brGDGTs over langere tijd goed met de gemiddelde temperatuur.

Dit suggereert dat brGDGTs nog steeds kunnen worden gebruikt als een paleothermometer in het tijdgeïntegreerde archief van meersedimenten.

Hoofdconclusies

Samenvattend benadrukt dit proefschrift het belang van uitgebreide studies van het hedendaagse meersysteem voorafgaand aan de interpretatie van lipide paleoklimaatproxy's in sedimenten. De biomarkers in het hedendaagse meersysteem vertonen een veel gecompliceerder beeld dan gewoonlijk wordt verwacht, en dit proefschrift benadrukt op verschillende manieren het belang van het bestuderen van moderne systemen voor paleoklimaatonderzoek. Ten eerste wordt aangetoond dat bepaalde biomarkers een andere oorsprong hebben dan algemeen gedacht (zoals het C_{28}-vetzuur en *des*-A-arborenen). Ten tweede beschrijft dit proefschrift belangrijke stappen in het koppelen van vaak gebruikte en nieuwe biomarkers (zoals de $C_{19:1}$ *n*-alkeen en de *n*-alk-1-enen) aan hun mogelijke microbiële bronnen. Ten derde kunnen de relatief ^{13}C-verarmde biomarkers in het Chala-meer en zijn sedimenten worden verklaard door fysische fractioneringsprocessen behorend bij de hoge pH in het oppervlaktewater, iets wat vaak voorkomt in Oost-Afrikaanse meren. Het herkennen van deze processen is zeer belangrijk voor de interpretatie van paleomilieureconstructies op basis van biomarker $\delta^{13}C$-waarden, niet alleen in het sedimentarchief van het Chala-meer, maar ook in dat van alle (Oost-Afrikaanse) meren. Tot slot benadrukt dit proefschrift dat monitoringprogramma's vele jaren moeten worden voortgezet om de relatie tussen de omgeving en de temporele patronen van de bestudeerde biomarkers volledig te karakteriseren, en om de drijvende krachten en onderliggende patronen van microbiële productiviteit en successie te onthullen. Hoewel dit tijdrovend, praktisch uitdagend en kostbaar is om te implementeren, is langdurige bestudering van moderne meersystemen cruciaal om ons begrip van sedimentaire klimaatreconstructies te verbeteren.

Local fishermen in wooden boats on the Tanzanian side of Lake Chala.

1 General introduction and synopsis

1.1 Climate change and paleoclimate archives

Anthropogenic climate change is expected to cause large societal and economical disruptions in the centuries to come (IPCC, 2013). With the current expected CO_2 level rise, by the end of the century the global annual average surface temperature is estimated to rise with 1.5 to 4.6°C compared to preindustrial times. In order to understand current and projected future climate change, we need to better understand the natural climate changes that have occurred in the (geologically recent) past. As instrumental records only go back a relatively short amount of time (for example, air temperature measurements have only been recorded since ca. 1850), past changes need to be reconstructed by so-called proxy records. These paleoclimate reconstructions provide critical knowledge for climate modelers to validate, test and improve their models to accurately predict future climate changes. As oceans play an important role in regulating the global heat transport, and thus have a large influence on the global climate (IPCC, 2013), a large part of the paleoclimate studies focuses on exploring marine sedimentary archives, which can cover many millions of years. However, also our understanding of climate change over the continents is crucial as this is where societal and economic impacts will be highest.

The study of continental paleoclimates faces various challenges, not only due to limited availability of long term, continuous, high-resolution climate archives on land, but also due to a scarcity of reliable proxies for paleoclimate reconstruction. Among the most promising continental climate archives are lake sediments, ice cores, tree rings and speleothems, each with their own advantages and disadvantages. Ice cores provide high-resolution archives of both past climate and atmospheric composition, the latter recorded in gas inclusions in the ice (e.g. Rasmussen et al., 2014), but are geographically limited to permanently ice-covered regions. Tree rings can record environmental conditions with a seasonal resolution, but these archives cover only relatively short time intervals and are hard to extract from tropical trees due to their year-round growth (Sheppard, 2010). Speleothems in caves can provide high-resolution paleoclimate reconstructions mainly based on their stable oxygen ($\delta^{18}O$) and carbon ($\delta^{13}C$) isotopic composition (e.g., Wang et al., 2001; Cheng et al., 2016), but the formation of high-quality speleothems is geographically limited, with many more containing hiatuses due to periods with dry conditions, and with limited accurate dating possibilities (currently restricted to <640-kyr with Uranium-Thorium dating). Lake sediment archives are sensitive to environmental changes in the lake itself or the surrounding catchment. Further, the sediment accumulation rate in lakes is generally high compared to that in the deep ocean, implying that reconstructions with high temporal resolution are possible. Especially in lakes with anoxic bottom water and finely laminated (varved) sediments it is possible to even reconstruct environmental conditions on an annual resolution. On the other hand, sediment continuity over sufficiently long periods of time can be compromised by complete ice cover during glacial intervals or mass-wasting events during climate extremes. Overall, however, lake sediments are the best archives of past continental climate change, especially in tropical areas where other archives are often lacking.

1.2 Lipid biomarkers and proxies

Information on paleoclimate can be obtained from lake-sediment archives using various methods. For example, the assemblages of microscopic remains of pollen, diatoms or chironomid larvae stored in lake sediments are often related to climate-driven changes in catchment vegetation or local environmental variables such as lake temperature and salinity (e.g. Heiri and Lotter, 2005; Eggermont et al., 2007), but as these assemblages can reflect many environmental parameters (e.g., temperature, precipitation, pH, nutrients, species occurrence), their proxy records are often qualitative and not quantitative. A different method that enables the reconstruction of environmental conditions in both the water column and the surroundings is based on lipid biomarkers. Biomarkers are organic compounds that can be linked, either by their specific structure, their stable-isotope composition, or both, to a known biological source or certain process. Hence, the (relative) abundance and stable isotopic composition of these biomarkers, or their degradation products in sediments can provide information on the environmental conditions at the time of deposition, and can thus act as qualitative and quantitative proxies for specific climate variables (see e.g., Meyers, 1997, 2003; Volkman et al., 1998; Castañeda and Schouten, 2011 for reviews).

1.2.1 Vegetation and phytoplankton biomarkers

Practically all higher plants produce leaf waxes, mainly to protect themselves against uncontrolled water loss. These plant waxes consist partly of 'simple' compounds such as long-chain *n*-alkanes (Fig. 1.1A), fatty acids and alcohols (e.g., Eglinton and Hamilton, 1967; Eglinton and Eglinton, 2008; Castañeda and Schouten, 2011; Freeman and Pancost, 2014) but also more complex cyclic compounds (Fig. 1.1B) such as non-hopanoid pentacyclic triterpenoids (e.g., Rullkötter et al., 1982; Freeman et al., 1994; Sabel et al., 2005; Diefendorf et al., 2012). The chain length of leaf waxes can be used to differentiate between trees/shrubs and grassland, where shrubs are characterized by relatively more C_{27} and C_{29}, and grasses by C_{31}, C_{33} and C_{35} *n*-alkanes (e.g. Rommerskirchen et al., 2006; Vogts et al., 2012; Freeman and Pancost, 2014; Garcin et al., 2014). Furthermore, the stable carbon isotopic composition ($\delta^{13}C$) of plant waxes is indicative of vegetation type (Collister et al., 1994), as C_3 and C_4 plants follow a different stable carbon isotopic fractionation pathway during photosynthesis. Similarly, the composition of precipitation is recorded in the hydrogen isotopic (δD) signature of plant waxes, as plants use environmental water as source of hydrogen to synthesize them. Plant waxes stored in lake sediments have been studied extensively and have resulted in many records of hydroclimate and vegetation history (e.g., Schefuß et al., 2005; Castañeda et al., 2007; Tierney et al., 2010a; Berke et al., 2012a; Feakins et al., 2013).

There are also several biomarkers that can be used to reconstruct changes in primary productivity and phytoplankton community composition within a lake. Although not all of these biomarkers can be linked to unique biological taxa, they can be attributed to the occurrence of a certain taxonomic group (see reviews of Volkman et al., 1998; Castañeda and Schouten, 2011). For example, phytol is derived from chlorophyll, and can be used as a non-specific marker for primary productivity (e.g., Rontani and Volkman, 2003). In the same way, short-chain *n*-alkanes and fatty acids are generic phytoplankton biomarkers (e.g., Gelpi et al., 1970; Meyers, 1997; Volkman et al., 1989, 1998), and sterols can be derived from a large suite of different algae (e.g., Volkman et al., 1998; Volkman, 2003; Rampen et al., 2010; Castañeda and Schouten, 2011). Next to these common compounds, species-specific biomarkers can be used to reconstruct the particular environmental parameters or conditions under which their producing organisms thrive. For example, Bacillariophyta (diatoms) can be traced by the occurrence of (iso)loliolide (Fig. 1.1D), a diagenetic

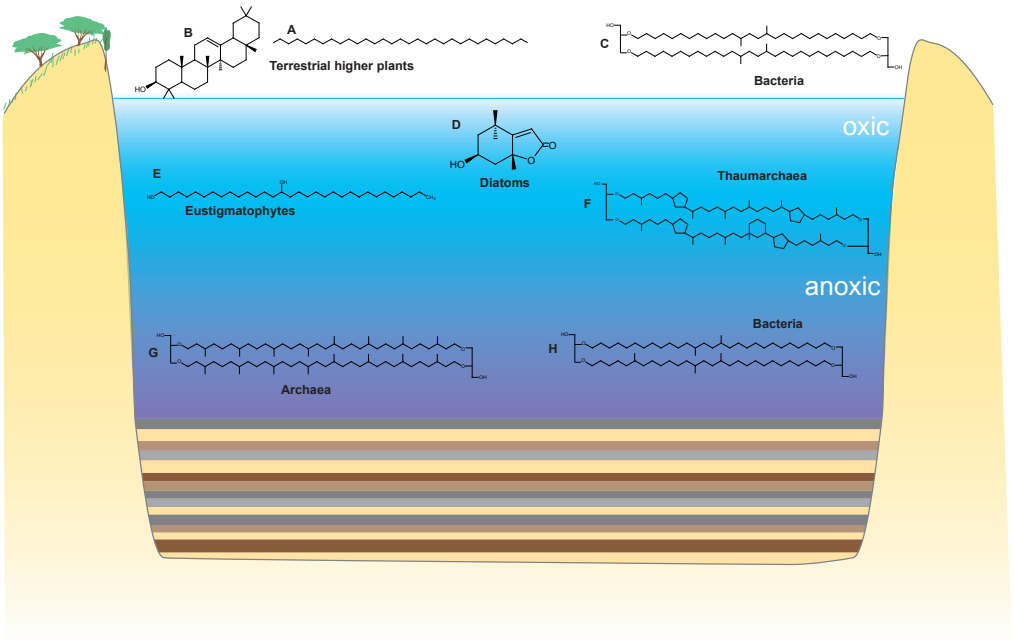

Figure 1.1 Overview of organic biomarkers typically found in tropical lake systems. Terrestrial vegetation is characterized by plant waxes such as C_{31} long chain *n*-alkanes (A) and functionalized pentacyclic triterpenoids such as β-amyrin (B). Next to vegetation biomarkers, soils contain biomarkers of soil bacteria, including brGDGT-Ia (C). Phytoplankton, bacteria and archaea all thrive in the open water column, producing a plethora of different biomarkers. In the oxic water column one often finds the diatom biomarker loliolide (D), eustigmatophyte long-chain 1,15 *n*-alkyl diols (E), and thaumarchaeotal crenarchaeol (F). Archaeal isoGDGT-0 (G) and bacterial brGDGTs such as IIa′ (H) are often found in the anoxic water column.

product of specific pigments (Klok et al., 1984; Repeta, 1989; Castañeda et al., 2009b; Castañeda and Schouten, 2011). Dinosterol is a biomarker for dinoflagellates (e.g., Boon et al., 1979; Volkman, 1999, 2003; Castañeda et al., 2011), and long-chain diols (Fig. 1.1E) in lacustrine environments are biomarkers for Eustigmatophyte algae (e.g., Volkman et al., 1992, 1998, 1999; Versteegh et al., 1997; Rampen et al., 2014; Villanueva et al., 2014). Tetrahymanol is typically derived from bacterivorous ciliates and used as indicator of stratified water column conditions under which these ciliates thrive (e.g., Harvey and McManus, 1991; Hanisch et al., 2003; Xu and Jaffé, 2008; Castañeda and Schouten, 2011 and references therein). However, many more lipids found in lake sediments have an unknown biological origin or even a molecular structure that is not yet fully resolved. In order to increase the biomarker toolbox, and thus the possibilities to improve the accuracy and reliability of paleoclimate reconstructions, it is important to further characterize these lipids, to identify their biological sources and the environmental processes associated with their occurrence and structure.

1.2.2 Archaeal and bacterial tetraether membrane biomarkers

A suite of relatively novel climate proxies is based on glycerol dialkyl glycerol tetraethers (GDGTs). Isoprenoid GDGTs (isoGDGTs) are membrane lipids of the Archaea (Fig. 1.1F-G), and can contain

up to 8 cyclopentyl moieties (DeRosa and Gambacorta, 1988). Crenarchaeol and its isomer are isoGDGTs with four cyclopentyl rings and an additional cyclohexyl moiety (Fig. 1.1F), and are specific biomarkers for Thaumarchaeota (e.g., Sinninghe Damsté et al., 2002, 2012b; Schouten et al., 2013). The relative distribution of isoGDGTs in marine surface sediments has been found to vary with sea surface temperature (SST), which has led to the development of the TEX_{86} paleotemperature proxy (Schouten et al., 2002; Powers et al., 2005). This proxy works well for isoGDGTs stored in marine sediments, but the application of TEX_{86} as lake surface temperature (LST) proxy has turned out to be more complicated, especially in small lakes, due to the possible contribution of isoGDGTs that are produced by species other than Thaumarchaeota, such as methanotrophs, methanogens or other archaea, to the isoGDGTs extracted from lake sediments (e.g., Blaga et al., 2009, 2011; Powers et al., 2010, 2011; Sinninghe Damsté et al., 2012; Buckles et al., 2013).

Another group of GDGTs consists of non-isoprenoidal alkyl chains, that can contain zero, one or two cyclopentyl moieties, and can be tetra-, penta-, or hexamethylated, where the outer methyl group can be attached to the 5^{th} (5-methyl) or 6^{th} (6-methyl) position (Figs. 1.1C and H). These branched GDGTs (brGDGTs) have a bacterial origin, possibly from Acidobacteria, although their exact producers are still unknown (Sinninghe Damsté et al., 2011a). As their fractional abundance in modern surface soils and peats shows an empirical relationship with mean annual air temperature (MAAT) and the pH of the soil or peat in which they are produced (Weijers et al., 2007b; Schouten et al., 2013; De Jonge et al., 2014a), they are used as a continental paleothermometer. In aquatic environments, the abundance of brGDGTs relative to that of crenarchaeol has been used to assess the terrestrial contribution to marine or lacustrine sediments, quantified in the Branched and Isoprenoid Tetraether (BIT) index (Hopmans et al., 2004). In lakes, the BIT index has been used as an indirect proxy for precipitation-induced runoff (e.g., Blaga et al., 2009; Verschuren et al., 2009), on the premise that archaeal isoGDGTs are mainly produced within the lake, while soil bacterial brGDGTs are washed in with rainfall. Subsequently, attempts were made to generate paleotemperature records based on the brGDGTs in lake sediments. However, the brGDGT signals in lake sediments appeared to be substantially different from those in the soils surrounding the lake, indicating that there must be an additional, likely *in situ* source of brGDGTs contributing to the lake sediments (e.g. Tierney and Russell, 2009; Bechtel et al., 2010; Loomis et al., 2011, 2014b; Pearson et al., 2011; Tierney et al., 2012; Schouten et al., 2013; Buckles et al., 2014). This finding stimulated the development of region- and lake-specific calibrations of the brGDGT-based temperature proxy. However, a mechanistic understanding of brGDGT production in lakes and the link with temperature and other environmental conditions is still lacking (Tierney et al., 2010a; Pearson et al., 2011; Sun et al., 2011; Loomis et al., 2012). Also the interpretation of BIT index records in lake settings is no longer straightforward since both isoGDGTs and brGDGTs are now known to be produced *in situ* (e.g., Sinninghe Damsté et al., 2009, 2012). To improve the applicability of GDGT-based proxies in the lacustrine environment we thus need to constrain the biological sources of GDGTs in lakes and reveal the intricate workings of these proxies.

1.3 Study site: Lake Chala in East Africa

The relative scarcity of climate archives in the tropics has resulted in an imbalance between the large number of paleoclimate records (lacustrine as well as marine) currently available from temperate and polar regions, versus a much smaller number available from (sub)tropical regions.

This hampers the understanding of timing and trends in continental paleoclimate evolution on a global scale. To help alleviate this imbalance, we chose as study site for this thesis a tropical crater lake in equatorial East Africa. Besides this favorable location, Lake Chala also contains in its bottom sediments a long and continuous, finely laminated paleoenvironmental record spanning at least the last two glacial-interglacial cycles (Moernaut et al., 2010), which makes it a prospective key site for continental paleoclimate history near the equator over the past 250 kyr.

Situated in the foothills of Mt. Kilimanjaro, Lake Chala straddles the border of Kenya and Tanzania. Lake Chala is locally known as 'Challa' (named after a nearby village) and is a relatively small (4.2 km²), but deep (~90 m) crater lake with steep crater walls rising up to 180 meter above the lake surface. It has a permanently stratified (meromictic) lower water column, and these permanently anoxic deep-water conditions are responsible for the excellent preservation of organic material in the lake sediments. The tropical rain belt associated with the Inter-Tropical Convergence Zone (ITCZ) passes over the Lake Chala region twice yearly, resulting in two distinct rain seasons, with relatively heavy 'short rains' from October to December, and 'long rains' from March to May (Nicholson, 2000; Verschuren et al., 2009). During these rain seasons, the water column is more

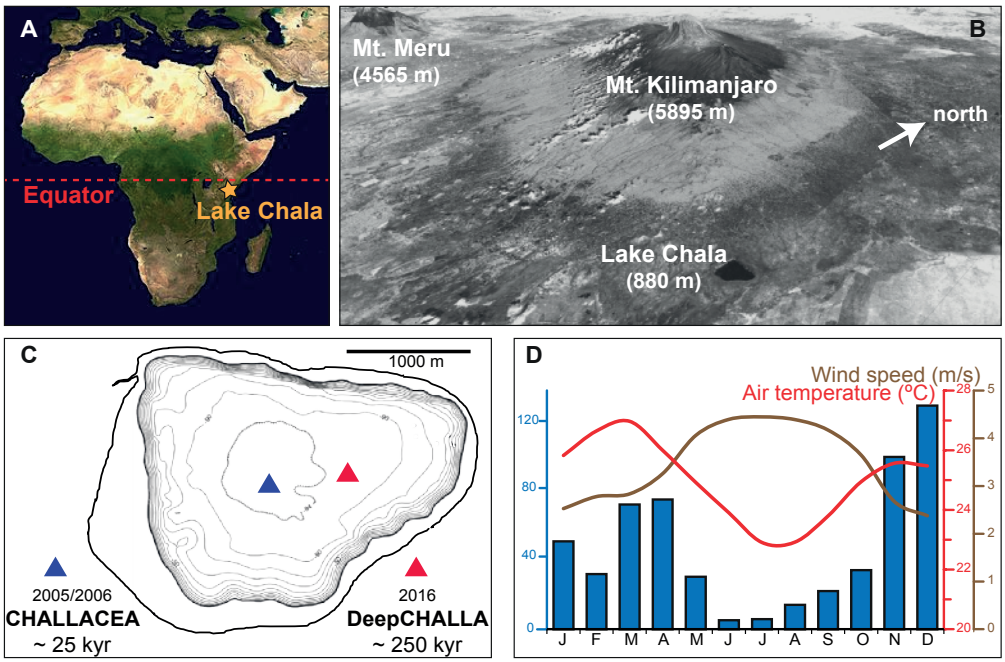

Figure 1.2 Lake Chala in equatorial East Africa, the focus lake system of this study. It is situated just south of the equator (A) on the border of Kenya and Tanzania in the foothills of Mount Kilimanjaro (B). The long sediment cores recovered by the CHALLACEA project (25 kyr; recovered in 2003-2005) and by the ICDP DeepCHALLA project (~250 kyr; recovered in 2016) were both taken at an offshore positions (C). Climate in the Lake Chala region is influenced by the twice-yearly passing ITCZ, which results in two rain seasons from October to December and from March to May, and one relatively cold and windy principal dry season (D). Climate variables for Voi, averaged over the period 1957-2008. Figure panels are adapted after Verschuren et al. (2009), Moernaut et al. (2010) and Wolff et al. (2014).

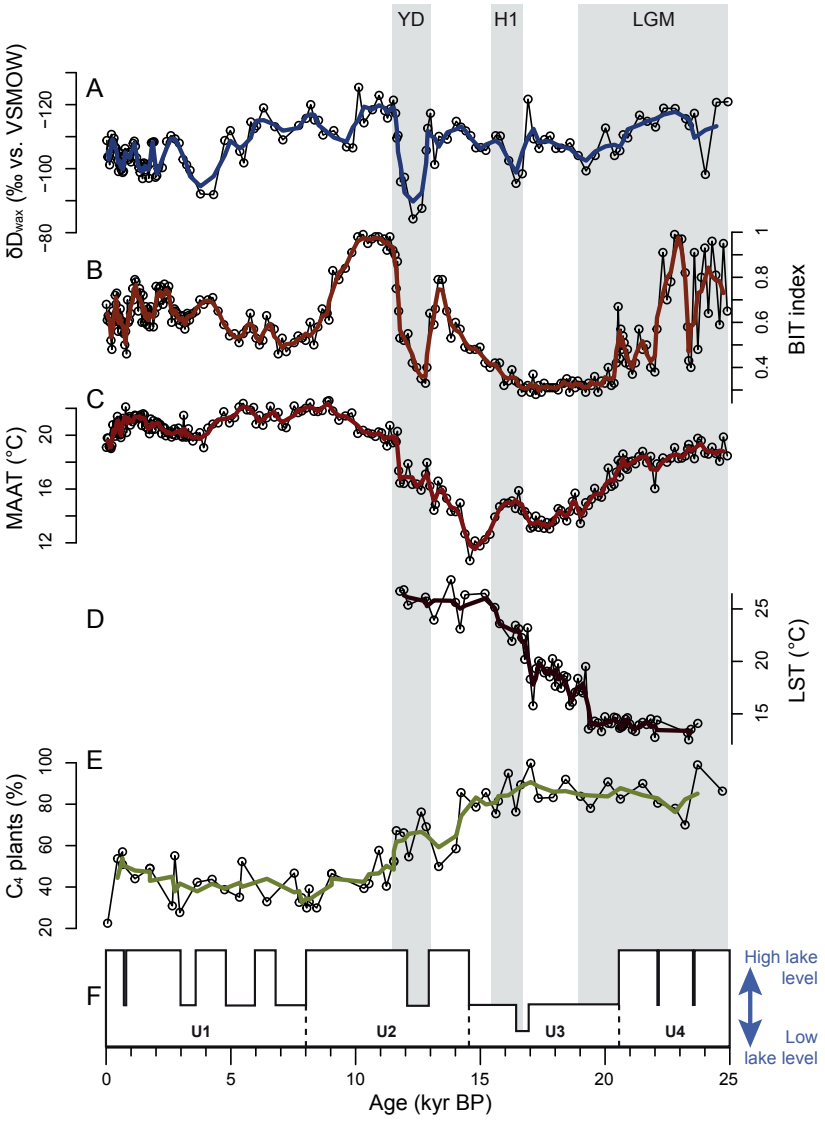

Figure 1.3 Climate and ecosystem proxy data based on organic biomarkers extracted from the sediments of Lake Chala over the past 25 kyr. A: δD_{wax} (in ‰ vs. VSMOW) based on the hydrogen composition of the C_{28} fatty acid (Tierney et al., 2011). B: the BIT index (Verschuren et al., 2009), here an indicator for monsoon rainfall intensity. C: Mean annual air temperature (MAAT; in °C) based on the MBT/CBT index using the Tierney et al. (2010a) calibration (Sinninghe Damsté et al., 2012). D: TEX_{86}-based reconstructed lake surface temperature (LST in °C; Tierney et al., 2010a calibration; Sinninghe Damsté et al., 2012). E: the proportion of C_4 plants, based on the $\delta^{13}C$ composition of the C_{31} *n*-alkane (Sinninghe Damsté et al., 2011b). F: the seismic-reflection record of lake level high- and lowstands (Moernaut et al., 2010). The three-point moving average (thick colored lines) in A-E are superimposed on the high-resolution proxy records (thin black lines). Shaded areas represent the Last Glacial Maximum (LGM; 26.5-19 kyr BP), Heinrich event H1 (16.8-15.4 kyr BP) and the Younger Dryas period (YD: 13-11.5 kyr BP).

or less strongly stratified with anoxic conditions extending high up into the water column, while during the cool and windy principal dry season between June and September, the water column is mixed down to 40-60 m (Wolff et al., 2011). The varved sediments of Lake Chala consist of alternating light and dark layers, with diatom-rich light varves deposited during the dry and windy southern-hemisphere winter months, and diatom-poor dark varves during the southern-hemisphere summer season when the water column is more strongly stratified (Wolff et al., 2014).

Previous studies of Lake Chala's sediment record were coordinated by the CHALLACEA project, and focused on the climate history of the last 25 kyr, covering the end of the Last Glacial Maximum (LGM), the deglaciation and the Holocene (Fig. 1.3). These studies included the analysis of plant wax (C_{28} fatty acids) δD, which showed that the Congo Air Boundary blocked the Atlantic Ocean influence on precipitation over Lake Chala (Fig. 1.3A; Tierney et al., 2011). A study on GDGTs and the BIT index indicated that the moisture-balance of Lake Chala predominantly reflected longer-term variation in low-latitude insolation, with wet and dry episodes at Lake Chala alternating at half-precessional intervals (Fig. 1.3B; Verschuren et al., 2009). The record of surface-water $\delta^{18}O$ as captured in diatom silica indicated that the duration of seasonal drought was decoupled from annual rainfall (Barker et al., 2011). Subsequently, charcoal records showed that these seasonal droughts controlled the long-term variations in the savannah fires in the Lake Chala region (Nelson et al., 2012). Furthermore, the $\delta^{13}C$ of *n*-alkanes revealed that vegetation shifted from predominantly C_4 plants (grasses) during the LGM, to a mix of C_4 and C_3 plants during the Holocene (Sinninghe Damsté et al., 2011b), indicating that next to variation in water availability, low CO_2 pressure during the LGM played a key role in the development of C_4 savannah vegetation during that time. Paleotemperature reconstructions based on brGDGTs (Fig. 1.3C) indicated a post-glacial rise in MAAT from 15 kyr BP onwards, while TEX_{86} reconstructions indicated that LST started increasing from shortly after the LGM (Fig. 1.3D; Sinninghe Damsté et al., 2009, 2012). Not only were the sediments of Lake Chala studied, but the occurrences and trends of selected biomarkers were also studied in the modern-day lake and it catchment, in both exploratory but also more detailed studies. For example, GDGTs in up to 3.5 years of settling particles showed a large variability over time, and depth profiles indicated *in situ* production of GDGTs (Sinninghe Damsté et al., 2009; Buckles et al., 2013, 2014). And one year of long-chain diols in settling particles revealed a seasonal variability in their occurrence, while a depth profile of these lipids coupled with 18S rRNA analysis indicated an eustigmatophyte source (Villanueva et al., 2014).

These novel insights and the general success of the CHALLACEA project led to a request to the ICDP (International Continental Scientific Drilling Program) to drill Lake Chala and enable the reconstruction of climate change and environmental history in tropical East Africa over the past 250 kyr. The DeepCHALLA expedition in November 2016 resulted in the recovery of almost 215 m of lake sediments that are finely laminated throughout most of the recovered sequence. Analyzing this new sediment record promises to enhance our understanding of tropical climate and ecosystem dynamics. The high-resolution multi-proxy record that will be generated may become the long-awaited equatorial counterpart to the high-latitude ice-core climate records. However, to ensure the reliability of the climate records based on lipid biomarker proxies, we need a more thorough understanding of the occurrence and production of these lipid biomarkers in the modern system, following the previous exploratory and detailed studies of biomarkers in modern-day lake Chala. Specifically, can we relate the occurrence of biomarkers in the modern system to certain environmental conditions? Can we reveal the mechanism(s) driving biomarker proxies? And can we identify more specific sources for general (e.g., *n*-alkenes, fatty acids) and orphan (e.g., brGDGTs and isoGDGTs) biomarkers?

1.4 Scope and framework

The main objective of this thesis is to identify organic compounds in modern-day Lake Chala that have biomarker potential, i.e. that characterize conditions and (climate-driven) processes in the water column of the lake, and to assess how the abundance, distribution and drivers of these biomarkers over short (seasonal to inter-annual) time-scales can be extrapolated to understand long (25 kyr) time-scales. To this end, a large variety of biomarkers was analyzed in water depth profiles of suspended particulate matter (SPM) collected monthly over a 17-month period; in settling particles collected monthly in a sediment trap over a period of 53 months; in the 25-kyr sediment record; and further in vegetation, litter and soils from within the catchment area of Lake Chala. **Chapter 2** of this thesis describes the occurrence and distribution of long-chain *n*-alk-1-enes of phytoplanktonic origin in the modern water column and the 25 kyr sediment record of Lake Chala, and shows that these microbial lipids become more prevalent during and after the glacial-to-Holocene transition. A newly defined index of the $C_{25:1}$ and $C_{27:1}$ *n*-alk-1-enes (Alkene Index) reveals that the relative abundance of $C_{27:1}$ *n*-alk-1-enes varies with a periodicity of ~2.3 kyr. This suggests that the production of *n*-alk-1-enes might be linked to variations in monsoon intensity, which in turn might be (in)directly forced by solar radiation. **Chapter 3** describes the occurrence and $\delta^{13}C$ signature of *des*-A-lupane in the 25 kyr sedimentary record of Lake Chala. *Des*-A-triterpenoids are degradation products of non-hopanoid pentacyclic triterpenoids that are generally regarded as terrestrial biomarkers. This chapter describes how *des*-A-lupane in Lake Chala sediments can be used as a novel and independent proxy for the stable carbon isotopic composition of local terrestrial C_3 plants, which is important as the usual assessment of $\delta^{13}C$ signature of plant waxes is influenced by the mixed signal of C_3/C_4 vegetation. **Chapter 4** describes the source and environmental significance of another group of triterpenoids, i.e., *des*-A-arborene isomers. These compounds are degradation products of isoarborinol, which is often regarded as a terrestrial biomarker. However, the occurrence, trends and $\delta^{13}C$ signatures of *des*-A-arborenes in the 25-kyr sediment record indicate that isoarborinol must have had a microbial source in the epilimnion of Lake Chala, and most likely also in other modern and ancient tropical lacustrine settings (typically crater lakes) with permanently anoxic bottom waters and sediments. Molecular mechanics calculations indicate that the transformations of *des*-A-arborene isomers are microbially mediated. In **Chapter 5**, both the seasonal variability in the occurrence and the $\delta^{13}C$ composition of various biomarkers in depth profiles of SPM collected over a 17-month period are studied to evaluate their capacity to trace seasonal microbial occurrences. Indeed, most of the studied biomarkers show a seasonal trend that can be linked to phytoplankton succession. Interestingly, the seasonal trend and $\delta^{13}C$ values of the C_{28} fatty acid, a compound that is often used as plant-wax biomarker in paleoenvironmental reconstructions, indicates that it has an aquatic origin in the water column of Lake Chala. The long-chain *n*-alk-1-enes and the C_{28} fatty acid most likely have an chlorophyte source, while the $C_{19:1}$ *n*-alkene probably is cyanobacterial. Furthermore, all targeted aquatic biomarkers become ^{13}C depleted at times of high primary productivity, indicating that processes of chemically-enhanced diffusion and fractionation associated with high lake-water pH occur in Lake Chala, and should be taken in consideration when interpreting aquatic biomarker-$\delta^{13}C$ records for Lake Chala and possibly also other alkaline lakes. **Chapter 6** focusses on the origin of brGDGTs found in 17 months of SPM and 53 months of settling particles in Lake Chala. The concentration and distribution of brGDGTs in the water column greatly varies over time, and reveals that they are primarily produced *in situ*, rather than washed into the lake by precipitation-induced erosion. Linked 16S rRNA gene-abundance data indicate that Acidobacteria are not the

main producers of brGDGTs in the water column of Lake Chala. Although modern-day brGDGT fluxes and distributions in Lake Chala cannot directly be linked to water column conditions, the overall brGDGT signature in settling particles does correspond to MAAT, suggesting that they can most likely still be used as paleothermometer in the time-integrated archive of lake sediments. In **Chapter 7**, the archaeal isoGDGTs in SPM and 98 months of settling particles are discussed. Overall, conditions of strong water-column stratification with a very shallow oxycline play a key role in isoGDGT production in Lake Chala. Strong stratification leads to i) a suppressed Thaumarchaeotal bloom, with low crenarchaeol production resulting in high BIT values; ii) high GDGT-0 production, resulting in high isoGDGT-0/crenarchaeol ratios; and iii) increased crenarchaeol isomer production. These findings indicate that the 25 kyr BIT record should be interpreted as indicating how strong stratification of the upper water column, itself associated with wetter and less windy climate conditions, restricted thaumarchaeotal blooms and thus indirectly reflecting past variation in hydroclimate conditions. Finally, **Chapter 8** provides an overview of seasonal and multi-annual variability in all aquatic biomarkers discussed in the previous chapters, in the settling-particle record over a 53-month period. All biomarkers show a large range of variation without systematic annual recurrence in their temporal pattern, although the mixing and stratification regime seems an important driver for biomarker variability over time. The irregularity in the presence of biomarkers in settling particles indicates that modest but unique changes in water-column conditions are required to initiate the large inter-annual variations in the aquatic productivity (including phytoplankton, bacteria and archaea) observed in Lake Chala, and shows that even 4.5 years of monitoring is not long enough to exactly pin-point the drivers of biomarker occurrence.

In summary, this thesis emphasizes the importance of extensive studies of the modern-day lake system prior to interpretation of climate-proxy records based on the occurrence and distribution of lipid biomarkers in its sediments. Firstly, certain biomarkers are shown to have a different origin than generally presumed (such as the C_{28} fatty acid, and *des*-A-arborenes). Secondly, this thesis describes significant steps in tying established and new biomarkers (such as the $C_{19:1}$ *n*-alkene, and long chain *n*-alk-1-enes) to their possible microbial sources. Thirdly, the ^{13}C-depleted aquatic biomarkers found in Lake Chala and its sediments can be explained by physical fractionation processes associated with high pH, a common condition in East African lakes. These findings are not only important for the quality and impact of paleoenvironmental reconstructions based on biomarker $\delta^{13}C$ values in the sediment record of Lake Chala, but for all (East African) lakes. Finally, this thesis highlights that monitoring programs need to run for many more years (>5) to fully characterize the relation between environmental conditions and the temporal patterns of the studied biomarkers, as well as to reveal the drivers and underlying patterns forcing the lake's microbial community. Although this is practically challenging and costly to implement, it is crucial in order to improve our understanding of paleoenvironmental reconstructions based on lake sediments.

Five baby cheetahs waiting for their mothers' signal before rushing to devour a fresh wildebeast in Masai Mara National Reserve.

2 Origin and paleoenvironmental significance of C_{25} and C_{27} *n*-alk-1-enes in a 25,000-year lake-sedimentary record from equatorial East Africa

L.G.J. van Bree, W.I.C. Rijpstra, C. Cocquyt, N.A. Al-Dhabi, D. Verschuren, J.S. Sinninghe Damsté and J.W. de Leeuw

adapted from: *Geochimica et Cosmochimica Acta* 145, 89-102 (2014)

Abstract

We studied the distribution of long-chain *n*-alkenes ($C_{23:1}$ to $C_{31:1}$) in well-dated sediments from Lake Chala, a deep crater lake near Mt. Kilimanjaro in equatorial East Africa, to reveal signatures of paleoenvironmental and paleoclimatic changes affecting the production of these compounds during the last 25 kyr. The apolar fractions of organic sediment extracts dated to the last 16 kyr showed an unusual dominance of $\delta^{13}C$-depleted $C_{25:1}$ and $C_{27:1}$ *n*-alk-1-enes. These *n*-alkenes were not detected in soil and litter from near the shoreline and from the inner rim of the crater, pointing to an autochthonous, aquatic source. Analysis of suspended particulate matter indicated that the *n*-alk-1-enes are produced in the well-oxygenated upper 30 m of the water column, indicating a phytoplanktonic origin. Sedimenting particles collected monthly from December 2006 to November 2007 showed increased fluxes of *n*-alk-1-enes following the locally prominent short rain season in November-December. Green algae and/or cyanobacteria were identified as candidate sources of these alkenes. Production of the $C_{25:1}$ and $C_{27:1}$ *n*-alk-1-enes in Lake Chala was much reduced during the Last Glacial Maximum and early late-glacial period, suggesting a temperature or CO_2 effect on habitat suitability. We explored the potential of *n*-alk-1-ene accumulation rates, and of a derived Alkene Index $[C_{27:1}]/([C_{25:1}]+[C_{27:1}])$, to record longer-term climatic changes. The Alkene Index record of Lake Chala over the past 25 kyr shows clear periodicity with a dominant frequency of ~2.3 kyr, potentially indicative of monsoon variability directly or indirectly forced by variation in solar radiation.

2.1 Introduction

Lake sediments are excellent archives of past environmental and climate changes. Organic biomarkers of lake sediments have contributed substantially to climate history reconstructions of Africa (e.g. Tierney et al., 2008; Verschuren et al., 2009; Sinninghe Damsté et al., 2011b). The occurrence of long-chain *n*-alkenes (C_{23} to C_{31}) in various types of lacustrine sediments has frequently been reported (e.g. Jaffé et al., 1996; Zhang et al., 2004, 2011; Theissen et al., 2005; de Mesmay et al., 2007), but even though these potential biomarkers sometimes dominate the apolar fraction of organic sediment extracts, their origin and fate remains ambiguous and are sometimes not even addressed. One major reason for this apparently modest interest is that sedimentary *n*-alkenes can have multiple natural sources. Short-chain *n*-alkenes ($<C_{22}$) can derive from cyanobacteria, microalgae, macroalgae and zooplankton, while long-chain *n*-alkenes ($>C_{22}$) are traditionally thought to be derived from either higher plant waxes (Eglinton and Hamilton, 1967) or microalgae (e.g. Gelpi et al., 1968, 1970; Cardoso et al., 1983; Jaffé et al., 1996; Volkman et al., 1998). Because of these different possible origins, the distribution of *n*-alkenes in lacustrine sediment records often leads to disparate interpretations. In some studies they are argued to derive from allochthonous sources such as higher plants, including marginal reeds, ferns and peat (Giger et al., 1980; Cardoso et al., 1983; Cranwell et al., 1987; Duan and Ma, 2001). In other studies the compounds are attributed to an autochthonous (aquatic) source, such as algae in general (Jaffé et al., 1996; Zhang et al., 2004; Xu and Jaffé, 2009), cyanobacteria (Gelpi et al., 1970), or specific algal species such as the green alga *Botryococcus braunii* race A (Theissen et al., 2005). Some studies interpret the *n*-alkenes as resulting from a mixture of both microalgae and higher plant input (e.g. Zhang et al., 2011).

In this paper we describe the stratigraphic distribution of two specific *n*-alkenes in the anoxic bottom sediments of Lake Chala, a permanently stratified crater lake on the border of Tanzania and Kenya. The origin and potential paleoenvironmental significance of these two long-chain *n*-alkenes are discussed based on ecological and sedimentary data.

2.2 Materials and methods

2.2.1 Study area: Lake Chala

Lake Chala (3°19′S, 37°42′E) is a crater lake of approximately 4.5 km² surface area with a maximum depth of 92 m in 2005. This tropical freshwater lake is located ~880 m above sea level, on the lower south-east slope of Mt. Kilimanjaro in equatorial East Africa (Fig. 2.1). Rainfall seasonality is mainly determined by the twice-annual passing of the Inter-Tropical Convergence Zone (ITCZ). This results in relatively moderate "long rains" from March to May, and heavy "short rains" from October to December. The local precipitation/evaporation balance is negative, and balanced by subsurface inflow of groundwater derived from rain falling higher up on Mt. Kilimanjaro. Temporary discharge from a creek breaching the northwestern crater rim can occur during heavy rains. Allochthonous organic matter in Lake Chala sediments consists of wind-blown particles from the surrounding savanna landscape, supplemented by soil erosion and litter input from the inner crater rim. Seasonal deep mixing of the water column extends down to 40-60 m between June and September, when air and surface water temperature are lowest, while daily wind-driven mixing is limited to 15-20 m year-round. A constant temperature of 22.2°C and complete anoxia at greater depths indicate

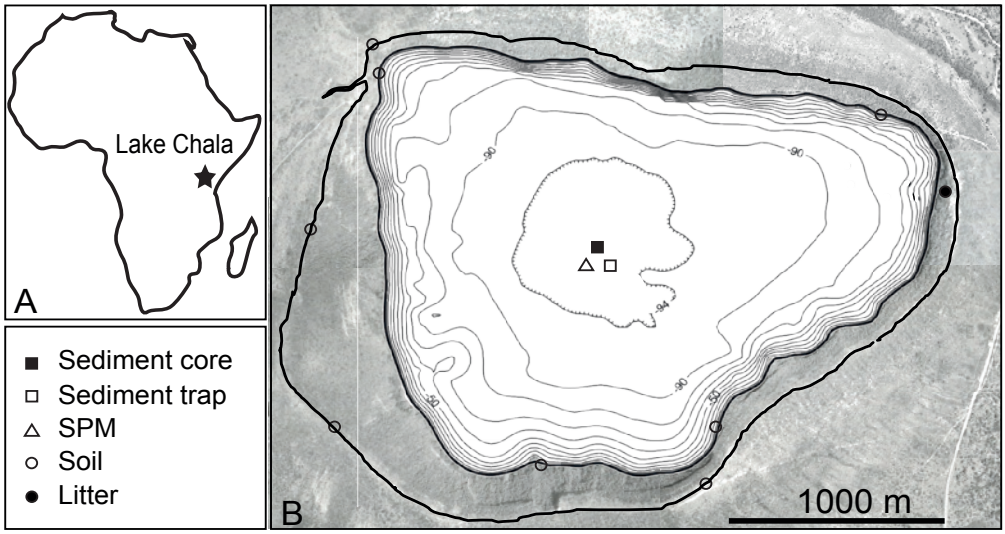

Figure 2.1 The location Lake Chala (3°19′S, 37°42′E) on the border of Kenya/Tanzania in equatorial East Africa (A), with bathymetry at 10 m intervals and sampling locations of the suspended particulate matter (SPM) profile, the sediment-trap and the sediment core, as well as catchment soil and litter samples (B). The inner bold line represents the lake shore at the time of coring in 2005, whereas the outer bold line indicates the crater rim, which forms the edge of the catchment area. Modified after Moernaut et al. (2010).

that the lower water column is permanently stratified, or at most mixes with a decadal or lower frequency (Wolff et al., 2011; Sinninghe Damsté et al., 2012a).

Rainfall in the Lake Chala area is mainly influenced by insolation-driven monsoon intensity. Today, both the El Nino-Southern Oscillation (ENSO) and the Indian Ocean dipole or Zonal Mode (IOZM) can have a strong non-linear impact on rainfall amount and intensity during the "short rains" in October-December (Black et al., 2003; Mölg et al., 2006; Tierney et al., 2011). Lake Chala is located east of the Congo Air Boundary (CAB) throughout the year, which minimizes the influence of northern high-latitude climate signatures propagated to low latitudes by the Atlantic Meridional Overturning Circulation (AMOC; Verschuren et al., 2009). Lake Chala is, therefore, an ideal location to study long-term changes in insolation-driven monsoon intensity and the associated precipitation.

2.2.2 Study material

We studied a 21.65 m long composite sequence of mostly finely laminated organic-rich muds, based on several cores from the center of Lake Chala (Fig. 2.1) obtained in 2003 and 2005 as reported by Verschuren et al. (2009). After excision of five turbidites, it yielded a 20.82 m long sequence of continuous offshore lacustrine sedimentation covering ca. 25,000 years (25 kyr). The age-depth model is based on a smoothed spline through INTCAL04-calibrated AMS ^{14}C ages of 164 bulk organic carbon samples, corrected for a variable old-carbon age offset of between 200 and 450 year (Blaauw et al., 2011). For the present analysis of organic biomarkers, sediment samples with 4-cm thickness, each comprising about 50 years, were extracted at ~200 year intervals throughout the last 25 kyr. In total, 146 sediment samples were analyzed both quantitatively and qualitatively, of

which 105 represent the Holocene (the last 11.7 kyr). The exceptionally precise age model (Blaauw et al., 2011) allowed the calculation of sedimentary biomarker fluxes. An additional 24 samples were analyzed only qualitatively, for determination of the alkene ratio. The stable-carbon isotopic composition of *n*-alkenes was analyzed in 12 samples.

A sediment-trap was installed in November 2006 at 35 m water depth (Fig. 2.1). Samples for biomarker analysis were retrieved at approximately 4-week intervals up to December 2007, as described by Sinninghe Damsté et al. (2009). For the purpose of this study, a preserved subsample of the filtered sediment-trap material was used for phytoplankton analyses. Algal and cyanobacterial remains were brought back in suspension with distilled water, and filters were carefully checked for any remaining material. The algal suspension was then diluted to a known volume and studied following the Uthermöhl (1931) method using sedimentation chambers of 10 ml and an inverted Olympus CX41 microscope.

Suspended particulate matter (SPM) was sampled on 10-11 September 2006 at 13 depth intervals along a vertical profile in the center of the lake (Fig. 2.1). Water volumes of 4 to 9 L were retrieved from every 5 m between 0 and 30 m, and every 10 m between 30 and 90 m depth. The water was filtered through precombusted GF/F filters and stored frozen until processing. As in Sinninghe Damsté et al. (2009), data from the deepest SPM sample (90 m) was excluded since a contribution of resuspended uppermost bottom sediments was evident. As the SPM samples were collected over a 2-day period, these data provide only a snapshot of the expected large changes in primary productivity, linked to the seasonal cycle of Lake Chala.

Eight soil samples were collected in the catchment area of Lake Chala in 2005 (Fig. 2.1) as described by Sinninghe Damsté et al. (2009). Sampling of litter was performed in September 2012 (Fig. 2.1). Three near-shore litter samples represent plant and fruit remains, decomposing flat leaves and leaf stalks of the hydrophilous sedge *Cyperus involucratus*; two litter samples from about halfway up the crater rim consist of leaf and twig remains and small non-determinable particles.

2.2.3 Lipid analysis

The freeze-dried and powdered sediments were extracted with a Dionex™ Accelerated Solvent Extractor (ASE) using a dichloromethane (DCM)/methanol (9:1, v/v) mixture at high temperature (100°C) and pressure (7.6×10^6 Pa). The total organic extracts were separated over a column with activated Al_2O_3 into an apolar and a polar fraction using hexane/DCM (9:1, v/v) and DCM/MeOH (1:1, v/v) as eluents, respectively. The apolar fraction was analyzed by gas chromatography (GC) and GC-mass spectrometry (MS) after adding a known amount of internal standard (pristane). Quantification of compounds was performed by peak area integration of the chromatograms. The double-bond position of the mono-unsaturated alkenes was determined on the basis of mass spectra of their dimethyl disulfide derivatives as described by Nichols et al. (1986). Fluxes (in mg m^{-2} yr^{-1}) of the quantified apolar compounds were calculated taking into account their concentration, the measured water content and the dry weight of sediment samples.

SPM and sediment-trap samples were extracted as described before (Sinninghe Damsté et al., 2009). The apolar fractions of the sediment extracts were obtained by column chromatography over Al_2O_3 by elution with hexane/DCM (9:1, v/v). Pristane was added as internal standard before analysis by GC and GC/MS. Fluxes of *n*-alkenes (in mg m^{-2} yr^{-1}) were calculated for sediment-trap samples, taking into account the dry sample weight, days of collection and funnel size of the sediment-trap device.

Leaf, stem and fruit remains present in some litter samples were cut into small pieces. All litter and soil samples were ultrasonically extracted with DCM/MeOH (2:1, v/v). The extracts were

evaporated to dryness, methylated with diazomethane in ether and separated over a column filled with activated Al_2O_3 into an apolar and polar fraction, as described above. The apolar fractions were analyzed by GC and GC-MS.

GC was performed using a Hewlett-Packard (HP6890) instrument equipped with an on-column injector and a flame ionization detector. A fused silica capillary column (25 m x 0.32 mm) coated with CP Sil-5 CB (film thickness 0.12 µm) was used with helium as carrier gas. The samples were injected at 70°C and the oven temperature was programmed to 130°C at 20°C min^{-1} and then at 4 °C min^{-1} to 320°C, at which it was held for 20 min. GC-MS was performed on a Finnigan Trace DSQ mass spectrometer operated at 70 eV with a mass range of *m/z* 40 to 800 and a cycle time of 1.7 s. The gas chromatograph was equipped with a fused silica capillary column as described above for GC. The carrier gas was helium, and the same oven temperature program as for GC was used. For the SPM samples, single ion monitoring (SIM) was conducted on the $M^{+\cdot}$ ions (*m/z* 350.0-351.0 and 378.0-379.0) of the C_{25} and C_{27} *n*-alk-1-enes to further support their identification, as their concentrations were low.

The apolar fractions of 12 selected sediments younger than 17 kyr BP and one sediment-trap sample were separated into a saturated and an unsaturated hydrocarbon fraction using a small column with Ag^+-impregnated silica and hexane and ethyl acetate as eluents, respectively. Both saturated and unsaturated hydrocarbon fractions were subjected to compound-specific $\delta^{13}C$ analysis using an Agilent 6800 GC coupled to a ThermoFisher Delta V isotope-ratio monitoring mass spectrometer. Carbon isotope values were measured against calibrated external reference gas and performance of the instrument was monitored by daily injections of a mixture of a C_{20} and a C_{24} perdeuterated *n*-alkane with known isotopic compositions. The $\delta^{13}C$ values are reported in the standard delta notation against the Vienna Pee Dee Belemnite (VPDB) standard. All samples were run at least in duplicate, with an average standard deviation of 0.5‰ for the C_{25} *n*-alkene and 0.4‰ for the C_{27} *n*-alkene.

Spectral analysis of the proxy data set was undertaken using AnalySeries software (Paillard et al., 1996). The Alkene Index record was detrended using a polynomial function, interpolated to a constant ~200 year interval and analyzed with the Blackman-Tukey method. Frequencies around ~2.3 kyr were filtered from the record (Gaussian filter centered at 0.00044, bandwidth 0.0001) excluding superimposed low and high frequencies. REDFIT analysis was conducted with PAST software (Hammer et al., 2001) for significance estimation.

2.3 Results

2.3.1 Sediments

Fig. 2.2 shows typical distribution patterns of apolar lipids in Lake Chala sediments. Most sediments contain *n*-alkanes, *n*-alkenes, phytadienes, hopenes and *des*-A-triterpenoids (with lupane, oleanane, ursane and arborane skeletons). In sediments younger than 16 kyr BP, two unusually dominant components are the $C_{25:1}$ and $C_{27:1}$ *n*-alkenes. DMDS adduction indicated a terminal position of the double bond in these alkenes. The $C_{23:1}$ *n*-alkene was found only at some depth intervals and in low concentrations, and low or trace amounts of $C_{26:1}$ and $C_{29:1}$ *n*-alkenes were encountered occasionally in the younger sediments. A few sediment intervals also contained traces of an C_{27} *n*-alkadiene.

The accumulation rate of *n*-alk-1-enes is highest in the younger, uppermost sediments (Fig. 2.3). The accumulation rate of the $C_{25:1}$ *n*-alk-1-ene mostly exceeds 1 mg m^{-2} yr^{-1} in sediments younger

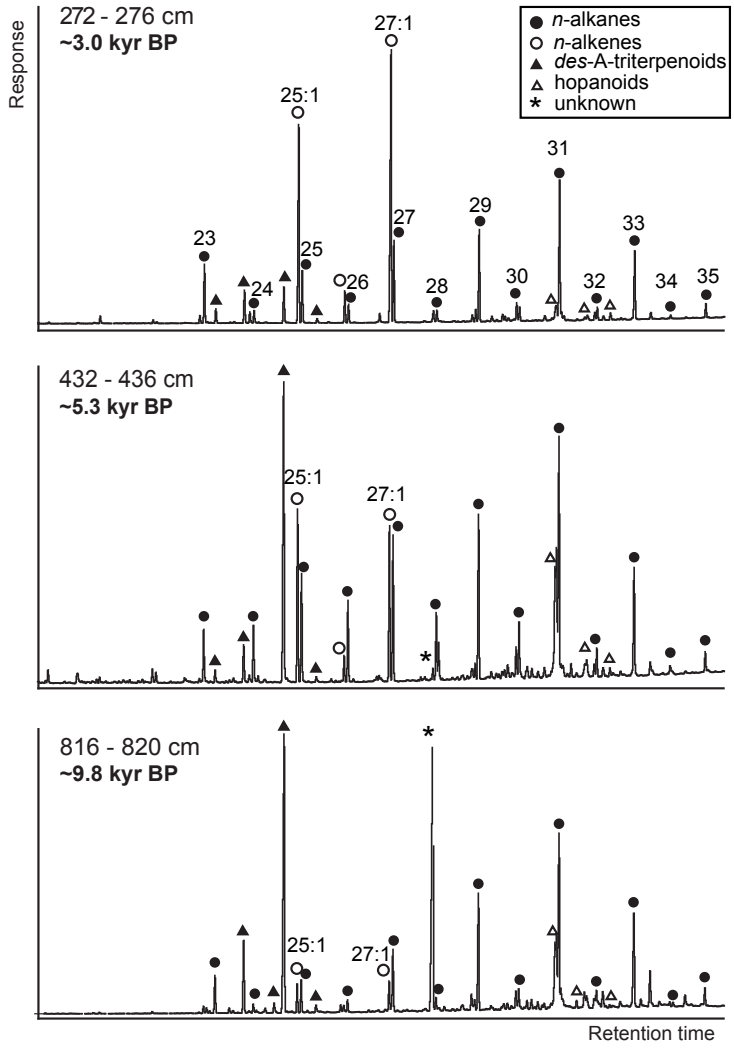

Figure 2.2 GC-FID traces of the apolar fractions of organic extracts from three sediment samples dated to the Holocene (age and composite profile depth indicated) attributable to *n*-alkanes, *n*-alk-1-enes, *des*-A-triterpenoid hydrocarbons, hopanoids and an unknown compound (*).

than 3.9 kyr BP, with a pronounced maximum (5 mg m^{-2} yr^{-1}) in sediments dated to ~600 year BP. The accumulation of the $C_{27:1}$ *n*-alk-1-ene is high between 8.8 and 7.2 kyr BP and after 3.5 kyr BP, with a pronounced peak of 4.5 mg m^{-2} yr^{-1} at 3.5-3.2 kyr BP. Accumulation rates of both the $C_{25:1}$ and $C_{27:1}$ *n*-alk-1-enes are low (<0.14 mg m^{-2} yr^{-1}) before 16 kyr BP, with slightly higher values at 23.1-22.5 and 19.3 kyr BP. The mean long-term trend in both *n*-alkenes is similar, with average accumulation rates of 0.1 mg m^{-2} yr^{-1} in the Last Glacial Maximum (LGM) and early late glacial periods (25 to ~16 kyr BP), and 1.8 mg m^{-2} yr^{-1} during the Holocene. The here defined Alkene Index, defined as $[C_{27:1}]/([C_{25:1}]+[C_{27:1}])$, varies from 0.36 to 0.92 over the past 25 kyr (Fig. 2.3D), with higher (>0.75) values mostly restricted to sediments older than 6 kyr BP.

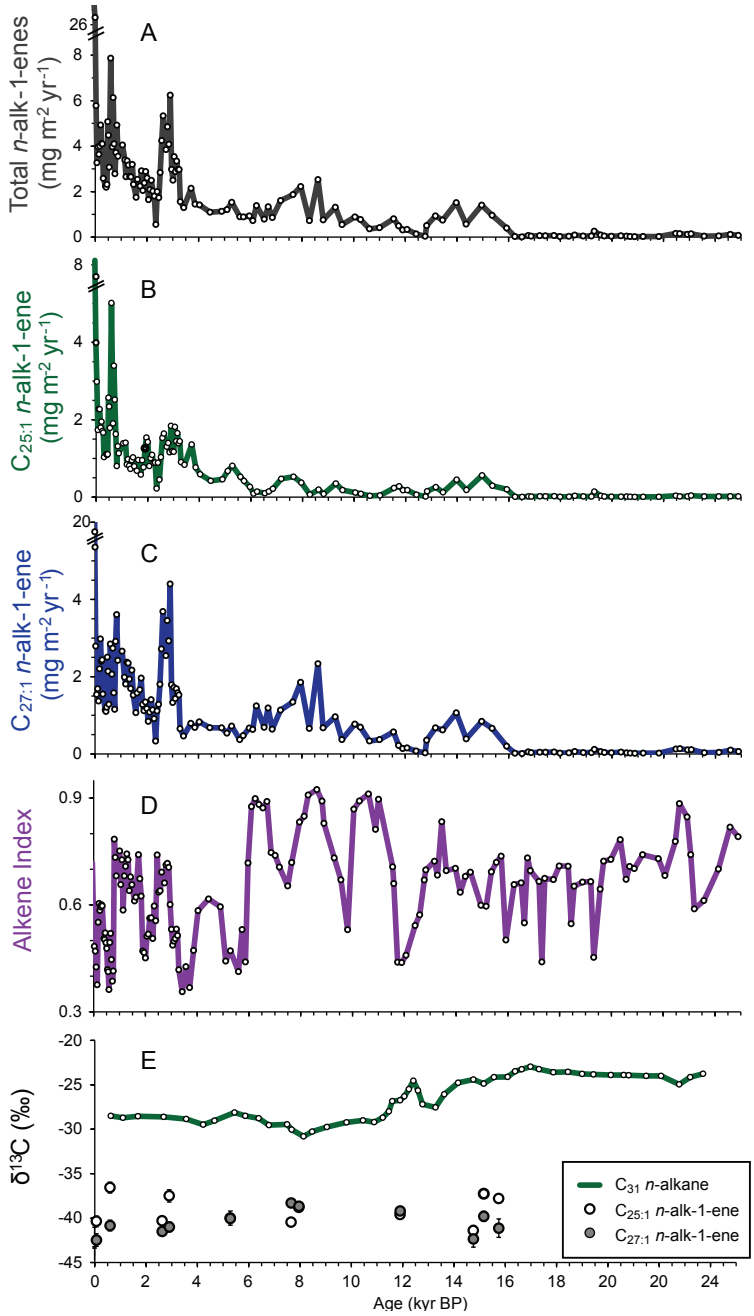

Figure 2.3 Accumulation of $C_{25:1}$ and $C_{27:1}$ *n*-alk-1-enes (in mg m^{-2} yr^{-1}), with summed (A), $C_{25:1}$ (B) and $C_{27:1}$ (C) *n*-alk-1-enes, compared to the Alkene Index (D), calculated as $C_{27:1}/(C_{25:1}+C_{27:1})$. Stable carbon-isotopic ($\delta^{13}C$) values of $C_{25:1}$ and $C_{27:1}$ *n*-alk-1-enes (E) compared with the $\delta^{13}C$ record of C_{31} *n*-alkanes (Sinninghe Damsté et al., 2011b), where error bars show ± 1 standard deviation based on at least duplicate measurements, and in many cases the error interval is smaller than the size of the symbol.

2.3.2 Settling particles

The apolar lipid fractions of the extracts of settling particles contain mainly *n*-alkanes (C_{23} to C_{35}), *n*-alkenes (C_{23} to C_{31}), hopenes and some *des*-A-triterpenoids (with ursane and lupane skeletons). The fluxes and distribution patterns of the $C_{25:1}$ and $C_{27:1}$ *n*-alk-1-enes varied through the year (Fig. 2.4). Fluxes of these alkenes (Fig. 2.4A-B) were both highest during the first month of deployment (December 2006) and lower thereafter, resembling the total mass flux of depositing material and organic carbon (Sinninghe Damsté et al., 2009). The annual flux of *n*-alk-1-enes into the sediment-trap is comparable but slightly lower (with $C_{25:1}$ and $C_{27:1}$ *n*-alk-1-ene accumulations of 1.1 and 1.3 mg m^{-2} yr^{-1}, respectively) than the average Holocene *n*-alk-1-ene accumulation rate in the sediment (1.2 and 1.8 mg m^{-2} yr^{-1}, respectively). The Alkene Index varied between 0.5 and 0.9 with highest values in January and August-November 2007 (Fig. 2.4D), i.e. generally coinciding with the dry seasons. The annual pattern in the flux of *n*-alk-1-enes is roughly similar to the combined monthly flux of small *Cosmarium* spp. (green algae) in the same sediment-trap samples (Fig. 2.4E).

2.3.3 Suspended particulate matter

The $C_{25:1}$ and $C_{27:1}$ *n*-alk-1-enes were detected in SPM from the upper water column down to 40 m depth, i.e., within the oxic part of the water column, in concentrations of up to 8.1 and 21 ng L^{-1},

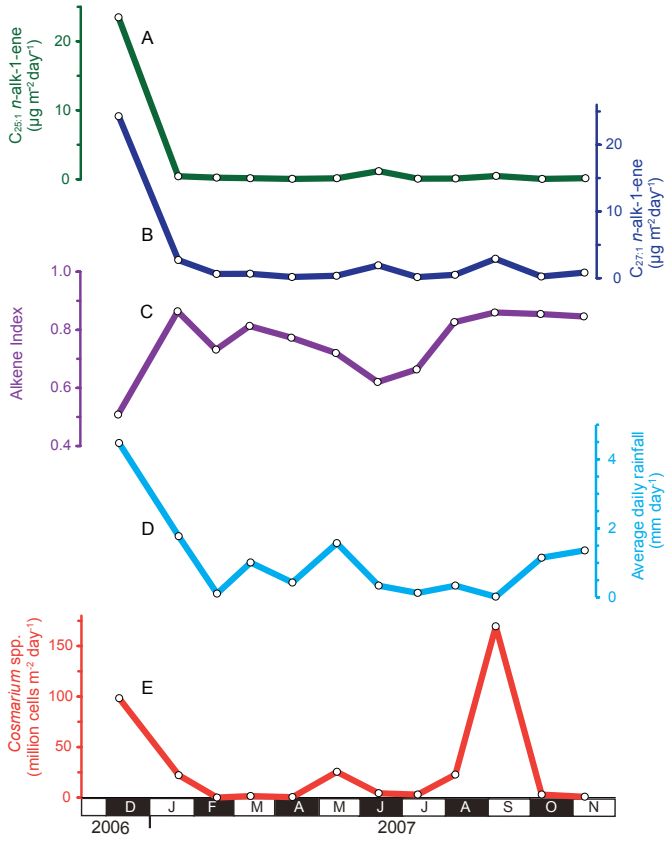

Figure 2.4 Monthly fluxes of *n*-alkenes and selected microalga in Lake Chala collected in a sediment trap from November 2006 to December 2007, with the flux (in µg m^{-2} day^{-1}) of $C_{25:1}$ (A) and $C_{27:1}$ *n*-alk-1-ene (B), compared to the Alkene Index. (C), average rainfall (mm day^{-1}) during monthly periods of sediment-trap deployment in 2006/2007 (D) from the Voi weather station 80 km to the east of Lake Chala (adapted from Sinninghe Damsté et al., 2009), and the monthly flux (in million cells m^{-2} day^{-1}) of the green alga *Cosmarium* spp (E).

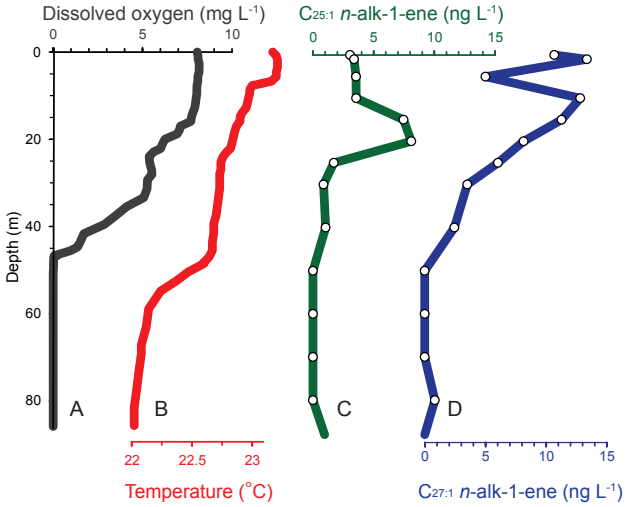

Figure 2.5 Vertical distribution of (A) dissolved oxygen (mg L^{-1}) and (B) temperature (°C) in the water column of Lake Chala, measured on 11-12 September 2006 (modified after Sinninghe Damsté et al., 2009), compared to the *in-situ* concentration of $C_{25:1}$ (C) and $C_{27:1}$ (D) *n*-alk-1-enes (ng L^{-1}) from SPM samples.

respectively (Fig. 2.5). In SPM from the lower water column these alkenes were not detected, or present in much lower concentrations only.

2.3.4 Soils and litter

The apolar lipid fractions of soil and litter from the Chala crater catchment contained mainly *n*-alkanes (C_{25} to C_{33}), squalene and plant-derived triterpenoids. Long-chain $C_{25:1}$ and $C_{27:1}$ *n*-alk-1-enes were not detected. In one litter sample containing plant fruit remains, *n*-alkenes (C_{23} to C_{35}) were present, but these compounds did not contain a terminal double bond.

2.3.5 Stable carbon isotopic composition

The stable carbon isotopic composition of the *n*-alk-1-enes from Lake Chala sediments varied substantially, from -44‰ to -37‰ within the last 17 kyr (Fig. 2.3E; Table 2.1). Typically, the $C_{25:1}$ *n*-alk-1-ene is slightly less depleted than the $C_{27:1}$ *n*-alk-1-ene, with average values of 39.4±0.5‰ and 40.8±0.5‰, respectively. The *n*-alk-1-enes are also isotopically depleted compared to the corresponding *n*-alkanes, the latter ranging from -40 to -25‰ (Table 2.1). The higher *n*-alkanes are less depleted and show an increasingly less negative average value than the average isotopic signatures of C_{25} (36‰), C_{27} (-35‰) and C_{29} (31‰) *n*-alkanes. The $\delta^{13}C$ values of $C_{25:1}$ and $C_{27:1}$ *n*-alk-1-enes in the sediment-trap sample of December 2006 are 34‰ and 39‰, respectively, which is in the range of measurements of the corresponding sedimentary *n*-alk-1-enes but notably somewhat more positive, especially in the case of the $C_{25:1}$ *n*-alk-1-ene.

2.4 Discussion

2.4.1 Origin of the $C_{25:1}$ and $C_{27:1}$ *n*-alk-1-enes

The origin of $C_{25:1}$ and $C_{27:1}$ *n*-alkenes in lacustrine sediments is not self-evident, as *n*-alkenes are biosynthesized by widely different (groups of) organisms. Diagenetic transformations of functionalized compounds such as alcohols are a possible source of *n*-alkenes in sediments. However, dehydration of the dominant even-carbon numbered alcohols found in Lake Chala

Table 2.1 Stable carbon isotopic composition ($\delta^{13}C$, in ‰ vs. VPDB) of *n*-alk-1-enes and *n*-alkanes in Lake Chala sediments and sediment-trap.

Sediment depth (cm)	Age (kyr BP)	$C_{25:1}$ *n*-alkene $\delta^{13}C$ in ‰	C_{25} *n*-alkane $\delta^{13}C$ in ‰	$C_{27:1}$ *n*-alkene $\delta^{13}C$ in ‰	C_{27} *n*-alkane $\delta^{13}C$ in ‰	C_{31} *n*-alkane $\delta^{13}C$ in ‰
4-8	-0.001	-42.2 ±1.2	-35.4±0.1	-44.0 ±0.8	-35.4±0.2	-32.2±0.2
12.2-16	0.07	-40.4 ±0.6	NA	-42.5 ±0.7	NA	NA
80-84	0.6	-36.6 ±0.6	-33.6±0.4	-40.8 ±0.6	-31.9±0.2	-27.5±0.1
248-252	2.6	-40.3 ±0.1	-39.4±1.0	-41.5 ±0.1	-38.1±0.3	-31.0±1.3
268-272	2.9	-37.5 ±0.7	-33.5±0.1	-41.0 ±0.6	-33.7±0.2	-31.5±0.4
432-436	5.3	-40.0 ±0.8	-33.1±0.6	-40.0 ±0.2	-32.5±1.4	-30.5±0.6
648-652	7.7	-40.5 ±0.5	-38.4±a	-38.3 ±0.4	-34.8±0.3	-30.8±0.5
672-676	7.9	-38.8 ±0.3	NA	-38.7 ±0.2	-35.2±1.1	-31.2±0.3
984-988	11.9	-39.6 ±0.1	-37.2±0.7	-39.2 ±0.1	-33.5±0.2	-27.7±0.1
1140-1144	14.8	-41.4 ±0.6	-40.0±0.1	-42.4 ±0.9	-38.8±0.6	-29.7±0.3
1200-1204	15.2	-37.3 ±0.2	-35.7±a	-39.8 ±0.6	NA	-27.2±a
1236-1240	15.7	-37.8 ±0.4	-33.8±0.0	-41.1 ±1.0	-33.4±0.0	-24.2±0.1
Sediment trap	Dec. 2006	-33.7 ±0.4	NA	-38.7 ±0.1	NA	NA

NA: Not available
a: No standard deviation: value based on one measurement

sediments would generate even-carbon numbered *n*-alkenes instead of the dominant $C_{25:1}$ and $C_{27:1}$ *n*-alk-1-enes. Decarboxylation of even-chain fatty acids could yield odd-chain hydrocarbons, but in Lake Chala this diagenetic origin is unlikely, since only two odd-chain *n*-alk-1-enes are encountered in high relative abundances in the study material.

A variety of higher plants are known to produce *n*-alkenes. Cardoso et al. (1983) identified the fern *Dryopteris dilatata* and erosion from peat deposits as most likely sources of sedimentary *n*-alkenes in Rostherne Lake (England). In that study, the fern and peat contained homologous series of *n*-alkenes (C_{18} to C_{32}) with a dominance of $C_{29:1}$ and $C_{31:1}$. This typical higher-plant distribution is not seen in the sediments of Lake Chala. The complete absence of *n*-alk-1-enes in all soil and litter samples from Chala crater further suggests an origin different than land plants. Aeolian input with $C_{25:1}$ and $C_{27:1}$ *n*-alkenes derived from regional terrestrial vegetation is not likely either. To the best of our knowledge, *n*-alkenes have not been reported as constituents of aeolian transported spores, pollen or wax components. Aquatic macrophytes can also be excluded as a source due to their absence along the very steep-sloping and rocky shoreline of Lake Chala (Fig. 2.1). Even the substantial lake-level lowering which occurred during the early late-glacial period (Moernaut et al., 2010) is not likely to have created more favorable conditions for development of aquatic macrophytes (Sinninghe Damsté et al., 2011b).

Insects are known to produce *n*-alkenes, and although Lake Chala sediments contain microfossil remains of chironomid larvae (Eggermont and Verschuren, 2004) an insect origin of *n*-alkenes in Lake Chala is unlikely. Insects show a characteristically broad range of (branched) *n*-alkenes with high carbon numbers (C_{24} to C_{45}; Blomquist and Jackson, 1979), including some $C_{25:1}$ and $C_{27:1}$ *n*-alkenes (Oudejans and Zandee, 1973; Chikaraishi et al., 2012), but also many others. In microbial mats (Boudou et al., 1986a, 1986b) predominantly C_{29} and C_{31} *n*-alkenes of insect origin were present. Furthermore, to the best of our knowledge, Eubacteria do not produce $C_{25:1}$ and $C_{27:1}$ *n*-alkenes. The *n*-alkenes produced by insects and in microbial mats do not match with the specific *n*-alkene distribution encountered in Lake Chala sediments.

Significant concentrations of the *n*-alk-1-enes were detected in SPM of the upper water column and in the sediment trap, indicating autochthonous biogenic production of the $C_{25:1}$ and $C_{27:1}$ alkenes by organisms living in the (most often) well-oxygenated upper 40 m of the water column. This origin is supported by the significant $\delta^{13}C$ offset between the *n*-alkenes and corresponding *n*-alkanes derived from terrestrial vegetation. The $\delta^{13}C$ values of the *n*-alkenes are up to 7‰ ($C_{25:1}$) and 9‰ ($C_{27:1}$) more negative than their corresponding *n*-alkanes (Table 2.1). The more negative $\delta^{13}C$ values of the *n*-alkenes compared to those derived from land plants (higher *n*-alkanes and also land-derived triterpenes, latter data discussed in Chapter 3) are consistent with the expected carbon-isotopic depletion of algal sources in Lake Chala.

Some freshwater species of both cyanobacteria and microalgae are known to synthesize *n*-alkenes. Cyanobacteria can contain a wide range of *n*-alkenes (e.g. Gelpi et al., 1968, 1970; Cardoso et al., 1983). Species include *Oscillatoria* sp., which contains $C_{21:1}$ to $C_{23:1}$ *n*-alkenes (Matsumoto et al., 1990) and *Anacystis montana,* common in eutrophic lakes, is reported as a source of C_{19} to C_{29} *n*-alkenes (Gelpi et al., 1968). Gelpi et al. (1968, 1970) detected predominantly $C_{25:1}$ and $C_{27:1}$ *n*-alkenes in *A. montana*, but this finding is disputed by Murray and Thomson (1977) since their axenic *A. montana* cultures contained no long-chain *n*-alkenes at all. Similarly, non-axenic cultures of *Microcystis aeruginosa* contained *n*-alk-1-enes, while they were not detected in axenic cultures (Cardoso et al., 1983). Paoletti et al. (1976) found only small or trace amounts of $C_{20:1}$, $C_{23:1}$ and $C_{27:1}$ *n*-alkenes in four nonaxenic cultures (*Spirulina platensis*, *Spirulina* sp., *Calothrix* sp. and *Nostoc commune*). It is questionable whether cyanobacteria produce *n*-alkenes. The *n*-alkene distribution so far observed in single cyanobacterial species does not fit the *n*-alkene distribution found in Lake Chala, and the often trace amounts of *n*-alkenes cannot explain the dominance of *n*-alkenes in the apolar lipid fractions of Lake Chala sediments.

Some microalgae produce *n*-alk-1-enes. The green alga *B. braunii* race A contains C_{23} to C_{33} *n*-alkenes (Gelpi et al., 1970) and the eustigmatophyte *Nannochloropsis* spp. contains C_{15} to C_{31} *n*-alkenes (Gelin et al., 1997). In both *Nannochloropsis* spp. and *B. braunii* race A, the *n*-alk-1-enes are accompanied by significant amounts of alkadienes, trienes or $C_{23:1}$ and $C_{29:1}$ *n*-alkenes. In the sediments of Lake Chala, only minor amounts of $C_{23:1}$ and traces of $C_{29:1}$ *n*-alkenes and one $C_{27:2}$ *n*-alkadiene were detected, but no other alkadienes or trienes. Traces of the $C_{23:1}$ *n*-alkene are present in the SPM from surface waters, and a larger range of *n*-alk-1-enes from C_{21} up to C_{31}, albeit in small quantities, are present in settling particles. Since no significant amounts of alkadienes or alkatrienes are encountered either in the water column or sediments of Lake Chala, it is unlikely that species like *Nannochloropsis* spp. and *B. braunii* contribute substantially to the *n*-alk-1-enes in Lake Chala. Nonaxenic cultures of the green algae *Ulothrix gigas, Uronema terrestre* and *Selenastrum gracile* contained small or trace amounts of C_{20}, C_{23} and C_{27} *n*-alkenes (Paoletti et al., 1976). The green alga *Scenedesmus quadricauda* is reported to contain a variable *n*-alkene mixture, with predominantly $C_{27:1}$ *n*-alkene (Gelpi et al., 1970), $C_{21:1}$, $C_{23:1}$ and $C_{25:1}$ *n*-alkenes (Cranwell et al., 1990) or with minor amounts of $C_{20:1}$, $C_{23:1}$ and $C_{27:1}$ *n*-alkenes (Paoletti et al., 1976). This latter study identified minor amounts of $C_{23:1}$ and $C_{27:1}$ *n*-alkenes in *Chlorella* sp., while *Chlorella emersonii*, a terrestrial green alga from Europe, is known to contain both $C_{25:1}$ and $C_{27:1}$ *n*-alkenes (Afi et al., 1996). Strikingly, *Chlorella vulgaris* produced predominantly $C_{25:1}$ and $C_{27:1}$ *n*-alkenes when grown under heterotrophic conditions, whereas no *n*-alkenes were detected under phototrophic conditions (Patterson, 1967). In contrast, Afi et al. (1996) reported the absence of $C_{25:1}$ and $C_{27:1}$ *n*-alkenes in axenic phototrophic incubation studies of *C. vulgaris*, and the heterotrophically grown *C. vulgaris* culture of Řezanka et al. (1982) also did not yield the $C_{25:1}$ and $C_{27:1}$ dominated *n*-alkene distribution of Patterson (1967).

Relatively modest correlation between the $\delta^{13}C$ values of $C_{25:1}$ and $C_{27:1}$ *n*-alk-1-enes (Fig. 2.6) suggests that these *n*-alkenes probably originate from two or more source organisms with varying relative abundances through time, since carbon-isotope fractionation during synthesis of the two *n*-alk-1-enes within a single organism should be similar at any one time. The compounds also have a similar trend but distinctively different depth profiles (Fig. 2.3A-B). Although the $C_{25:1}$ and $C_{27:1}$ *n*-alk-1-enes are closely related in structure and hence a single source organism seems likely, the $\delta^{13}C$ values and depth profiles suggest multiple source organisms.

Multiple species of green algae (including *Chlorella* sp. and *Cosmarium* spp.) were recovered by us in monthly sediment-trap samples from Lake Chala. The *n*-alkene distributions in Lake Chala sediments seem to be consistent with those reported in the literature for the green algae *Chlorella emersonii*, *C. vulgaris* and *Scenedesmus quadricauda*. Of all organisms that were microscopically identified, the pattern of *Cosmarium* spp. cells settling in the sediment-trap (Fig. 2.4E) is most similar to that of the *n*-alkenes extracted from the bulk sediment-trap samples. The accumulation rates of *Cosmarium* spp. and *n*-alkenes are by no means identical, but show the most similar distribution of all phytoplankton. On the basis of this data, and supported by the literature, we surmise that this group of green algae potentially synthesizes the $C_{25:1}$ and $C_{27:1}$ *n*-alkenes. Although our current hypothesis is that green algae are responsible for the synthesis of *n*-alk-1-enes in Lake Chala, more (culturing) research is needed to test this. Variation in the Alkene Index through time (Fig. 2.3D) could then possibly be explained by different (groups of) green algae – and possibly other algae – producing the bulk of the $C_{25:1}$ and $C_{27:1}$ *n*-alk-1-enes at different times in the past, and /or indicate periodic adaptation of one producer group to changes in their abiotic environment. Selective degradation of individual *n*-alk-1-enes is a hypothetical possibility but chemically unlikely and not supported by the sedimentary record, since the Alkene Index does not show a single sustained trend with time.

The distribution of *n*-alk-1-enes in SPM from the water column in Lake Chala is comparable to the *n*-alkene distribution in SPM of Lake Valencia in Venezuela, a larger (~350 km²), hypereutrophic tropical lake situated at 400 m above sea level, but like Lake Chala with anoxic bottom waters during (most of) the year (Jaffé and Hausmann, 1995; Jaffé et al., 1996). The

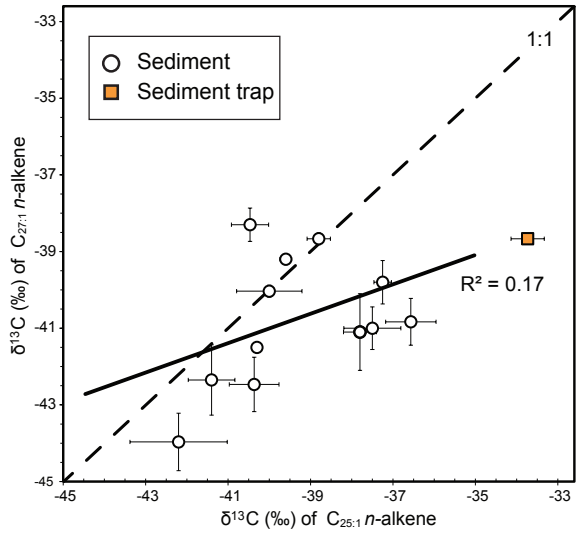

Figure 2.6 The stable carbon-isotopic composition ($\delta^{13}C$ in ‰ vs. VPDB) of $C_{25:1}$ versus $C_{27:1}$ *n*-alk-1-enes of 12 sediment samples spanning the last 16 kyr and one modern-day sediment-trap sample. Error bars indicate ±1 standard deviation based on duplicate or triplicate measurements. In some cases the error intervals are smaller than the size of the symbol. The reported R^2 value of the trend line excludes the sediment-trap sample.

concentrations of $C_{25:1}$ and $C_{27:1}$ *n*-alkenes in Lake Valencia were highest within the oxygenated part of the water column (Jaffé et al., 1996). Also the sedimentary record of Lake Valencia similarly includes relatively high concentrations of $C_{25:1}$ and $C_{27:1}$ *n*-alkenes. The origin of the *n*-alk-1-enes in Lake Valencia has not been discussed in previous studies, but Lake Chala SPM and sediment do display a comparable distribution including an origin in the oxygenated water column. The $C_{25:1}$ and $C_{27:1}$ *n*-alkenes could, therefore, possibly be used more generally as a biomarker for the unknown source microalgae.

2.4.2 *n*-alk-1-enes and hydrology

The highly variable accumulation rate of $C_{25:1}$ and $C_{27:1}$ *n*-alk-1-enes in Lake Chala over the past 25 kyr must reflect changes in the abundance of the organism(s) producing them, and / or changes in the amount of *n*-alk-1-enes they biosynthesize depending on ambient environmental conditions. The most prominent feature of the Chala *n*-alk-1-ene record is their near-absence prior to 16 kyr BP (Fig. 2.3A, C). Their fairly abrupt appearance at that time corresponds with the post-glacial onset of a strengthened southeasterly monsoon across equatorial East Africa (Gasse et al., 2008), and thus a longer or more intense principal rain season (Verschuren et al., 2009). However, since both the periods before and after 16 kyr BP include episodes of high rainfall and episodes of drought (Fig. 2.7), climate-driven changes in the hydrological balance of Lake Chala are unlikely the primary cause of the long-term trend in *n*-alk-1-ene production. The principal change in environmental conditions which occurred around that time is the postglacial transition from a slightly cooler (3-4°C) glacial climate under reduced atmospheric CO_2 concentrations to the interglacial (and present-day) warm tropical climate of this equatorial region. The TEX_{86}-inferred record of temperature change from Lake Chala (Sinninghe Damsté et al., 2012a) indicates that regional warming was gradual and occurred mostly between 19 and 14 kyr BP, consistent with the timing reported elsewhere in East Africa (Powers et al., 2005; Tierney et al., 2008). The low glacial atmospheric CO_2 concentration (and thus possibly higher surface-water pH) may also have influenced the composition of the phytoplankton community at Lake Chala. We surmise that either directly or indirectly, by 16 kyr BP the increased temperature and CO_2 must have created a more optimal habitat for the local *n*-alk-1-ene producing organisms. During the Holocene period (the last 11.7 kyr), temperature variation in the tropics is generally considered to have been limited to 1-2°C (at least at low or modest surface elevations), although actual data for intertropical Africa remain notably scarce (e.g., Nicholson et al., 2013) and evidence for more significant Holocene temperature anomalies have occasionally been reported (Rietti-Shati et al., 1998; Berke et al., 2012b). In any case, it seems unlikely that temperature change has been the main driver of the highly variable rates of *n*-alk-1-ene accumulation in Lake Chala since 16 kyr BP. In contrast, as indicated by both the seismic-reflection stratigraphy of past lake-level changes and the BIT-index of rainfall intensity (Fig. 2.7D-E), the hydrological balance of Lake Chala has varied strongly during this period. However, notwithstanding their sizable implied magnitude, these lake-level changes do not appear to have fundamentally altered the lake's mixing regime and internal nutrient cycling. This conclusion was inferred earlier from the uninterrupted deposition of finely laminated sediments (Wolff et al., 2011), implying the persistence of deep water anoxic conditions; in this study it is suggested by the relative constancy of *n*-alk-1-ene $\delta^{13}C$ depletion during the Holocene (Fig. 2.3E).

As indicated by the year-long sediment-trap record (Fig. 2.4) the settling flux of *n*-alk-1-enes in Lake Chala is positively correlated with the amount of monthly rainfall during 2006-2007. Some caution is advised about the significance of this correlation, given that seasonal rainfall patterns in the Lake Chala area can be quite variable from year to year. The catchment area of Lake Chala

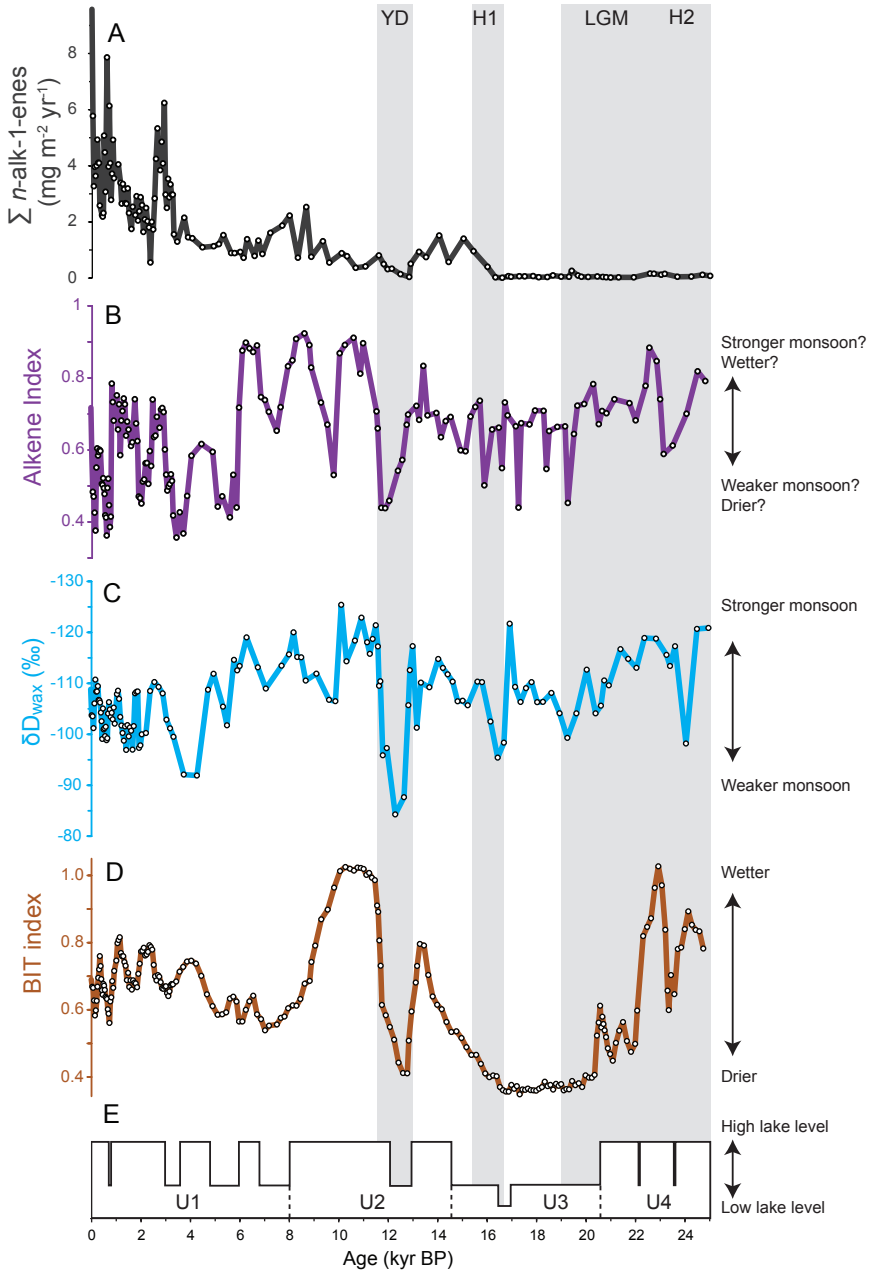

Figure 2.7 Summed accumulation of $C_{25:1}$ and $C_{27:1}$ *n*-alk-1-enes (A), in mg m^{-2} yr^{-1}, compared to the Alkene Index (B). The δD_{wax} record (‰ vs. VSMOW) is shown on a reversed axis (C) to highlight negative anomalies as episodes of inferred drought; adapted from Tierney et al. (2011). The BIT-index (D), three-point moving average (Verschuren et al., 2009). Lake Chala lake-level record (E) derived from seismic-reflection data (Moernaut et al., 2010). Shaded areas represent Heinrich events H1 (16.8-15.4 kyr BP) and H2 (around 24 kyr BP), LGM (26.5-19 kyr BP) and YD (13-11.5 kyr BP).

is small and there is limited surface inflow by direct runoff due to the steep crater wall. Nutrients in the surface waters are mainly replenished by deep water-column mixing in the dry southern hemisphere winter months of June to August, and known to stimulate diatom blooms in Lake Chala (Barker et al., 2011; Wolff et al., 2011). Selective growth of the alkene-producing algae during the ensuing "short" rain season may occur because most diatoms are disadvantaged by the developing water-column stratification. The alkene-producing algae may also benefit from a temporarily increased influx of land-derived debris during heavy rainfall. Incidental episodes of murky waters have been reported, turning Lake Chala brown. In extreme cases one might even consider heterotrophic growth of some algae during such episodes. As indicated above, certain *Chlorella* species can produce high amounts of the $C_{25:1}$ and $C_{27:1}$ *n*-alkenes during heterotrophic growth (Patterson, 1967).

Based on currently available data we conclude that accumulation of $C_{25:1}$ and $C_{27:1}$ *n*-alk-1-enes in Lake Chala sediments reflects autochthonous production by non-diatom microalgae, and mainly during the short period of heavy rains in November-December. This connection with the seasonal pattern of precipitation may be employed as a tentative key to interpret the longer-term variation in $C_{25:1}$ and $C_{27:1}$ *n*-alk-1-ene production observed in the sedimentary record.

Variations in *n*-alk-1-ene accumulation through time (Fig. 2.7A) do not show a clear, unambiguous correspondence with any of the existing paleohydrological proxy records for Lake Chala (Fig. 2.7C-E). At some times low *n*-alkene accumulation corresponds with episodes of relative drought as inferred from the BIT index and seismic record, e.g. during the Younger Dryas (YD), and high accumulation with inferred wet periods such as the wet late-Holocene conditions. At other times the high *n*-alk-1-ene accumulation corresponds with episodes of inferred drought (e.g., mid- and late-Holocene). The alkene accumulation rate thus cannot be used directly as a precipitation proxy.

The Alkene Index, on the other hand, displays broad visual correspondence with the long-term hydrogen-isotope record of leaf wax (δD_{wax}; Tierney et al., 2011) and has some features in common with the BIT index and seismic records (Fig. 2.7B, E). Tierney et al. (2011) suggested that the δD_{wax} records a mixture of δD in local precipitation during the two rain seasons, and thus sedimentary δD_{wax} is firstly influenced by the intensity of East African monsoon circulation, and secondly by the seasonal distribution of annual rainfall. Most lake lowstands recorded in the seismic reflection data of the past ca. 13 kyr (Verschuren et al., 2009; Moernaut et al., 2010) are accompanied by a decrease in the Alkene Index (Fig. 2.7E). The long lowstand U3 dated to between 20.5 and 14.5 kyr BP is a notable exception, possibly due to very low accumulation of *n*-alk-1-enes during that period. Features shared by the *n*-alkene and BIT index records (Figs. 2.7B and 2.7D) occur in the periods 25 to 22 kyr BP, around the YD and in the last 5.5 kyr. The BIT index is used as a proxy for monsoon rainfall intensity (Verschuren et al., 2009; Barker et al., 2011), although the direct mechanistic link remains partly unresolved (Sinninghe Damsté et al., 2009, 2012a). In conclusion, the relation between the Alkene Index and other hydrological proxies is not unambiguous, but shows interesting features nonetheless.

2.4.3 Cyclicity in the Alkene Index

The 25-kyr Alkene Index record from Lake Chala (Fig. 2.7B) displays a well-developed cyclic pattern. Since the Lake Chala sediment sequence is well-dated, sampled at high resolution and deposited through time in a stable and year-round anoxic bottom-water environment, it has the appropriate integrity to discern cyclicity in climate proxies on sub-Milankovitch time-scales. Spectral analysis (Fig. 2.8A) reveals a main frequency of ~2.3 kyr (p = 0.0062). Frequencies around

~2.3 kyr were filtered from the record (Gaussian filter centered at 0.00044, bandwidth 0.0001) excluding low and high frequencies superimposed on the ~2.3 kyr cycle (Fig. 2.8B). The filtered cyclicity pattern (Fig. 2.8B) describes the predominant variability of the Alkene Index, with high amplitude between 14 and 4 kyr BP and considerably lower amplitude between 20-15 kyr BP and during the last 3 kyr.

Similar periodicities are found in hydrological proxy records within the broader East African region. For example in the diatom-based $\delta^{18}O$ record from Lake Malawi (Barker et al., 2007), the foraminiferal record of upwelling in the Arabian Sea (Gupta et al., 2003) and the Qunf cave (Oman) speleothem $\delta^{18}O$ record (Fleitmann et al., 2007). The latter is interpreted to reflect the amount of Indian summer monsoon precipitation. The long-term variability in the Alkene Index may indeed reflect some aspect of Lake Chala paleohydrology.

Frequencies of ~2.1 to ~2.4 kyr have been reported previously in diverse climate proxy records with a worldwide distribution. They are for example identified in $\delta^{18}O$ of Greenland ice cores and Asian speleothems (~2.0-3.0 kyr; Wang et al., 2008), in dust records in peat deposits (~2.2 kyr; McGowan et al., 2010), in sediment texture in marine settings (~2.8 kyr, attributed to a 2.2 kyr cycle; Nederbragt and Thurow, 2005), in tropical sea surface temperature variability based on alkenones (~2.3 kyr; Rimbu et al., 2004) and in primary productivity of foraminifera (~2.2 kyr; Naidu and Malmgren, 1995), coccolithophores (~2.4 kyr; de Garidel-Thoron et al., 2001) and diatoms (~2.1 kyr; Hausmann et al., 2006). In these studies, the ~2.3 kyr cyclicity has been attributed either to changes in oceanic circulation and upwelling as primary drivers (e.g., Naidu and Malmgren, 1995), influenced in turn by solar activity variation such as the Hallstattzeit solar cycle (~2.1 to ~2.4 kyr; e.g., Damon and Jirikowic, 1992), or the coupling between solar irradiation and oceanic processes (e.g., de Garidel-Thoron et al., 2001). Recently it was proposed that the Hallstattzeit solar

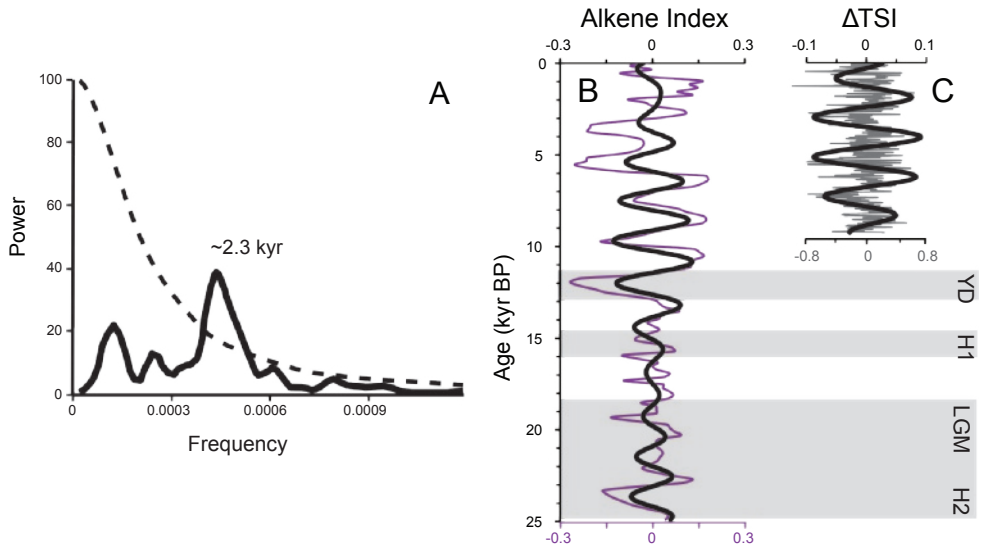

Figure 2.8 The REDFIT power spectrum estimation of the 25 kyr Alkene Index record (A), revealing a main frequency of 2.3 kyr (p = 0.0062). The dashed line represents the 99% significance level. Spectral analysis of resampled, detrended (thin lines) and filtered records (thick lines) of the Chala Alkene Index (B), and ΔTSI (C) the difference of total solar irradiance (in W m^{-2}; modified from Steinhilber et al., 2009).

cycle may have directly influenced Holocene monsoon variability (southeast Australia: McGowan et al., 2010; Holocene East Asian monsoon: Liu et al., 2012). A dominant periodicity similar to that of the Lake Chala Alkene Index record also occurs in ^{14}C and ^{10}Be records from tree rings (~2.4 kyr: Vasiliev and Dergachev, 2002; ~2.3 kyr: Mordvinov and Kramynin, 2010). Reconstructed changes in total solar irradiance (ΔTSI) based on ^{10}Be in polar ice cores (Steinhilber et al., 2009) displays clear periodicities of ~2.3 and ~1.0 kyr. The filtered Alkene Index record is mostly in phase with the filtered ΔTSI record. Generally speaking, in periods of higher total solar irradiance relatively more $C_{27:1}$ *n*-alk-1-ene was produced in the Lake Chala water column. Considering the marked cyclicity in the Lake Chala Alkene Index record, we suggest that the population of microalgae involved in *n*-alk-1-ene production in Lake Chala have been influenced by solar irradiation variability, which in turn can be mediated by the (sun-driven) variation in Indian Ocean monsoon strength and wind patterns.

2.5 Conclusion

Long-chain *n*-alkenes preserved in the Lake Chala sediment record are dominated by $C_{25:1}$ and $C_{27:1}$ *n*-alk-1-enes. These compounds are predominantly produced in the oxic upper water column, probably by (mixotrophic) green algae, following the heavy "short rains" in November to December. Production of $C_{25:1}$ and $C_{27:1}$ *n*-alk-1-enes in Lake Chala was much reduced during the LGM and early late-glacial period, suggesting a temperature or CO_2 effect on habitat suitability. Given the positive correlation with precipitation over the annual cycle, we explored the potential of individual *n*-alk-1-ene accumulation rates, and of a derived Alkene Index, to record longer-term hydrological changes in Lake Chala. The Alkene Index record of the past 25 kyr shows clear periodicity with a dominant frequency of ~2.3 kyr, indicative of monsoon variability directly or indirectly forced by solar radiation.

Acknowledgements
We like to thank the editor and one anonymous reviewer for valuable comments that have improved the manuscript. The fieldwork for this study was carried out with permission of the Permanent Secretary of the Ministry of Education, Science and Technology of Kenya under research permit 13/001/11C to D.V. We thank C.M. Oluseno for the sediment-trap sampling, C. Wolff for TOC measurements on settling particles, J. Moernaut for the bathymetric map, A. Mets, M. Verweij and J. Ossebaar for technical assistance, and M.L. Goudeau and especially L. Lourens for helpful discussions on spectral analysis. This work was performed in preparation of the International Continental Scientific Drilling Programme (ICDP) DeepCHALLA project, on research materials made available through the ESF Euroclimate project CHALLACEA which is financially supported by Grants from the Dutch Organization for Scientific Research (NWO) and FWO Vlaanderen (Belgium) to J.S.S.D. and D.V., respectively.

A clear view of the lush near-shore vegetation of Lake Chala during a water-column sampling trip near the Tanzanian shoreline during the rainy season in November 2016.

3 *Des*-A-lupane in an East African lake sedimentary record as a new proxy for C_3-plant stable carbon isotopic composition

L.G.J. van Bree, W.I.C. Rijpstra, N.A. Al-Dhabi, D. Verschuren, J.S. Sinninghe Damsté and J.W. de Leeuw

adapted from: *Organic Geochemistry* 101, 132-139 (2016)

Abstract

We studied the high-resolution and well-dated 25,000 year sedimentary record of Lake Chala, a deep tropical crater lake in equatorial East Africa, to explore new proxies for paleoenvironmental and paleohydrological change. Sedimentary biomarker analysis revealed the presence of *des*-A-triterpenoids with oleanane, ursane and lupane carbon skeletons, microbial degradation products of angiosperm plant triterpenoids. Their increased influx from 16,000 years ago corresponds with previously documented changes in the terrestrial vegetation of the Lake Chala basin during postglacial warming, in particular the relative increase in C_3/C_4 plant ratio inferred from the stable carbon isotopic signature ($\delta^{13}C$) of sedimentary *n*-alkanes derived from plant leaf waxes. In contrast to this *n*-alkane $\delta^{13}C$, the $\delta^{13}C$ of *des*-A-lupane maintains a constant value of -27.4±1.1‰ across the glacial – interglacial transition. Since *des*-A-lupane is derived from C_3 plants, its $\delta^{13}C$ signature is here proposed to represent a novel and independent proxy for the time-variable carbon isotopic composition of local terrestrial C_3 plants, which can improve estimates of the C_3/C_4 plant ratio based on two-end member mixing models of *n*-alkane $\delta^{13}C$ values.

3.1 Introduction

Non-hopanoid pentacyclic triterpenoids preserved in lake and marine sediments are relatively well studied biomarkers, and used in organic geochemistry as a proxy for the input of terrestrial angiosperm plants (e.g. Rullkötter et al., 1982; Freeman et al., 1994; Sabel et al., 2005). These wax components are synthesized almost exclusively by higher plants as a defense mechanism against insects, pathogens and herbivores (Langenheim, 1994). Pentacylic triterpenoids with, for example, lupane, oleanane and ursane skeletons, are widely accepted as general biomarkers for angiosperms, yet most of these triterpenoids are not species-specific (e.g. Ohmoto et al., 1970; ten Haven and Rullkötter, 1988; Regnery et al., 2013). *Des*-A-triterpenoids, in turn, are diagenetic products of triterpenoid A-ring degradation (Trendel et al., 1989), a process probably mediated by microorganisms under anoxic conditions (Lohmann et al., 1990).

Plant wax lipids, such as *n*-alkanes, can be used as indicators of the composition of local vegetation, as their compound-specific stable carbon isotopic value ($\delta^{13}C$) depends on the dominant biochemical pathway used by plants for photosynthesis. Higher plants usually fix CO_2 by either the C_3 (Calvin-Benson) or C_4 (Hatch-Slack) cycle. In C_4 photosynthesis, atmospheric CO_2 entering the plant stomata is pre-concentrated, resulting in less carbon isotopic depletion. In tropical Africa, lowland vegetation consists mostly of C_4 grasses and C_3 trees and shrubs, and (seasonal) moisture availability is the dominant control on the distribution and abundance of these C_4 grasses across the modern-day landscape. On glacial-interglacial time scales, variation in atmospheric pCO_2 exerted important control on the composition of savanna vegetation of East Africa (Sinninghe Damsté et al., 2011b). When pCO_2 varies little, as within the Holocene, the distribution of C_3 and C_4 vegetation can be used as a measure of past water availability (Castañeda et al., 2007).

During an earlier high-resolution stratigraphic study of *n*-alk-1-enes in the continuous and well-dated 25,000-year (25 kyr) sedimentary record of Lake Chala, a deep crater lake in equatorial East Africa (van Bree et al., 2014), we also encountered a wide range of *des*-A-triterpenoids. In this paper, we report our findings regarding the origin and potential paleoenvironmental application of the pentacyclic triterpenoid degradation products derived from higher plants. A study of *des*-A-arborenes/fernenes also present in Lake Chala sediments, but of microbial origin, is reported separately in Chapter 4.

3.2 Material and Methods

3.2.1 Study area

Lake Chala (3°19′S, 37°42′E) is a relatively unproductive, tropical freshwater lake, situated ~880 m above sea level on the lower south-eastern slope of Mt. Kilimanjaro (Fig. 3.1). Shared by Kenya and Tanzania, it has a surface area of 4.5 km², a steep-sided crater catchment of ~3.4 km² and a maximum depth of ~90 m. Rainfall seasonality is mainly determined by the semi-annual passing of the Inter-Tropical Convergence Zone (ITCZ), resulting in moderate 'long rains' (March-May) and more intense 'short rains' (October-December) separated by a long dry season during Southern Hemisphere winter (June-September). Since the local balance between precipitation and evaporation is negative by three to one, the lake's water budget must be maintained by substantial groundwater inflow, derived from rainfall on the forested mid-elevation slopes of Mt. Kilimanjaro. Also temporary creek discharge breaching the crater's northwestern rim can occur during very heavy rains (Buckles et al., 2014). Daily wind-driven mixing of the water column is limited to the

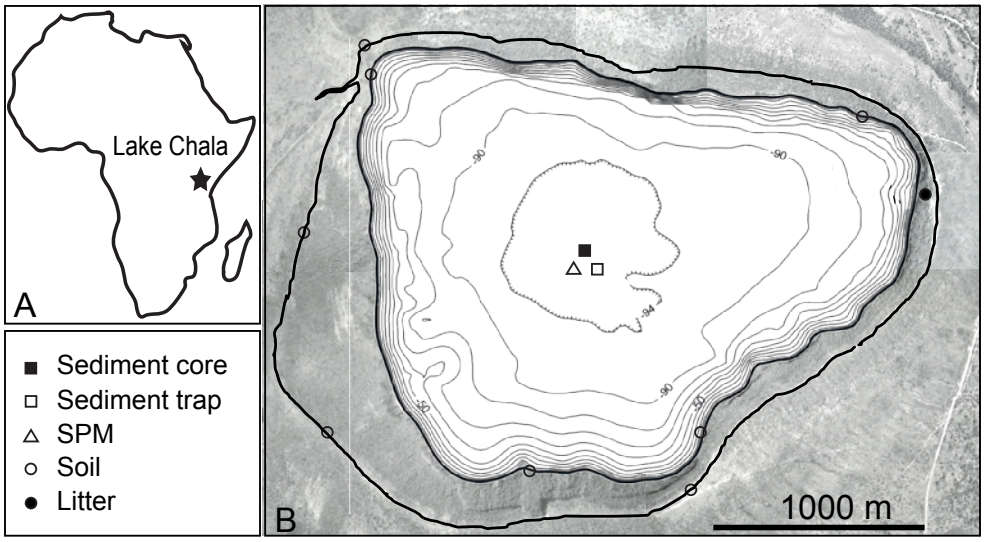

Figure 3.1 The location of Lake Chala (3°19′S, 37°42′E) in equatorial East Africa (A), and the sampling locations of the suspended particulate matter (SPM), the sediment trap and the 25,000-year sediment record, as well as catchment soils and litter. The outer bold line indicates the crater rim, which defines the lake's catchment area, and the crater basin with bathymetry at 10-m intervals. Modified after Moernaut et al. (2010) and van Bree et al. (2014).

uppermost 15-20 m year-round. Seasonal deeper mixing (June-September) extends to 40-60 m, implying a permanently stratified lower water column. Given limited density stratification, the possibility of complete mixing cannot be excluded but its recurrence frequency is likely decadal or longer, rather than inter-annual (Wolff et al., 2011, 2014). Wind-blown (aeolian) particles, supplemented by soil and litter input from the steep-sided inner slopes of the crater, contribute allochthonous organic matter to Lake Chala sediments. The vegetation outside the crater and on top of the rim is a woodland-savannah with shrubs, trees and C_4 grasses, while inside the crater rim a more varied vegetation occurs, including CAM plants in a dry succulent forest occupying the middle slopes, and a fringe of evergreen forest around the lake shore (Hemp, 2006; Sinninghe Damsté et al., 2011b).

3.2.2 Study material

A 21.65 m composite core of mostly finely-laminated organic muds was retrieved from the center of Lake Chala (Fig. 3.1) during coring activities in 2003 and 2005 (Verschuren et al.,2009). This yielded, after excision of five turbidites, a 20.82 m long master sequence covering the last 25 kyr of continuous offshore lacustrine sedimentation. The age-depth model is based on a smoothed spline through INTCAL04-calibrated AMS ^{14}C ages of 164 bulk organic carbon samples (Blaauw et al., 2011). For this study, a total of 148 sediment samples with 4-cm thickness were extracted and processed for biomarker analysis, generally at ~200-year intervals, with a higher resolution of ~50 year intervals in the youngest 3.2 kyr. In addition, we analyzed the compound-specific $\delta^{13}C$ of selected biomarkers in 52 sediment samples distributed throughout the sequence.

In order to trace the origin of the biomarkers found in Lake Chala sediments, we further analyzed soil and litter samples from around the lake, suspended particulate matter (SPM) and settling particles collected by a sediment trap (Sinninghe Damsté et al., 2009; Buckles et al., 2014). This sediment trap was deployed at 35 m water depth in a most often suboxic part of the water column, and samples were retrieved at ca. 4-week intervals between November 2006 and December 2007 (Sinninghe Damsté et al., 2009). The SPM sampling was conducted on 10-11 September 2006 along a vertical profile in the center of the lake, every 5 m between 0 and 30 m, and every 10 m between 30 and 90 m water depth. The water samples (4 to 9 L) were filtered through precombusted GF/F filters and stored frozen until processing. Eight soil samples were collected from within the catchment area of Lake Chala in 2005 (Sinninghe Damsté et al., 2009; Fig. 3.1). Sampling of litter in September 2012 included three near-shore samples representing leaf and fruit remains from forest trees and shrubs, and two samples from just below the crater rim consisting of leaf and twig remains and small non-diagnostic organic debris. These samples were also stored frozen until analysis.

3.2.3 Lipid extraction

The freeze-dried and powdered sediment samples were extracted with a Dionex™ Accelerated Solvent Extractor (ASE), using a dichloromethane (DCM)/methanol (9:1, v/v) mixture at high temperature (100°C) and pressure (7.6×10^6 Pa) (Sinninghe Damsté et al., 2011b). The total extracts were separated over an activated Al_2O_3 column into an apolar and a polar fraction with hexane/DCM (9:1, v/v) and DCM/MeOH (1:1, v/v), respectively. Accumulation rates of apolar compounds (in mg m^{-2} yr^{-1}) were calculated based on their concentration, the wet weight and water content of the sediment samples, and the sediment's age-depth profile. For analysis of stable carbon isotopic composition, a subset of the apolar fractions were separated into a saturated and an unsaturated hydrocarbon fraction using a small Ag^+-impregnated silica column with hexane and ethyl acetate as eluents, respectively.

SPM and sediment trap samples were extracted previously (Sinninghe Damsté et al., 2009). Fluxes of apolar compounds (in mg m^{-2} yr^{-1}) in the sediment trap samples were calculated using the concentration of each of these components relative to total particle flux.

Litter and soil samples were extracted ultrasonically with DCM/MeOH (2:1, v/v), after cutting the larger leaf, stem or fruit remains into small pieces. The extracts were evaporated to dryness, methylated with diazomethane in diethyl ether and separated over an activated Al_2O_3 column into apolar, ketone and polar fractions, using hexane/DCM (9:1, v/v), hexane/DCM (1:1, v/v) and DCM/MeOH (1:1, v/v) as eluents, respectively.

3.2.4 Lipid identification and quantification

The apolar fractions of sediments, SPM, sediment trap, soil and litter extracts were analyzed by gas chromatography (GC) and GC-mass spectrometry (GC/MS), after addition of a known amount of internal standard. A few polar fractions of sediment and SPM samples were methylated, silylated and screened for functionalized triterpenoids. GC analysis was performed using a Hewlett-Packard (HP6890) instrument equipped with an on-column injector and a flame ionization detector (FID). A fused silica capillary column (25 m x 0.32 mm) coated with CP Sil-5 CB (film thickness 0.12 µm) was used with helium as carrier gas. The samples were injected at 70°C and the oven temperature was programmed to rise at 20°C min^{-1} to 130°C, and then at 4°C min^{-1} to 320°C, at which it was held for 20 min. GC-MS was performed on a Finnigan Trace DSQ mass spectrometer operated at 70 eV with a mass range of *m/z* 40 to 800 and a cycle time of 1.7 s. The gas chromatograph was equipped with a fused silica capillary column as described above. The carrier gas was helium and

the same oven temperature program as for GC was used. Identification of the *des*-A-triterpenoids and other triterpenoid hydrocarbons is based on relative retention times, published mass spectra (including the NIST98 spectral library), and interpretation of observed fragmentation patterns. Quantification of compounds was performed by peak area integration of appropriate peaks (including that of the internal standard) in the FID chromatograms.

3.2.5 Compound-specific carbon isotope analyses

We subjected 52 saturated hydrocarbon fractions to compound-specific $\delta^{13}C$ analysis using an Agilent 6800 GC coupled to a ThermoFisher Delta V isotope-ratio monitoring mass spectrometer. The isotope values were measured with reference to a calibrated external reference gas, and performance of the instrument was monitored daily by injections of a mixture of a C_{20} and a C_{24} perdeuterated *n*-alkane with known isotopic composition. The $\delta^{13}C$ values are reported in standard delta notation against the Vienna Pee Dee Belemnite (VPDB). All samples were run at least in duplicate, allowing estimation of the standard deviation of these measurements. $\delta^{13}C$ values of the *n*-alkanes in these same samples have been published previously (Sinninghe Damsté et al., 2011b).

3.3 Results

3.3.1 The sedimentary record of *des*-A-triterpenoids in Lake Chala

Our analysis of the apolar fractions of 148 biomarker extracts from Lake Chala sediments covering the last 25 kyr showed the presence of *n*-alkanes, *n*-alk-1-enes, phytadienes, aromatic triterpenoids, hopenes, and a suite of *des*-A-triterpenoid hydrocarbons with lupane, oleanane, ursane, and fernane or arborane skeletons. The stratigraphic distribution, origin and paleoenvironmental significance of the *n*-alkanes and *n*-alk-1-enes have been discussed by Sinninghe Damsté et al. (2011b) and van Bree et al. (2014), respectively.

We detected 11 distinct *des*-A-triterpenoid hydrocarbon compounds on the basis of their relative retention times, published mass spectra, and interpretation of mass spectrometric fragmentation patterns. The mass spectra of ten *des*-A-triterpenes and one *des*-A-triterpane exhibit molecular ions at *m/z* 324, 326, 328 or 330. Here we focus on the distribution, origin and potential paleoenvironmental application of the five *des*-A-triterpenoids with lupane, oleanane and ursane skeletons (Fig. 3.2A). The identification and geochemical significance of the other, arborane-derived *des*-A-triterpenoids will be discussed elsewhere (Chapter 4). Next to these *des*-A-triterpenoids with arborane or fernane skeleton, several other, non-identified *des*-A-triterpenoids co-elute, occur infrequently or in low relative abundance and are not further discussed.

Compound **1** ($M^{+\bullet}$ at *m/z* 328; Fig. 3.2B) was identified as *des*-A-olean-13(18)-ene (Corbet, 1980; Logan and Eglinton, 1994; Jacob et al., 2007; Huang et al., 2008), and compound **2** ($M^{+\bullet}$ at *m/z* 328; Fig. 3.2B) was tentatively assigned to *des*-A-olean-12-ene (Corbet, 1980; Logan and Eglinton, 1994; Jacob et al., 2007). *Des*-A-triterpenoid **3** ($M^{+\bullet}$ at *m/z* 328; Fig. 3.2B) was identified as *des*-A-urs-13(18)-ene (Corbet, 1980; Logan and Eglinton, 1994; Jacob et al., 2007). Compound **4** ($M^{+\bullet}$ at *m/z* 328; Fig. 3.2B) represents a mixture of *des*-A-ursenes, which could not be further identified. *Des*-A-triterpenoid **5** exhibiting an $M^{+\bullet}$ at *m/z* 330 (Fig. 3.2B) was identified as *des*-A-lupane (Corbet, 1980; Schmitter et al., 1981; Trendel et al., 1989; Boreham et al., 1994; Jacob et al., 2007; Huang et al., 2008).

The accumulation rates (in mg m^{-2} yr^{-1}) of these *des*-A-triterpenoid hydrocarbons in the sedimentary record vary considerably over time (Fig. 3.3). The stratigraphic distributions of

Table 3.1 List of *des*-A-triterpenoids in the Lake Chala sediment record with retention times, mass spectral data and (tentative) identifications. References: **A**: Corbet (1980); **B**: Logan and Eglinton (1994); **C**: Trendel et al. (1989); **D:** Jacob et al. (2007); **E**: Huang et al. (2008); **F:** Schmitter et al. (1981); **G:** Boreham et al. (1994)

Peak number	Retention time (GCMS)	Most significant ions (in order of decreasing abundance)	M+	Formula	Tentative identification	References
1	18.16	109, 313, 189, 328 [M^+], 205, 204, 218, 161	328	$C_{24}H_{40}$	*des*-A-olean-13(18)ene	**A B C D E**
2	18.30	203, 218, 313, 189, 328 [M^+], 231, 243	328	$C_{24}H_{40}$	*des*-A-olean-12-ene	**A B D**
3	18.52	313, 177, 189, 121, 175, 328 [M^+], 218	328	$C_{24}H_{40}$	*des*-A-urs-13(18)ene	**A B D**
4	19.01	218, 203, 313, 189, 133, 328 [M^+], 231	328	($C_{24}H_{40}$)	Mixture, i.a. *des*-A-ursenes	
5	19.60	123, 149, 163, 191, 287, 206, 330 [M^+], 315	330	$C_{24}H_{42}$	*des*-A-lupane	**A C D E F G**

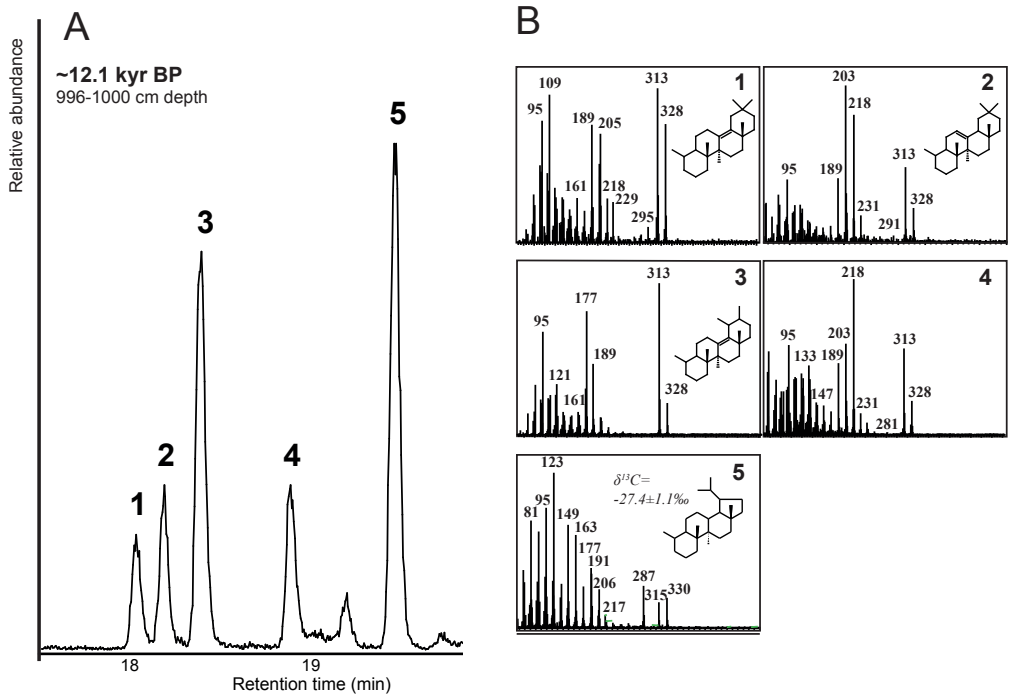

Figure 3.2 Higher plant derived *des*-A-triterpenoids in the Lake Chala sediments. Panel (A) shows a partial summed mass chromatogram (*m/z* 163+177+189+203+218+309) of the distribution of *des*-A-triterpenoids in the apolar fraction of the lipid biomarker extract from 996-1000 cm core depth, deposited ~12.1 kyr BP. Panel (B) shows the electron-impact mass spectra of *des*-A-triterpenoids in the Lake Chala sediment record: *des*-A-olean-13(18)-ene (compound **1**); *des*-A-olean-12-ene (**2**); *des*-A-urs-13(18)-ene (**3**); mixture of *des*-A-ursenes (**4**); *des*-A-lupane (**5**). Additional information on these compounds is presented in Table 3.1.

des-A-triterpenoids with lupane (**5**), ursane (**3**) and oleanane (**1**+**2**) skeletons are all similar and significantly inter-correlated: *des*-A-lupane with *des*-A-oleanenes (R^2 = 0.53), *des*-A-oleanenes with *des*-A-ursene (R^2 = 0.62) and *des*-A-lupane with *des*-A-ursene (R^2 = 0.81). Throughout the record, *des*-A-lupane is more abundant than *des*-A-ursene, whereas *des*-A-oleanenes concentration is lowest (Fig. 3.3). They all exhibit low accumulation rates from 25,000 to 15,000 years ago (the glacial and early post-glacial period) and much higher (on average 5 to 11 times) accumulation rates in last 12,000 years (the Holocene).

The $\delta^{13}C$ values of *des*-A-lupane (Fig. 3.4) vary between -25.1‰ and -29.4‰ (-27.4‰±1.1‰ on average) with no significant trend over time (R^2 = 0.042; n = 38; p = 0.22). Determinations of $\delta^{13}C$ of other *des*-A-triterpenoids of the oleanane and ursane type in the unsaturated hydrocarbon fraction were unsuccessful due to co-elution or low abundances.

3.3.2 Triterpenoids and *des*-A-triterpenoids in soil and litter surrounding the lake

No *des*-A-triterpenoids were identified in the hydrocarbon fraction of extracts from soils and litter. Functionalized triterpenoids in soils along the crater rim were identified as urs-12-en-3β-ol (α-amyrin), olean-12-en-3β-ol (β-amyrin), olean-13(18)-en-3β-ol, ursa-9(11),12-dien-3-one, taraxerone, lup-20(29)-en-3-one, lup-20(29)-en-3-ol acetate and friedelan-3-one and, tentatively, methyl-ursa-2,12-dien-28-oate. Also three pentacyclic triterpene methyl ethers (PTMEs) with oleanane and taraxerane skeletons were detected: 3β-methoxy-olean-12-ene (iso-sawamilletin; β-amyrin ME), 3β-methoxy-olean-18-ene ME (miliacin; germanicol ME) and 3β-methoxy-taraxer-14-ene (sawamilletin, crusgallin or taraxerol ME). Litter samples contained the oleanane-type triterpenoids β-amyrenone, olean-18-en-3β-one (germanicone), olean-18-en-3β-ol (germanicol) and β-amyrin acetate. The functionalized ursane-type triterpenoids present were α-amyrinone and α-amyrin acetate. One litter sample contained a lupeol acetate.

3.3.3 *Des*-A-triterpenoids in settling particles and suspended particulate matter

In the extracts of settling particles, only low concentrations of *des*-A-urs-13(18)-ene and *des*-A-lupane were detected, next to traces of functionalized triterpenoids such as α-amyrin. Hydrocarbon concentrations in the SPM extracts were too low for identification of specific triterpenoid compounds.

3.4 Discussion

The strong correlation between accumulation rates of *des*-A-oleanenes, *des*-A-ursene and *des*-A-lupane (Fig. 3.3) suggest a common origin for these *des*-A-triterpenoids. Higher plant material originates predominantly from washed-in debris of local terrestrial vegetation from within the crater catchment, because of the absence of riverine input, the limited amount of leaf waxes deposited from the air, and the near-absence of submerged or emergent aquatic macrophytes due to the steep crater walls both above and below the lake surface (Sinninghe Damsté et al., 2011b). While various *des*-A-triterpenoids are present both in the sediment record and to some extent in settling particles, these compounds are lacking in the collected litter and soil. *Des*-A-triterpenoids are thought to result from microbial degradation of functionalized triterpenoids, under anoxic or reducing conditions (e.g., Lohmann et al., 1990; Jacob et al., 2007; Huang et al., 2008); but their presence in the sediment trap material indicates that microbial degradation is not restricted to the anoxic lower water column in Lake Chala. One other mechanism for *des*-A-triterpenoids to

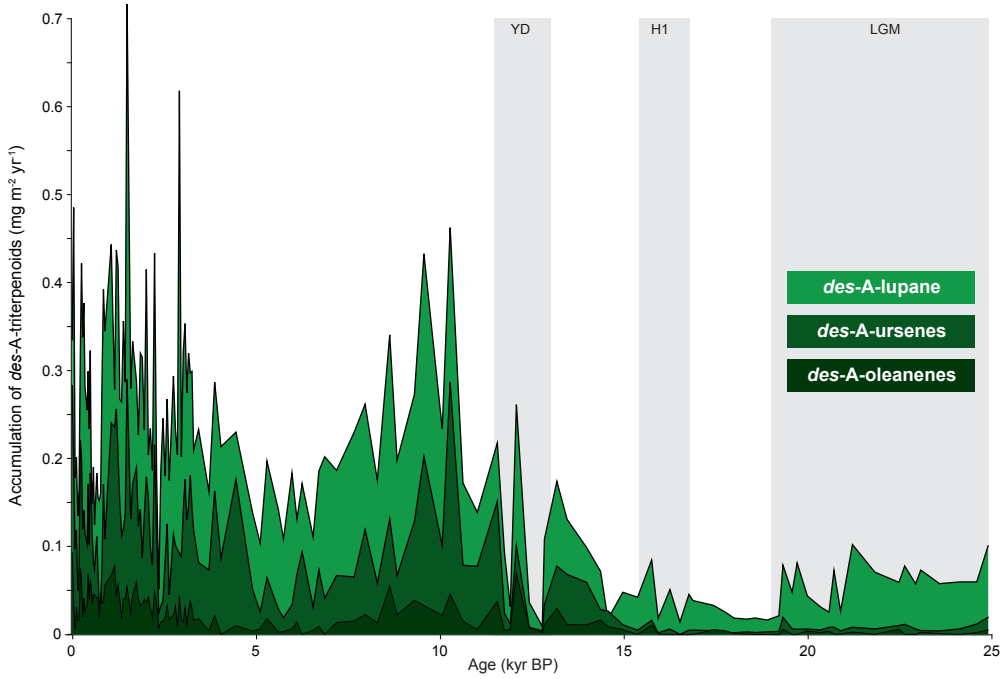

Figure 3.3 Variation through time in the accumulation rates (in mg m^{-2} yr^{-1}, not cumulative) of the *des*-A-triterpenoid compounds for *des*-A-lupane, *des*-A-ursenes and *des*-A-oleanenes in Lake Chala sediments. Shaded areas represent the LGM (26.5-19 kyr BP), Heinrich event H1 (16.8-15.4 kyr BP) and YD (13-11.5 kyr BP).

enter the system, namely the washing-in of microbial degradation products from (anoxic) soils, is unlikely in Lake Chala, as the studied litter and soils did not contain *des*-A-triterpenoids.

The principal degradation processes affecting pentacyclic triterpenoids have been described by various authors (e.g., Trendel et al., 1989; Hauke et al., 1992a, 1992b; Jacob et al., 2007), although not all transformation routes are completely established. Early diagenetic degradation of C-3 oxygenated triterpenoids involves either A to D-ring aromatization or the loss of the A-ring, followed by progressive aromatization from ring B to D (Trendel et al., 1989; Lohmann et al., 1990). The dominant transformation pathway of non-hopanoid triterpenoids in Lake Chala sediments is loss of the A-ring. This loss can be initiated by the formation of A-seco-intermediates, a process that can already occur within the vegetation by photochemical or photomimetic influences (Corbet, 1980; Baas, 1985), but in Lake Chala sediments such intermediates were not identified.

3.4.1 *Des*-A-oleanenes and *des*-A-ursenes

Oleanane- and ursane-type triterpenoids are generally considered to be biomarkers of terrestrial higher plants, specifically angiosperms (e.g. Diefendorf et al., 2012). Smetanina et al. (2001) identified miliacin (3β-methoxy-olean-18-ene) in a marine fungus, which would imply that oleanoid-type triterpenoids are not exclusively produced by terrestrial higher plants. However, a new study on this fungal species did not yield any miliacin (Bossard et al., 2013). We therefore consider all oleanane- and ursane-type triterpenoids as angiosperms biomarkers.

Functionalized triterpenoids with ursane and oleanane skeletons occur in the local vegetation, soils and litter of Lake Chala, often as α- or β-amyrin. The accumulation of their *des*-A-counterparts in the sediments increased markedly from 15 kyr BP onwards (Fig. 3.3). A comparatively low accumulation of higher plant *des*-A-triterpenes occurred during the C_4-plant dominated glacial and early late-glacial periods (Sinninghe Damsté et al., 2011b), suggesting that the C_4 grasses which dominated the vegetation inside the crater at that time did not produce (much of these) triterpenoids. The increase in higher plant *des*-A-triterpenoid accumulation after 15 kyr BP (Fig. 3.3) broadly coincides with the shift towards a mixed C_3/C_4 vegetation as inferred from $\delta^{13}C$ signature of n-C_{31} alkanes (Fig. 3.4; Sinninghe Damsté et al., 2011b) and palynological data (van Geel et al., 2011), following the post-glacial intensification of the region's monsoon rainfall (Verschuren et al., 2009).

Concentrations of *des*-A-oleanenes in Lake Chala sediments are relatively low compared to the other *des*-A-triterpenoids, especially considering the predominance of oleanane-type functionalized triterpenoids in the investigated soils and litter. Future studies on the hydrocarbons in local Lake Chala vegetation might shed light on this apparent discrepancy. Possibly, aromatization of some triterpenoid types is favored over the loss of the A-ring, although the low and infrequent occurrence of aromatic triterpenoids in the sedimentary record does not seem to fit this scenario.

3.4.2 *Des*-A-lupane: a tracer of C_3-plant vegetation composition

The only saturated *des*-A-triterpenoid present in Lake Chala sediments is *des*-A-lupane, as has also been reported from other late-Quaternary lake-sediment records (see e.g. Jacob et al., 2007; Huang et al., 2008). This saturation may be a result of its specific precursors such as lupeol, lupanol or lupanone, or because *des*-A-lupane is more resistant to diagenesis compared to other saturated *des*-A-triterpenoids (Jacob et al., 2007; Huang et al., 2008).

Des-A-lupane records have been interpreted in different ways. Huang et al. (2008), who studied the Dajiuhu peat deposit in China, used *des*-A-lupane as a proxy for the depositional environment at the time of burial, linking sections of the biomarker record with more *des*-A-lupane to episodes of limited degradation (i.e. better preservation). This mechanism is less likely to apply to Lake Chala, because of its relatively constant sedimentation rate and continuously anoxic bottom-water conditions. In a study on the Brazilian Lake Caçó, *des*-A-lupane was thought to be derived from a belt of spike-rush (*Eleocharis* sp.), an emergent aquatic macrophyte (Jacob et al., 2007). As already mentioned, aquatic macrophytes are not a likely source of organic matter input in Lake Chala, as the shoreline of Lake Chala is rocky and near-vertical (Fig. 3.1), which largely prevents aquatic macrophyte growth. Even substantial lake-level lowering, which occurred during the early late-glacial period (Moernaut et al., 2010), is not expected to have created more favorable conditions for development of aquatic macrophytes (Sinninghe Damsté et al., 2011b). Given the absence of functionalized triterpenoids in the sedimentary record of Lake Chala, we consider the sedimentary *des*-A-lupane record (Fig. 3.3) to reflect the input of its precursors in the lake, with a constant transformation of these precursors into *des*-A-lupane, and minor or no degradation of *des*-A-lupane over the last 25-kyr.

Most non-hopanoid triterpenoids are not species-specific, and the lupane-type triterpenoids are no exception. Although these compounds occur in both C_3 and C_4 plants (e.g. Misra et al., 1988; Macías-Rubalcava et al., 2007; Saleem, 2009; Singariya et al., 2012, 2014), the specific $\delta^{13}C$ value of *des*-A-lupane (-27.4‰ on average, SD=±1.1‰, n=38; Fig. 3.4) clearly indicates a C_3-plant origin (*cf.* Castañeda et al., 2009a; Diefendorf et al., 2012). Regnery et al. (2013) reported a comparable $\delta^{13}C$ signature (ranging from -28‰ to -30.6‰) of *des*-A-lupane in lake sediments from the

Holsteinian interglacial (*cf.* Marine Isotope Stage 11c) at Dethlingen in Germany, also similar to *des*-A-lupane isotope values in Tertiary brown coal from China (-28.1±0.6‰; Schoell et al., 1994). Some genera of the Betulaceae (birch family) biosynthesize *des*-A-lupane precursors and, therefore, this C_3 plant family is regularly designated as an important biological source of *des*-A-lupane (Regnery et al., 2013; Schnell et al., 2014). However, Betulaceae do not naturally occur in tropical Africa and no Betulaceae vegetation or pollen are found in Lake Chala (van Geel et al., 2011; Sinninghe Damsté et al., 2011b), so in this setting, *des*-A-lupane must originate from other C_3-plant species. In line with Regnery et al. (2013), and in contrast to Jacob et al. (2007), Huang et al. (2008) and Diefendorf et al. (2012), the concentration of *des*-A-lupane in Lake Chala sediments correlates well with oleanane- and ursane-type *des*-A-triterpenoids. We propose that this dichotomy can be explained by one or more different sources of *des*-A-lupane in these latter studies.

An interesting feature of the *des*-A-lupane $\delta^{13}C$ record is the apparent lack of trend over longer timescales (Fig. 3.4). This record does show some variability over time, but, unexpectedly, no trend, even though large changes in pCO_2 (and its carbon isotopic composition), rainfall and vegetation occur over the glacial-interglacial transition. Recently it was shown that carbon isotope discrimination in C_3 land plants is independent of natural variations in pCO_2 (e.g. Kohn, 2016). Furthermore, the $\delta^{13}C$ value of CO_2 varies by only ~1‰ (between -7‰ and -6‰) over the LGM and Holocene, a variability that is hard to differentiate within the analytical error margins of compound specific $\delta^{13}C$ analysis. Lastly, the modest variability in the *des*-A-lupane $\delta^{13}C$ record in Lake Chala that does occur shows no clear connection to the regional vegetation changes and the alternation of wetter and drier periods documented from other proxies. This absence of a clear trend in $\delta^{13}C$ values of *des*-A-lupane was also noted by Regnery et al. (2013) in their interglacial record from Dethlingen paleolake.

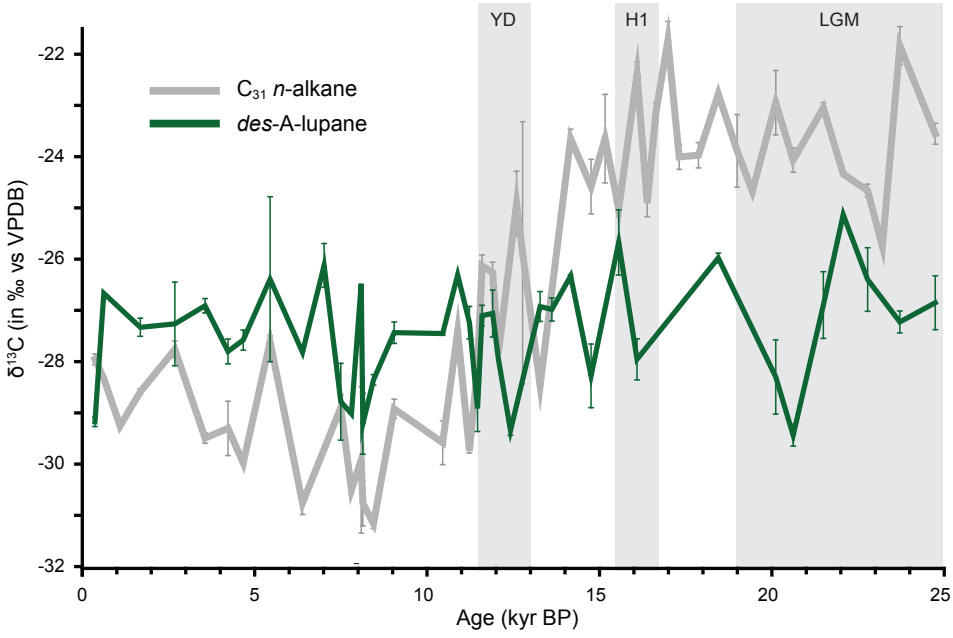

Figure 3.4 Variation through time in the stable carbon isotopic composition ($\delta^{13}C$, in ‰ vs. VPDB) of C_{31} *n*-alkanes (gray line; Sinninge Damsté et al., 2011) and *des*-A-lupane (green line).

Recent studies have indicated the need for more direct proxies of C_3 and C_4 higher plants (Diefendorf et al., 2010; Castañeda and Schouten, 2011), and our findings may be an important step in this development. Firstly, the concentration of *des*-A-triterpenoids with ursane/oleanane/lupane skeletons in the Lake Chala record is high when C_3 plants (trees and shrubs) are common in local/regional vegetation (van Geel et al., 2011; Sinninghe Damsté et al., 2011b). Therefore, we might be able to use these compounds as an absolute measure of C_3 plant abundance, instead of the usual estimate of C_3 or C_4 percentage based on variation in *n*-alkane $\delta^{13}C$ values. Secondly, we introduce a new way of estimating the average $\delta^{13}C$ value of C_3 vegetation at any point in time, which can be important for carbon cycle studies, as $\delta^{13}C$ records of C_3 plants could be used by modelers to assess the possible pCO_2-effect of plant $\delta^{13}C$ (Kohn, 2016). Thirdly, we can use this C_3-plant specific $\delta^{13}C$ record for improving estimates of the C_3/C_4 ratio in past vegetation. Recently, the relative contribution of C_3 and C_4 plants in terrestrial vegetation has been modeled using the $\delta^{13}C$ value of long-chain *n*-alkanes (e.g. Castañeda et al., 2007; Sinninghe Damsté et al., 2011b; Berke et al., 2012). In the Holocene section of our Lake Chala record, *des*-A-lupane $\delta^{13}C$ values are on average less depleted (-27.6‰) than those of C_{31} *n*-alkanes (-29.1‰; Sinninghe Damsté et al., 2011b); the situation is reversed during the glacial period, where average *des*-A-lupane $\delta^{13}C$ values (-27.2‰) are more depleted than those of C_{31} *n*-alkanes (-24.3‰; Sinninghe Damsté et al., 2011b). During the Holocene period, C_3 plants are estimated to contribute ca. 50% of the C_{31} *n*-alkanes (Sinninghe Damsté et al., 2011b). This value was calculated using a simple binary box model, in which a 50/50 mixture of C_3- and C_4-derived *n*-alkanes (with mean values of respectively -35.2‰ and -21.7‰ in modern plants; Castañeda et al., 2009a) yields an average $\delta^{13}C$ value of -28.5‰. During the glacial period, vegetation in the Lake Chala region was dominated by C_4 grasses; the mixed C_3/C_4 composition developed only from 16.5 kyr BP onwards (Sinninghe Damsté et al., 2011b), when a riparian forest of C_3 trees and shrubs started growing inside the crater (van Geel et al., 2011). This local growth of C_3 vegetation is also clearly evident in the record of *des*-A-triterpenoid hydrocarbons with lupane, ursane and oleanane skeletons (Fig. 3.3).

The carbon isotopic fractionation between acetyl CoA-based compounds (e.g. *n*-alkanes) and the isoprene-based isoprenoids essentially depends on the biosynthetic pathways by which they are produced (e.g. MVA for isoprenoids in angiosperms). In their study of North American C_3 plants, Diefendorf et al. (2012) showed that this biosynthetic offset between terpenoids and *n*-alkanes is ~4-6‰. Correspondingly, also in sedimentary records, the ^{13}C of terpenoids is typically reported to be enriched by 5-6‰ compared to *n*-alkanes. We do not expect this biosynthetic offset between triterpenoids and *n*-alkanes to be different in East African vegetation. Temperate C_3 plants may have significantly lower 'overall' lipid fractionation values compared to tropical species (Diefendorf et al., 2011), but this will influence the *n*-alkanes and the terpenoids in the same way. Hence, we can use the $\delta^{13}C$ of *des*-A-lupane as a temporal (i.e. time-specific) C_3 endmember in modeling the C_3/C_4 ratio of local vegetation. To this end we subtracted an average terpenoid enrichment of 5.5‰ from the individual *des*-A-lupane $\delta^{13}C$ values of to estimate the $\delta^{13}C$ values of C_{31} *n*-alkanes derived from local C_3-plants at each time interval. We use the average offset as recorded in sediments (Diefendorf et al., 2012) for this down-core correction exercise, as sediments contain more integrated, averaged signals compared to fresh plant material. Introduction of these corrected C_{31} *n*-alkane $\delta^{13}C$ values in the binary box model for C_3/C_4 ratio calculation, using a constant C_{31} *n*-alkane $\delta^{13}C$ value of -21.7‰ derived from C_4 plants (*cf.* Castañeda et al., 2009a), results in an estimated increase in the relative proportion of C_3 plants by 0 and 19% (Fig. 3.5) as compared to values obtained by Sinninghe Damsté et al. (2011b). Our $\%C_3$ estimates are different from the previous estimates (t-test; $p < 0.0001$, $n = 35$), and the difference remains significant throughout the

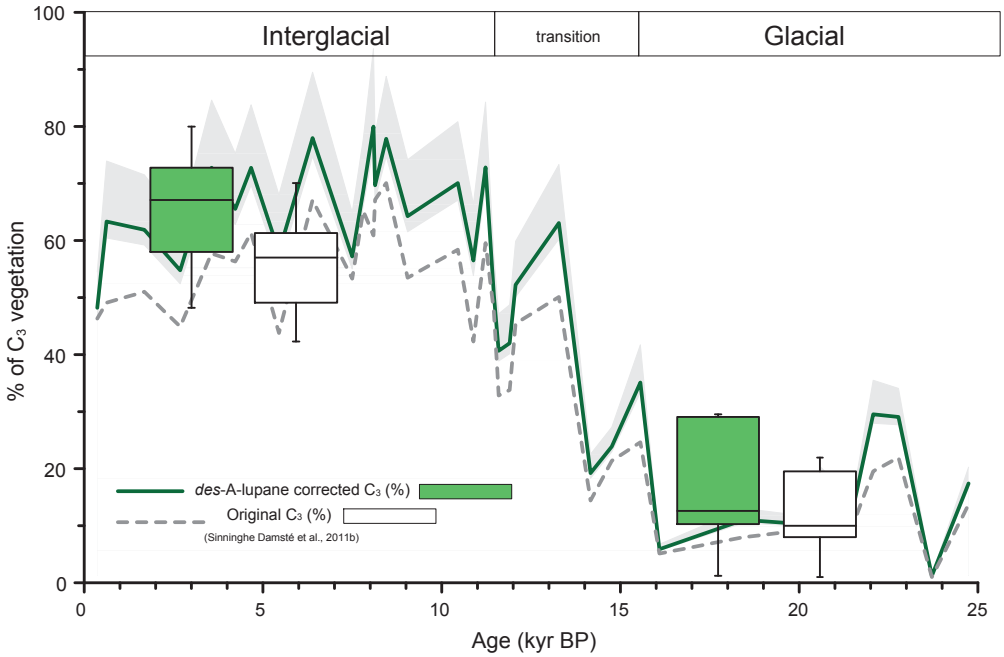

Figure 3.5 Percentage of C_3 vegetation, based on C_{31} *n*-alkane $\delta^{13}C$ values (data from Sinninghe Damsté et al., 2011b), calculated in two different ways: first (solid line) using *des*-A-lupane as the local and temporally variable C_3-plant endmember and an average terpenoid fractionation of 5.5‰ relative to the *n*-alkanes, and second (dashed line) based on fixed $\delta^{13}C$ values for the C_3-plant (-35.2‰) and C_4-plant (-21.7‰) endmembers taken from the literature (Sinninghe Damsté et al., 2011b). The range of C_3 estimates when the modern terpenoid fractionation range of 4 to 6‰ is taken into account is plotted as a grey band. Boxplots show the differences between the original and *des*-A-lupane (grey, left-hand side) corrected C_3 estimate in the glacial and early late-glacial (25 to 16 kyr BP) and in the interglacial period (Holocene, 12.3 to 0 kyr BP) (thus excluding the glacial-interglacial transition), with median, first and third quartiles, and whiskers depicting the minimum/maximum values.

terpenoid to *n*-alkane offset range of 4 to 6‰ (i.e. the range that exists in modern plants; Diefendorf et al., 2012). From this exercise we conclude that especially in the Holocene part of the Lake Chala record, when local vegetation had a mixed C_3/C_4 composition, a reconstruction using fixed C_3-plant $\delta^{13}C$ values underestimates the fraction of C_3 vegetation, while there is less discrepancy during the glacial and early late-glacial periods when C_4 plants (here mostly grasses) were dominant. This result is especially valuable for carbon-cycle modeling studies, where correct assessment of climate-vegetation feedbacks strongly depends on correct estimates of past C_3/C_4 (and hence biome) distribution.

Our method for time-specific correction of the fraction of C_3 plants in local vegetation has the potential to enhance the accuracy of C_3/C_4 vegetation reconstructions in all situations where the local C_3-plant signal is as strong as during the Holocene around Lake Chala (Fig. 3.5). Using sample-specific *des*-A-triterpenoid $\delta^{13}C$ values for estimating this local C_3 vegetation component is convenient, as for example *des*-A-lupane is present in the saturated aliphatic lipid fraction, just like the *n*-alkanes, and can therefore be measured in the same analysis.

3.5 Conclusion

We investigated the possibility to use the degradation products of terrestrial higher plant pentacyclic triterpenoids as a proxy for local vegetation reconstructions. The accumulation of *des*-A-triterpenoids with oleanane/ursane/lupane skeletons serves as a proxy record for the local abundance of C_3 vegetation. The $\delta^{13}C$ signature of *des*-A-lupane can be used as a proxy for the stable carbon isotopic composition of local C_3 plants if, as in our study site of Lake Chala, *des*-A-lupane is exclusively of C_3-plant origin. Therefore, it can be applied as a temporally variable C_3-plant end member representing the local C_3 vegetation component in reconstructions of the C_3/C_4 ratio through time.

Acknowledgements
Sample collection for this study was carried out with permission of the Permanent Secretary of the Ministry of Education, Science and Technology of Kenya under research permit 13/001/11C to D.V. This work was performed as contribution to the ESF EuroClimate project CHALLACEA and the ICDP project DeepCHALLA, financially supported mainly by grants from the Dutch Organization for Scientific Research (NWO) and FWO-Vlaanderen (Belgium) to J.S.S.D. and D.V., respectively. Part of the work was carried out under the program of the Netherlands Earth System Science Centre (NESSC), financially supported by the Ministry of Education, Culture and Science (OCW). We thank C.M. Oluseno for field assistance, and A. Mets, M. Verweij, J. Ossebaar and M. van der Meer for technical assistance. We further thank J. Jacob and an anonymous reviewer for their valuable comments, which greatly improved this manuscript.

Majestic cows at Lake Jipe. Legend has it that when you swim across Lake Chala, you will get sucked into the lake and will be spat out in Lake Jipe.
Photo credit: D. van der Velden

4 Origin, formation and environmental significance of *des*-A-arborenes in the sediments of an East African crater lake

L.G.J. van Bree, M.M. Islam, W.I.C. Rijpstra, D. Verschuren, A.C.T. van Duin, J.S. Sinninghe Damsté and J.W. de Leeuw

adapted from: *Organic Geochemistry* 125, 95-108 (2018)

Abstract

Non-hopanoid pentacyclic triterpenoids occur widespread in lake sediments, but their biological sources and diagenetic pathways are not fully resolved. We tentatively identified a number of the *des*-A-arborene isomers occurring in relatively high abundance in the 25,000-year (25-kyr) sedimentary record of Lake Chala, a deep crater lake in tropical East Africa. The mono-, di- and tri-unsaturated *des*-A-arborenes are transformation products of isoarborinol/arborinone. These precursors have an aquatic source, and are most likely biosynthesized by algae or aerobic bacteria in the epilimnion. The relatively depleted $\delta^{13}C$ values (on average -32.3‰±1.3‰) of *des*-A-arbor-9(11)-ene are consistent with an aquatic source (algae or aerobic bacteria). In general, isoarborinol and its microbially induced transformation products are found in present and ancient tropical lacustrine settings (typically crater lakes) with permanently anoxic bottom waters and sediments. Based on molecular mechanics calculations of *des*-A-arborenes it is clear that these transformation products are not in thermodynamic equilibrium, strongly indicating that their formation is microbially-mediated. Subtle temporal and spatial differences in the microbial community might therefore not only dictate the variable relative contributions of different *des*-A-arborenes found in the sediments of Lake Chala over the last 25 kyr, but also explain the distribution of arborane derivatives in comparable crater-lake settings elsewhere.

4.1 Introduction

Non-hopanoid pentacyclic triterpenoids preserved in lake and marine sediments are relatively well-studied biomarkers and are predominantly used as a proxy for the terrestrial input of angiosperm higher plants (e.g., Rullkötter et al., 1982; Freeman et al., 1994; Sabel et al., 2005). The biological origin of sedimentary triterpenoids with an arborane carbon skeleton is, however, relatively unknown (e.g., Borrego et al., 1997; Volkman, 2005), so their use as biomarkers in paleoenvironmental reconstruction is limited. Arborane-type triterpenoids such as isoarborinol are known to occur in members of a few angiosperm families (Rutaceae: Vorbrüggen et al., 1963; Rubiaceae: Hui and Lam, 1965; Poaceae: Ohmoto et al., 1970; Euphorbiaceae: Hemmers et al., 1989), but their general scarcity in higher plants seems to be at odds with the widespread occurrence and relative abundance of arborane-type triterpenoids found in lake sediments (e.g., Albrecht and Ourisson, 1969; Jaffé and Hausmann, 1995). Furthermore, aromatic isoarborinol derivatives have been found in sediments predating the evolution of angiosperm plants (Hauke et al., 1992a;,1992b, 1995). Alternative sources for arborane triterpenoid hydrocarbons, such as algae or aerobic bacteria, have also been proposed (Ourisson et al., 1982; Hauke et al., 1992b, 1995; Borrego et al., 1997; Volkman, 2005), but it has proven difficult to confirm their biosynthesis by these alternative sources. Only recently, the aerobic marine heterotrophic bacterium *Eudoraea adriatica* has been shown to produce arborane triterpenols (Banta et al., 2017).

During high-resolution stratigraphic analysis of *n*-alkanes (Sinninghe Damsté et al., 2011b), *n*-alk-1-enes (van Bree et al., 2014) and *des*-A-lupane (van Bree et al., 2016) in the continuous and well-dated 25,000-year (25-kyr) sedimentary record of Lake Chala, a deep equatorial crater lake on the border of Kenya and Tanzania, we also encountered a series of *des*-A-arborenes. *Des*-A-arborenes are diagenetic products of pentacyclic triterpenoids with an arborane skeleton such as isoarborinol and arborinone produced by microbial cleavage of the A-ring (Trendel et al., 1989; Lohmann et al., 1990). In this paper we report on the origin, transformation pathways and potential applications of the pentacyclic triterpenoid transformation products with an arborane skeleton in Lake Chala, and compare our setting with other known lacustrine deposits with arboranes. Molecular mechanics were applied to provide critical information regarding the relative stability of various (stereo-)isomers of *des*-A-arborenes, and the likeliness of diagenetic pathways of these compounds to more stable sedimentary biomarkers (*cf.* van Duin et al., 1997; van Duin and Sinninghe Damsté, 2003).

4.2 Material and Methods

4.2.1 Study area

Lake Chala (3°19′S, 37°42′E; locally 'Challa', after a nearby village) is a small, deep and relatively unproductive tropical freshwater crater lake on the lower south-eastern slope of Mt. Kilimanjaro (Fig. 4.1). It is located on the border of Kenya/Tanzania, ~880 m above sea level, with a surface area of ~4.2 km², a catchment area of ~3.4 km² and a maximum depth of around 90 m. The bi-annual passing of the Inter-Tropical Convergence Zone (ITCZ) results in moderate 'long rains' (March-May) and heavy 'short rains' (October-December), and consequently a long dry season (June-September). Subsurface groundwater inflow originating from rainfall on the mid-elevation slopes of Mt. Kilimanjaro is the main water source into the lake (Payne, 1970), although temporary discharge from a creek breaching the crater rim in the northwest can occur during very heavy rains

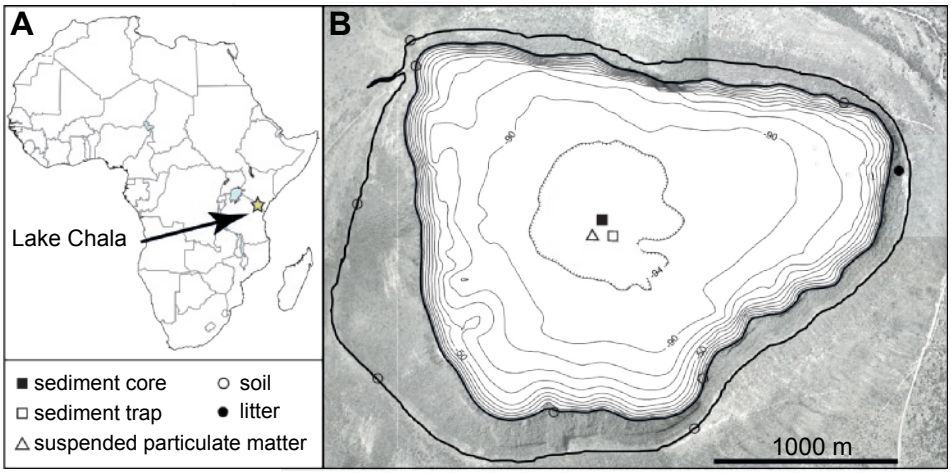

Figure 4.1 The location of Lake Chala (3°19′S, 37°42′E) in East Africa, on the border of Kenya and Tanzania (A), with the sampling location of the suspended particulate matter (SPM), the sediment-trap, the 25-kyr sediment core, catchment soil and litter (B). The outer bold line is the crater rim confining the catchment area, the inner bold line the shoreline at the time of coring in 2005, and lake bathymetry is indicated at 10-m intervals. Modified after Moernaut et al. (2010) and van Bree et al. (2014, 2016).

(Buckles et al., 2014). Daily wind-driven water-column mixing is limited to 15-20 m year-round, while seasonal deep mixing (June-September) extends to 40-60 m. Consequently, the lower water column is permanently stratified. Due to the limited density stratification, complete mixing cannot be excluded, but its recurrence frequency is almost certainly decadal or longer, not inter-annual (Wolff et al., 2011, 2014).

4.2.2 Study materials

We studied Lake Chala's finely-laminated organic muds retrieved mid-lake (Fig. 4.1) in 2003 and 2005 (see Verschuren et al., 2009). The well-dated 20.82 m long master sequence covers the last 25 kyr of continuous offshore lacustrine sedimentation (see Blaauw et al., 2011). For this study, a total of 141 sediment samples with 4-cm thickness were extracted and processed for biomarker analysis, generally at ~200-year intervals, with a higher resolution of ~50 year intervals in the youngest 3.2 kyr, similar to previous studies (van Bree et al., 2014, 2016). In addition, we analyzed the compound-specific stable carbon isotopic composition of selected biomarkers in 14 sediment samples distributed throughout the sequence.

We also analyzed sediment trap, suspended particulate matter (SPM), soil and litter samples (Sinninghe Damsté et al., 2009; Buckles et al., 2014; van Bree et al., 2014, 2016). A sediment trap deployed at 35 m water depth in oxic water (~5 mg L^{-1}) was retrieved at ca. 4-week intervals between November 2006 and December 2007 as described by Sinninghe Damsté et al. (2009). On 10-11 September 2006 SPM samples were obtained from throughout the water column, filtered and processed as described in van Bree et al. (2014, 2016). Soil (n = 8) and litter (n = 5) samples were collected within the catchment area of Lake Chala in 2005 and 2012, respectively (Fig. 4.1). These were stored and processed as described by Sinninghe Damsté et al. (2009) and van Bree et al. (2016).

4.2.3 Lipid extraction

Lipid extraction has been performed in the context of previous studies (Sinninghe Damsté et al., 2011b; van Bree et al., 2014, 2016). In short, the freeze-dried and powdered sediments were extracted with a Dionex™ Accelerated Solvent Extractor (ASE), using a dichloromethane (DCM)/methanol (9:1, v/v) mixture at high temperature (100°C) and pressure (7.6 x 10^6 Pa). Subsequently the extracts were separated into an apolar and a polar fraction over an activated Al_2O_3 column with hexane/DCM (9:1, v/v) and DCM/MeOH (1:1, v/v), respectively. A subset of the apolar fractions were separated with a small Ag^+-impregnated silica column into a saturated (hexane eluent) and an unsaturated hydrocarbon fraction (ethyl acetate eluent) prior to stable carbon isotopic composition analysis.

SPM and sediment-trap samples were extracted previously (Sinninghe Damsté et al., 2009). Fluxes of apolar compounds (in mg m^{-2} yr^{-1}) in the water column were calculated using the concentration of each of these components relative to total particle flux measured in the sediment trap. Litter and soil samples were extracted ultrasonically with DCM/MeOH (2:1, v/v) as described by van Bree et al. (2016). In short, the extracts were methylated with diazomethane in diethyl ether and separated over an activated Al_2O_3 column into apolar, ketone and polar fractions, using hexane/DCM (9:1, v/v), hexane/DCM (1:1, v/v) and DCM/MeOH (1:1, v/v) as eluents, respectively.

4.2.4 Lipid identification and quantification

As described previously (Sinninghe Damsté et al., 2011b; van Bree et al., 2014, 2016), the apolar fractions of sediments, SPM, sediment-trap, soil and litter extracts were analyzed by gas chromatography (GC) and GC-mass spectrometry (GC-MS). A selection of polar samples of sediment, sediment-trap and SPM were methylated, silylated and screened for funtionalized triterpenoids. GC was performed using a Hewlett-Packard (HP6890) instrument equipped with an on-column injector, a flame ionization detector (FID), a fused silica capillary column (25 m, 0.32 mm) coated with CP Sil-5 CB (film thickness 0.12 µm), and helium as carrier gas. The samples were injected at 70°C with an oven program of 20°C min^{-1} to 130°C, 4°C min^{-1} to 320°C, and held for 20 min. GC-MS was performed on a Finnigan Trace DSQ mass spectrometer operated at 70 eV with a mass range of *m/z* 40 to 800 and a cycle time of 1.7 s. The GC was equipped with a fused silica capillary column as described above, with helium as carrier gas, and the same oven temperature program as for GC. Identification of the *des*-A-triterpenoids and other triterpenoid hydrocarbons is based on relative retention times, published mass spectra (including the NIST98 spectral library), and interpretation of observed fragmentation patterns. Quantification of compounds was performed by peak area integration of peaks in the FID chromatograms, including an internal standard. The concentration of apolar compounds are normalized to µg $gTOC^{-1}$.

4.2.5 Compound-specific carbon isotope analyses

We measured the compound-specific $\delta^{13}C$ signature of 20 unsaturated hydrocarbon fractions with an Agilent 6800 GC coupled to a ThermoFisher Delta V isotope-ratio monitoring mass spectrometer. Samples were run in duplicate or triplicate, allowing an estimation of the standard deviation of the measurements. The isotope values were measured with reference to a calibrated external gas. Instrument performance was monitored daily by injections of a mixture of a C_{20} and a C_{24} perdeuterated *n*-alkane with known isotopic composition. The $\delta^{13}C$ values are reported in standard delta notation against the Vienna Pee Dee Belemnite (VPDB).

4.2.6 Molecular mechanics

We performed both quantum-chemistry-based Density Functional Theory (DFT) and ReaxFF classical-force-field simulations to calculate the relative stabilities of various stereo-isomeric configurations of the *des*-A-arborenes. DFT calculations are deemed more accurate, but require more computational power than ReaxFF. The ReaxFF method has been well-established over the last decade to describe a wide range of systems including catalysis, combustion, pyrolysis, batteries, and other complex chemical systems (e.g., van Duin et al., 2001; Senftle et al., 2016). In the main text, we will only discuss the DFT results. Background, methodology and results from the ReaxFF simulations are available in Appendix 4.1, including a discussion on similarities and differences compared to DFT.

The DFT calculations were carried out with the Jaguar 7.5 program with the B3LYP (Becke, 1988; Lee et al., 1988) hybrid functional and the 6-311++G** basis set. The mixture composition of various stereo-isomers at equilibrium was calculated using the following formula:

$$\%C_i = 100 \times \frac{\exp\left(\frac{\Delta G_i - \Delta G_1}{RT}\right)}{1 + \sum_{n=2}^{nc} \exp\left(\frac{\Delta G_n - \Delta G_1}{RT}\right)}$$

where ΔG_i is the relative Gibbs free energy of isomer *i*, n_c the number of compounds, R the universal gas constant, and T the temperature. In the equilibrium composition calculations at 298K, the entropic contributions are approximated negligible, thus Gibbs free energies are replaced by the ground state energies.

4.3 Results

4.3.1 The sedimentary record of *des*-A-triterpenoids in Lake Chala

Analysis of the apolar fractions of biomarker extracts from 141 well-dated sediment horizons covering the last 25 kyr revealed the presence of various biomarkers, including *n*-alkanes, *n*-alk-1-enes, phytadienes, di- and tri-aromatic triterpenoids, hopenoids, and *des*-A-triterpenoids with oleanane, ursane, lupane and arborane skeletons. The origin and paleoclimatic significance of some of these biomarkers have been discussed previously, and include terrestrial long-chain *n*-alkanes (Sinninghe Damsté et al., 2011b), aquatic $C_{25:1}$ and $C_{27:1}$ long-chain *n*-alk-1-enes (van Bree et al., 2014), and the higher plant-derived *des*-A-triterpenoids with oleanane, ursane and lupane skeletons (van Bree et al., 2016). Here we focus on the origin, transformation, distribution and potential paleoenvironmental application of the arborane-type *des*-A-triterpenoid hydrocarbons.

In the C_{23} to C_{26} *n*-alkane region of the chromatograms (Fig. 4.2A-B), six different peaks were identified as *des*-A-arborenes with one to three double bonds, based on their relative retention times, published mass spectra, and fragmentation patterns. Fig. 4.2C shows a representative summed mass chromatogram (*m/z* 161+177+189+203+218+309) of a sediment horizon dated to 12.1 kyr BP, exemplifying their distribution. Compounds **1**, **2**, **3** and **4** ($M^{+\bullet}$ at *m/z* 328, base peak at *m/z* 161) reflect mass spectral fragmentation patterns similar to mono-unsaturated *des*-A-arborenes (Fig. 4.2D). The presence of a fragment at *m/z* 326 in the mass spectrum of compound **2** indicates co-elution with an unknown *des*-A-arboradiene. The mass spectral fragmentation

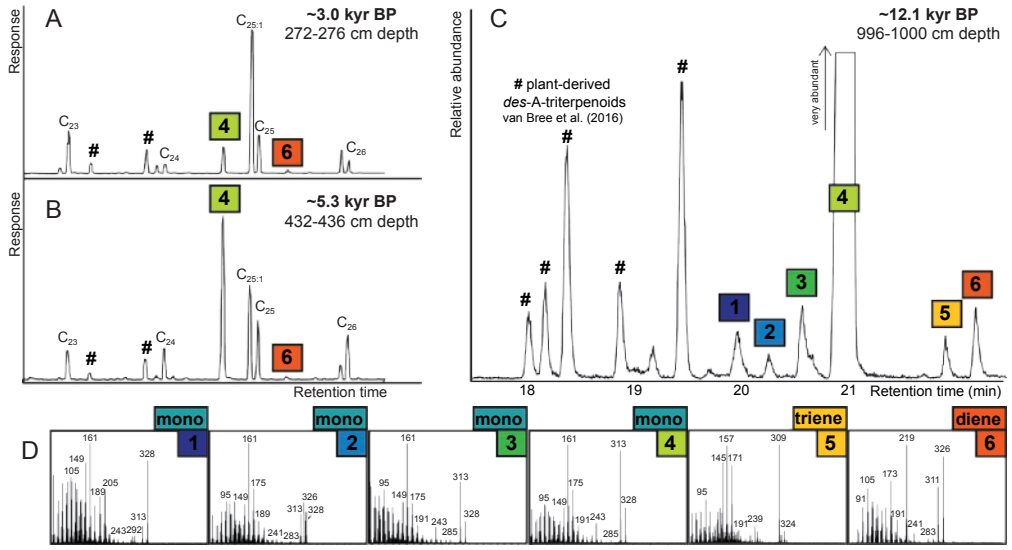

Figure 4.2 Distribution of *des*-A-triterpenoids in the Lake Chala sediment record with partial GC-FID traces of the apolar fractions of hydrocarbon extract from representative sediment horizons at 272-276 cm (A) and 432-436 cm (B) depth, deposited ~3.0 and ~5.3 kyr BP, respectively. Panel (C) shows a summed mass chromatogram (*m*/*z* 163+177+189+203+218+309) illustrating the distribution of *des*-A-triterpenoids from the apolar lipid fraction of a sample taken at 996-1000 cm depth, which is dated ~12.1 kyr BP; # indicates plant-derived *des*-A-triterpenoids (van Bree et al., 2016). Panel (D) shows the mass spectra of compounds **1** and **2** (mono/di-unsaturated *des*-A-triterpenes with an arborane skeleton), **3** and **4** (*des*-A-arbor-9(11)-ene), **5** (*des*-A-arbora-5,7,9-triene), and **6** (*des*-A-arbora-5(10),9(11)-diene); these identifications are tentative. Possible structures are shown in Figure 4.5.

patterns of compounds **3** and **4** are similar to that of *des*-A-arbor-9(11)-ene as tentatively described by Jaffé and Hausmann (1995) and Jacob et al. (2007), possibly indicating the presence of two stereoisomers. Compound **5** ($M^{+\bullet}$ at *m*/*z* 324) is tentatively identified as *des*-A-arbora-5,7,9-triene (Hauke et al., 1992a). Compound **6** ($M^{+\bullet}$ at *m*/*z* 326) is tentatively identified as *des*-A-arbora-5(10),9(11)-diene (Jaffé and Hausmann, 1995). Some sedimentary horizons contain traces of other *des*-A-arboradienes, including two that are coeluting with a compound containing a mass fragment at *m*/*z* 329. Several other, non-identified *des*-A-triterpenoids occur infrequently or in trace amounts; these compounds are not further discussed. In addition, trace amounts of isoarborinol were found in polar fractions of suspended particulate matter (in the sample set discussed by van Bree et al., 2018b) and in surface sediments.

The distributions and abundances of these unsaturated *des*-A-arborenes in the sedimentary record vary considerably over time. The summed record of the *des*-A-arborenes (compounds **1** to **6**) shows three periods of high concentrations, namely 23.1 to 19.2 kyr BP, 14.0 to 8.3 kyr BP and around 0.4 kyr BP (Fig. 4.3A and D). *Des*-A-arborenes, and compound **4** in particular, are at times dominant in the apolar fraction of Lake Chala's lipid extracts. The overall average concentration is ~300 µg $gTOC^{-1}$ with peak values up to 3 mg $gTOC^{-1}$ for the summed *des*-A-arborenes. The relative proportion of mono-enes, dienes and trienes fluctuates over the past 25 kyr (Fig. 4.3B). The mono-enes are dominated by compound **4**, in few cases by compound **3** (Fig. 4.3C). The mono-

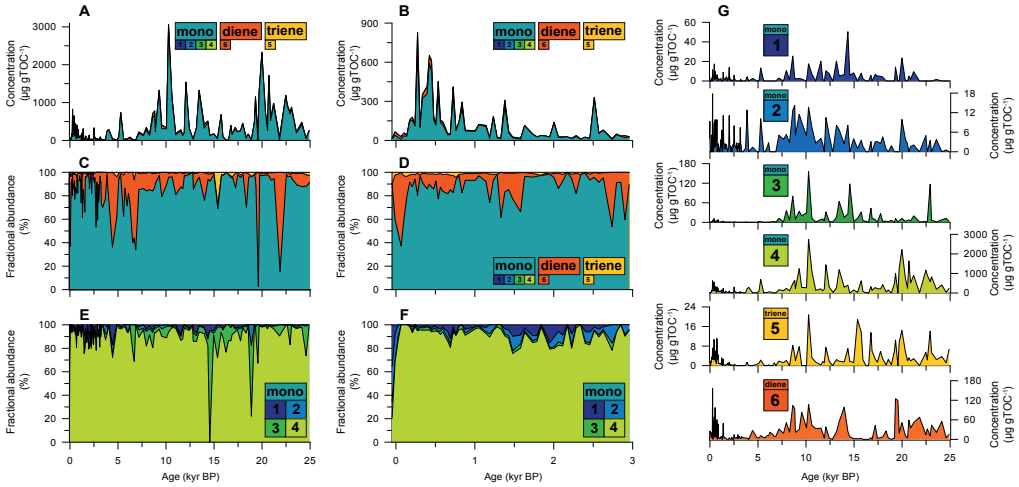

Figure 4.3 Distribution of *des*-A-arborenes (in µg $gTOC^{-1}$) in Lake Chala sediments over the past 25 kyr. (A) shows the summed concentration of *des*-A-arborenes (in µg $gTOC^{-1}$) in Lake Chala sediments. Panel (B) shows the relative abundances, revealing a large proportion of monoenes (sum of 1, 2, 3 and 4; green), and smaller proportions of the triene (**5**; yellow) and diene (**6**; orange). (C) shows the fractional abundance of the mono-enes. Panels (D), (E), and (F) zoom in on these plots over the past 3 kyr, the section investigated at high temporal resolution. In (G) the *des*-A-arborene concentrations (in µg $gTOC^{-1}$) of compounds **1, 2, 3, 4, 5** and **6** over the last 25 kyr are plotted separately.

enes are dominant most of the time (average 83%, median 91%). The fractional abundance of the diene (**6**) is highly variable and ranges between 0 and 100% (average 15%, median 8%). The triene (**5**) is typically present as a minor (<5%) component (average 1.8%, median 0.8%), but has peak occurrences of up to 35%, and is entirely absent in some intervals even though the sedimentary record has been sampled at very high resolution (e.g., between 2.7 and 3.7 kyr BP; $n = 14$). When the dienes and trienes are relatively abundant, the overall concentration of unsaturated *des*-A-arborenes is always relatively low (Fig. 4.3).

The stable carbon-isotopic composition of compound **4** was determined successfully in 14 out of 20 sediment horizons (Fig. 4.4), and ranges from -29.8‰ to -33.8‰ (-32.3‰±1.3‰ on average). Reliable determination of the stable carbon-isotopic composition of other *des*-A-arborenes was unsuccessful due to co-elution or low abundances.

4.3.2 (*Des*-A-)triterpenoids in soil, litter, settling particles and suspended particulate matter

No *des*-A-triterpenoids were identified in the hydrocarbon extracts from soils and litter, and no functionalized arborane-type triterpenoids were detected in other fractions. Van Bree et al. (2016) reported the presence of functionalized triterpenoids with oleanane, ursane and lupane skeletons in the soil and litter, but arborane or fernane-type triterpenoids were not encountered. In the extracts of particulate matter recovered with the sediment trap, only low concentrations of *des*-A-urs-13(18)-ene and *des*-A-lupane were detected, next to traces of functionalized triterpenoids such as α-amyrinol. Hydrocarbon concentrations in the SPM were too low for identification of specific triterpenoid compounds.

4.3.3 Molecular mechanics: DFT simulation

DFT molecular mechanics calculations were performed to calculate the stabilities of the isomers of mono/di/tri-unsaturated *des*-A-arborenes (Table 4.1; Fig. 4.5). If isomerization of double bonds via relatively stable tertiary carbocations (de Leeuw et al., 1989) should occur, five double-bond isomers, i.e. $\Delta^{5(10)}$, Δ^{7}, Δ^{8}, Δ^{9}, and $\Delta^{9(11)}$, may result from the original $\Delta^{9(11)}$ *des*-A-arborene. Isomerization of the $\Delta^{9(11)}$-isomer via the tertiary carbocation at C-9 can produce Δ^{8}- and Δ^{9}-isomers. The Δ^{8}-isomer can give rise to Δ^{7}-isomers via the tertiary carbocation at C-8, whereas the Δ^{9}-isomer can evolve into the $\Delta^{5(10)}$-isomer via the tertiary carbocation at C-10. Chiral centers in *des*-A-arbora-monoenes occur at C-8, C-9, and C-10, and, hence, stereoisomers may occur as well. As the double-bond isomers of *des*-A-arbora-monoenes can have 2 or 4 stereo-isomers each, there are 16 possible configurations (see Fig. 4.5 for roman numeral codes). DFT calculations indicate that generally, the $\Delta^{9(11)}$-isomers are most stable (**IIIa-b**), followed by Δ^{7} (**IIIg**), Δ^{8} (**IIIe-f**) and Δ^{9} (**IIIk**). More specifically, DFT molecular mechanics calculations indicate that $\Delta^{9(11)}$-8βH,10βMe (**IIIa**) is the most stable *des*-A-arbora-monoene (Table 4.1, Fig. 4.5). The DFT calculations predict stabilities for $\Delta^{9(11)}$-8αH,10αMe (**IIIb**), Δ^{8}-10αMe (**IIIe**), Δ^{8}-10βMe (**IIIf**), Δ^{7}-9αH,10αMe (**IIIg**), and Δ^{9}-8βH (**IIIk**) that are less stable but are within 2 kcal/mol, compared to that of $\Delta^{9(11)}$-8βH,10βMe (**IIIa**).

Table 4.1 DFT molecular calculation results of double-bond and stereoisomers of *des*-A-arborene, *des*-A-arbor-diene and *des*-A-arbor-triene. ΔE_{DFT} marked with an * are significantly present in equilibrium compositions calculated at 298K, and their equilibrium composition (%) is calculated for mono-enes and dienes separately. ΔE was calculated compared to compounds **IIc** and **IIIe**, marked with an **#**.

Structure	*des*-A-arborene double-bond position	Stereoisomer configuration	DFT (kcal/mol)	ΔE_{DFT} (kcal/mol)	Equilibrium composition (%)
IIa	$\Delta^{5(10),9(11)}$	8βH	-588380.49	-4.29 *	99.9
IIb	$\Delta^{5(10),9(11)}$	8αH	-588376.94	-0.74	-
IIc	$\Delta^{5(10),8}$	-	-588376.80	# 0.00	-
IId	$\Delta^{7,9}$	-	-588335.71	40.48	-
IIIa	$\Delta^{9(11)}$	8βH,10βMe	-589145.22	-0.84 *	57.5
IIIb	$\Delta^{9(11)}$	8αH,10αMe	-589144.48	-0.09 *	16.4
IIIc	$\Delta^{9(11)}$	8βH,10αMe	-589141.99	2.40	0.2
IIId	$\Delta^{9(11)}$	8αH,10βMe	-589140.16	4.23	0.0
IIIe	Δ^{8}	10αMe	-589144.39	# 0.00 *	14.0
IIIf	Δ^{8}	10βMe	-589143.70	0.69 *	4.4
IIIg	Δ^{7}	9αH,10αMe	-589143.88	0.51 *	6.0
IIIh	Δ^{7}	9αH,10βMe	-589140.93	3.46	0.0
IIIi	Δ^{7}	9βH,10βMe	-589139.49	4.90	0.0
IIIj	Δ^{7}	9βH,10αMe	-589138.26	6.13	0.0
IIIk	Δ^{9}	8βH	-589143.02	1.36 *	1.4
IIIl	Δ^{9}	8αH	-589138.22	6.17	0.0
IIIm	$\Delta^{5(10)}$	8βH,9αH	-589140.74	3.65	0.0
IIIn	$\Delta^{5(10)}$	8αH,9αH	-589138.55	5.83	0.0
IIIo	$\Delta^{5(10)}$	8βH,9βH	-589135.09	9.29	0.0
IIIp	$\Delta^{5(10)}$	8αH,9βH	-589131.80	12.58	0.0
IV	$\Delta^{5,7,9}$	-	-587639.18	-	-

Hence, if thermodynamic equilibrium should exist for the *des*-A-arborenes, these compounds should be present in significant amounts (Table 4.1).

Isomerization of *des*-A-arboradienes (**IIa** to **IId**) can only occur via relatively stable allylic tertiary carbocations (de Leeuw et al., 1989). Hence, only four possible *des*-A-arboradienes may be formed starting from the $\Delta^{9(11)}$-isomer: $\Delta^{5(10),9(11)}$-8βH (**IIa**), $\Delta^{5(10),9(11)}$-8αH (**IIb**), $\Delta^{5(10),8}$ (**IIc**), and $\Delta^{7,9}$ (**IId**; Fig. 4.5). The DFT calculations indicate that $\Delta^{5(10),9(11)}$-8βH (**IIa**) is the most stable isomer, and would dominate the mixture (~99.9%) if at equilibrium.

We also calculated the inter-conversion energetics of the most stable monoene (**IIIa**), diene (**IIa**) and B-ring aromatized $\Delta^{5,7,9}$ *des*-A-arboratriene (**IV**), considering molecular hydrogen as reference for hydrogenation and dehydrogenation reactions. DFT calculations predict an exothermic conversion process of diene **IIa** to monoene **IIIa** (ΔE_1 = -14.10 kcal/mol), and endothermic conversions for both diene **IIa** to triene **IV** (ΔE_2 = 1.13 kcal/mol), and monoene **IIIa** to triene **IV** (ΔE_3 = 15.50 kcal/mol).

4.4 Discussion

4.4.1 Arborane vs. fernane precursors

One important issue regarding *des*-A-arborenes is the possibility that they may have been formed by transformation of fernane-type triterpenoids, since *des*-A-fernenes are enantiomers of *des*-A-arborenes (Jaffé and Hausmann, 1995). Arborane and fernane skeletons (Fig. 4.5: **Ia**-**Id**) differ only in stereochemistry due to chair and boat conformations of the B-ring when they are synthesized (Ohmoto et al., 1970). Therefore, its precursor skeleton is no longer identifiable when aromatized or when the A-ring is removed. Fernane-type triterpenoids have been reported from different biological sources including plants, lichens and bacteria (e.g., Ohmoto et al., 1970; Bottari et al., 1972; Howard et al., 1984; Hemmers et al., 1989; Shiojima and Ageta, 1990; González et al., 1991; Hauke et al., 1992b; Paull et al., 1998; Maier et al., 2009). Although a fernane-type origin cannot be ruled out completely, it is highly unlikely in Lake Chala, firstly due to the presence of trace amounts of isoarborinol and absence of functionalized fernenes in the modern water column and surface sediments; and secondly due to the similarity of Lake Chala with other lacustrine environments from where large amounts of arborane-triterpenoids have been reported (Section 4.2). Therefore, we are most likely dealing with compounds derived from functionalized arboranes, more specifically isoarborinol and/or arborinone.

4.4.2 Comparison with other lacustrine records

Isoarborinol and its derivatives are often found in lake settings similar to Lake Chala. Sometimes large quantities of isoarborinol/arborinone are typically found in small (sub)tropical freshwater lakes with a permanently anoxic hypolimnion (Table 4.2). This includes modern lakes such as Lake Valencia (in Venezuela; Jaffé and Hausmann, 1995) and Lake Albano (in Italy; Hanisch et al., 2003), but also paleolake deposits such as the Eocene Lake Messel (~47.8±0.2 Ma; Albrecht and Ourisson, 1969; Kimble et al., 1974; Hauke et al., 1992a), Eckfeld Maar (~44.3 Ma; Sabel et al., 2005), the Bouxwiller shales (Arpino et al., 1971; Hauke et al., 1995), the Ménat shales (Hauke et al., 1992a, 1995), and the Miocene Clarkia deposits (Logan and Eglinton, 1994; Huang et al., 1995). Isoarborinol/arborinone is usually found in highly productive (eutrophic to hypereutrophic) lakes, while Lake Chala is oligotrophic. Typically, isoarborinol is found in tropical or warm and humid climates, but it has also been detected in the Pleistocene sediments of the Arctic Lake El'gygytgyn

(D'Anjou et al., 2013). Lake Valencia and paleolake Messel are the most comparable to Lake Chala. Lake Valencia is much larger than Lake Chala, but its sedimentary lipid content is very similar, not only with respect to arborane-triterpenoid derivatives (isoarborinol, *des*-A-arbor-9(11)-ene, *des*-A-arbora-5(10),9(11)-diene), but also for example with respect to the abundance of algal long-chain *n*-alk-1-enes (van Bree et al., 2014). The depositional environment of Lake Chala is similar to that of the Eocene Lake Messel, which contains *des*-A-arbor-5,7,9-triene **IV** and high abundances of isoarborinol/arborinone (Albrecht and Ourisson, 1969; Hauke et al., 1992a).

4.4.3 Microbial origin of isoarborinol/arborinone

There are various potential biological sources of the *des*-A-arborene precursors isoarborinol and arborinone. Traditionally they are attributed to a terrestrial higher plant source (e.g., Albrecht and Ourisson, 1969; Ohmoto et al., 1970; Vliex et al., 1994; Jacob et al., 2005), but they have also been assigned to phytoplankton and bacteria (Ourisson et al., 1982; Hauke et al., 1992b, 1995; Jaffé and Hausmann, 1995; Volkman, 2005). Oxidosqualene cyclases (OSCs), the enzymes responsible for the biosynthesis of C3-oxygenated cyclic triterpenoids, are predominantly occurring in the eukaryotic domain, but a limited number of bacterial OSCs has also been identified (Banta et al., 2017). The only confirmed bacterial production of arborane triterpenols is by the aerobic marine heterotrophic bacterium *Eudoraea adriatica* (Banta et al., 2017). However, metagenomic sequences from both marine and lacustrine environments indicated the presence of the bacterial OSC responsible for the biosynthesis of arborane triterpenols, suggesting the possibility of other bacterial sources for these type of triterpenols.

4.4.3.1 Stable carbon-isotopic composition

One way of differentiating between an terrestrial and aquatic source of lipid biomarkers is the stable carbon isotopic composition of specific lipids (Fig. 4.4). In Lake Chala, $\delta^{13}C$ values of compound **4** range from -29.8‰ to -33.8‰ (-32.3‰±1.3‰ on average). No isotopic fractionation is expected to occur during transformation of triterpenoids (Freeman et al., 1994), therefore these $\delta^{13}C$ values are thought to reflect the $\delta^{13}C$ signature of the parent compound, and can be used to distinguish between alternative plant or microbial sources. The relative ^{13}C depletion found in Lake Chala is comparable to that reported for arborane compounds in other lake settings. In a study of Eocene shales (Hauke et al., 1992a), *des*-A-arbora-5,7,9-triene (**IV**) has a $\delta^{13}C$ value of -28.7‰, contrasting with significantly less depleted $\delta^{13}C$ values (-23 to -25‰) of lupane or ursane-type triterpenoids. Such a clear offset between the $\delta^{13}C$ values of terrestrial triterpenoid derivatives and arborane derivatives is also seen in Lake Chala (Fig. 4.4), where compound **4** is significantly more depleted in ^{13}C (29.8‰ to -33.8‰; -32.3‰±1.3‰ on average) than the plant-derived *des*-A-lupanes (-25.1 to -29.4‰; -27.4‰±1.1‰ on average; van Bree et al., 2016). Isoarborinol is reported with $\delta^{13}C$ values of -28.0 to -28.4‰ in Miocene Lake Clarkia (Logan and Eglinton, 1994; Huang et al., 1995), and -24.7 to -27.9‰ in Lake Valencia (Xu and Jaffé, 2008). The significant ^{13}C depletion of compound **4** in Lake Chala sediments indicates that also here an aquatic source is much more likely than a terrestrial higher plant source of arborane-type triterpenoids.

4.4.3.2 Distribution patterns of *des*-A-arborenes

Besides the depleted $\delta^{13}C$ values, also the distribution of *des*-A-arborenes in Lake Chala sediments is different from those of known higher plant-derived biomarkers. Indeed, the concentration of *des*-A-arborenes in the sediment is often higher than those of bona fide terrestrial higher-plant biomarkers such as *n*-alkanes and the plant-derived *des*-A-triterpenoids. The concentration of

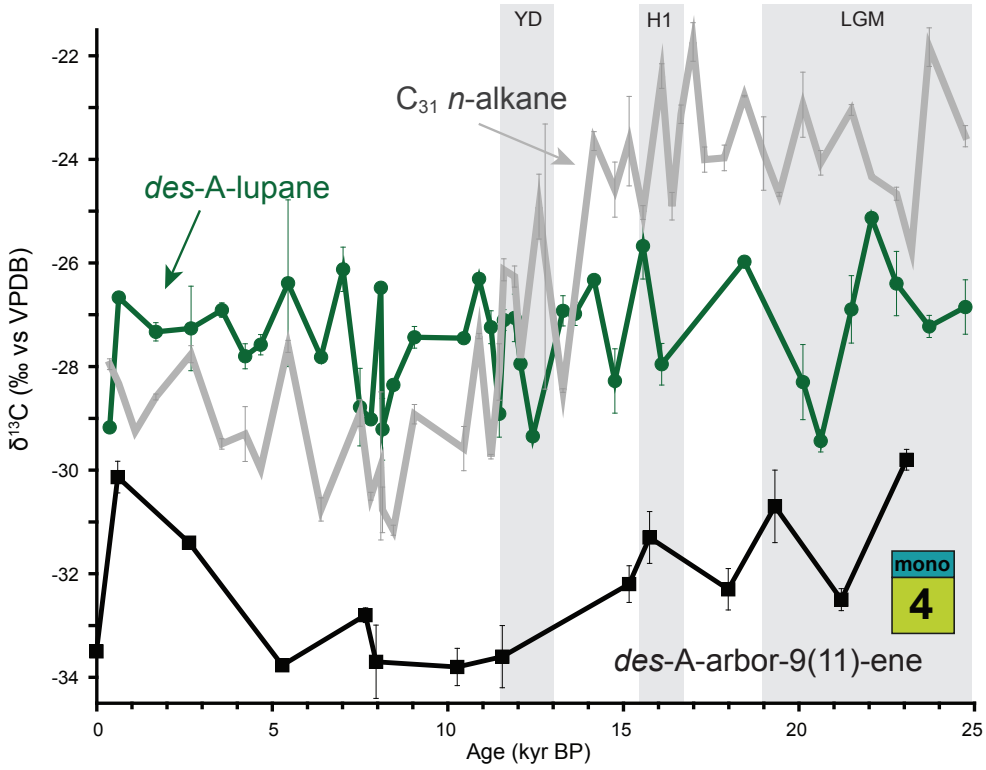

Figure 4.4 The stable carbon-isotopic composition ($\delta^{13}C$, in ‰ vs. VPDB) of *des*-A-arborene compound **4** over time, in comparison with the records for the C_3-plant derived *des*-A-lupane (van Bree et al., 2016) and the C_{31} *n*-alkane plant waxes (Sinninghe Damsté et al., 2011b).

compound **4** is not correlated with that of *des*-A-lupane, *des*-A-ursenes and *des*-A-oleanenes (R^2 = 0.01, 0.02, and 0.08, respectively; van Bree et al., 2016). Although the *des*-A-arborenes are at times dominant in apolar sediment extracts from Lake Chala, their potential precursors (i.e. triterpenoid ketones, alcohols, methyl ethers, acetates and acids with an arborane skeleton) were not found in the soil and litter of the Lake Chala area, and only trace amounts of isoarborinol have been detected in selected sediment samples. In conclusion, a land-derived origin of the *des*-A-arborenes in Lake Chala is much less likely than an aquatic, microbial origin.

4.4.3.3 Comparison with similar geochemical settings

Not only in Lake Chala, but also in many small and permanently stratified tropical lakes (Table 4.2) an aquatic microbial origin is much more likely than a terrestrial one. Ourisson et al. (1982) already predicted an aerobic bacterial source for isoarborinol, as this compound has been found in many different sediments and is relatively rare in plants. Hauke et al. (1992a, 1992b) proposed that sedimentary arborane-type triterpenoids originate from aerobic bacteria or algae, based on their stable carbon-isotopic composition and the requirement of molecular oxygen for their biosynthesis. A bacterial origin was also proposed by Jaffé and Hausmann (1995) in their study

Table 4.2 Characteristics of Lake Chala compared to other (paleo)lakes with a sedimentary record of various arborane-type triterpenoid compounds.

Lake	Location	(paleo)climate	Salinity	Age	References
Chala	Kenya/Tanzania	tropical	fresh	0-25 kyr BP (Quaternary)	this study
Valencia	Venezuela	tropical	fresh	0-13 kyr BP (Quaternary)	**A B**
Messel oil shales	Germany	tropical	fresh	47.8±0.2 Ma (Eocene)	**C**
Eckfeld Maar	Germany	tropical	fresh	44.3±0.4 Ma (Eocene)	**D**
Albano	Italy	Mediterranean	fresh	Holocene (Quaternary)	**E**
Clarkia lacustrine deposits	Idaho, USA	tropical	fresh	15.4-16 Ma (Miocene)	**F G**
Kupfer- schiefer	Germany		lagoonal	Permian	**H I J K**
Bouxwiller shales	France	tropical	fresh	Eocene	**K L**
Caçó	Brazil	tropical	fresh	0-20 kyr BP (Quaternary)	**M N**
Orbagnoux basin	France		lagoonal	Kimmeridgian (Late Jurrassic)	**K O**
Puertollano oil shale	Spain		fresh	~300 Ma (Carboniferous; late Stephanian)	**C**
El'gygytgyn	Russia	Arctic	fresh	275-475 kyr BP (Quaternary)	**P**
Kinneret	Israel		fresh	Holocene (Quaternary)	**Q**

A: Jaffé and Hausman (1995), **B**: Xu and Jaffé (2008), **C**: Borrego et al. (1997), **D**: Sabel et al. (2005), **E**: Hanisch et al. (2003), **F**: Logan and Eglinton (1994), **G**: Huang et al. (1995), **H**: Schwark and Püttmann (1990), **I**: Bechtel and Püttmann (1992), **J**: Hauke et al. (1992a), **K**: Hauke et al. (1995), **L**: Arpino et al. (1971), **M**: Jacob et al. (2005), **N**: Jacob et al. (2007), **O**: Hauke et al. (1992b), **P**: D'Anjou et al. (2013), **Q**: Robinson et al. (1986)

Table 4.2 (continued)

Lake characteristics	Arborene-compounds reported	Interpretation precursor origins
Volcanic crater lake with an area of 4.5 km^2. Average depth 81 m, maximum depth ~90 m. Oligotrophic. Permanently anoxic hypolimnion.	*des*-A-arbor-9(11)-enes; *des*-A-arbora-5(10),9(11)-diene; *des*-A-arbora-5,7,9-triene; isoarborinol (trace)	Microbial
Origin lake due to faulting and damming of the Valencia river. Hypereutrophic lake with an area of 350 km^2. Average depth 19 m, maximum depth 40 m. Permanently anoxic hypolimnion.	*des*-A-arbor-9(11)-ene; *des*-A-arbora-5(10),9(11)-diene; isoarborinol; arborinone	Microbial
Volcanic crater lake with an area of 1.7 km^2. Depth between 10s-100s of meter. Hypereutrophic with a permanently anoxic hypolimnion.	isoarborinol; arborinone; *des*-A-arbora-5,7,9-triene; 24,25-dinorarbora-1,3,5(10),9(11)-tetraene; 24,25-dinorarbora-1,3,5,7,9-pentaene	Microbial
Small crater lake (< 1 km^2). Depth estimation of 160-210 m. Eutrophic, with a permanently anoxic hypolimnion.	arborinone, *des*-A-arbora-9(11)-ene, *des*-A-arbora-5,7,9-triene, 24,25-dinorarbora-1,3,5,7,9,11-hexaene, 24,25-dinorarbora-3,5,7,9-tertraene, 24,25-dinorarbora-1,3,5,7,9-pentaene, 24,25-dinorarbora-5,7,9-triene	Microbial
Volcanic crater lake with an area of 6 km^2. Average depth of 77 m, 175 m maximum. Trophic state is meso- to eutrophic, with a permanently anoxic hypolimnion.	isoarborinol; arborinone	Phytoplankton, other microbial origin possible
Drainage basin dammed by flood basalts. Deeper than 12 m. Trophic state is meso- to eutrophic, with a permanently anoxic hypolimnion.	isoarborinol; arborinone	Terrestrial interpretation in the cited studies, but microbial possible
Permanently anoxic hypolimnion.	*des*-A-arbor-8-ene; B-ring aromatized fernenes; *des*-A-arbora-5,7,9-triene; 24,25-dinorarbora-1,3,5(10),9(11)-tetraene; 24,25-dinorarbora-1,3,5,7,9-pentaene	Pre-angiosperm deposits, therefore interpreted as gymnosperm terrestrial origin (**H**, **I**), but possible microbial source. B-ring aromatized compounds are fernane-type (optical rotation), while the triene is from isoarborinol (NMR)
	isoarborinol; arborinone	-
Lake with an area < 2.5 km^2, and less than 12 m deep. Oligotrophic, no permanently anoxic hypolimnion.	arbor-9(11)-en-3β-ol methyl ester	Terrestrial
	des-A-arbora-5,7,9-triene	Microbial origin in pre-angiosperm deposits. Derived from fernenes (**O**) or derived from isoarborinol (**K**)
	des-A-arbora-5,7,9-triene; *des*-E-D:C-friedo-25-norhopa-5,7,9-triene; 25-norarbora(ferna)-triene; 24,25-dinorarbora(ferna)-1,3,5,7,9-pentaene; iso-25-norarbora(ferna)-1,3,5,7,9-pentaene	Microbial (bacterial) origin in pre-angiosperm deposits. Uncertain from arbora- or fernane-type triterpenoids.
Impact crater lake with an area of 110 km^2 and a depth of 175 m. Oligotrophic, no permanently anoxic hypolimnion.	isoarborinol	Terrestrial interpretation (**P**); microbial or phytoplankton origin not discussed but possible.
Lake with an area of 168 km^2, and a maximum depth of 42 m. Holomictic (no permanently anoxic hypolimnion), but with anoxic sediments.	isoarborinol; arborinone	Bacterial

of the hypereutrophic Lake Valencia. Analysis of SPM from Lake Valencia showed the absence of arborane-type triperpenoids (Jaffé et al., 1996), whereas these hydrocarbons occurred abundantly in the sediment. Isoarborinol derivatives from the Eocene Eckfeld Maar in Germany are also thought to have a bacterial origin and coincide with the occurrence of a diatom-rich community (Sabel et al., 2005), which is of interest since diatoms are also the dominant group of phytoplankton in Lake Chala. The occurrence of isoarborinol derivatives in other lacustrine deposits predating the development of angiosperm higher plants in the Cretaceous (Hauke et al., 1995; Borrego et al., 1997) is interpreted as a strong argument for a non-higher plant source of the precursor compounds.

Although most studies conclude that a microbial aquatic origin of arborane triterpenoids is most probable, in some settings a terrestrial origin is possible. For example, in Lake Caçó the arborane triterpenoids are of terrestrial origin (Jacob et al., 2007). Although Lake Caçó is a small, tropical, oligotrophic, freshwater lake like Chala, it is relatively shallow and has no permanent anoxic hypolimnion and is in that respect different to the small crater lakes where arborane triterpenoids are most likely of microbial aquatic origin (Table 4.2). In other lakes and shales, the interpretation of arborane derivatives as of terrestrial or aquatic origin is more ambiguous, for example when there is known input of fernane-type triterpenoids or when the depositional setting is different (e.g., the Kupferschiefer and Orbagnoux sites; see Table 4.2), or when the possibility of a microbial aquatic origin has not been studied. For example, *des*-A-arbor-8,9-enes from the Permian Kupferschiefer sediments have been interpreted as terrestrial, due to the large co-occurring quantities of bisaccate conifer pollen in the sedimentary record during anoxic freshwater depositional conditions (Bechtel and Püttmann, 1992). Using optical rotation techniques, Hauke et al. (1995) demonstrated that the arborenes/fernenes **IV** in these Permian sediments where in fact isoarborinol-derived transformation products. Therefore, co-occurrence of pollen and arborenes by no means excludes a microbial aquatic origin, but this is not discussed in the original study. Based on interpretation of isoarborinol $\delta^{13}C$ values a terrestrial origin has also been suggested for arborane compounds in the Miocene Clarkia deposits (Logan and Eglinton, 1994; Huang et al., 1995). However, isoarborinol from Clarkia is more depleted in ^{13}C (-28.0 to -28.4‰) than are terrestrial *des*-A-lupane (-25.1‰) and oleanane-triterpenoids (-26.2‰; Logan and Eglinton, 1994; Huang et al., 1995). Due to their biosynthetic pathway, triterpenoids in plants are 5-6‰ enriched in ^{13}C compared to straight-chain compounds (Diefendorf et al., 2012). When Clarkia $\delta^{13}C$ values of isoarborinol (-28.0 to -28.4‰) are compared to those of *n*-alkanes (-27.4 to -32.8‰) taking into account this triterpenoid enrichment, it is not evident that the isoarborinol is of terrestrial origin. An aquatic source of isoarborinol in Lake Clarkia is therefore more likely.

4.4.3.4 Aerobic production of *des*-A-arborenes precursors

The mere presence of ring-A degraded arborene-type triterpenoids in sediments indicates that their functionalized precursors must be produced by aerobic organisms in a (sub)oxic environment, because *des*-A-triterpenoids can only be formed when there is an oxygenated function present at C-3 (Lohmann et al., 1990). Triterpenoids with an oxygenated function at C-3 are formed by OSCs, which require oxidosqualene as the substrate. The biosynthesis of oxidosqualene requires molecular oxygen (Ourisson et al., 1982; Summons et al., 2006; Fischer and Pearson, 2007). This constrains the depth of production of the *des*-A-arborenes precursor(s) to the upper portion of the water column in Lake Chala, since the water column below 45-55 m is anoxic year-round. Oxygen penetration in the water column varies seasonally (Wolff et al., 2011, 2014; Buckles et al., 2014; van Bree et al., 2018b), and during some stratified periods, anoxic conditions extend upwards to ~15 m depth.

However, production of arborane triterpenoids in the modern-day water column of Lake Chala seems to be low. Isoarborinol is only present in trace amounts in settling particles and SPM, and *des*-A-arborenes were not detected at all. This makes the identification of a microbial production zone more challenging, although it is certain they are produced in the oxic or suboxic water column due to the aforementioned C-3 oxygenation. As the extent of the epilimnion and chemocline depth is seasonally variable, we do expect seasonal changes in the microbial production of isoarborinol, which may in turn be reflected in the variable concentration of arborane compounds in the sediment record (Fig. 4.3; see Section 4.5).

4.4.4 Transformation pathways of isoarborinol: abiotic diagenesis vs microbial transformations

A suite of transformation products of isoarborinol/arborinone occurs in the sedimentary record of Lake Chala, including mono-unsaturated (**1**-**4**), di-unsaturated (**5**) and tri-unsaturated/mono-aromatic (**6**) *des*-A-arborenes. One of the remaining questions is how these transformations from functionalized arborane triterpenoids to the *des*-A compounds take place, and if this is an abiotic or microbially-mediated process. Molecular mechanics calculations can help solve this question. If abiotic transformations occur, such as the loss of ring A and possible isomerization through tertiary carbocations, one may expect that the mixture of *des*-A-arborenes is either in thermodynamic equilibrium or approaches it with depth.

4.4.4.1 Microbial A-ring removal: diene formation

Des-A-arboradienes are probably the first product formed after A-ring removal. The process of A-ring removal is thought to be mediated by microbial activity under anoxic or reducing conditions (Lohmann et al., 1990; Jaffé and Hausmann, 1995; Jacob et al., 2007; Huang et al., 2008) and may yield four possible isomers of *des*-A-arboradienes: **IIa** to **IId** (Fig. 4.5), if we assume that double-bond isomerization can take place through allyl-stabilized tertiary carbocations after loss of ring A. In Lake Chala sediments we detected only one diene in high abundance (compound **6**) and only minor traces of three other dienes in some of the sedimentary horizons. Compound **6** is, therefore, likely 8βH-*des*-A-arbora-5(10),9(11)-diene **IIa**, which is the most likely microbial product of (iso)arborinol and/or arborinone after A-ring loss and by far the most stable diene isomer based on molecular mechanics calculations (Table 4.1). Hence, we cannot conclude that **IIa** or **IIb** is the dominant *des*-A-arbora-diene produced after the loss of ring A, or if this dominant diene results from other dienes upon double-bond isomerizations through tertiary carbocations.

4.4.4.2 Mono-unsaturated *des*-A-arborenes: abiotic isomerisation vs microbially induced variation

Des-A-arbor-monoenes are formed by hydrogenation of *des*-A-arboradienes. As the $\Delta^{5(10)}$ double-bond hydrogenation (from **IIa** to **IIIa**) is exothermic (Fig. 4.6), this process is likely to happen spontaneously. This could explain the dominance of compound **4** in Chala sediments (Fig. 4.3C), which most likely has the **IIIa** (8αH,10αMe-$\Delta^{9(11)}$) configuration. In the sedimentary record, we observe substantial variation in the distributions of mono-unsaturated *des*-A-arborenes but no distinct trend with time (Fig. 4.3C and F). When we compare the sedimentary distribution of these isomers with their modeled distribution at thermodynamic equilibrium (Table 4.1), we see that the *des*-A-arbora-monoene isomers present in Lake Chala sediments are not in thermodynamic equilibrium, nor is there a trend towards thermodynamic equilibrium over time. This also indicates that even over a time span of 25 kyr, there is no significant abiotic transformation between the *des*-A-arborene isomers. This implies that the four different monounsaturated *des*-A-arborenes are more likely formed microbially, either directly after the loss of ring A or after microbial

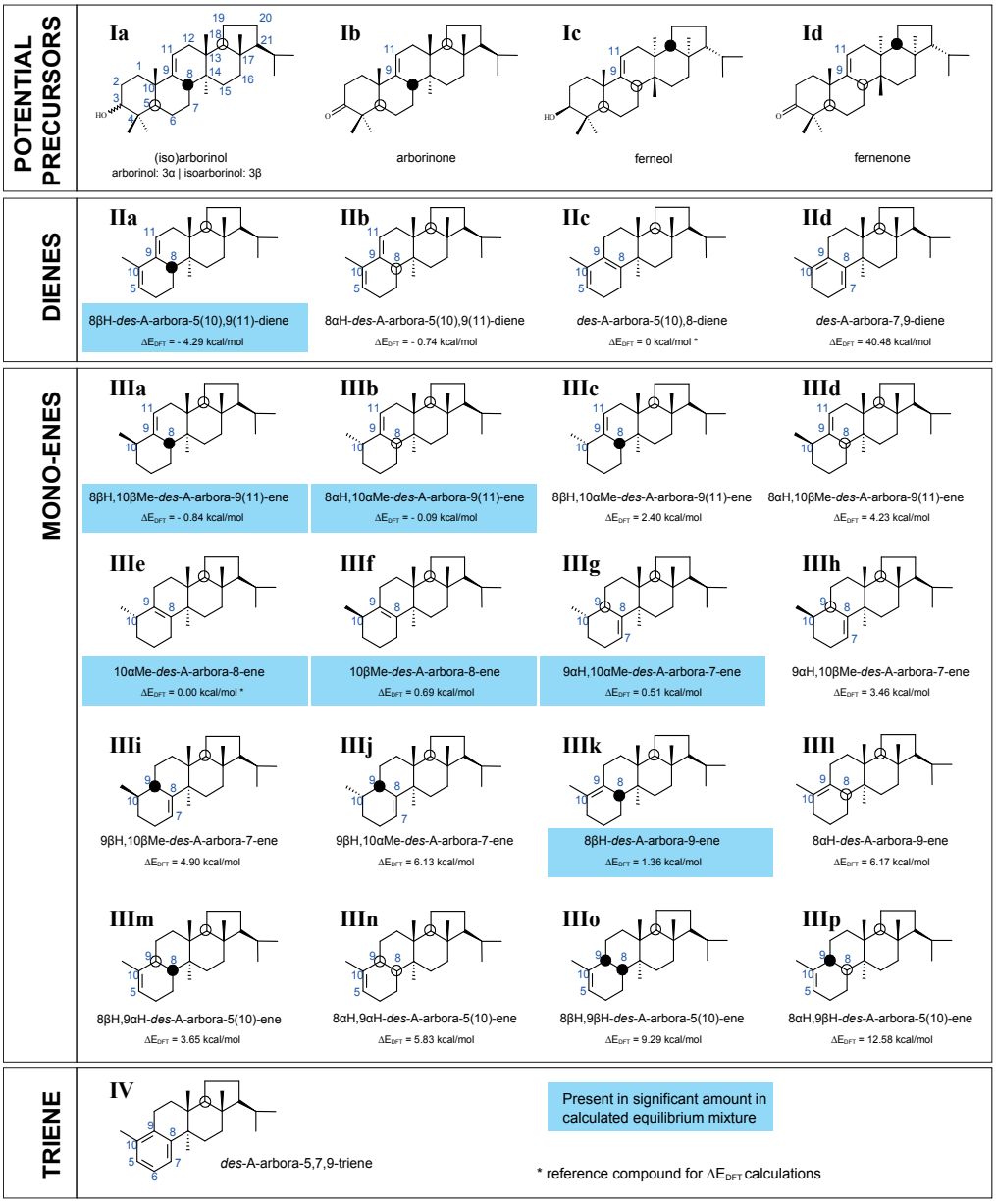

Figure 4.5 Molecular structures and configuration of potential precursors (**Ia**-**Id**), *des*-A-arbora-dienes (**IIa**-**IId**), *des*-A-arborenes (**IIIa**-**IIIp**) and *des*-A-arbora-triene (**IV**). Also indicated are the ΔE_{DFT} values calculated for the dienes and mono-enes relative to **IIc** and **IIIe**, respectively. Isomers accentuated in blue are present in significant amounts in the calculated equilibrium mixtures. The reference compounds for ΔE_{DFT} calculations (**IIc** and **IIIe**) are indicated with an asterisk (*).

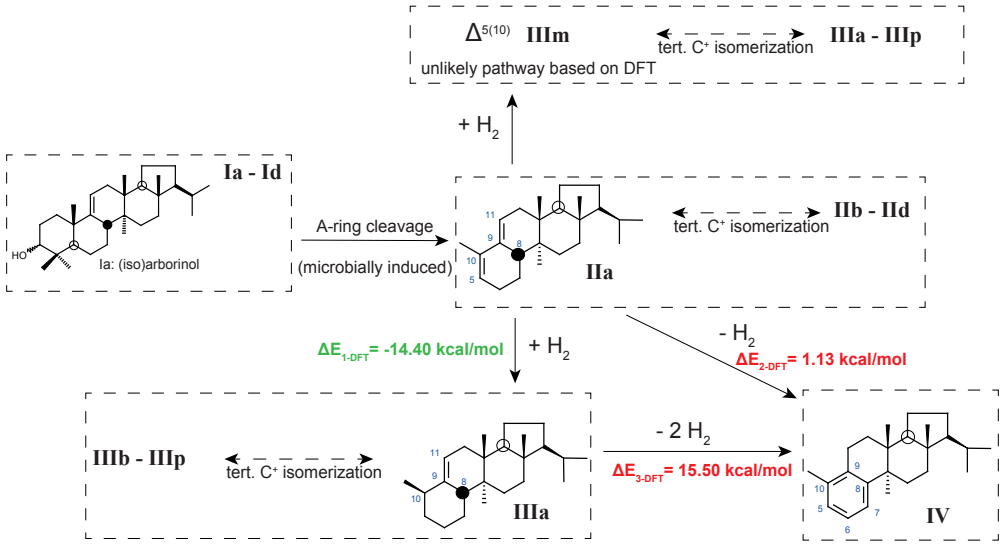

Figure 4.6 Schematic diagenetic pathway of (iso)arborinol. For clarification, only **Ia**-(iso)arborinol is depicted, but the pathways are valid for all possible parent compounds **Ia**-**Id**. Hydrogenation of the $\Delta^{9(11)}$ double bond is unlikely based on DFT calculations, but is depicted for completeness. Hydrogenation of **IIa** to **IIIa** is exothermic (green values), and the dehydrogenation of **IIa** and **IIIa** to **IV** is endothermic (red values). Tertiary C^+ isomerization is indicated where possible.

hydrogenation, and that the isomerization of double bonds via tertiary carbocations can be excluded as a transformation process. This implies further that spatial or temporal variations within the microbial community could be reflected in the different monoene distributions observed.

The $\Delta^{9(11)}$ arbora-monoene has four possible stereoisomers: 8αH,10αMe (**IIIa**), 8αH,10βMe (**IIIb**), 8βH,10αMe (**IIIc**), and 8βH,10βMe (**IIId**). Two *des*-A-arbora-monoenes (compounds **3** and **4**) in Lake Chala sediments have mass spectra similar to *des*-A-arbora-monoenes published previously (Jaffé and Hausman, 1995; Jacob et al., 2007). Double-bond positions in arborane-type compounds are however difficult to differentiate based on mass-spectrometric fragmentation patterns alone, as they are similar for isomers of various pentacyclic triterpenoids and their diagenetic derivatives (*cf.* Shiojima et al., 1992; Lavrieux et al., 2011). Therefore, mass spectrometry alone will not be able to distinguish all four stereoisomers. The order of elution of the various *des*-A-arborene isomers is also unknown. Since there is no thermodynamic equilibrium observed, it is not possible to use molecular mechanics calculations to determine the individual stereochemical isomers of the $\Delta^{9(11)}$-ene isomers.

In other lacustrine settings, only *des*-A-arborenes with a $\Delta^{9(11)}$ double bond have been described. In oil shales of the Duaringa Basin, Boreham et al. (1994) tentatively identified two *des*-A-arbor-9(11)-ene isomers with identical mass spectra but different retention times. 10αMe-*des*-A-arbor-9(11)-ene was tentatively identified in sediments of Lake Valencia (Jaffé and Hausmann, 1995) and Lake Caçó (Jacob et al., 2007). The identification of *des*-A-arborenes in all studies is tentative, and the stereochemistry at C-10 is either not discussed (Boreham et al., 1994)

or inferred to be 10αMe (Jaffé and Hausmann, 1995; Jacob et al., 2007), although 10βMe is the most stable isomer based on molecular mechanics calculations (Table 4.1). It can be expected that the most abundant compound **4** has the most stable configuration, which is 8βH,10βMe-*des*-A-arbor-9(11)-ene (**IIIa**), in contrast to **IIIc** (8βH,10αMe) that was postulated by Jaffé and Hausmann (1995). Further studies, based on synthesized *des*-A-arborenes, are required to elucidate the stereochemistry of these compounds.

4.4.4.3 Microbially induced *des*-A-arbor-triene formation

The mono-aromatic *des*-A-arborene **IV** occurs throughout the sedimentary record of Lake Chala (compound **5**, Fig. 4.3G). The transformation of dienes **II** and mono-enes **III** to the B-ring aromatized compound **IV** are strongly endothermic (Fig. 4.6), and although **IV** features an aromatic ring, and is therefore expected to be more stable than non-aromatic *des*-A-arborenes, molecular mechanics calculations indicate it is not. The strongly endothermic transformation must thus involve enzymatic and/or inorganic catalytic processes. The idea that micro-organisms can induce molecular aromatization is not new. For example, Wakeham et al. (1980) and Lohmann et al. (1990) stress the importance of microorganisms in the degradation of triterpenoid precursors to polycyclic aromatic hydrocarbons within sediments. In Lake Chala, **IV** is already present in the profundal surface sediments. This whole transformation process from A-ring removal to B-ring aromatization, therefore, must take place relatively rapidly, within 40 years. This is much faster than observed in Lake Valencia sediments (Jaffé and Hausmann, 1995), where only small amounts of the B-ring aromatized *des*-A-arborene were detected at 45 cm depth, indicating that it took ~180 years to form small amounts of this compound. This difference could be due to different microbial communities in the water column and sediments.

4.4.5 Application in paleoenvironmental reconstruction

As the transformation of isoarborinol and arborinone to the different *des*-A-arborenes depends on enzymatic action, it is likely that the microbial community is influenced by subtle spatial variation in the water-column environment and thereby the structures and relative abundances of *des*-A-arborenes in the sediment. These differences in microbial communities will be most pronounced between different lake systems, but also within one system, microbial communities will differ seasonally and along a depth gradient. Although these microbial changes are likely to occur on short spatial and temporal scales, sediments can record these changes cumulatively in the form of long-term trends, and hence examining absolute and relative changes in sedimentary *des*-A-arborene degradation products through time provide insight in some physical aspects of Lake Chala. As only low (trace) amounts of isoarborinol are found in Lake Chala at present, it is reasonable to assume that the vast majority of triterpenoids originally present have been subjected to microbial transformation. Therefore, the accumulation of *des*-A-arborenes in the sediment record can be used as proxy for the production rates of isoarborinol/arborinone in the water column. These parent compounds are most likely synthesized by aerobic bacteria residing just above the chemocline of the lake (Section 4.4.3).

To elucidate possible paleoclimatological and -environmental controls on the concentration of *des*-A-arborenes in Lake Chala sediments, this record is compared with two independent proxy records (Fig. 4.7) of climatic moisture balance (the precipitation/evaporation ratio), namely the seismic-reflection record of lake-level fluctuation (Moernaut et al., 2010) and the branched isoprenoid tetraether (BIT) index of past rainfall variations (Verschuren et al., 2009; Buckles et al., 2016). The concentration of *des*-A-arborenes is somewhat higher during inferred wetter periods,

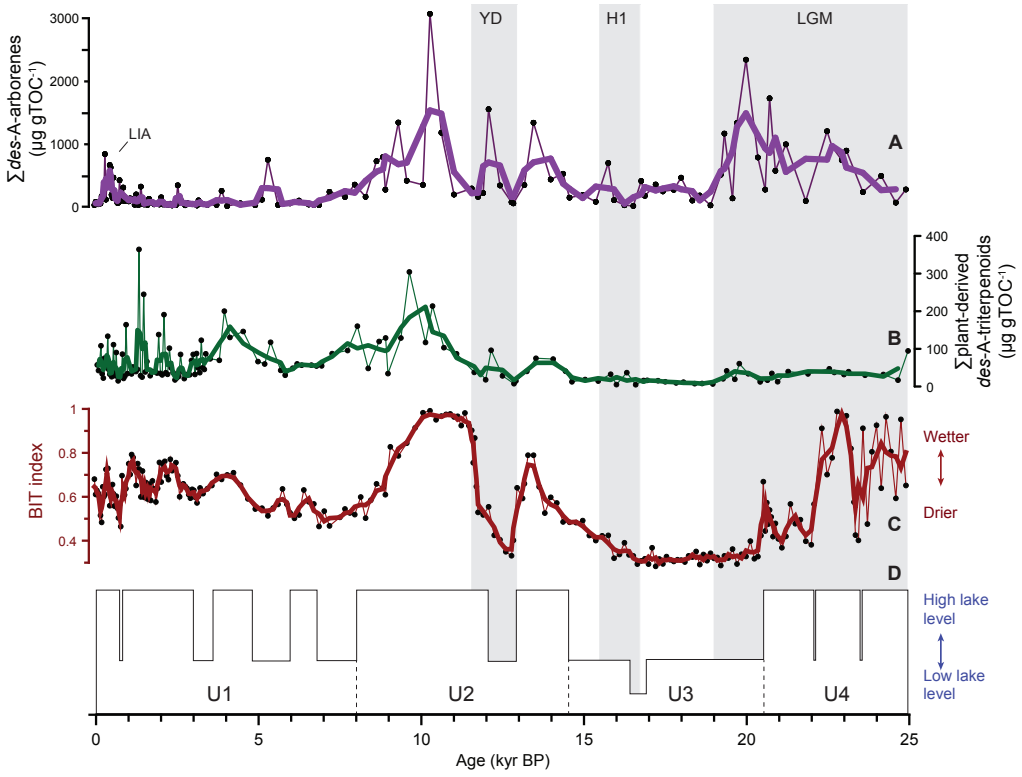

Figure 4.7 Summed concentration (in µg $gTOC^{-1}$) of *des*-A-arborenes in Lake Chala sediments (A), compared to the plant-derived *des*-A-triterpenoid record (µg $gTOC^{-1}$) (B), the BIT-index (C) record of Verschuren et al. (2009), and the seismic-reflection record of lake level high- and lowstands (D) (Moernaut et al., 2010). Shaded areas represent the Last Glacial Maximum (LGM: 26.5-19 kyr BP), Heinrich event H1 (16.8-15.4 kyr BP) and the Younger Dryas period (YD: 13-11.5 kyr BP). The Little Ice Age is also marked (LIA: 1270-1750 CE). Points connected by a thin line are individual data, while thicker lines represent a three-point moving average.

and lower during inferred drier periods (Fig. 4.7). While concrete evidence for a mechanistic link explaining this relation is not provided by this study, we can infer that *des*-A-arborene production must have been higher during times of more pronounced water-column stratification and/or higher precipitation than today. Variations over time between the different *des*-A-arborene compounds could indicate changes in the activity of different microbial assemblages producing and degrading isoarborinol or arborinone. It would be interesting to compare the proliferation of microbial communities in different lake systems where *des*-A-arborenes and their precursors have been found, as this could be informative to understand the subtleties in microbial transformation patterns of isoarborinol/arborinone. Future metagenomic studies of the modern lake system of Lake Chala and its sediments may reveal the connection between microbial communities and isoarborinol production and its microbial transformations.

4.5 Conclusion

The sedimentary record of Lake Chala contains a variety of transformation products of pentacyclic triterpenoids with an arborane skeleton. The functionalized triterpenoids are synthesized by an unverified microbial source in the water column, most likely algae or aerobic bacteria. After production in the (sub)oxic water column, microbially mediated A-ring loss of isoarborinol/arborinone occurs in the suboxic/anoxic water column, producing 8βH-*des*-A-arbor-5(10),9(11)-diene, which is hydrogenated forming predominantly 8βH-10βMe-*des*-A-arbor-9(11)-ene. The process of aromatization from mono- and di-unsaturated *des*-A-arborenes to *des*-A-arbor-5,7,9-triene is endothermic, and therefore most likely microbially mediated. Although their precise biological source remains unknown, *des*-A-arborenes are specific biomarkers with high preservation potential in the anoxic sediments of Lake Chala, and in the anoxic sediments of similar small, tropical crater lakes with permanently anoxic hypolimnion. The varying proportion of *des*-A-arborenes in these systems could be a reflection of subtle differences in the physical parameters of the water column along the depth gradient, resulting in changing microbial communities and activity. Differences in arborane-type triterpenoids and their distribution patterns between different lakes, both extant and in the geological past, are likely due to different microbial communities producing and transforming isoarborinol and/or arborinone and *des*-A-arborenes with one, two and three unsaturations.

Acknowledgements
We thank A. Diefendorf and one anonymous reviewer for their constructive feedback on this manuscript, and J. Jacob and an anonymous reviewer for extensive feedback on a previous version of this work. C.M. Oluseno is thanked for field assistance, and M. Baas, A. Mets, J. Ossebaar, and M. Verweij for their technical assistance at the Royal NIOZ. N.A. Al-Dhabi is thanked for plant-derived triterpenoid analysis of soils. This study was carried out with permission of the Permanent Secretary of the Ministry of Education, Science and Technology of Kenya under research permit 13/001/11C to D.V. The fieldwork was performed as part of the ESF EuroClimate project CHALLACEA, financially supported by grants from the Dutch Organization for Scientific Research (NWO) and FWO Vlaanderen (Belgium) to J.S.S.D. and D.V., respectively. The work was supported by funding from the Netherlands Earth System Science Center (NESSC) through a gravitation grant (NWO 024.002.001) from the Dutch Ministry for Education, Culture and Science to J.S.S.D.

Appendix 4.1: ReaxFF

Introduction

Over the last decade, the capability of the ReaxFF method has been well demonstrated in a wide range of systems including catalysis, combustion, pyrolysis, batteries, and other complex chemical systems (Chenoweth et al., 2008, 2009; Salmon et al., 2009b; Ding et al., 2013; Fan et al., 2013; Monti et al., 2013; Raju et al., 2013; Islam et al., 2014; Golkaram and van Duin, 2015; Verlackt et al., 2015). A detailed description of the ReaxFF method can be found elsewhere (van Duin et al., 2001; Chenoweth et al., 2008; Senftle et al., 2016). The ReaxFF molecular force field has been employed in a number of geochemical and microbiological studies, such as the cyclization of isorenieratene to its tetracyclic derivatives (van Duin and Sinninghe Damsté, 2003), thermal decomposition of the algaenan *Botryococcus braunii* race L biopolymer (Salmon et al., 2009a), and the stereochemistry of

Table A.4.1. Double-bond and stereoisomers of *des*-A-arborenes, -diene and -triene, with calculated ReaxFF and DFT energy. Isomers marked with an * are significantly present in equilibrium compositions calculated at 298K approximating negligible entropic contribution, and their equilibrium composition (%) is calculated for mono-enes and dienes separately. ΔE was calculated compared to compounds **IIc** and **IIIe**, marked with an #.

	des-A-arborene double-bond position	Stereoisomer configuration	DFT (kcal/mol)	ΔE_{DFT} (kcal/mol)	DFT-%	ReaxFF (kcal/mol)	ΔE_{ReaxFF} (kcal/mol)	ReaxFF-%
IIa	$\Delta^{5(10),9(11)}$	8βH	-588380.49	-4.29 *	99.9	-7182.80	7.00	-
IIb	$\Delta^{5(10),9(11)}$	8αH	-588376.94	-0.74	-	-7179.70	10.10	-
IIc	$\Delta^{5(10),8}$	-	-588376.80	# 0.00	-	-7189.80	# 0.00 *	99
IId	$\Delta^{7,9}$	-	-588335.71	40.48	-	-7169.70	20.10	-
IIIa	$\Delta^{9(11)}$	8βH,10βMe	-589145.22	-0.84 *	57.47	-7331.00	**1.02** *	9.75
IIIb	$\Delta^{9(11)}$	8αH,10αMe	-589144.48	-0.09 *	16.43	-7330.50	**1.52** *	4.19
IIIc	$\Delta^{9(11)}$	8βH,10αMe	-589141.99	2.40	0.24	-7328.20	3.82	0.09
IIId	$\Delta^{9(11)}$	8αH,10βMe	-589140.16	4.23	0.01	-7326.30	5.72	0.00
IIIe	Δ^{8}	10αMe	-589144.39	# 0.00 *	14.02	-7332.02	# 0.00 *	54.61
IIIf	Δ^{8}	10βMe	-589143.70	**0.69** *	4.39	-7330.70	**1.32** *	5.88
IIIg	Δ^{7}	9αH,10αMe	-589143.88	**0.51** *	5.95	-7331.45	**0.57** *	20.85
IIIh	Δ^{7}	9αH,10βMe	-589140.93	3.46	0.04	-7329.45	2.57	0.71
IIIi	Δ^{7}	9βH,10βMe	-589139.49	4.90	0.00	-7328.14	3.88	0.08
IIIj	Δ^{7}	9βH,10αMe	-589138.26	6.13	0.00	-7327.38	4.64	0.02
IIIk	Δ^{9}	8βH	-589143.02	**1.36** *	1.41	-7330.41	**1.61** *	3.6
IIIl	Δ^{9}	8αH	-589138.22	6.17	0.00	-7327.68	4.34	0.04
IIIm	$\Delta^{5(10)}$	8βH,9αH	-589140.74	3.65	0.03	-7328.47	3.55	0.14
IIIn	$\Delta^{5(10)}$	8αH,9αH	-589138.55	5.83	0.00	-7327.84	4.18	0.05
IIIo	$\Delta^{5(10)}$	8βH,9βH	-589135.09	9.29	0.00	-7323.85	8.17	0.00
IIIp	$\Delta^{5(10)}$	8αH,9βH	-589131.80	12.58	0.00	-7321.73	10.29	0.00
IV	$\Delta^{5,7,9}$	-	-587639.18	-	-	-7065.75	-	-

crenarchaeol (Sinninghe Damsté et al., 2002), a glycerol dibiphytanyl glycerol tetraether (GDGT) membrane lipid of thaumarchaeotal origin. In these studies, ReaxFF calculations highlighted the reaction pathways and the corresponding reaction energies for the conversion of isomers, reaction mechanisms of pyrolysis of the biopolymer, as well as the effect of the cyclohexane moiety on the dense packing of biphytanyl chains in GDGT membrane lipids of thaumarchaeota (Sinninghe Damsté et al., 2002).

Methods

The molecular mechanics calculations were performed using the ReaxFF reactive force field method. ReaxFF is a general bond order (BO) (Abell, 1985; Tersoff, 1988; Brenner, 1990) based empirical force field method, which allows on-the-fly bond breaking and formation during simulations. All the bonded (2-, 3-, and 4-body) interactions are calculated as a function of BOs. Non-bonded interactions, i.e. the van der Waals and Coulomb, are calculated between every pair of atoms. Excessive repulsion at short distances is circumvented by adding a shielding parameter in non-bonded energy expressions (Liang et al., 2013). A seventh order taper function in the non-bonded interaction energies is used to eliminate any energy discontinuity (van Duin et al., 2003). This treatment of non-bonded interactions enables ReaxFF to describe a wide range of covalent, ionic, and intermediate materials and a greater transferability (Nielson et al., 2005). The ReaxFF{C/H} parameters developed by Chenoweth et al. (2008) are used in this study. Sixteen different stereo-isomeric configurations of *des*-A-triterpenes are investigated for their relative stabilities and their equilibrium mixture compositions at room temperature. The structural relaxation simulations were performed using a conjugate gradient based energy minimization scheme with a root mean square gradient (RMSG) of the system energy equal to 0.25 (kcal/mol)/Å as convergence threshold.

Results and discussion

ReaxFF calculations predict the **IIc** isomer as the most stable diene structure, dominating the equilibrium mixture by ~99%. Hydrogenation of this isomer would yield **IIIe** (the most stable monoene isomer based on ReaxFF) and **IIIf** isomers, both of which are expected in significant amounts in the monoene equilibrium mixture. Generally, the ReaxFF and DFT methods are in agreement, but the *des*-A-arbor-dienes are an exception. For example, when we compare the stability of **IIc** based on ReaxFF to the DFT calculations that indicates a dominance of **IIa** that would mainly yield **IIIa** after hydrogenation (Table A.4.1; Fig. 4.5). Overall, ReaxFF predict stabilities of **IIIa**, **IIIb**, **IIIe**, **IIIf**, **IIIg** and **IIIk** that are within 2 kcal/mol, and predicts their presence in a mono-ene equilibrium mixture. This is similar to the DFT calculations. We calculated the ReaxFF inter-conversion energetics for the most stable structures **IIc** and **IIIe**. This indicates an exothermic **IIc** to **IIIe** conversion process ($\Delta E_{1\text{-ReaxFF}}$ = -33.4 kcal/mol), and endothermic **IIc** to **IV** ($\Delta E_{2\text{-ReaxFF}}$ = 13.6 kcal/mol) and **IIIe** to **IV** ($\Delta E_{3\text{-ReaxFF}}$ = 48.90 kcal/mol) conversions. Both ReaxFF and DFT calculations predict qualitatively a similar trend with the exothermic diene-to-monoene conversion, and endothermic diene-to-triene and monoene-to-triene conversions, even though these inter-conversion energetics are calculated for the most stable structures of monoenes and dienes that are different for the ReaxFF (**IIc**-**IIIe**-**IV**) and DFT (**IIa**-**IIIa**-**IV**) methods.

Wooden rowing boat used for all monthly water column sampling on the shore of Lake Chala, September 2014. Home-made production by field assistant Caxton.
Photo credit: F. Peterse

5 Seasonal variability in the abundance and stable carbon-isotopic composition of lipid biomarkers in suspended particulate matter from a stratified equatorial lake (Lake Chala, Kenya/Tanzania): Implications for the sedimentary record

L.G.J. van Bree, F. Peterse, M.T.J. van der Meer, J.J. Middelburg, A.M.D. Negash, W. De Crop, C. Cocquyt, J.J. Wieringa, D. Verschuren and J.S. Sinninghe Damsté

adapted from: *Quaternary Science Reviews* 192, 208-224 (2018)

Abstract

We studied the distribution and stable carbon-isotopic ($\delta^{13}C$) composition of various lipid biomarkers in suspended particulate matter (SPM) from the water column of Lake Chala, a permanently stratified crater lake in equatorial East Africa, to evaluate their capacity to reflect seasonality in water-column processes and associated changes in the lake's phytoplankton community. This lake has large seasonal variation in water-column dynamics (stratified during wet seasons and mixing during dry seasons) with associated phytoplankton succession. We analyzed lipid biomarkers in SPM collected monthly at 5 depths (0-80 m) from September 2013 to January 2015. Seasonal variation in total phytoplankton biovolume is strongly reflected in the concentration of phytadienes, a derivative of the general photosynthetic pigment chlorophyll. The wax and wane of several specific biomarker lipids between June and December 2014 reflect pronounced phytoplankton succession after deep mixing, starting with a long and sustained chlorophyte bloom (reflected by $C_{23:1}$, $C_{25:1}$ and $C_{27:1}$ *n*-alkenes, and C_{21} and C_{23} *n*-alkanes), followed by a peak in diatoms between July and October (loliolide and isololiolide), and then eustigmatophytes (C_{30} and C_{32} 1,15 *n*-alkyl diols) once stratification resumes in October. Peak abundance of the $C_{19:1}$ *n*-alkene during shallow mixing of the water column in January-February 2014 can be tentatively linked to the seasonal distribution of cyanobacteria. The concentration, seasonal variability and low $\delta^{13}C$ values of the C_{28} fatty acid in the SPM suggest that this biomarker is produced in the water column of Lake Chala instead of having the typically assumed vascular plant origin. The $\delta^{13}C$ signature of particulate carbon and all aquatic biomarkers become increasingly more negative (by up to 16‰) during mixing-induced episodes of high productivity, whereas enrichment would be expected during such blooms. This reversed fractionation may be attributed to chemically enhanced diffusion, which generates depleted HCO_3^- under high pH (>9) conditions, as occur in the epilimnion of Lake Chala during periods of high productivity. The influence of this process can potentially explain previously observed ^{13}C-depleted carbon signatures in the paleorecord of Lake Chala, and should be considered prior to paleorecord interpretation of organic-matter $\delta^{13}C$ values derived (partially) from aquatic organisms in high-pH, i.e. alkaline, lakes.

5.1 Introduction

Lipid biomarkers are organic molecules used as indicators for the past presence of certain organisms and consequently for the past environmental conditions in which these organisms occur. For example, long-chain fatty acids ($\geq C_{24}$) and *n*-alkanes ($\geq C_{23}$) are major components of terrestrial higher (vascular) plant leaf waxes (Eglinton and Hamilton, 1967), and are, therefore, often used as biomarkers for vascular plants (e.g., Tierney et al., 2011; Sinninghe Damsté et al., 2011b). Similarly, short-chain fatty acids and *n*-alkanes ($<C_{21}$) are general phytoplankton biomarkers (e.g. Gelpi et al., 1970; Meyers, 1997; Volkman et al., 1998), mid-chain *n*-alkanes (C_{21}-C_{25}) are often used as biomarkers for aquatic macrophytes (Ficken et al., 2000), and 1,15 *n*-alkyl diols are biomarkers for Eustigmatophyte algae (Volkman et al., 1992; Versteegh et al., 1997; Rampen et al., 2014; Villanueva et al., 2014).

The stable carbon-isotopic composition ($\delta^{13}C$) of these lipid biomarkers may provide further information on their origin or environmental conditions at the time of their production, and are, therefore, increasingly used in paleoclimate reconstructions (Castañeda and Schouten, 2011; Berke et al., 2012; Leng and Henderson, 2013). For example, terrestrial plants can follow several pathways of carbon fixation (C_3, C_4 and crassulacean acid metabolism (CAM)), each resulting in a different degree of fractionation of atmospheric CO_2 (Collister et al., 1994; Hobbie and Werner, 2004; Diefendorf and Freimuth, 2017). As a result, analyzing compound-specific $\delta^{13}C$ of leaf waxes preserved in a lake-sediment record can be used to reconstruct vegetation history (e.g. Sinninghe Damsté et al., 2011b), whereas the hydrogen isotopic composition (δD) of these leaf waxes provides additional information on past hydroclimate (e.g. Tierney et al., 2008). The $\delta^{13}C$ signature of biomarkers specific to phytoplankton can be used to trace their inorganic carbon source and the fractionation during carbon fixation (Castañeda and Schouten, 2011).

Lake sediments are a prominent archive for long-term continental paleoclimate reconstructions (Castañeda and Schouten, 2011), and especially so in tropical regions, where long ice-core and speleothem records are scarce (Verschuren, 2003; Verschuren and Russell, 2009). Organic biomarkers stored in lake sediments reflect ambient climate conditions such as temperature and precipitation prevailing in the lake's catchment at the time of their deposition. Hence, down-core variations in the occurrence, distribution, and isotopic composition of these biomarkers are increasingly used as proxies to reconstruct paleoclimate (e.g. Huang et al., 1999; Tierney et al., 2011; Berke et al., 2012). In order to strengthen the interpretation of such proxy records it is critical to understand the origin(s) and spatiotemporal variations of lipid biomarkers in modern lakes (e.g. Castañeda and Schouten, 2011). Studies documenting the distribution of specific biomarkers in sediment-trap material over a complete annual cycle, or in suspended particulate matter (SPM) along a depth profile in a stratifying lake, have improved insight in the validity of these compounds as paleoenvironmental proxies. For example, in both tropical and temperate lakes (e.g. Buckles et al., 2013, 2014; Loomis et al., 2014b) the seasonal distribution of glycerol dialkyl glycerol tetraether (GDGT) membrane lipids has revealed unexpected complexity, with important implications for GDGT-based paleothermometry. This situation calls for more detailed investigations, in which the occurrence of a large range of biomarkers is analyzed both over the complete water column and through the annual cycle, and is subsequently linked to changes in environmental conditions and the composition of the lake's living microbial community.

In this study, we determine the distribution and stable carbon-isotopic composition of lipid biomarkers present in SPM from the permanently stratified water column of Lake Chala in equatorial East Africa, over a 17-month period. This tropical lake has been well-monitored,

offering an excellent setting to link biomarker dynamics to water-column processes and microbial-community composition, especially in the light of future studies using lipid biomarker proxies preserved in its sedimentary record. Unique in its extent, this study provides a first thorough assessment of the occurrence and sources of organic biomarkers in lakes.

5.2 Material & Methods

5.2.1 Study site

Lake Chala (locally 'Challa', after a nearby village) is a ~90 m deep and relatively unproductive crater lake on the border of Kenya and Tanzania (3°19′S, 37°42′E; Fig. 5.1). It is situated at ~880 m above sea level, on the lower east slope of Mt. Kilimanjaro. It has a surface area of ~4.5 km² and features a permanently stratified (meromictic) water column. As the Inter-Tropical Convergence Zone (ITCZ) is passing over the region twice a year, Lake Chala has two rain seasons, with relatively heavy 'short' rains from October to December and 'long' rains from March to May (Nicholson, 2000; Verschuren et al., 2009). The seasonal cycle of stratification and mixing in Lake Chala's water column is mainly driven by variation in air temperature and wind speed (Buckles et al., 2014; Wolff et al., 2014), with low wind speeds during the warm rain seasons leading to stratified water-column conditions, while higher wind speeds during dry seasons cause mixing, particularly during the colder southern-hemisphere winter of June-September. Evaporation (~1700 mm yr^{-1}) is higher than local precipitation (~600 mm yr^{-1}; Payne, 1970). As the small crater catchment also provides only limited surface inflow, the lake is maintained mainly by subsurface groundwater input, probably originating from Mt. Kilimanjaro's forest belt (Hemp, 2006). Mean air temperatures are lowest in July-August (20-21°C), and highest in January-February (25-27°C), while water-column temperature ranges from 22°C to 28°C (Buckles et al., 2014, 2016). Water-column mixing extends down to 40-60 m depth during the main dry season, depending on wind speed and air temperature (Verschuren et al., 2009). The resulting convective upwelling brings nutrients to the surface, which subsequently initiates phytoplankton blooms.

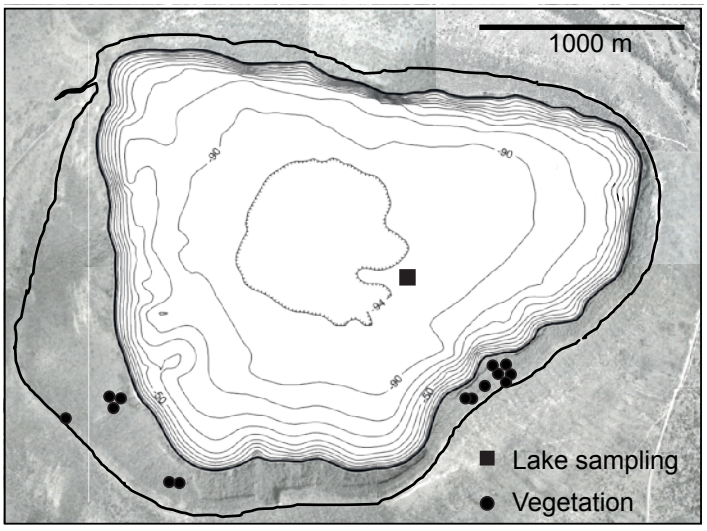

Figure 5.1 Location of the measurements of the physical water-column properties and the sampling of suspended particulate matter (SPM), phytoplankton, TIC and PC (black square) in Lake Chala; and locations of terrestrial vegetation sampling inside the crater catchment (black circles). Crater-basin map and bathymetry from Moernaut et al. (2010).

5.2.2 Field observations and sample collection

5.2.2.1 Water-column monitoring

The water column of Lake Chala was monitored at approximately four-week intervals at an offshore location 03°19.064′S, 37°42.147′E (Fig. 5.1). Physical-property profiles of the upper 50 m of the water column were collected at 1 m (0-24 m) and 2 m (24-50 m) intervals using a Hydrolab Quanta® Multiprobe which registered temperature, dissolved oxygen (DO), conductivity (K25) and pH. The pH data were corrected for drift between calibrations. Further, an air pocket in the DO sensor created unreliable DO data in the oxygenated part of the water column between 30 April and 30 June 2014.

5.2.2.2 Total Inorganic Carbon (TIC)

TIC samples were collected at the same location as the physical-property profiles, on or close to the first day of each month between September 2013 and January 2015, and from a total of 13 water depths (0, 10, 20, 25, 30, 35, 40, 45, 50, 60, 70, 80 and 90 m depth; total n = 221). Lake water was collected unfiltered in airtight 12 ml exetainer vials pre-poisoned with mercury chloride, and stored at room temperature. Months mentioned in the text refer to a sampling or observation date at the start of that month, or, in some cases, at the end of the previous month. The precise sampling dates are listed in Table S5.2.

5.2.2.3 Suspended Particulate Matter (SPM)

SPM was collected according to the same schedule as TIC. At each depth, between 5 and 10 L of water was collected using an UWITEC water sampler. The water samples were transported in dark plastic jerrycans, filtered over pre-combusted GF/F filters (142 mm ø; Whatman) and stored frozen on the same day. The SPM samples were transported to Utrecht University on dry ice, where the filters were freeze-dried.

5.2.2.4 Terrestrial vegetation

Leaves from 49 plants were collected on the crater rim and near the shoreline on the Kenyan side of Lake Chala during the dry season in September 2014. The leaves were stored frozen prior to transport on dry ice, and freeze-dried at Utrecht University. Species identification was done at the National Herbarium of the Netherlands; 28 plants were identified to species level, three to genus level and five to family level, while 13 remain unidentified. Six specimens were deposited in the herbarium and can be consulted online (http://bioportal.naturalis.nl/).

5.2.2.5 Phytoplankton

Quantitative phytoplankton samples (n = 85) were taken at five depth intervals (0, 5, 10, 15 and 20 m depth) in 100 ml vials, parallel to the SPM collection but as part of an independent study of phytoplankton dynamics (C. Cocquyt, unpublished data). Immediately after collection, the lake water was fixed with an alkaline Lugol's solution prior to adding formalin.

5.2.3 Sample preparation and instrumental analyses

5.2.3.1 Bulk carbon properties

Each filter (n = 221) was subsampled for particulate carbon (PC) content and carbon-isotopic composition ($\delta^{13}C_{PC}$), by punching out small circles (5 mm ø). Plant samples were visually checked to remove possible contaminants such as insects and subsequently freeze-dried. A subsample of each plant was powdered for bulk organic carbon (OC) content and $\delta^{13}C$ analysis. Bulk OC

(PC in case of SPM) and $\delta^{13}C$ of SPM and plants was measured using an elemental analyzer (Fisons Instruments NA1500), coupled online to an IRMS (Thermo Delta$^+$). Samples were not acidified prior to analysis, therefore representing a mixture of organic and inorganic PC in the SPM. Reproducibility of PC content was typically <0.03 µg L^{-1} (n = 12) for SPM, and 0.5% for OC in vegetation (n = 7). Reproducibility of $\delta^{13}C$ measurements was usually better than 0.1‰ based on in-house standards (nicotinamide and graphite quartzite), and <0.4‰ for PC duplicates (n = 20) for SPM, and 0.1‰ for vegetation (n = 7).

5.2.3.2 Total inorganic carbon

TIC concentrations in lake water were measured on a Shimadzu TOC-5050A carbon analyzer. Concentrations were calibrated using an in-house seawater standard (precision <0.3 mg L^{-1}). Replication of samples was better than 1.2 mg L^{-1} (n=8). For $\delta^{13}C$ analysis of TIC, H_3PO_4 was added to vials, and vials were flushed with helium. The subsequent addition of lake water created CO_2 gas that was measured for $\delta^{13}C$ using a gas bench coupled online to an IRMS (Thermo Delta V advantage). The $\delta^{13}C$ values are reported against VPDB, using Li_2CO_3 (IAEA) and Na_2CO_3 (in-house) as standards.

5.2.3.3 Biomarkers

SPM filters from 0, 10, 25, 50 and 80 m depth (n = 85) were extracted using a modified Bligh-Dyer method (*cf.* Buckles et al., 2013). The extract was acid-hydrolyzed using 1.5N hydrochloric acid (HCl) in methanol (MeOH; 2 h reflux at 70°C) with a known carbon isotopic composition (determined offline), and then separated into apolar, fatty-acid and polar fractions, using an activated Al_2O_3 column with hexane/dichloromethane (DCM) (9:1, v/v), DCM, and DCM/MeOH (1:1, v/v) as eluents, respectively. An aliquot of the apolar fractions was passed over an Ag^+-impregnated silicagel column with hexane and ethyl acetate (EtOAc) as eluents, respectively, to separate the saturated and unsaturated hydrocarbons.

A subset of 14 plants was selected for fatty acid analysis based on their $\delta^{13}C_{bulk}$ values (which revealed the plant's biosynthetic pathway) and habitat. Between 0.1 and 1.6 g dry weight of the leaves of each plant species was cut into small pieces, extracted ultrasonically with DCM/MeOH (2:1, v/v), and dried under a stream of N_2. An aliquot of total lipid extract was acid-hydrolyzed and separated following the same approach as for the SPM.

The apolar, fatty acid and polar fractions of SPM, as well as the fatty acid fractions of the plant samples were analyzed with a known amount of standard (pristane or 5α-cholestane) added for quantification on a gas chromatograph (GC) coupled to a flame ionization detector (GC-FID; Hewlett Packard 6890 series). All fatty acids were measured as their methyl-ester derivatives. The samples (in hexane or EtOAc as solvent) were injected on-column at 70°C, with helium as carrier gas with a flow rate of 2 ml min^{-1}. The oven was programmed to 130°C at 20°C min^{-1}, and then at 4°C min^{-1} to 320°C at which it was held isothermal for 10 min. Selected samples were analyzed on a GC-mass spectrometer (GC-MS; Finnigan Trace GC Ultra, DSQ MS) for compound identification, with similar column properties and temperature program as the GC analysis. The mass spectral identification of biomarkers was based on comparison with a NIST library and interpretation of mass fragmentation patterns. Double-bond positions were determined by forming the adduct with dimethyl-disulfide (DMDS) and subsequent mass spectral interpretation of the products formed (Francis, 1981). Based on the GC analyses, n-alkane average chain length (ACL), carbon preference index (CPI) and P_{aq} were calculated as:

$$CPI = 0.5 \cdot [(\Sigma C_{25\text{-}33\text{-}odd}/\Sigma C_{26\text{-}34\text{-}even}) + (\Sigma C_{25\text{-}33\text{-}odd}/\Sigma C_{24\text{-}32\text{-}even})]$$

$$ACL = \Sigma(C_n \cdot n)/\Sigma C_n, \text{ where } C_n \text{ is the abundance of each } n\text{-alkane with } n \text{ carbon atoms (23 to 35)}$$

$$P_{aq} = (C_{23}+C_{25})/(C_{23}+C_{25}+C_{29}+C_{31})$$

Selected fractions for compound-specific $\delta^{13}C$ measurement were injected on a GC combustion isotope-ratio-monitoring mass spectrometer (GC-C-irMS), Thermo Scientific Trace 1310 GC coupled to a Delta V mass spectrometer via an Isolink II and Conflo IV. The gas chromatograph was equipped with a PTV injector in on-column mode (on-column liner, glass, S+H Analytic, Germany) connected to a fused silica capillary column (l = 25 m; O.D. 0.32 mm) coated with CP Sil-5 (film thickness = 0.12 µm) with helium as carrier gas at a constant flow of 2 ml min^{-1}, and a similar temperature program as GC analysis, except for an additional 10 min hold at 320°C for the plant samples. GC-C-irMS performance was checked daily by injecting an in-house GC standard combined with two fully deuterated *n*-alkanes (C_{18} and C_{24}) with known isotopic composition (IAEA). The reported values are based on at least duplicate analyses, with results averaged to obtain a mean value and standard deviation. Reproducibility is typically better than 0.7‰. $\delta^{13}C$ values are reported against the VPDB standard, with those of fatty acid methyl esters corrected for the carbon atom added during methylation. Due to co-elution with other compounds, such as non-specified triterpenoids, two of the 14 selected plant extracts were not suitable for $\delta^{13}C_{FAME}$ analysis.

5.2.3.4 Phytoplankton abundance

The major groups of pelagic phytoplankton (chlorophytes, diatoms, dinophytes, euglenophytes, chrysophytes, cryptophytes and cyanobacteria) were identified and counted with an inverted Olympus CKX41 microscope equipped with an Olympus UC30 digital camera, following the Utermöhl method (Utermöhl 1931, 1958) using sedimentation chambers of 10 ml. At least 500 solitary phytoplankton cells (≥3 µm) or colonies were counted per sample, as well as the number of cells per colony. The total biovolume of each taxon present was calculated based on mean cell dimensions of the phytoplankton species, and expressed in $\mu m^3\ L^{-1}$. Euglenophytes and dinophytes are excluded from total phytoplankton biovolume due to their heterotrophic and assumed heterotrophic nature, respectively, in Lake Chala. The biovolume values were averaged across multiple sampled depths to eliminate missing values, both over the 0-10 m interval as conservative measure of the standing biomass of actively photosynthesizing phytoplankton (being proportional to primary productivity), and over the 0-20 m interval for optimal correlation with the taxon-specific biomarker concentrations. At times during the year when the latter interval extends below thermocline depth (Fig. 5.2), some of the phytoplankton encountered at 15 and 20 m depth must represent recently dead or dying cells in the process of sinking.

5.3 Results & Discussion

5.3.1 Physical and chemical properties of the water column

5.3.1.1 Mixing and stratification

Variations in physical water-column properties over the period September 2013 to January 2015 (Fig. 5.2) mostly reflect the seasonal cycle of mixing and stratification. Changes in stratification are revealed by the temperature profiling (Fig. 5.2A), with high surface temperatures

during stratification and lower surface temperatures particularly during the periods of deep mixing. Dissolved oxygen (DO) concentrations are influenced by oxygen diffusion from the atmosphere, temperature-driven convection, primary productivity, and oxygen consumption by the remineralization of organic matter. This interaction results in the DO profiles (Fig. 5.2B) being characterized by i) a shallow oxycline (between 15 and 30 m depth) during water-column stratification until June 2014, ii) oxic conditions extending down to ~40 m during July to September 2014 when deep mixing coincided with peak primary productivity, and iii) subsequent shallowing of the oxycline from October 2014 onwards due to the onset of stratification and enhanced remineralization after the algal-bloom period has ended. The difference in conductivity between epilimnion and hypolimnion over the studied interval ranges between 15 and 43 µS cm^{-1} (Fig. 5.2C), being small during periods of deep mixing, and larger during stratification. The epilimnion has a high pH year-round (8.3 to 9.0). The pH decreases from the epilimnion (pH > 8) to deeper anoxic waters in the hypolimnion (pH < 8), due to remineralization of sinking organic matter. High pH values extend down to 38 m depth during deep mixing in August-September 2014 (Fig. 5.2D). The seasonal trends in the water-column properties of Lake Chala observed in this study are comparable to those in previous studies (Wolff et al., 2011, 2014), but the exact timing and extent of deep mixing varies between years.

Based on these profile data (Fig. 5.2), three different states of the Lake Chala water column can be recognized during the studied time interval: stratification (S), shallow mixing (SM) and deep mixing (DM). Consistent with its status as a permanently stratified (meromictic) lake, there is no evidence for complete water-column mixing during our study period. Our observations from September 2013 represent the end of a period of deeper mixing (DM), followed by stratified conditions (S) between October 2013 and May 2014. This period is shortly interrupted by a period of shallow mixing (~15 m; SM) during January-February 2014. The water column then experiences deeper mixing between June and September 2014 (DM), stratification from October 2014 to December 2014 (S), and a period of shallow mixing (SM) starting in January 2015.

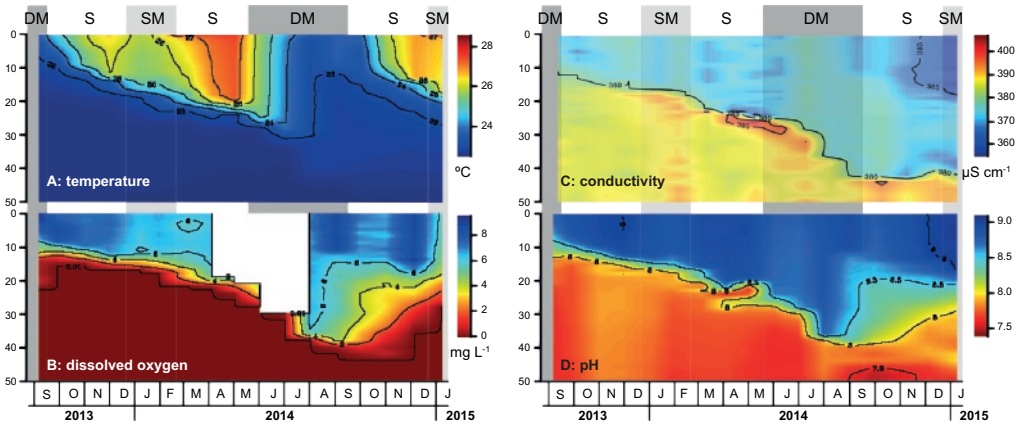

Figure 5.2 Interpolated monthly profiles of temperature (A; °C), dissolved oxygen (B; mg L^{-1}), conductivity (C; K25 in µS cm^{-1} at 25°C) and pH (D) through the upper water column of Lake Chala (0-50 m depth), from early September 2013 until early January 2015, in relation to the periods of water-column stratification (S), shallow mixing (SM) and deep mixing (DM).

5.3.1.2 Vertical distribution and seasonal variability in TIC and PC

The concentration of (dissolved) inorganic carbon in lakes is determined by atmospheric CO_2 exchange, primary productivity, remineralization of terrestrial and aquatic organic matter, and carbon input from runoff and groundwater inflow (Bade et al., 2004). TIC in the water column of Lake Chala consists of dissolved inorganic carbon (DIC) and suspended calcium carbonate ($CaCO_3$). TIC concentrations range from 32 mg C L^{-1} in the surface water to 56 mg C L^{-1} at depth (Fig. 5.3A). In a meromictic lake this increase with depth is expected, since respiration products accumulate at depth. The relatively high DIC levels in Lake Chala are primarily due to evaporation strongly exceeding precipitation, but may also originate partly from calcite-bearing tuffaceous breccia within its catchment, and make it a hard-water lake where HCO_3^- is the main anionic component (Wolff et al., 2014). The depth gradient in TIC concentration is minimal during early stratification (November 2013 to January 2014; October 2014), and TIC concentrations are low throughout the whole water column from the end of deep mixing until the end of 2014 (Fig. 5.3A). Within a lake the balance of production and respiration is a prime factor governing $\delta^{13}C_{TIC}$ (Striegl et al., 2001; Bade et al., 2004). The $\delta^{13}C$ of TIC is relatively high (values are less negative) in the epilimnion due to primary production preferentially removing ^{12}C, while relatively low (more negative) values occur in the hypolimnion down to 60 m (except in the early months of stratification October-December 2014), which is interpreted to reflect the remineralization of this ^{13}C-depleted

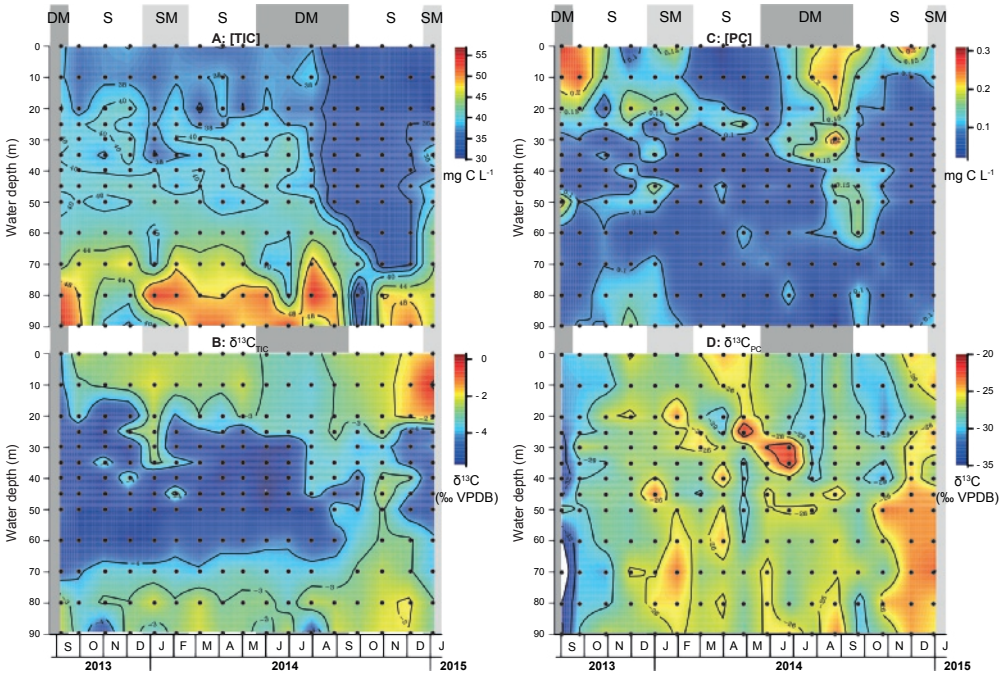

Figure 5.3 Interpolated monthly profiles of concentrations (mg C L^{-1}) and $\delta^{13}C$ signature (‰ VPDB) of total inorganic carbon (TIC; A-B) and particulate carbon (PC; C-D) through the water column of Lake Chala (0-90 m depth), from early September 2013 until early January 2015, in relation to the periods of water-column stratification (S), shallow mixing (SM) and deep mixing (DM). Black dots represent the sampling depths.

organic matter as it sinks through the water column. The $\delta^{13}C$ of this respired carbon had an average value of -16.6‰, as indicated by the y-intercept of a linear trendline of $\delta^{13}C_{TIC}$ versus 1/TIC concentration between 0 and 60 m depth (Keeling plot; Fig. 5.4). The deepest part (60 to 90 m) of the water column has again less negative $\delta^{13}C_{TIC}$ values, especially when TIC concentrations are also high (Fig. 5.3A-B). These atypically high deep-water $\delta^{13}C_{TIC}$ values can be produced by three different processes: i) subsurface inflow of water with high DIC concentration and higher $\delta^{13}C$ values; ii) methanogenesis in the bottom water or surficial sediments; and iii) $CaCO_3$ dissolution (*cf.* 'mode C' lakes; Myrbo and Shapley, 2006). In Lake Chala, all three mechanisms may be involved. Firstly, substantial subsurface inflow is needed to balance the lake's water budget (Payne, 1970), but the chemical composition of this water and depth of inflow remain unconstrained. Secondly, biomarkers for methanogenesis have been found both in the surficial sediments (Sinninghe Damsté et al., 2012a) and in the anoxic deep water column (Buckles et al., 2013). And thirdly, calcite and aragonite oversaturation due to seasonal phytoplankton blooms combined with continuous strong lake-surface evaporation causes seasonally variable precipitation of $CaCO_3$ (Wolff et al., 2014). Partial dissolution of this $CaCO_3$ in the under-saturated upper hypolimnion could then enrich $\delta^{13}C_{TIC}$ in the deepest water column, while the increased TIC concentrations reflect the local accumulation of $CaCO_3$ due to its reduced sinking speed in the denser bottom water. However, the continuous pH decline with depth (Wolff et al., 2014) and presence of intact calcite crystals in the sediment record (Wolff et al., 2011) suggest that the third process may be relatively unimportant in Lake Chala.

PC concentrations range from 0.02 to 0.30 mg C L^{-1}, and generally decrease with depth (Fig. 5.3C), suggesting that most algae have disintegrated by the time they have sunk below 30-40 m. During mixing of the lake and until after the onset of stratification, PC concentrations are higher due to high primary productivity and greater amounts of sinking organic matter (September-October 2013; July-October 2014), while during times of prolonged stratification, PC concentrations are very low (December 2013; March-May 2014). The $\delta^{13}C_{PC}$ values range from -37.9‰ to -20.4‰ and show greater variation through time than with depth (Fig. 5.3D), arguing for relatively rapid sinking of organic matter. Despite substantial scatter (Fig. 5.3D), the lowest (most negative) $\delta^{13}C_{PC}$ values generally occur during mixing and at the onset of stratification. Overall, seasonal variation in $\delta^{13}C_{PC}$ is greater than that in $\delta^{13}C_{TIC}$, indicating that $\delta^{13}C_{PC}$ is strongly influenced by primary productivity, remineralization and mixing processes, while $\delta^{13}C_{TIC}$ is less dynamic because the TIC pool is much larger than that of PC.

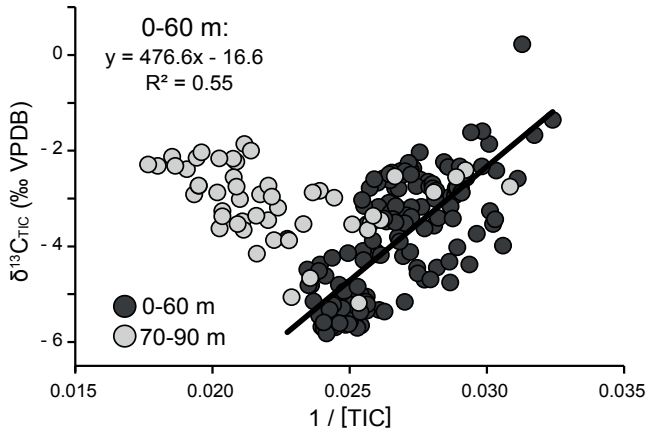

Figure 5.4 Keeling plot showing the relationship between TIC $\delta^{13}C$ values (‰ VPDB) and 1/TIC concentrations (in 1/mg C L^{-1}), with y-intercept determined by linear regression of data from the 0-60 m depth range (black circles), and data from the 70-90 m depth range plotted for comparison (white circles).

5.3.2 Seasonal occurrence and possible sources of lipid biomarkers

A variety of lipid biomarkers were identified in the SPM of Lake Chala, including C_{17}-C_{35} *n*-alkanes; $C_{19:1}$ *n*-alkene; $C_{23:1}$, $C_{25:1}$ and $C_{27:1}$ *n*-alk-1-enes; phytadienes; saturated fatty acids ranging from C_{14} to C_{32} (excluding C_{19}); mono-unsaturated fatty acids (MUFAs) of C_{16}, C_{18}, C_{20}, C_{22} and C_{24}; poly-unsaturated fatty acids (PUFAs) of C_{16}, C_{18}, C_{20} and C_{22}; branched fatty acids *ai*C_{15} and *i*C_{15} to *i*C_{19}; loliolide and isololiolide; and the C_{30} and C_{32} 1,15 *n*-alkyl diols. Their respective concentrations are listed in Table S5.2 to S5.4, and their $\delta^{13}C$ values in Table S5.5. To permit comparison to other variables, SPM biomarker concentrations were integrated over the upper 25 m of the water column (average of 0, 10 and 25 m), unless stated otherwise. Here we discuss a selection of the most common biomarkers (Fig. 5.5) that show strong seasonal changes and/or have clear potential as paleo-environmental proxy.

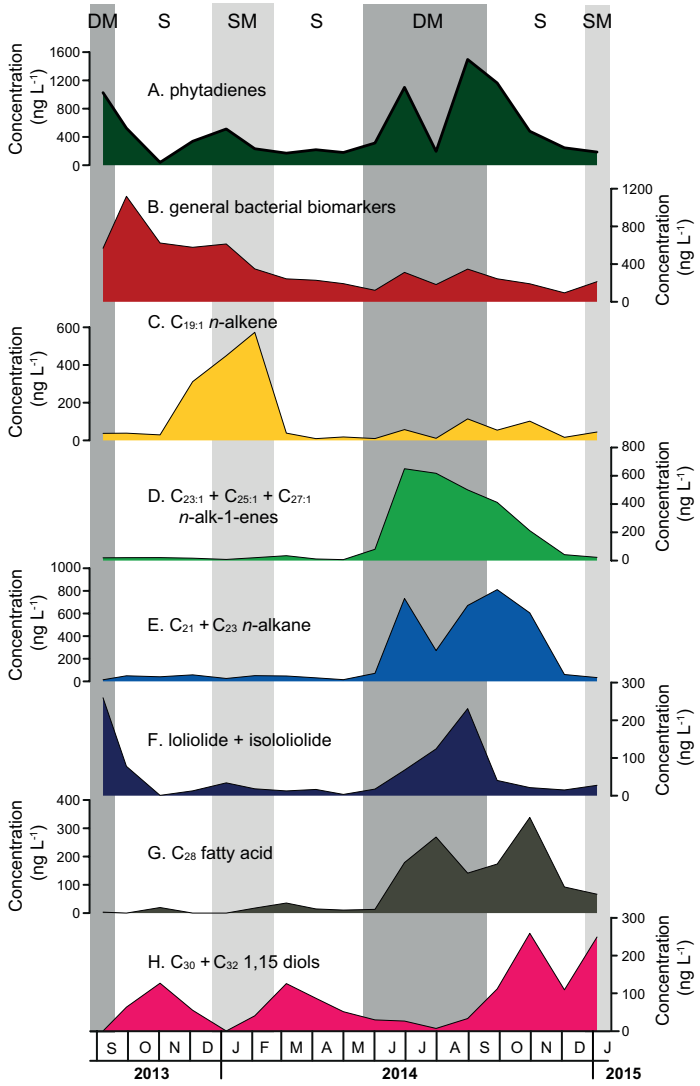

Figure 5.5 Seasonal variation in the concentration (in ng L^{-1}) of selected biomarkers in SPM from the upper 25 m (average of 0, 10 and 25 m depth) of Lake Chala, in relation to the periods of water-column stratification (S), shallow mixing (SM) and deep mixing (DM). A: Summed phytadienes. B: Summed general bacterial biomarkers *ai*-C_{15}, *i*-C_{15}, *i*-C_{16}, *i*-C_{17} and *i*-C_{19} fatty acids. C: $C_{19:1}$ *n*-alkene. D: Summed $C_{23:1}$, $C_{25:1}$ and $C_{27:1}$ *n*-alk-1-enes. E: Summed C_{21} and C_{23} mid-chain *n*-alkanes. F: Summed loliolide and isololiolide. G: C_{28} fatty acid. H: Summed C_{30} and C_{32} 1,15 *n*-alkyl diols.

5.3.2.1 Biomarkers of eukaryote phytoplanktonts

Most groups of primary producers contain chlorophyll, a source of phytol (e.g. Rontani and Volkman, 2003). Acid hydrolysis of lipid extracts containing phytol can produce phytadienes (Grossi et al., 1996). Although phytadienes are thus secondary products, they are a direct reflection of phytol (and thereby chlorophyll) concentration in the SPM. Therefore, we here use the sum of all phytadienes (Fig. 5.5A) as a general indicator of changes in the total biomass of aquatic primary producers in Lake Chala. The $\delta^{13}C$ value of these phytadienes in our data set ranges between -34.4 and -30.3‰, i.e. relatively enriched in ^{13}C compared to other aquatic biomarkers, due to their isoprenoidal structure (*cf.* Schouten et al., 1998). The concentration of phytadienes is highest in September 2013 and between June and November 2014 (i.e. during and immediately after deep mixing), and also elevated between December 2013 and February 2014, at the start of shallow mixing. The phytadiene concentrations have a seasonal pattern similar to that of the total biomass of autotrophic phytoplankton (as measured by their total biovolume; Fig. 5.6A-B) and PC concentrations (Fig. 5.6C) in the upper 0-10 m. This also confirms that our PC values mainly represent POC, although PIC, in the form of precipitating calcite crystals, likely contributed to the modest PC maxima during the warm shallow-mixing periods of January-February 2014 and January 2015 (*cf.* Wolff et al., 2014). Additionally, seasonal variation in Secchi-disk depth (Fig. 5.6D), an indicator of light penetration, corresponds with the PC concentrations. The seasonal pattern in all these variables is conform the expectation that primary productivity is enhanced during and just after periods of deep water-column mixing, due to upwelling of nutrients from the hypolimnion (Buckles et al., 2014).

The concentration of long-chain *n*-alk-1-enes ($C_{23:1}$, $C_{25:1}$ and $C_{27:1}$) increases during the main period of deep mixing (Fig. 5.5D), with relatively high concentrations extending down to 80 m water depth in October 2014 (Table S5.2). The highest concentrations of these long-chain *n*-alk-1-enes were found between July and November 2014 in the epilimnion, up to 1.3 µg L^{-1} at the surface in August 2014. The distribution of these long-chain *n*-alk-1-enes is similar in all

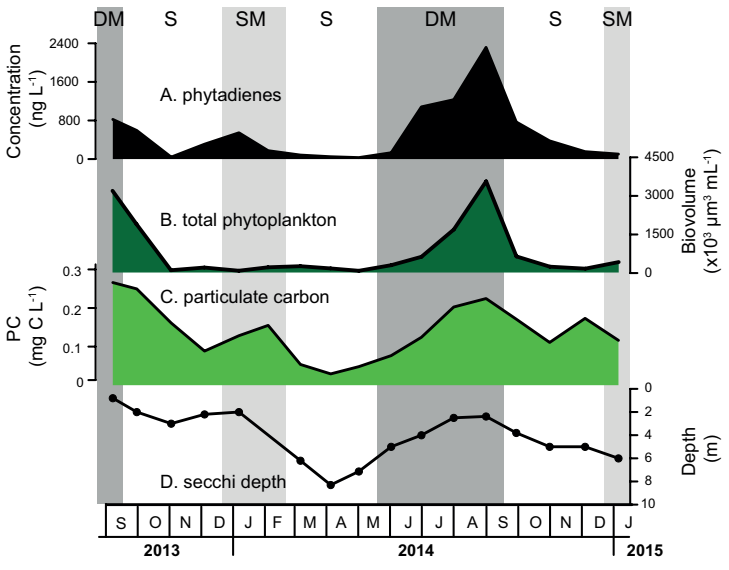

Figure 5.6 Seasonal variation in summed phytadiene concentration in SPM (A) and three measures of total primary production (B-D), all in relation to the periods of water-column stratification (S), shallow mixing (SM) and deep mixing (DM). A-C represent average values over the 0-10 m depth interval. A: Summed phytadienes (in ng L^{-1}). B: Phytoplankton biomass, expressed as biovolume (x10^3 µm^3 L^{-1}). C: Concentration of particulate carbon (mg C L^{-1}). D: Secchi depth (m).

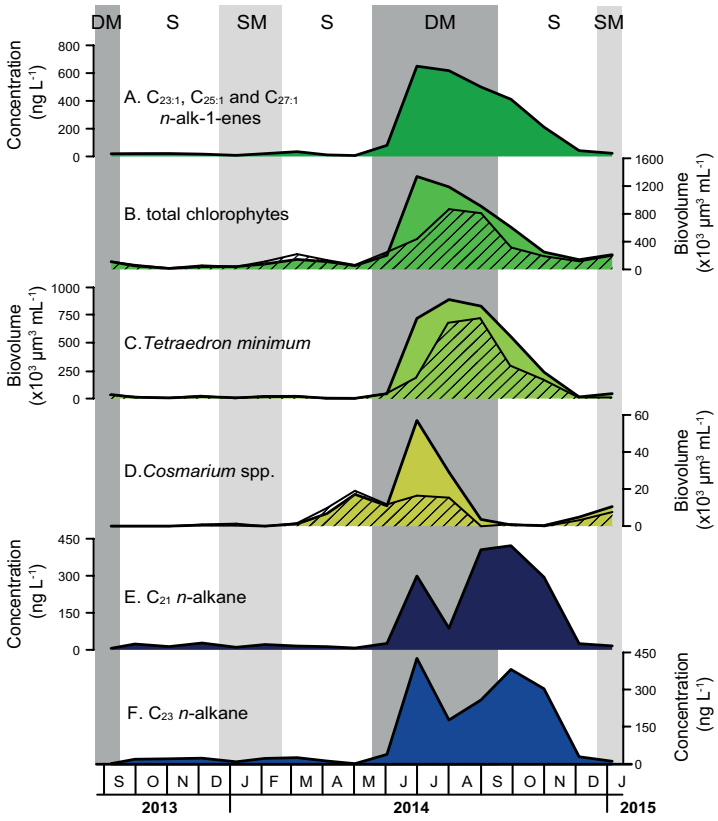

Figure 5.7 Seasonal variation in summed $C_{23:1}$, $C_{25:1}$ and $C_{27:1}$ *n*-alk-1-ene (A), C_{21} *n*-alkane (E) and C_{23} *n*-alkane (F) concentrations in Lake Chala SPM (all in ng L^{-1}) compared with seasonal patterns in total (B) and selected (C-D) chlorophyte algae, in relation to the periods of water-column stratification (S), shallow mixing (SM) and deep mixing (DM). B: Total chlorophytes. C: *Tetraedron minimum*. D: *Cosmarium* spp., all total biomass expressed as biovolume (x10^3 µm^3 L^{-1}). A, E and F represent average values over 0-25 m depth, whereas B-D show average values integrated over 0-10 m depth (open diagonal lines) and 0-20 m depth (filled surfaces); see text of Section 5.2.3 for argumentation.

samples, translated in strong correlation of their individual concentrations ($C_{23:1}$-$C_{25:1}$ R^2 = 0.96; $C_{25:1}$-$C_{27:1}$ R^2 = 0.96; $C_{23:1}$-$C_{27:1}$ R^2 = 0.90; n = 72); in general, the concentration of $C_{27:1}$ is higher than that of $C_{25:1}$ and $C_{23:1}$. Also the $\delta^{13}C$ values of the *n*-alk-1-enes are similar, and range between -41.0 and -36.6‰ ($C_{23:1}$), -40.9 and -35.3‰ ($C_{25:1}$), -41.8 and -35.8‰ ($C_{27:1}$) (Fig. 5.13, Table S5.5), suggesting a common source. Their seasonal pattern (Figs. 5.5C and 5.7A) matches well with that of total biovolume estimates for Chlorophyta (green algae; Fig. 5.7B). Specifically, *Tetraedron minimum*, which is often the dominant chlorophyte in Lake Chala (Fig. 5.7C), is similarly distributed with time as the *n*-alk-1-enes (Fig. 5.7A) and seems, therefore, the most likely source organism of those compounds in Lake Chala, even though *n*-alk-1-enes had previously not been detected in cultures of *T. minimum* (Gelpi et al., 1970). Based on similarities between the *n*-alk-1-enes and phytoplankton abundances in settling particles and SPM collected in 2007, van Bree et al. (2014) proposed that the green algae *Cosmarium* spp. might be a possible source for these compounds in Lake Chala. Our present study indicates that *T. minimum* is more likely the dominant source organism, given that the total biovolume of *Cosmarium* spp. is an order of magnitude lower than that of *T. minimum,* and the timing of its bloom (Fig. 5.7D) is more distinct from that of the long-chain *n*-alk-1-enes. Nevertheless, it remains possible that the long-chain *n*-alk-1-enes in Lake Chala are produced by several chlorophyte taxa.

The seasonal distribution of the mid-chain length *n*-alkanes C_{21} and C_{23} are highly similar to each other (Fig. 5.7E-F; Table S5.2), and their summed distribution (Fig. 5.5E) is comparable

to those of the *n*-alk-1-enes. The $\delta^{13}C$ values of C_{21} and C_{23} *n*-alkanes range between -43.8 and -36.2‰ (Fig. 5.13, Table S5.5) and are nearly identical at specific times and depths (R^2 = 0.97, *n* = 5). The relative abundance of these mid-chain *n*-alkanes in lake sediment records (expressed as P_{aq}; Ficken et al., 2000) is often linked to the past presence of submerged or emergent macrophytes, although these compounds also occur in algae (like in the green alga *Tetraedron* sp.; Gelpi et al., 1970). In our data, P_{aq} is always above 0.4, excluding two samples that lack C_{23} and C_{25} *n*-alkanes altogether. This would normally be interpreted as a macrophyte-dominated *n*-alkane pool. However, a significant source of submerged macrophytes is unlikely in Lake Chala (Sinninghe Damsté et al., 2011b; van Bree et al., 2016) due to its steep rocky shores (Moernaut et al., 2010), and also our isotope data indicate that an algal source is much more likely. Most probably, the C_{21} and C_{23} *n*-alkanes in Lake Chala SPM are biomarkers for chlorophyte algae, considering their seasonal timing, $\delta^{13}C$ values, and similarity between the total chlorophyte and *n*-alk-1-ene abundances.

Bacillariophyta (diatoms) are important primary producers in Lake Chala, as reflected in the high fractional abundance of diatom valves in the sediment record (Wolff et al., 2011; Barker et al., 2011, 2013). The biomarkers loliolide and isololiolide are degradation products of the diatom pigment fucoxanthin (Klok et al., 1984; Repeta, 1989). Although some Haptophyta and Dinophyta species have also been reported as possible sources of this pigment (Klok et al., 1984; Jeffrey and Vesk, 1997), loliolide and isololiolide are generally held indicative of diatom input, especially when haptophyte algae are absent (Castañeda et al., 2009b; Castañeda and Schouten, 2011), such as in Lake Chala. The combined loliolide and isololiolide concentration (Fig. 5.5F) peaks in September of both 2013 and 2014, reaching up to 450 ng L^{-1} (September 2014, 25 m depth). The seasonal pattern of loliolide and isololiolide is indeed similar to that of total diatom biovolume (Fig. 5.8A-B).

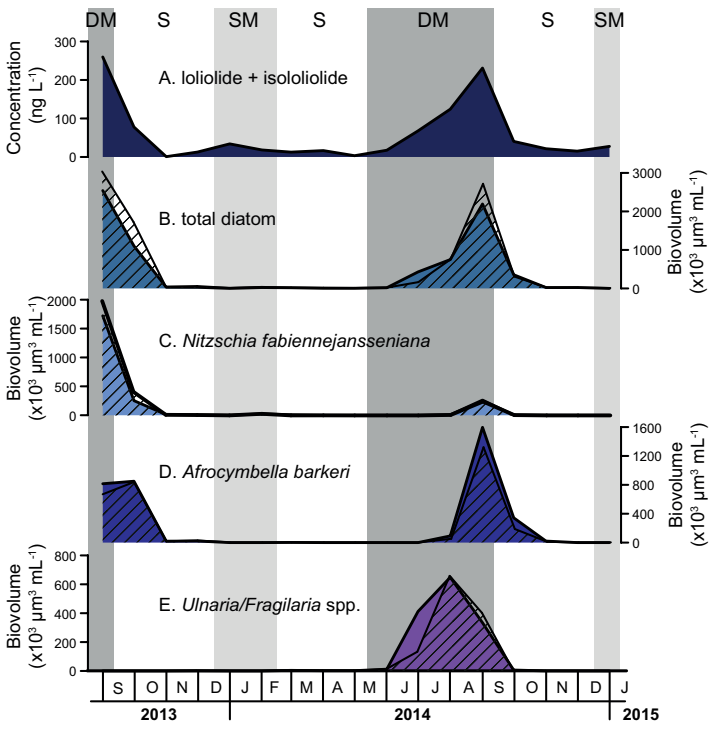

Figure 5.8 Seasonal variation in summed loliolide-isololiolide concentration in Lake Chala SPM (A; in ng L^{-1}) compared with seasonal patterns in total (B) and selected (C-E) diatom algae, in relation to the periods of water-column stratification (S), shallow mixing (SM) and deep mixing (DM). B: Total diatoms. C: *Nitzschia fabiennejansseniana*. D: *Afrocymbella barkeri*. E: *Ulnaria/Fragilaria* spp., all expressed as biovolume (x10^3 µm^3 L^{-1}). A represents average values over 0-25 m depth, whereas B-E show average values over 0-10 m depth (open diagonal lines) and 0-20 m depth (filled surfaces).

The most important diatom species in Lake Chala are *Nitzschia fabiennejansseniana* (Cocquyt and Ryken 2017; Fig. 5.8C), *Afrocymbella barkeri* (Cocquyt and Ryken 2016, Fig. 5.8D) and, to a lesser extent, *Ulnaria/Fragilaria* spp. (Fig. 5.8E). Although there is large variation in the relative abundance of these diatoms between the deep-mixing periods of 2013 and 2014, loliolide and isololiolide do not seem to track a specific species, but appear to reflect total diatom production in Lake Chala, in line with the ubiquitous occurrence of fucoxanthin in diatoms.

C_{30} and C_{32} 1,15 *n*-alkyl diols commonly occur in lake sediments, and are known biomarkers for Eustigmatophyta in marine and freshwater environments (Volkman et al., 1992, 1999; Rampen et al., 2014; Villanueva et al., 2014). In Lake Chala they occur in high abundance between October and December 2013, February to June 2014, and October 2014 to January 2015 (Fig. 5.5H), i.e. consistently during the periods with a stratified water column. Relatively little is known about eustigmatophyte ecology in lakes, as these cells are often overlooked in phytoplankton counts due to their small size and non-diagnostic appearance. Their absence in our phytoplankton dataset indicates that the cells of Lake Chala species are either smaller than 3 µm, or not preserved intact despite fixation with an alkaline Lugol's solution prior to adding formalin. The C_{30} and C_{32} 1,15 *n*-alkyl diols in Lake Chala were previously studied in sediment-trap samples as part of material settling through the water column between August 2009 and 2010 (Villanueva et al., 2014). That study identified five eustigmatophyte groups based on the detection of 18S rRNA genes, and showed that these algae are important producers of long-chain diols in Lake Chala. The documented seasonal changes in diol abundance are also in line with our findings. This indicates that eustigmatophytes thrive, more than other algal groups, under stratified conditions, and hence that sedimentary C_{30} and C_{32} 1,15 *n*-alkyl diol records have the potential to serve as proxy for past stratified conditions in Lake Chala.

5.3.2.2 Biomarkers of (cyano-)bacteria

In our data from the upper water column of Lake Chala, generic biomarkers for bacteria such as short-chain *iso* and *anteiso* fatty acids (FA) reach peak values during or immediately after periods of high primary production, and decrease in abundance during periods of stratification (Figs. 5.5B, 5.9A). The magnitude of the peak that developed after the main mixing season of 2014 is much less than the one that developed after the mixing season of 2013, notwithstanding the comparable total phytoplankton abundance (Fig. 5.6B). Although some bacterial biomarkers such as *iso*C_{16} and *iso*C_{19} FAs were mostly found in the anoxic deeper water column, and concentrations of *iso*C_{15} and *anteiso*C_{15} FAs decrease noticeably below the epilimnion, in general bacterial biomarkers are found throughout the water column (Table S5.3).

One bacterial biomarker with a distinct seasonal pattern is the $C_{19:1}$ *n*-alkene, which develops a prominent peak between December 2013 and March 2014, i.e. mostly during the period of shallow mixing (Fig. 5.9B). Concentrations of $C_{19:1}$ *n*-alkene reach 0.7 µg L^{-1} in the upper 10 m of the water column in January-February 2014, and decrease in deeper water. Its compound-specific $\delta^{13}C$ values range from -43.2 to -35.6‰. Short-chain *n*-alkenes ($<C_{22}$) are generally assumed to be derived from cyanobacteria or microalgae (e.g. Gelpi et al., 1968, 1970; Volkman et al., 1998). Although the $C_{19:1}$ *n*-alkene is not commonly used in biomarker studies, it can be synthesized by cyanobacteria, and has been reported in cultures of the marine cyanobacteria *Coccochloris elabens* and *Agmenelium quadruplicatum* (Winters et al., 1969), *Synechococcus sp*. (marine strain PCC7002; ~38% of total hydrocarbons; Coates et al., 2014; Mendez-Perez et al., 2014) and *Leptolyngbya* sp. (strain PAC 10-3; ~98% of total hydrocarbons; Coates et al., 2014). The peak $C_{19:1}$ *n*-alkene concentration during shallow mixing does indeed suggest a cyanobacterial source rather than other

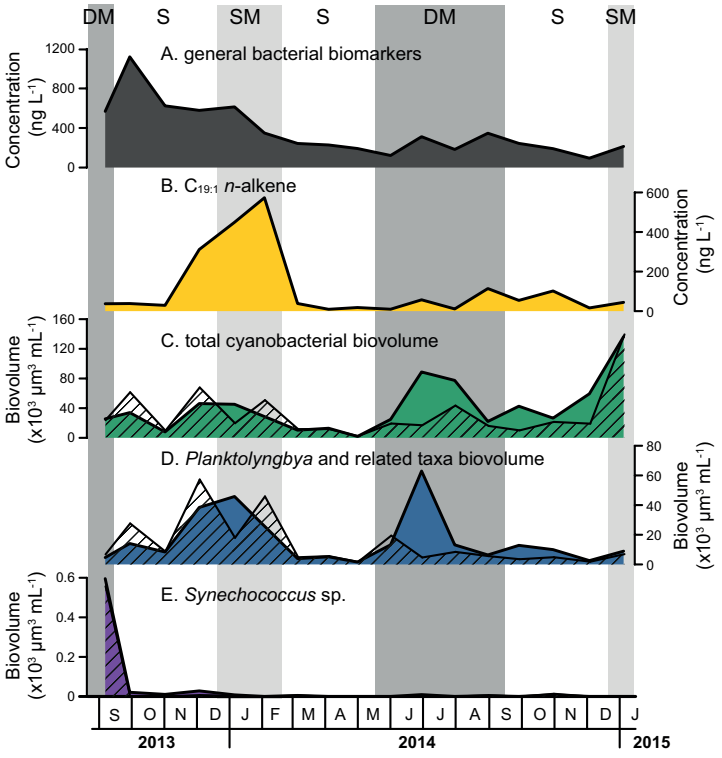

Figure 5.9 Seasonal variation in the summed concentrations of general bacterial biomarkers *ai*-C_{15}, *i*-C_{15}, *i*-C_{16}, *i*-C_{17} and *i*-C_{19} FAs (A) and the $C_{19:1}$ *n*-alkene in Lake Chala SPM (B; both in ng L^{-1}) compared with seasonal patterns in total (C) and selected (D-E) cyanobacteria, in relation to the periods of water-column stratification (S), shallow mixing (SM) and deep mixing (DM). C: Total cyanobacteria. D: *Planktolyngbya* and related taxa. E: *Synechococcus* sp., all expressed as biovolume (x10^3 µm^3 L^{-1}). A-B represent average values over 0-25 m depth, whereas C-E show average values over 0-10 m depth (open diagonal lines) and 0-20 m depth (filled surfaces).

phytoplankton groups, which all display other seasonal patterns (Figs. 5.6B, 5.7B, 5.8B). Although the seasonal trend in total biovolume of all identified cyanobacteria (Fig. 5.9C) does not directly correspond to that of $C_{19:1}$ *n*-alkene (Fig. 5.9B), the seasonal pattern of *Planktolyngbya* and related taxa, one of the dominant groups of cyanobacteria in Lake Chala, is similar in that it also displays a prominent peak during the shallow mixing season of 2014 (Fig. 5.9D). *Planktolyngbya* is closely related to *Leptolyngbya* species, which is known to produce $C_{19:1}$ *n*-alkenes (Coates et al., 2014). *Synechococcus* sp. (>3 µm) seems a less likely source of the $C_{19:1}$ *n*-alkenes here (Fig. 5.9E). Further, the seasonal trend in $C_{19:1}$ *n*-alkene concentration closely matches that of the cyanobacterial photoactive pigment myxoxanthophyll (pers. comm. H. Tanttu, Ghent University). Considering this similar timing and the relatively high concentration of $C_{19:1}$ *n*-alkene in Lake Chala, and its occurrence in cyanobacterial cultures (Winters et al., 1969; Coates et al., 2014; Mendez-Perez et al., 2014), it seems most likely that the $C_{19:1}$ *n*-alkene in Lake Chala has a cyanobacterial origin, and may potentially be used as biomarker specific to cyanobacteria.

5.3.2.3 Biomarkers of terrestrial vegetation

Long-chain *n*-alkanes derived from vascular plants are present in low concentrations (max. 92 ng L^{-1}, July 2014 at the surface; Table S5.2), often too low for accurate quantification. Vascular plants typically have a strong odd-over-even *n*-alkane distribution. Therefore, high carbon preference index (CPI) values are indicative of a terrestrial plant origin, while CPI values ~1 indicate a bacterial or algal *n*-alkane source (Gelpi et al., 1970; Cranwell et al., 1987). The CPI of

the *n*-alkanes in Lake Chala SPM varies between 0.2 and 4.6 (1.6 on average), indicating limited contribution of terrestrial-plant *n*-alkanes. ACL varies between 23.3 and 28.6 (26.3 on average). The mean $\delta^{13}C$ values of long-chain *n*-alkanes are -29.5±0.8‰ (C_{29}, $n = 4$), -30.9±1.7‰ (C_{31}, $n = 4$) and -31.2±1.6‰ (C_{33}, $n = 3$). Long-chain FAs are present mainly during the deep-mixing period and subsequent start of stratification. The most abundant FA is C_{22}, followed by C_{28} and C_{24}. Their $\delta^{13}C$ values range from -41.5 to -27.3‰ (C_{20} FA), -39.6 to -26.8‰ (C_{24} FA), -41.9 to -26.7‰ (C_{26} FA, Fig. 5.13G), and -46.3 to -34.3‰ (C_{28} FA, Fig. 5.13H). Due to co-elution, $\delta^{13}C$ of the C_{22} FA could only be determined in five samples, and ranges from -39.3 to -31.5‰. Compared to the long-chain *n*-alkanes, the $\delta^{13}C$ of long-chain FAs have a larger range and reach much greater negative values. Since their concentration maxima also have a different timing over the studied period, the long-chain FAs are, therefore, likely not exclusively terrestrial (see Section 5.3.3).

The (near-) absence of biomarkers for terrestrial vegetation in the SPM of Lake Chala during the sampled period is striking, as these biomarkers are clearly present in the sediments (e.g. Sinninghe Damsté et al., 2011b; van Bree et al., 2016). This suggests that SPM, even when sampled throughout a full year, must still be considered to represent a 'snapshot' in time, mainly reflecting processes within the water column, rather than a reflection of all preserved settling particles that contribute to the sedimentary record.

5.3.2.4 Inter-annual variability

In this unproductive lake with permanently anoxic bottom waters and strong seasonal stratification of the upper water column, primary productivity critically depends on the annual recurrence of deep mixing (to 45-60 m depth since 1999; Buckles et al., 2014) and associated upwelling of nutrients. Overall, phytoplankton biomass (as reflected in phytadiene and PC concentrations, and in total biovolume) is highest during the two periods of deep mixing covered by this study (Fig. 5.6). However, when looking at specific biomarkers, substantial inter-annual differences are evident between the periods September 2013 to January 2014 and September 2014 to January 2015. Diatom blooms (producing loliolide and isololiolide) recur yearly and have similar timing and abundance, while chlorophytes (C_{21} and C_{23} *n*-alkanes; $C_{23:1}$, $C_{25:1}$ and $C_{27:1}$ *n*-alkenes) bloomed only in 2014. Eustigmatophytes (C_{30} and C_{32} 1,15 *n*-alkyl diols) were common during all periods with a stratified water column in both years. Physical water-column conditions, such as the duration and depth of seasonal water-column mixing, are key controls on phytoplankton abundance and species succession. In Lake Chala, inter-annual variation in the duration and depth of mixing, and hence the inter-annual variation in biomarker succession, is partly due to local climate variability linked to the El Niño-Southern Oscillation (ENSO), where El Niño years are wetter, and La Niña years drier (Nicholson, 2000; Nicholson and Selato, 2000; Wolff et al., 2014). In particular, the phytoplankton blooming season in Lake Chala is extended during La Niña years, while El Niño years have a shorter blooming season and more abrupt onset of water column stratification (Wolff et al., 2011). During the time interval covered by this study, El Niño conditions (although relatively weak) from October 2014 onwards (http://www.cpc.ncep.noaa.gov/products/analysis_monitoring/ensostuff/ensoyears.shtml) are reflected in a more abrupt onset of temperature stratification in 2014 than in 2013 (Fig. 5.2A), which may in turn have influenced the seasonal succession of phytoplankton and the biomarkers derived from them. The time period covered by this study is, however, too short to draw firm conclusions about the proximate and ultimate causes of inter-annual variation in the biomarker distributions.

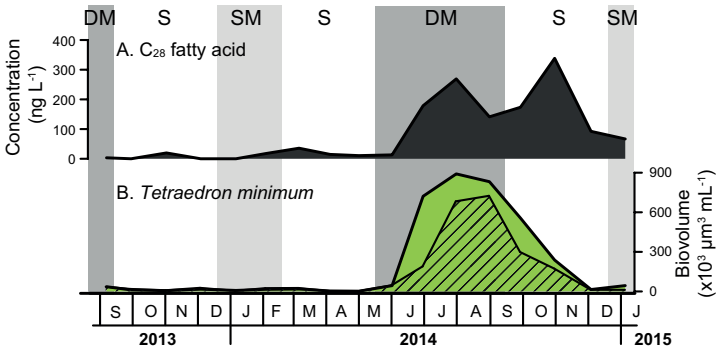

Figure 5.10 Seasonal variation in C_{28} fatty acid concentration in Lake Chala SPM (A; in ng L^{-1}; average over 0-25 m depth) compared to the chlorophyte algae *Tetraedron minimum* (B; in biovolume in x10^3 µm^3 L^{-1}; average over 0-10 m (open diagonal lines) and 0-25 m (filled)).

5.3.3 Aquatic source of C_{28} FA in Lake Chala

The C_{28} FA is the most abundant long-chain fatty acid in SPM between C_{26} and C_{32} (76% of C_{max}; n = 64), with concentrations up to 390 ng L^{-1} in November 2014 (Fig. 5.10A). The strong seasonal pattern of C_{28} FA in the water column of Lake Chala suggests that this compound has an aquatic source. However, long-chain FAs in sediment records are usually assumed to be derived from terrestrial vascular plants (e.g., Eglinton and Eglinton, 2008; Tierney et al., 2010a; Castañeda and Schouten, 2011; Freeman and Pancost, 2014; Hemingway et al., 2016), because they are a major component of leaf waxes (Eglinton and Hamilton, 1967; Kolattukudy, 1976). Yet long-chain FAs are also known to occur in algae and (cyano-)bacteria (e.g. Volkman et al., 1980, 1998), and there have been several, although infrequent, warnings about possible aquatic production interfering with the terrestrial plant signal (e.g., Feakins et al., 2007; Kusch et al., 2010; Holland et al., 2013).

In order to check whether long-chain FAs in Lake Chala are indeed derived from terrestrial plants, we started by comparing the distribution and $\delta^{13}C$ values of long-chain FA homologues in the SPM with that in vegetation from the crater, i.e. the most likely source of vascular plant wax lipids in Lake Chala (Sinninghe Damsté et al., 2011b). The distribution of FAs in plant leaves (n = 14) varies widely between plant species (Table S5.1) and ranges from C_{14} to C_{37} with an average chain length ($ACL_{FAME20-37}$) of 26.4±1.4. Further, C_{max} varies between 24 and 32, and the FAs have a strong even-over-odd carbon number predominance. The $\delta^{13}C$ values of leaf waxes from C_3 plants vary between -41.3 and -32.4‰ (with a weighted average $\delta^{13}C$ value between -37.8 and -34.7‰ among species), while the C_4 grasses have FA $\delta^{13}C$ values between -20.9 and -24.5‰ (weighted average of -21.6‰ and -22.7‰; Table S5.1). An overview of biosynthetic fractionation of the FAs from plant leaves can be found online in Table S5.1. Vegetation-derived FA distributions (n = 14) are clearly different from those in SPM (averaged; n = 71) (Fig. 5.11), as C_{28} and C_{30} FAs co-dominate in vegetation, whereas C_{30} FAs are hardly detected in SPM and C_{28} is by far the most dominant long-chain FA. Further, the $\delta^{13}C$ of FA homologues in SPM (Fig. 5.12A) and terrestrial plants (Fig. 5.12B) also indicate that the latter C_{28} FA does not reach the level of ^{13}C depletion recorded in SPM. Considering that vegetation around Lake Chala is a mixture of C_3, C_4 and CAM plants (Sinninghe Damsté et al., 2011b), the average plant-derived C_{28} FA signature in the sediment would be relatively enriched, due to the C_{28} FAs contributed by C_4 and CAM plants. Moreover, C_{28} FAs in SPM show a ~12‰ shift in $\delta^{13}C$ between July and November 2014, that cannot be explained other than by aquatic production (see Section 5.3.4). Although some contribution of C_{28} FAs from terrestrial plants cannot be excluded, the distinct FA-homologue distribution patterns and $\delta^{13}C$ values clearly indicate that there is extensive aquatic C_{28} FA production in the water column of

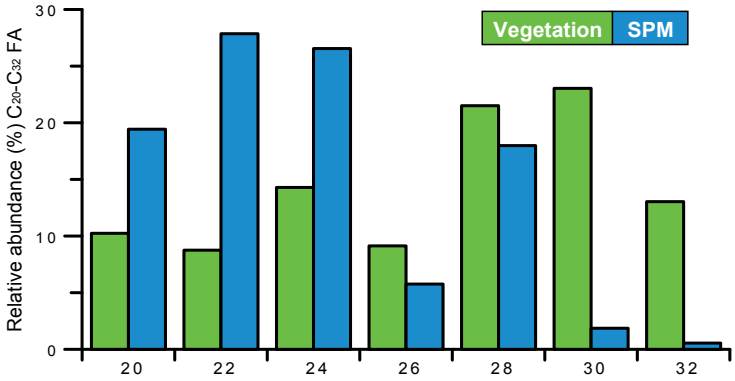

Figure 5.11 Contrasting average distribution of fatty acids with carbon number C_{20} to C_{32} in SPM from Lake Chala (blue; n = 79) and in terrestrial vegetation surrounding the lake (green; n = 14).

Lake Chala. A few microalgae, including (marine) diatoms and chlorophytes, are known to produce some long-chain FAs between C_{20} and C_{30}, usually in small amounts (Volkman et al., 1980, 1989, 1998; Řezanka and Podojil, 1986). Specifically, C_{28} FA was found in the fresh-water chlorophyte *Scenedesmus communis* (recently transferred to the genus *Desmodesmus*) and a batch culture of *Tetraedron minimum* (Schouten et al., 1998), and was part of the insoluble biopolymer algaenan of both species (Blokker et al., 1998). *Scenedesmus* can be excluded as possible significant source organisms in Lake Chala, considering its overall rarity (three occurrences of small colonies entailing <0.5% of total counted cells of these samples) and a seasonal distribution entirely different from that of the C_{28} FA. *T. minimum* is a more likely source, because it is a common species and reaches greatest abundance during the mixing season of July-September 2014, coincident with one of two prominent peaks in the seasonal pattern of C_{28} FA (Fig. 5.10). However, we hesitate to assign the origin of C_{28} FA to *Tetraedron* species, because C_{28} FA concentration peaks during both the mixing and subsequent stratification periods, and it also occurs (albeit in lesser quantities) during the two other monitored stratification periods when *Tetraedron* is almost absent from the phytoplankton counts.

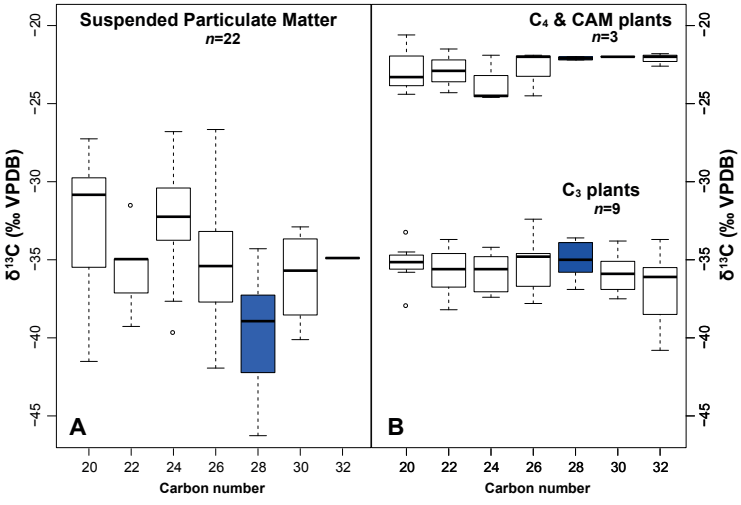

Figure 5.12 Boxplots of the $\delta^{13}C$ values (‰ VPDB) of C_{20} to C_{32} fatty acids (median, first and third quartiles, whiskers depicting minimum and maximum values, and outliers as open symbols) in SPM from Lake Chala (A; n = 22) and in C_3 plants (B; n = 9) and C_4+CAM plants (C; n = 2+1) from surrounding terrestrial vegetation. The C_{28} fatty acid is accentuated in purple.

5.3.4 Seasonal trends in particulate-carbon and biomarker $\delta^{13}C$

An overview of seasonal trends in the $\delta^{13}C$ values of selected biomarkers (Fig. 5.13) shows that all lipid biomarkers that are probably derived from algae blooming during (or immediately following) the June-to-September 2014 period of deep mixing (long-chain *n*-alk-1-enes, C_{21} and C_{23} *n*-alkanes, C_{26} and C_{28} FAs) become increasingly depleted in ^{13}C (up to 14.7‰ lighter), reaching values as low as -41.8‰ ($C_{27:1}$ *n*-alkene) and -46.3‰ (C_{28} FA) by the end of October 2014. This depletion is also reflected in the moderately decreasing values of $\delta^{13}C_{PC}$ during this deep-mixing period (up to 4.5‰, averaged over the depth interval 0-10 m; Fig. 5.3D), but is not seen in $\delta^{13}C_{TIC}$, which shows a slight enrichment of ~1‰ within the epilimnion during this time period (Fig. 5.3B). Whereas the latter trend is expected, the depletion trend in biomarker and particulate-carbon $\delta^{13}C$ is not, because growing phytoplankton preferentially takes up ^{12}C, thereby enriching the epilimnetic pool of DIC. During a pronounced blooming period, the phytoplankton also incorporate this relatively enriched DIC and become more and more enriched in ^{13}C themselves. However, instead of this expected enrichment we see a systematic depletion (ranging from ~4.4‰ to ~14.7‰) in bulk $\delta^{13}C_{PC}$ and various lipid biomarkers derived from algal organic matter. A temporal switch from CO_2 to HCO_3^- uptake by these primary producers cannot explain the large difference in fractionation, because HCO_3^- is enriched in ^{13}C relative to CO_2 by ~8‰ (Mook et al., 1974) and hence HCO_3^- utilization would lead to ^{13}C enrichment, and not depletion, of the resulting organic matter. The $\delta^{13}C$ depletion trend during times of higher productivity is also reflected in the $C_{19:1}$ *n*-alkene, the suspected cyanobacterial biomarker which is produced primarily during the shallow mixing period of January-February 2014 (Fig. 5.13A), indicating that this atypical ^{13}C depletion is not a time-specific or species-specific phenomenon, but strongly suggests a universal phenomenon in the water column of Lake Chala during episodes of enhanced primary production. In order to explain this large depletion in PC and aquatic-biomarker $\delta^{13}C$, we need a source of depleted DIC that is not reflected in the $\delta^{13}C_{TIC}$.

Several possible water-column sources of ^{13}C-depleted DIC exist, such as upwelling of ^{13}C-depleted hypolimnetic water, or enhanced input of ^{13}C-depleted CH_4 and its oxidation to CO_2. It is possible that part of the depleted DIC pool in the photic zone of Lake Chala originates from respired DIC ($\delta^{13}C$ of approximately -16.6‰, Fig. 5.4) that is brought upwards from the hypolimnion during deep mixing, but it is unlikely that all depleted DIC results from upwelling as the difference in $\delta^{13}C_{TIC}$ between surface and the most depleted water around 50 m depth is not very large (between -1.3 and -5.4‰; Fig. 5.3B). Moreover, the long duration of enhanced depletion is inconsistent with mixing from deeper water as the primary mechanism, as the largest depletion occurs after the onset of stratification in October 2014, when any upwelling of depleted carbon must have stopped.

Release of CH_4 depleted in ^{13}C from the lower water column and bottom sediments, and its subsequent oxidation to CO_2, might also contribute to ^{12}C-rich DIC. Although it would be expected that methanotroph biomarkers have low $\delta^{13}C$ values, it is surprising that all phytoplankton-derived biomarkers become increasingly depleted in ^{13}C. Unless there is an extremely tight coupling between methanotrophy and primary production in Lake Chala, it is unlikely that methanotrophy plays a substantial role in the ^{13}C depletion of its DIC. Thus, the depletion of $\delta^{13}C$ in PC and aquatic biomarkers cannot be explained with carbon sources from 'the deep', i.e. upwelling of respired or CH_4-derived carbon.

The main alternative source of ^{13}C-depleted carbon is the atmosphere, since CO_2 dissolves into undersaturated lake waters. Typically, dissolved CO_2 reacts with H_2O to form HCO_3^-. However, at high pH conditions it increasingly reacts with OH^- (Herczeg and Fairbanks, 1987), which leads to

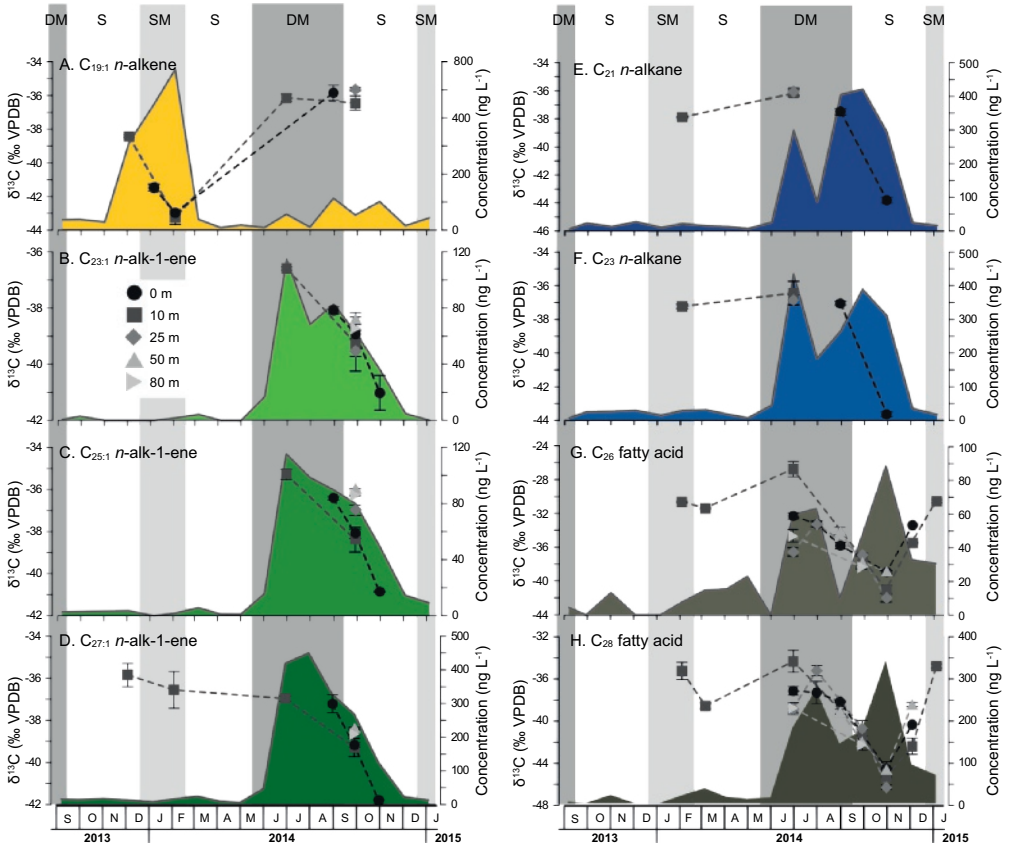

Figure 5.13 Variation in the $\delta^{13}C$ values (‰ VPDB) of selected biomarkers (A-H) in the SPM of Lake Chala over the period September 2013 to January 2015, from the surface (0 m) and 10, 25, 50 and 80 m depth (symbol legend in panel B), in relation to periods of stratification (S), shallow mixing (SM) and deep mixing (DM). The concentration of each biomarker (ng L^{-1}; averaged over 0-25 m depth) is depicted in the background. Note that $\delta^{13}C$ values of the $C_{19:1}$ *n*-alkene decrease coincident with high production during the SM period (A), whereas $\delta^{13}C$ values of all other biomarkers decrease coincident with high production during the DM period (B-H). B: $C_{23:1}$ *n*-alk-1-enes. C: $C_{25:1}$ *n*-alk-1-enes. D: $C_{27:1}$ *n*-alk-1-enes. E: C_{21} *n*-alkane. F: C_{23} *n*-alkane. G: C_{26} fatty acid. H: C_{28} fatty acid.

chemically enhanced diffusion. This process can mitigate carbon limitation in aquatic biological processes (Portielje and Lijkema, 1995), and can have significant influence on the air-water CO_2 flux and carbon residence time in lakes (Wanninkhof and Knox, 1996). The process of chemically enhanced diffusion is well documented in gas-transfer models and laboratory measurements, and has also been reported in a few natural lake settings (Bade and Cole, 2006, and references therein; Portielje and Lijkema, 1995; Bontes et al., 2006; Lammers et al., 2017). This process may take place in Lake Chala, as it has high epilimnetic pH values (8.3-9.1 during our period of observation) particularly during episodes of high primary production (Fig. 5.2D). Not only is the flux of CO_2 into the water column enhanced, the reaction of CO_2 with OH^- results in strong carbon-isotopic fractionation: +8‰ in the common reaction of CO_2 with H_2O to produce HCO_3^-, but -15‰ in

the reaction of CO_2 with OH^- (Mook et al., 1974; Herczeg and Fairbanks, 1987; Bade and Cole, 2006). There are two periods when this process of chemically enhanced fractionation seems evident in the PC and biomarker $\delta^{13}C$ values in Lake Chala: during shallow mixing in January-February 2014, and during/after deep mixing between August and November 2014. The biomarkers are on average ~12.8‰ (long-chain fatty acids), ~7.4‰ (C_{21} and C_{23} *n*-alkanes), and ~4.9‰ (long-chain *n*-alk-1-enes) more depleted in November 2014 than at the start of the mixing induced phytoplankton bloom. The variation in $\delta^{13}C_{PC}$ within the epilimnion is relatively small (~4.5‰) compared to that in the biomarkers, which is unexpected. At this time, we speculate that this might be due to strong CO_2 depletion and high pH halos immediately around the microorganisms generating strongly ^{13}C-depleted HCO_3^- locally, which is not reflected in overall $\delta^{13}C_{TIC}$ values but does substantially influence the $\delta^{13}C$ values of the algal biomarkers.

5.3.5 Implications for paleoenvironmental reconstruction

The high seasonal variability in the modern lake system of Lake Chala implies that seasonal variability may on the one hand complicate interpretation of the paleoenvironmental record, but on the other hand provide new insights on past seasonality. Given the atypical carbon-isotope fractionation process occurring in modern-day Lake Chala, we need to be careful when interpreting sedimentary carbon-isotope signatures as reflecting the enrichment or depletion of various carbon sources in the past. Whether chemically enhanced fractionation could be an important confounding factor will likely depend on the extent to which the naturally high pH of Lake Chala (and many other East African lakes, fresh or saline) is increased further by seasonally high photosynthetic activity. Not only the compound-specific carbon-isotopic signature of aquatic lipid biomarkers, but also of organic matter encapsulated in diatom frustules (Barker et al., 2013), and of bulk algal matter contributing to the $\delta^{13}C$ value of sedimentary TOC (Blaauw et al., 2011) are likely to be influenced by this process. The magnitude of ^{13}C depletion which we recorded in the SPM of Lake Chala during the peak phytoplankton bloom may also hint at the importance of chemically enhanced fractionation in the past, i.e. whether in any particular period the boundary conditions of epilimnetic water pH >8 were met. At least throughout the studied 25-kyr sediment record of Lake Chala, aquatic-biomarker $\delta^{13}C$ values have been characteristically low. The $\delta^{13}C$ values of $C_{25:1}$ *n*-alk-1-ene and $C_{27:1}$ *n*-alk-1-ene vary, respectively, from -42.2 to -37.3‰, and from -44.0 to -38.8‰ (van Bree et al., 2014), and those of the C_{23} *n*-alkane reach values as low as -48‰ (Sinninghe Damsté et al., 2011b). The organic matter within diatom frustules is also relatively depleted in ^{13}C, with values between -36.4 and -27.3 ‰ (Barker et al., 2013).

Secondly, paleohydrological and paleovegetation reconstructions based on the hydrogen-isotope and carbon-isotope signatures of the C_{28} fatty acid, respectively, are made on the premise that this compound is solely terrestrial, as are the leaf-wax alkanes. An aquatic or mixed terrestrial/aquatic origin of C_{28} FA therefore poses a problem for paleoclimate studies. When the $\delta^{13}C$ signature of long-chain FAs is used as proxy for vegetation type, input of the relatively ^{13}C-depleted aquatic C_{28} FA may substantially overestimate the fraction of C_3 vegetation present. Because compound-specific δD measurement requires relatively high biomarker concentrations, and C_{28} FA is often the most abundant FA homologue in East African lakes, it has frequently been used to reconstruct past δD fluctuations in precipitation, not only in Lake Chala (Tierney et al., 2011) but also in Lake Tanganyika (Tierney et al., 2008), Lake Victoria (Berke et al., 2012), Lake Turkana (Morrissey, 2014) and Lake Tana (Costa et al., 2014). Moreover, this dominance of the C_{28} FA is not exclusively an East African phenomenon but also occurs in, for example, Lake El'gygytgyn in Siberia (Holland et al., 2013). A predominantly aquatic production of the C_{28} FA

indicates that its δD signature records photic-zone lake-water composition rather than meteoric water modified by the evapotranspiration processes in soils and plants. While long-term trends in δD may still be comparable, the amplitude of the paleorecord will be smoothed as precipitation δD is spatially and temporally integrated in aquatic δD sources (Sachse et al., 2012), and the potential temporal resolution of the paleorecord will be limited by (and be proportional to) lake residence time. Consequently, regional/global syntheses of paleohydrological studies should be careful when interpreting absolute δD changes based on the C_{28} FA, and when integrating those δD records with those based on "real" plant waxes. When using *n*-alkanes as plant-wax biomarkers for δD reconstruction is not feasible, we recommend supplementary $\delta^{13}C$ measurements on the FA used, to check if their values are consistent with a vascular plant origin. Meanwhile, more research is also needed to identify the specific aquatic sources of C_{28} FA.

5.4 Conclusion

This study used monthly collections of SPM from throughout the water column of Lake Chala, supplemented by $\delta^{13}C$ analyses of the TIC and PC, to trace seasonal variability in the concentration, distribution and carbon-isotopic signature of lipid biomarkers in relation to seasonal succession in the lake's algal and microbial communities. After deep mixing started upwelling nutrients from the hypolimnion in June 2014, there is a succession in the phytoplankton from chlorophyte to diatom and then eustigmatophyte dominance, each producing characteristic biomarker compounds: $C_{23:1}/C_{25:1}/C_{27:1}$ *n*-alk-1-enes and C_{21}/C_{23} *n*-alkanes (chlorophytes), loliolide/isololiolide (diatoms), C_{30}/C_{32} 1,15 *n*-alkyl diols (eustigmatophytes). The $C_{19:1}$ *n*-alkene can be tentatively linked to cyanobacteria. Based on concentration, seasonal variability and the $\delta^{13}C$ values of C_{28} FA in SPM, we argue that this biomarker is produced in the water column of Lake Chala, instead of having a terrestrial vascular plant origin as is usually assumed. While future research will have to clarify the actual source of this C_{28} FA in lakes, this aquatic production should be kept in mind when interpreting the $\delta^{13}C$ and δD signatures of long-chain FAs extracted from sediment records. Finally we observed strong ^{13}C depletion in various aquatic carbon pools during seasons of high primary production. This is likely the result of high pH (>9) in Lake Chala's photic zone during such bloom periods, a condition promoting chemically enhanced carbon fractionation. This process can explain the strongly depleted organic carbon in the sediment record of Lake Chala as well as other high-pH lakes, and might potentially form the basis to develop a new biomarker-based surface-water pH proxy.

Data availability

Supplementary data tables (S5.1 to S5.5) can be found online at:
https://data.mendeley.com/datasets/wsjpnjzbh7/1

Acknowledgements
We thank P. Meyers and an anonymous reviewer for their feedback on the manuscript. We thank C.M. Oluseno for conducting the monthly sampling and other field assistance in Kenya. Sample collection was carried out with permission of the Permanent Secretary of the Ministry of Education, Science and Technology of Kenya, through research permit 13/001/11C to D.V. We thank W.I.C. Rijpstra and J.W. de Leeuw (NIOZ) for discussions on analytical methods; H. Tanttu (Ghent University) for providing unpublished pigment data; J.F. Veldkamp (Naturalis, Leiden) for help with taxonomy of the grass species; and C. Wolff (Max Planck Institute of Chemistry, Mainz) and M. Lammers (UU) for discussions on the carbon system in lakes. We are also grateful to A. van Dijk, D. Kasjaniuk, A. van Leeuwen-Tolboom, D. van den Meent-Olieman, C. Mulder, K. Nierop (UU) and J. Ossebaar (NIOZ) for technical and analytical support. This research was supported by the NESSC Gravitation Grant (024.002.001) from the Dutch Ministry of Education, Culture and Science (OCW) to J.S.S.D.

Young african bush elephant on the savannah, Masai Mara National Reserve.

6 Seasonal variability of *in situ* brGDGT production in a permanently stratified African crater lake

L.G.J. van Bree, F. Peterse, W. De Crop, S. van Grinsven, L. Villanueva, D. Verschuren and J.S. Sinninghe Damsté

To be submitted to: *Geochimica et Cosmochimica Acta*

Abstract

Lake sediments are important archives of continental climate history, and their lipid biomarker content can be used to reconstruct paleoenvironmental conditions. Branched glycerol dialkyl glycerol tetraethers (brGDGTs) are bacterial membrane lipids that are increasingly used in paleoclimate studies to reconstruct past temperature. However, major gaps exist in our understanding of these biomarkers in modern lake systems, in particular regarding environmental controls on the *in situ* (i.e., aquatic) production and spatio-temporal distribution of individual brGDGT compounds. Working on Lake Chala, a tropical crater lake in East Africa with a permanently anoxic deep water column, we analyzed depth profiles of brGDGTs in suspended particulate matter (SPM) during 17 consecutive months between September 2013 and January 2015, and in settling particles collected monthly between August 2010 and January 2015. We find that brGDGTs in the water column of Lake Chala are primarily produced *in situ*, and that their concentrations and distributions greatly vary with depth and over time. Direct comparison of the brGDGTs with the distribution and abundance of microbial taxa, as based on 16S rRNA gene amplicon sequencing and quantification, strongly indicates that Acidobacteria are not the main producers of brGDGTs in Lake Chala. Shallowing of the oxic-anoxic boundary during episodes of stratification promoted anoxic production of brGDGTs Ib and IIb in 2013-2014, and IIa' and IIIa' in 2014-2015. The distribution of individual brGDGTs does not consistently relate with ambient temperature, pH or dissolved oxygen, but does respond to transitions between mixing and stratification, as does the lake microbial community. Hence, the general link between brGDGT distributions and temperature in brGDGT-based paleothermometry is more likely driven by a change in microbial community composition than by membrane adaptation in a stable community to changing environmental conditions. While temperature is not the principal driver of distributional changes in aquatic brGDGTs in this system, at least not during the studied interval, abundance-weighted and time-integrated averages of brGDGT fractional abundance in settling particles reveal systematic variability over longer time scales that indirectly relates to temperature. Thus, although we do not as yet fully understand the drivers of modern-day brGDGT fluxes and distributions in Lake Chala, our data do support the application of brGDGT paleothermometry to time-integrated archives such as sediments.

6.1 Introduction

Lake sediments are important archives of continental climate history, especially in (sub-)tropical areas where other long-term, high-resolution natural archives such as ice cores or speleothems are lacking. Lipid biomarkers preserved in those sediments can be used to examine present and past environmental conditions, and often provide more specific information on those conditions than bulk geochemical proxies. For example, plant waxes stored in lake sediments are used to reconstruct past vegetation and hydroclimate changes (e.g., Freeman and Pancost, 2014; Diefendorf and Freimuth, 2017), while the presence and distribution of (iso)loliolide, long-chain *n*-alk-1-enes or 1,15 *n*-alkyl diols can be linked to shifts in algal community composition and/or primary productivity (e.g., Volkman et al., 1998; Castañeda and Schouten, 2011; van Bree et al., 2018b).

Temperature is probably the most important climate parameter that is challenging to reconstruct quantitatively from lacustrine settings. One promising proxy for continental paleothermometry is based on a suite of membrane lipids supposed to be derived from certain soil bacteria, the branched glycerol dialkyl glycerol tetraethers (brGDGTs). These consist of tetra- (I), penta- (II) or hexa-methylated (III) components, with none (suffix a), one (b) or two (c) cyclopentyl moieties, and with methyl groups on the 5th (5-methyl) or 6th (6-methyl; indicated with a prime notation) carbon position of their alkyl chain (Fig. S6.1). The fractional abundance of these different brGDGTs in modern surface soils and peats shows empirical relationships with mean annual air temperature (MAAT) and the pH of the soil or peat in which they are produced (Weijers et al., 2007b; De Jonge et al., 2014a; Naafs et al., 2017a, 2017b). Although the microbiota that produce brGDGTs are still largely unknown (Sinninghe Damsté et al., 2018), this relationship is increasingly used as proxy for continental air temperature in paleoclimate reconstructions. For example, analysis of brGDGTs in loess soils, peats and marine sediments has produced paleotemperature records across a wide range of geological ages (e.g., Weijers et al., 2007a; Peterse et al., 2011; Naafs et al., 2017a; Zheng et al., 2017).

The application of this temperature proxy on lake-sediment records was initially based on the premise that all sedimentary brGDGTs are derived from soil and washed into the lake by erosion. However, when brGDGT distributions in lake sediments were found to differ substantially from those in the soils surrounding the lake, it became clear that there must be an additional, *in situ* source of brGDGTs contributing to the lake sediments (e.g., Tierney and Russell, 2009; Tierney et al., 2009; Loomis et al., 2011; Schouten et al., 2013; Buckles et al., 2014; Colcord et al., 2015; Li et al., 2016). In addition, brGDGT isomers of type IIIa with methyl branches at the 5th position on the one end and the 6th position on the other end (IIIa"), have so far been detected exclusively in lakes and not in soils, providing further evidence for their *in situ* production (Weber et al., 2015, 2018). Furthermore, comparison of the stable carbon-isotopic composition ($\delta^{13}C$) of brGDGTs in lakes and nearby soils indicates distinctive signatures for, and thus sources of lacustrine and soil-derived brGDGTs, with the lacustrine brGDGTs being significantly more ^{13}C-depleted (Weber et al., 2015, 2018; Colcord et al., 2017).

Water-column studies show that brGDGT concentrations generally increase below the thermocline, suggesting that they are mainly produced in the anoxic hypolimnion (Sinninghe Damsté et al., 2009; Bechtel et al., 2010; Blaga et al., 2011; Woltering et al., 2012; Buckles et al., 2014; Loomis et al., 2014b; Miller et al., 2018). Also brGDGT production often varies seasonally (Sinninghe Damsté et al., 2009; Woltering et al., 2012; Buckles et al., 2014), which may introduce a temperature bias towards the season(s) with high brGDGT production (Loomis et al., 2014b; Miller et al., 2018). The contribution of aquatic brGDGTs, especially that of IIIa, generally results

in large underestimates of present-day temperature when the transfer function based on brGDGTs in soils is applied (Tierney et al., 2010b). This stimulated development of lake-specific temperature calibrations (Tierney et al., 2010b; Pearson et al., 2011; Sun et al., 2011; Loomis et al., 2012). Like in soils, the amount and distribution of brGDGTs in lakes seems to be influenced mostly by temperature and lake-water pH (Tierney et al., 2010b; Sun et al., 2011; Loomis et al., 2014a), although a wide range of other factors such as oxygen availability (e.g., Tierney et al., 2012; Loomis et al., 2014a; Weber et al., 2018), light and mixing regime (Loomis et al., 2014b), nutrients (Tierney et al., 2010b; Loomis et al., 2014a), water chemistry including alkalinity (Schoon et al., 2013), redox state (Weber et al., 2018) and conductivity (Tierney et al., 2010b) have also been suggested to influence the *in situ* production of brGDGTs in lakes.

Temperature calibrations based on brGDGTs in soils and peats have substantially improved since the identification and chromatographic separation of 5-methyl and 6-methyl brGDGT isomers (De Jonge et al., 2014a; Naafs et al., 2017a, 2017b). Initial scanning of surface sediments from East African lakes revealed that especially 6-methyl brGDGTs behave differently in lakes compared to soils, suggesting that they are produced by different bacteria, or that brGDGT producers in lakes respond differently to environmental changes than those in soils (Russell et al., 2018). Separation of the 5-methyl and 6-methyl brGDGTs yields slightly better error statistics for the East African lake calibration and lacks outliers such as are present in the calibration without separation of these isomers, re-affirming the potential of brGDGTs for paleotemperature reconstructions in lakes (Russell et al., 2018). Still, little is known about the environmental drivers, season or depth of brGDGT production in lakes, about their producers, or about variation in the terrestrial and aquatic contributions to brGDGTs stored in lake sediments.

Here we study temporal variation in the abundance and distribution of brGDGTs in suspended particles (SPM) from the water column of a permanently stratified lake in tropical Africa over a 17-month period. These SPM brGDGT data are compared with data on the environmental variables temperature, pH and dissolved oxygen obtained by concurrent water-column monitoring. The brGDGT distributions are also compared with the composition and abundance of microbial taxa in the SPM (based on 16S rRNA gene amplicon sequencing and quantification), in an attempt to identify the main producers of brGDGTs in Lake Chala. Finally, we studied the brGDGTs in settling particles collected at monthly intervals over a 4.5-year (53-month) period, to reveal possible long(er)-term trends in the seasonality of brGDGT production in this lake which may help elucidate its environmental drivers.

6.2 Material and methods

6.2.1 Location

Lake Chala (locally "Challa", after a nearby village) is a small (4.2 km^2), deep (~90 m) and permanently stratified crater lake at ~880 m above sea level bridging the border of Kenya and Tanzania (3°19′S, 37°42′E) in the foothills of Mt. Kilimanjaro. The tropical rain belt associated with latitudinal migration of the Inter-Tropical Convergence Zone (ITCZ) passes across this region twice yearly, resulting in two wet seasons and two dry seasons. 'Short rains' occur from late October to December, and 'long rains' from March to mid-May. The main dry season occurs during the southern hemisphere winter (June-September) and is characterized by lower air temperature and higher wind speeds that drive deep mixing of the water column of Lake Chala down to ~40-60 m depth, while the deeper water remains permanently stratified and anoxic (Wolff et al., 2011; Buckles

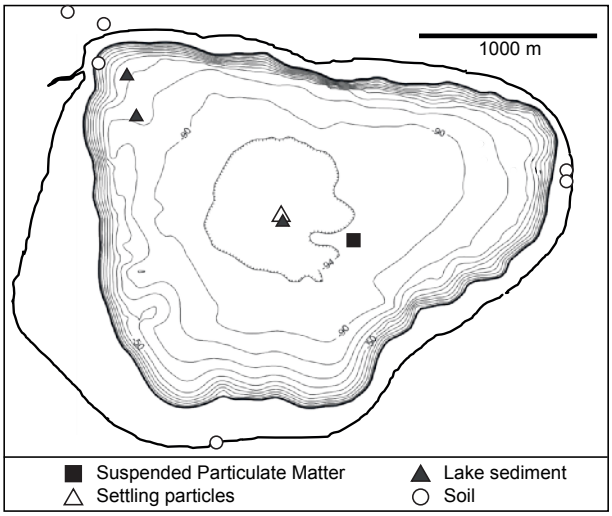

Figure 6.1 Bathymetry of Lake Chala with sample locations of suspended particulate matter (SPM; black square), settling particles (Sediment Trap; open triangle) and surficial lake sediments (grey triangles), and of terrestrial soils (open circles) within the crater catchment (bold full line). Bathymetry adapted from Moernaut et al. (2010).

et al., 2014; van Bree et al., 2018b). Primary productivity is highest during the long dry season (June to October), when nutrient-rich deep water is mixed upwards into the normally unproductive epilimnion (Wolff et al., 2014; van Bree et al., 2018b). Part of the lake's water budget is maintained by rainfall on the lake surface and over the steep-sloping crater basin; only occasionally after high rainfall a small creek is activated which breaches the north-western crater rim (Buckles et al., 2014). As lake-surface evaporation (1700 mm yr^{-1}) greatly exceeds annual rainfall (600 mm yr^{-1}), the lake's water budget must be maintained by substantial subsurface inflow (Payne, 1970), of water which originates from percolation in or above the forest belt on Mt. Kilimanjaro (Hemp, 2006; Bodé et al., submitted). Generally, mean monthly air temperature (MMAT) is lowest in July-August (20-21°C) and highest in January-February (25-27°C); during our study period of 2013-2014 surface-water temperature ranged between 22.5°C during the mixing season and 28.4°C during thermal stratification (van Bree et al., 2018b).

6.2.2 Field observations and sample collection

6.2.2.1 Temperature monitoring of the water column

Mid-lake (Fig. 6.1) vertical profiles of temperature, dissolved oxygen (DO), conductivity (K25) and pH were measured at 2-m intervals through the upper 50 m of the water column using a Hydrolab Quanta® multi-sensor probe, at monthly intervals between September 2013 and January 2015 (van Bree et al., 2018b). Additionally, water temperature was measured by automatic temperature loggers, at 2-hourly intervals between September 2010 and January 2015, suspended at a selection of the following water depths: 2, 10, 20, 25, 30, 35, 40, 45, 50 and 85 m (Fig. 6.2). The set of monitoring depths varied over time due to the occasional malfunctioning and subsequent replacement of loggers. Due to loss of logger data during retrieval, no water-column temperature information is available for the period between 7 January and 11 September 2012. The entire 53-month temperature record was corrected for drift of individual loggers, using the Hydrolab profiles as reference. Periods of deep water-column mixing and stratification were determined on the basis of the temperature-logger time series, or estimated on the basis of mean monthly air temperature (MMAT) data from Buckles et al. (2014) for the abovementioned hiatus period.

6.2.2.2 SPM

Collection of the suspended particulate matter (SPM) profiles used in this study has been described in detail by van Bree et al. (2018b). In short, 5 to 10 L of lake water was collected at 13 discrete depths, monthly between September 2013 and January 2015. The samples were filtered on pre-combusted glass fiber GF/F filters (142 mm diameter, Whatman), stored frozen and freeze-dried prior to analysis. For this study we analyzed SPM from all depths for the months November 2013 and August 2014, as well as from 0, 10, 25, 50 and 80 m depth for all other months (n = 101). The SPM was collected at or near the start of every month as discussed here, with the sample taken at, for example, 07-09-2013 representing September 2013, and the sample taken at 30-09-2013 representing October 2013 (see Table S.1).

6.2.2.3 Sediment trap

A sediment trap (UWITEC, double-funneled, 86 mm diameter) suspended in 35 m water depth at a mid-lake position (Fig. 6.1) was installed in November 2006, after which it was emptied and redeployed at about monthly intervals (Table S.1). The collected material was allowed to settle for two days, and stored frozen after decantation of excess water. Prior to analysis, the samples were thawed, filtered over pre-weighed and pre-combusted (400°C, 5h) glass fiber GF/F filters (110 mm diameter, Whatman), frozen and freeze-dried. Bulk mass flux was calculated for each month by taking the dry weight, days of collection, and the surface area of the sediment trap (58 cm^2), and is expressed as mg m^{-2} day^{-1}. This study focuses on the brGDGTs in settling particles representing September 2010 to January 2015 (n = 53; Table S.2).

6.2.2.4 Soil

Seven soil samples from the collection made by Buckles et al. (2014) were selected for brGDGT analysis (Fig. 6.1) based on site dissimilarity, i.e. from different origins (lakeshore forest, crater rim, savanna hinterland, small ravine; Table S.3) as described in the original study.

6.2.2.5 Lake sediment

Intact surficial lake sediment (3-5 cm depth) from 3 sites (CH10-06G: 3°19.049′S, 37°41.879′E; CH10-09G: 3°18.704′S, 37°41.448′E and CH10-10G: 3°18.575′S, 37°41.419′E; see Table S.4) forming a transect from close to the creek inlet towards the middle of the lake (Buckles et al., 2014) was collected by gravity coring in January-February 2010, then freeze-dried and homogenized prior to extraction.

6.2.3 Sample preparation and extraction

6.2.3.1 Lipid extraction

Sample preparation for SPM was described in detail by van Bree et al. (2018b). In short, the freeze-dried filters were cut in small pieces and extracted using a modified Bligh-Dyer method. Each extract was acid-hydrolyzed with 1.5N hydrochloric acid (HCl) in methanol (MeOH). After 2h reflux at 80°C, the pH was adjusted to 4-5 with KOH/MeOH, and washed three times with DCM. The combined supernatant was dried over a Na_2SO_4 column and dried under N_2. This total lipid extract (TLE) was separated on an activated Al_2O_3 column into an apolar, neutral and polar fraction, using hexane: dichloromethane DCM (9:1, v/v), DCM, and DCM: MeOH (2:1, v/v) as eluents, respectively. The freeze-dried filters with sediment-trap material were cut in small pieces and extracted directly by acid hydrolysis. The then obtained TLE was further processed similar to the SPM TLE. The lake sediments were extracted and processed in similar fashion as the SPM.

A known amount of internal standard (99 ng $GDGT_{46}$) was added to the polar fraction of SPM, settling particles and sediments. All polar fractions of SPM, sediment trap, surface sediments and soils were re-dissolved in hexane: isopropanol (99:1, v/v) and passed over a 0.45 µm PTFE filter.

6.2.3.2 DNA extraction, 16S rRNA gene sequencing and analysis, quantitative PCR of 16S rRNA gene sequences

DNA was extracted from 1/32 section of the SPM filters using the PowerSoil DNA extraction kit (Mo Bio Laboratories, Carlsbad, CA, USA). The 16S rRNA gene amplicon sequencing and analysis was performed with the general 16S rRNA archaeal and bacteria primer pair 515F and 806RB targeting the V4 region (Caporaso et al., 2012), as described in Besseling et al. (2018). PCR products were gel-purified using the QIAquick Gel-Purification kit (Qiagen), pooled and diluted. Sequencing was performed at the Utrecht Sequencing Facility (Utrecht, the Netherlands), using an Illumina MiSeq 2x300 bp sequencing platform. The 16S rRNA gene amplicon sequences were analyzed by an in-house pipeline including quality assessment by FastQC (Andrews, 2010), assembly of the paired-end reads with PEAR (Zhang et al., 2013), and taxonomic assignment (including picking of a representative set of sequences with the 'longest' method; Caporaso et al., 2010) with BLAST (Altschul et al., 1990) by using the Silva 128 release as reference database (https://www.arb-silva.de/). The 16S rRNA gene copies were quantified using quantitative PCR (qPCR) with the same primer pair as used for amplicon sequencing (515F, 806RB). The qPCR reaction mixture (25 µl) contained 1 U of Pico Maxx high fidelity DNA polymerase (Stratagene, Agilent Technologies, Santa Clara, CA) 2.5 µl of 10x Pico Maxx PCR buffer, 2.5 µl 2.5 mM of each dNTP, 0.5 µl BSA (20 mg ml^{-1}), 0.02 pmol μl^{-1} of primers, 10,000 times diluted SYBR Green® (Invitrogen) (optimized concentration), 0.5 µl of $MgCl_2$ (50 mM), and ultrapure sterile water. The cycling conditions for the qPCR reaction were the following: initial denaturation at 98°C for 30s, 45 cycles at 98°C for 10 s, at 56°C for 20 s, followed by a plate read, at 72°C of 30 s and at 80°C for 25 s. Specificity of the reaction was tested with a gradient melting-temperature assay, from 55°C to 95°C with a 0.5°C increment for 5 seconds. The qPCR reactions were performed in triplicate with standard curves from 100 to 10^7 molecules per microliter. qPCR efficiency for the 16S rRNA quantification was on average 95% ($R^2 = 0.998$).

6.2.4 Instrumental analysis

6.2.4.1 GDGT analysis

GDGT analysis was performed with an Agilent 1260 Infinity ultrahigh performance liquid chromatography (UHPLC) coupled to an Agilent 6130 single quadrupole mass detector, either at Utrecht University (most SPM, soil, surface sediments) or at the NIOZ (settling particles, SPM at 0 m, except November 2013 and September 2014) following the method of Hopmans et al. (2016). Separation was achieved by two silica Waters Acquity UPLC HEB Hilic (Ø1.7 µm) columns at 30°C, preceded by a guard column with similar packing. Isocratic elution was used for GDGT separation, starting with 82% A (hexane) and 18% B (hexane:isopropanol, 9:1) for 25 min at a flow rate of 0.2 mL min^{-1}, followed by a linear gradient to 70% A and 30% B for 25 min. Injection volume was 10 µL for settling particles, sediment and soils, and 20 µL for SPM. Ionization of the GDGTs was achieved by atmospheric pressure chemical ionization with gas temperature of 200°C, vaporizer temperature of 400°C, N_2 flow of 6 L min^{-1}, capillary voltage of 3500 V, nebulizer pressure of 25 psi and corona current of 5.0 µA as source conditions.

GDGTs were identified by detecting the $[M+H]^+$ ions in selected ion monitoring (SIM) mode for *m/z* 1018, 1020, 1022, 1032, 1034, 1036, 1046, 1048, 1050 (brGDGTs) and 744

(internal standard). Peak area integration of the GDGTs was done with Chemstation (SPM, soil, sediment) or Agilent Masshunter (settling particles, SPM at 0 m) software. For quantification, areas were compared to that of the internal standard, assuming a comparable response of the mass spectrometer for all GDGTs. Selected sediment trap samples were measured twice in different concentrations (n = 13), which yielded comparable fluxes, fractional abundances and index values (e.g., difference between duplicates of total brGDGT flux typically <5% ng m^{-2} day^{-1}; BIT <0.013; MAAT_SFS calibration <0.4°C).

6.2.4.2 Proxy calculation

The Roman numerals in the following equations refer to the molecular structures of GDGTs as shown in Fig. S6.1, with 6-methyl brGDGTs distinguished by a prime symbol, and square brackets indicating the fractional abundances of the 15 different brGDGTs. The Cyclisation of Branched Tetraethers (CBT') is defined by De Jonge et al. (2014b) as

$$CBT' = -\log [(Ic + IIa' + IIb' + IIc' + IIIa' + IIIb' + IIIc')/(Ia + IIa + IIIa)]$$

The abundance ratio of the 6-methyl penta- and hexa-methylated brGDGTs over 5-methyl and 6-methyl brGDGTs was modified after De Jonge et al. (2014b) and Sinninghe Damsté (2016):

$$IR_{6ME} = (IIa' + IIb' + IIc' + IIIa' + IIIb' + IIIc')/(IIa + IIb + IIc + IIIa + IIIb + IIIc + IIa' + IIb' + IIc' + IIIa' + IIIb' + IIIc')$$

Mean annual air temperature (MAAT) is reconstructed with the stepwise-forward-selection (SFS) calibration of brGDGT distribution in the East African lakes dataset (Russell et al., 2018), with brackets indicating the fractional abundances of the respective brGDGTs:

$$MAAT_{SFS} = 23.81 - 31.02[IIIa] - 41.91[IIb] - 51.59[IIb'] - 24.70[IIa] + 68.80[Ib]$$

Surface-water pH is reconstructed with the Russell et al. (2018) transfer function for East African lakes:

$$\text{Surface water pH} = 8.95 + 2.65 \cdot CBT'$$

6.2.5 Statistical analysis

To assess variability in brGDGT distribution among (types of) samples we performed principal component analysis (PCA) in the R-package FactoMineR (Lê et al., 2008). For SPM statistics only the fractional abundance of the most abundant brGDGTs, i.e., Ia, Ib, IIa, IIa', IIb, IIb', IIIa and IIIa' were used. Water temperature and pH were also included in the PCA, with pH between 50 and 90 m water depth assumed to be similar to the pH measured at 50 m depth. Although complete pH profiles from Lake Chala show that pH still decreases slightly (~0.5 pH units) with depth below 50 m (Wolff et al., 2014), this represents only a quarter of the total pH range.

Concentrations of brGDGTs (ng L^{-1}) were correlated with the estimated abundance of microbial groups to assign a possible source of the former. Microbial abundance was estimated by multiplying their relative abundance as obtained by 16S rRNA gene amplicon sequencing analysis with the absolute abundance of microorganisms in a given sample based on qPCR. For simplicity it was assumed that each microbe contains a single 16S rRNA copy in their genome; abundance is then

expressed as 16S rRNA gene copies L^{-1}. On the premise that potential brGDGT producers must be frequently present in the water column, microbial species present in less than one third of the samples were excluded from this comparison.

6.3 Results

6.3.1 Seasonal mixing and stratification

Surface-water temperature as measured by temperature loggers at 2 m depth, over the 29-month period from September 2012 to January 2015, ranged between 22.8°C during the mixing-season in August 2013 and 27.6°C during stratification in April 2013. Temperature in the deep water layer remained stable at ~22.4°C (Fig. 6.2) due to a lack of mixing. Over the 4.5-year monitoring period from September 2010 until January 2015 the water column of Lake Chala developed stratified conditions generally between September and April, with strongest stratification (greatest temperature contrast between the surface and deep water) during the SH summer months (Fig. 6.2). However, this long period of stratification was punctured by instances of shallow mixing (SM; extending to 20-25 m depth), which started between early December and mid-January, and ended between mid-February and mid-March, i.e. during the generally dry period in between the 'short' and 'long' rains. Deep mixing (DM; extending beyond 30-35 m depth) generally started at the end of April (between 25 April and 2 May), and ended in the first half of September (between 31 August and 14 September). During the 17-month period between September 2013 and January 2015, the oxygenated upper part of the water column, as based on the depth to anoxia (shallowest depth with <0.2 mg L^{-1} dissolved oxygen), varied between 17 m at the start of stratification in October-November 2013, and 44 m at the start of stratification in October-November 2014 (Fig. 6.2).

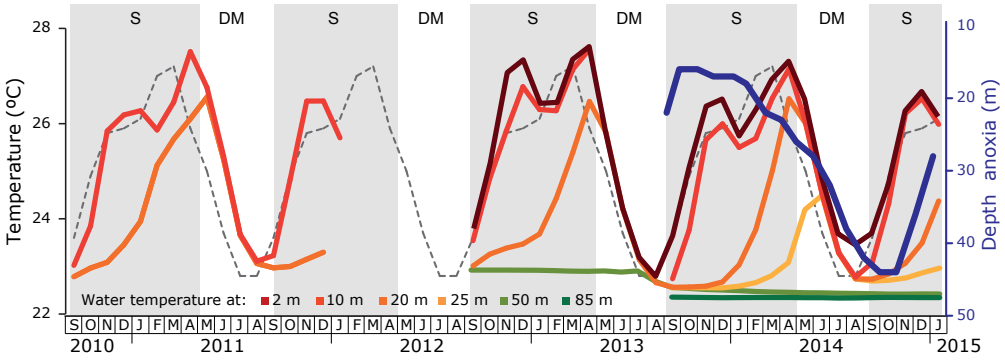

Figure 6.2 Variation in temperature (°C) within the upper 50 m of the water column of Lake Chala between August 2010 and January 2015, based on temperature loggers suspended at 2, 10, 20, 25, 50 and 80 m depth (where available), in relation to mean monthly air temperature (MMAT; stippled line). The dark blue line shows the extent of the oxygenated upper part of the water column, with depth to anoxia (right axis) referring to the shallowest depth with a dissolved oxygen level <0.2 mg L^{-1}, based on monthly water-column profiling between September 2013 and December 2015 (van Bree et al., 2018b). Grey shading highlights the periods of seasonal water-column stratification (S) and deep mixing (DM); the timing of the deep mixing to stratification transition in 2012 was estimated from MMAT due to a hiatus in the water-column temperature logging data.

6.3.2 Spatial and temporal distribution of brGDGTs in SPM

BrGDGTs were detected in all 101 SPM samples analyzed (Fig. 6.3). However, the abundance of compounds with one or two cyclopentyl moieties (types b and c) was often too low (i.e., peak area less than three times baseline) for reliable integration and quantification. Specifically, concentrations of brGDGTs IIIc and IIIc' were always below detection limit. Further, brGDGTs Ic, IIc, IIc', IIIb and IIIb' were present in less than 12% of the samples and in very modest amounts: the fractional abundances of IIc, IIc', IIIb and IIIb' were always <0.02, and that of Ic also rarely exceeded this value. The IIIa'' isomer (Weber et al., 2015) was not detected at all. In the following analysis, we focus on the eight brGDGTs that were found in at least 50% of the samples (i.e., Ia, Ib, IIa, IIa', IIb, IIb', IIIa and IIIa') unless stated otherwise.

The total concentration of all brGDGTs in the water column (ΣbrGDGTs) varied between 0.2 and 15.5 ng L^{-1} (n = 101), and generally increased with depth especially in the anoxic portion of the water column (Fig. 6.3). The overall mean fractional abundance of the individual brGDGTs in SPM collected at all depths above (0-35 m; $SPM_{abovetrap}$) and below the sediment trap (40-90 m; $SPM_{belowtrap}$), concentration-weighted and temporally integrated over the 17-month sampling period, are shown in Fig. 6.4A. Pentamethylated (type II) brGDGTs were most common in the SPM, overall having a fractional abundance ranging from 0.44 to 0.74 (n = 101); and concentration-weighted and temporally integrated values of 0.63 in $SPM_{abovetrap}$ (n = 57) and 0.68 in $SPM_{belowtrap}$ (n = 44). Compound IIa' is generally the dominant brGDGT in the SPM of Lake Chala, with a fractional abundance varying between 0.20 and 0.60, and its integrated $SPM_{abovetrap}$

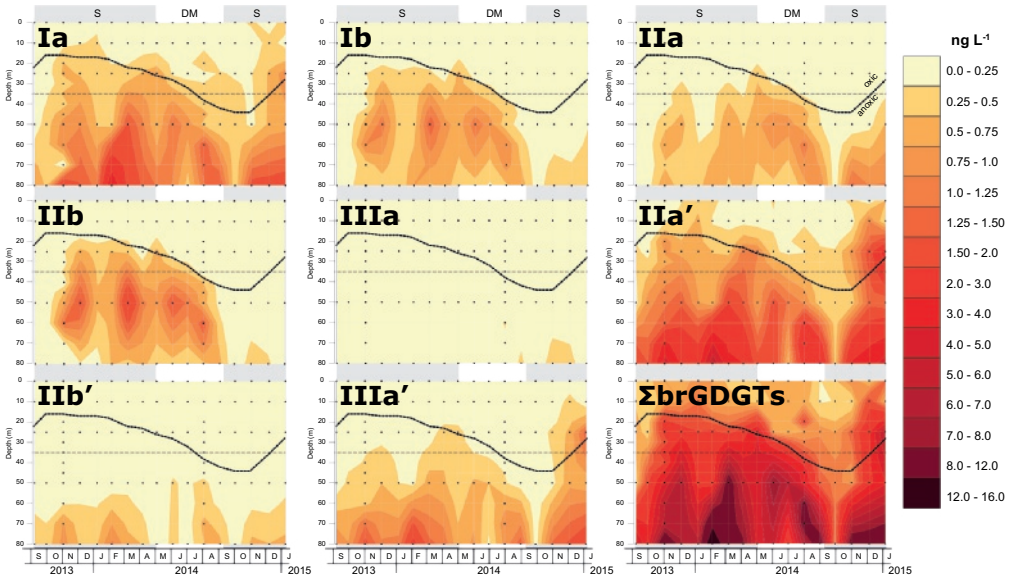

Figure 6.3 Interpolated concentrations (in ng L^{-1}) of the summed and eight most common individual brGDGT compounds in SPM from between 0 and 80 m water depth in Lake Chala, at approximately monthly intervals between September 2013 and January 2015. Grey background shading indicates the periods of seasonal water-column stratification (S) and deep mixing (DM); also indicated is the varying position of the oxic-anoxic boundary (depth to anoxia, as in Fig. 6.2) and the static position of the sediment trap at 35 m depth, which separates the $SPM_{abovetrap}$ and $SPM_{belowtrap}$ zones (see text).

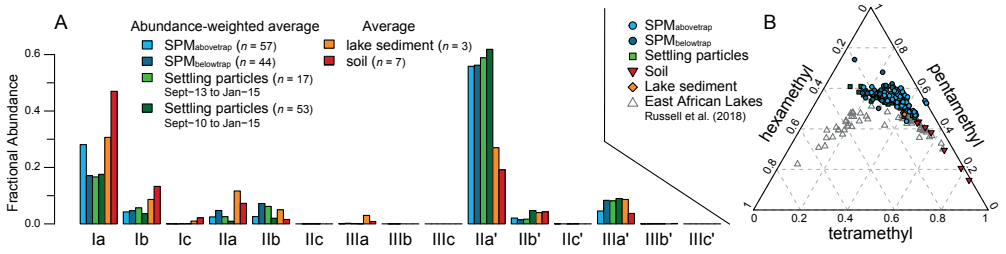

Figure 6.4 Distribution of brGDGTs in the various sample types analyzed in this study. A: Temporally-integrated, concentration- or flux-weighted average fractional abundances of individual brGDGT compounds in SPM from above (light blue) and below (dark blue) the sediment trap, and settling particles trapped over the 17-month period of SPM sampling (Sept-2013 to Jan-2015; light green) and over a longer 53-month period starting three years earlier (Sept-2010 to Jan-2015, dark green) are compared with the average fractional abundances of the same brGDGTs in lake sediments (orange) and catchment soils (red). B: Proportion of tetra-methyl, penta-methyl and hexa-methyl brGDGTs in SPM from above (light blue circles) and below (dark blue circles) the sediment trap, and in settling particles (green squares), lake sediments (orange diamonds) and soils (red triangles) plotted over the surface sediments from 65 East African Lakes (grey triangles; Russell et al., 2018).

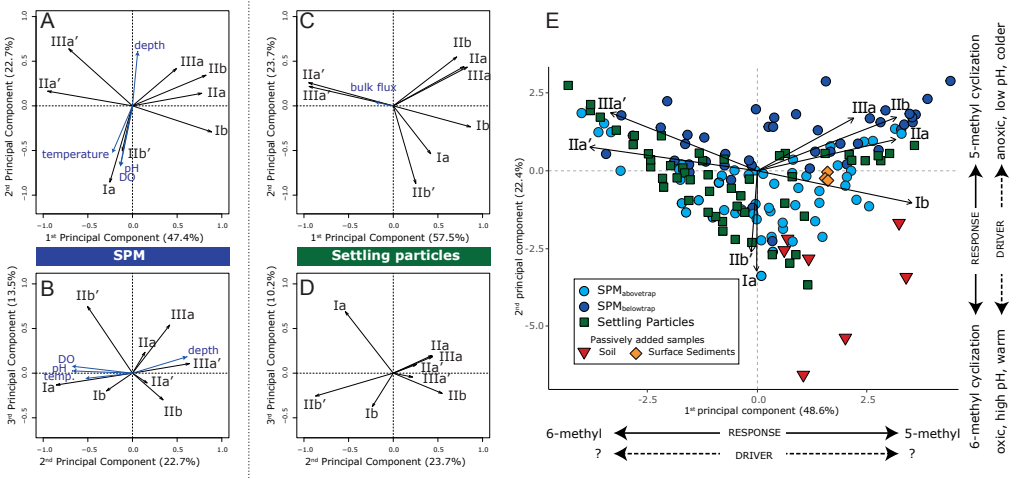

Figure 6.5 Principal component analysis (PCA) of fractional abundances of the eight major brGDGTs in SPM (n = 101) and settling particles (n = 53) from Lake Chala. PC1 vs PC2 (A) and PC2 vs PC3 (B) of the SPM samples, with black vectors indicating the PCA scores of individual brGDGTs, and blue vectors showing the PCA scores of environmental variables added passively. Temperature and pH are measured (0-50 m depth, van Bree et al., 2018b) and assumed similar to 50 m at 80 m depth. PC1 vs PC2 (C) and PC2 vs PC3 (D) of the settling particles, with with black vectors indicating the PCA scores of individual brGDGTs, and blue vector showing the PCA score of the total bulk settling flux added passively. Combined PCA of the fractional abundances of the (mainly aquatic) brGDGTs in all SPM (blue circles) and settling-particle (green squares) samples (E), with distinction between SPM from above (light blue) and below (dark blue) the sediment trap. The PCA scores of lake sediments (orange diamonds) and soils (red triangles) were added passively.

and $SPM_{belowtrap}$ values both equaling 0.56 (Fig. 6.4A). Although the concentration of IIb' is generally low (Fig. 6.3), it has a higher fractional abundance in the surface water and at the end of deep mixing periods. The tetramethylated (type I) brGDGTs amount to between 0.06 and 0.47 of total brGDGTs (n = 101), with a concentration-weighted mean of 0.32 ($SPM_{abovetrap}$) and 0.22 ($SPM_{belowtrap}$), with brGDGT Ia being the second-most abundant of all brGDGTs (Fig. 6.4A). Finally, hexamethylated (type III) brGDGTs have a fractional abundance of up to 0.25 (n = 101), dominated mostly by compound IIIa', and a concentration-weighted mean of 0.05 ($SPM_{abovetrap}$) and 0.09 ($SPM_{belowtrap}$). Thus, although the concentrations of brGDGTs increase with depth, overall the type I brGDGTs are relatively more common in the upper water column (with fractional abundances $SPM_{abovetrap} > SPM_{belowtrap}$) whereas the type II and III brGDGTs are relatively more common in the lower water column ($SPM_{abovetrap} < SPM_{belowtrap}$).

In >90% of the collected SPM samples, 6-methyl brGDGTs were more abundant than 5-methyl brGDGTs. The 5-methyl brGDGTs were relatively abundant only between November 2013 and August 2014, and peaked at 50 m depth with a summed concentration of up to 3.3 ng L^{-1} (in March 2014). This pattern is mainly on account of high concentrations of IIb (up to 2.2 ng L^{-1}, and a fractional abundance of 0.26). The concentration of 6-methyl brGDGTs was typically highest at 80 m depth (up to 9.3 ng L^{-1} in February 2014). However, concentration-weighted and temporally integrated mean fractional abundance of the 6-methyl brGDGTs were quite similar in shallow and deep water, with $SPM_{abovetrap}$ values of 0.63, and $SPM_{belowtrap}$ values of 0.67.

BrGDGT concentrations in the anoxic part of the water column were highest under stratified conditions (Fig. 6.3). Importantly, depth-integrated concentrations over the entire water column were also highest during the periods of stratification, and lowest towards the end of the mixing period in 2014 when the depth to anoxia reached its maximum. In both 2013 and 2014, brGDGT concentrations increased when stratification developed after the period of deep mixing. However, the fractional abundance of individual brGDGTs was different during the two periods of stratification covered by this study. During stratification in 2013/2014, the brGDGT assemblage mainly consisted of Ib and IIb at 25-50 m water depth, and IIa' and IIIa' at 80 m; during stratification in 2014/2015, Ib and IIb concentrations were strongly reduced and especially IIa' and IIIa' extended up to 25 m water depth (Fig. 6.3).

The first three components of a PCA on the fractional abundances of the eight major brGDGTs in all SPM samples (n = 101) together explain 83.3% of the observed variation (Fig. 6.5A-B). PC1 explains 47.4% of the variance, has strong negative loadings for brGDGTs IIa' and IIIa', and strong positive loadings for Ib, IIa, IIb and IIIa. PC2 explains 22.7% of the variance, and mainly shows strong negative loadings for Ia and IIb'. PC3 explains 13.5% of the variance and shows a strong positive loading for IIb'.

6.3.3 BrGDGTs in settling particles

The total flux of brGDGTs varied by two orders of magnitude (between 84 and 5268 ng m^{-2} d^{-1}) over the 53-month period of sediment-trap deployment (Fig. 6.6B). Total brGDGT flux is not related to the bulk flux (Fig. 6.6A) of settling particles (R^2 = –0.02, p = 0.91), and does not seem to be restricted to or dominated by a specific season of production and/or sedimentation. The brGDGT concentrations in settling particles were generally higher than in the 'snap-shot' SPM samples, enabling quantification of all studied brGDGTs except IIIc. Nevertheless, like in SPM, the fractional abundance of brGDGTs IIc, IIIb and IIIc' is <0.02 each at all times, and rarely >0.02 in Ic, IIc', IIIa and IIIb' (Fig. 6.4A). BrGDGTs IIc, IIIb and IIIc' were also found in only 62-77% of the 53 samples, whereas all other brGDGTs were found in at least 94%.

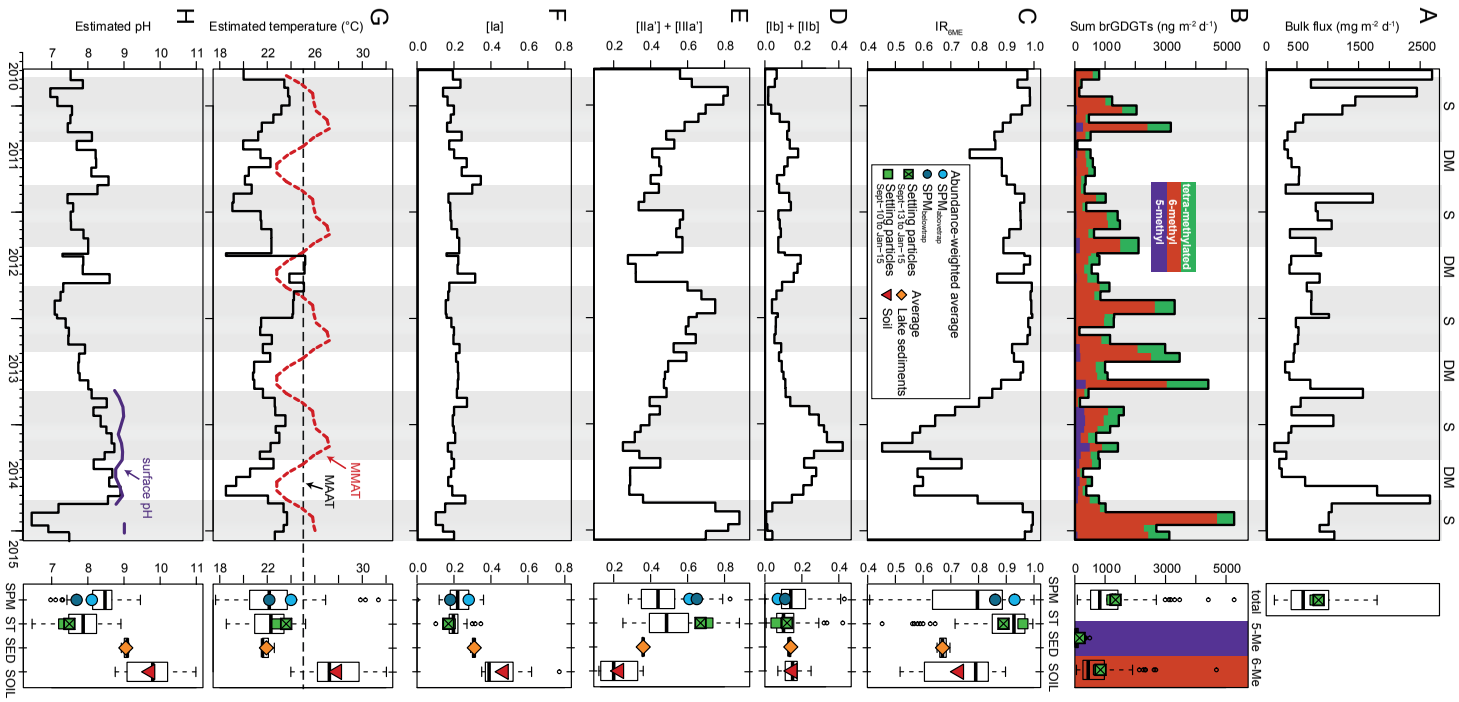

Figure 6.6 Time series of settling-particle data from Lake Chala, based on 53 months of sediment trapping from August 2010 to January 2015. A: Temporal variation in total bulk dry flux (mg m^{-2} day^{-1}). B: Total brGDGT flux (ng m^{-2} day^{-1}) with indication of the proportions of 5-methyl (purple) and 6-methyl (brown) brGDGTs; the remainder are tetra-methylated brGDGTs (green). C: Fraction of 6-methyl of penta- and hexamethylated brGDGTs (IR_{6ME}). D-F: Fractional abundances of brGDGTs Ib+IIb (D), IIa'+IIIa' (E) and Ia (F). G: Reconstructed mean annual air temperature (MAAT), using the EAL SFS calibration of Russell et al. (2018). Also indicated are MMAT (red dashed line) and MAAT (black dashed line). H: Reconstructed surface-water pH, using the EAL calibration of Russell et al. (2018), and pH measured at the surface (0 m) during the period September 2013 to January 2015 (van Bree et al., 2018b). The right-hand panels show boxplots indicating median, interquartile, minimum, maximum and outlier proxy values of the bulk and brGDGT fluxes (A-B), suspended-particulate data (SPM in C-H; n = 101), settling-particle data (ST in C-H; n = 53), lake-sediment data (SED in C-H; n = 3) and catchment soil data (SOIL in C-H; n = 7). These box plots are superimposed with flux- or abundance-weighted average values of the same for $SPM_{abovetrap}$ (light blue circle), $SPM_{belowtrap}$ (dark blue circle), settling particles trapped over the 17-month period of SPM sampling (September 2013 to January 2015, crossed green square) or over the 53-month period starting three years earlier (September 2010 to January 2015, green square), lake sediments (orange diamond) and soils (red triangle). Grey background shading highlights the periods of seasonal water column stratification (S) and deep mixing (DM).

The distribution of individual brGDGTs shows large variation throughout the sediment-trap record (Fig. 6.6B-F). With a combined fractional abundance ranging between 0.46 and 0.61 (n = 53), the majority of brGDGTs in settling particles were penta-methylated, similar to what was found in SPM. BrGDGT IIa' was again most often the dominant compound (fluxes of up to 3157 ng m^{-2} day^{-1}, in November 2014; Fig. 6.4A), although at times IIb (343 ng m^{-2} day^{-1} in March 2014) and IIb' (531 ng m^{-2} day^{-1} in August 2013) were substantial as well. The fractional abundance of tetra-methylated brGDGTs ranged from 0.11 to 0.46 (mostly of Ia, as in the SPM), and hexa-methylated brGDGTs ranged from 0.07 to 0.28 (mostly IIIa', as in the SPM). The 6-methyl brGDGTs most often (41 out of 53 months) comprised at least 80% of the total 5- and 6-methyl brGDGTs (IR_{6ME} >0.8, Fig. 6.6C), except in June 2011 and from November 2013 to September 2014.

The first three components of the PCA on the fractional abundances of the eight brGDGTs most common in settling particles (Ia, Ib, IIa, IIa', IIb, IIb', IIIa, and IIIa', as in the SPM) together explain 91.4% of the observed variation through time (n = 53; Fig. 6.5C-D). PC1 explains 57.5% of the variance and has strong negative loadings for brGDGTs IIa' and IIIa', and positive loadings for Ia, Ib, IIa, IIb and IIIa. PC2 explains 23.7% of the total variance and has strong negative loadings for Ia and IIb', and positive loadings for especially IIa, IIb and IIIa. PC3 explains 10.2% of the total variance and has a strong positive loading for Ia. Thus, overall the variation in fractional abundances of individual brGDGTs are similar in SPM and settling particles. The PCA of both the 101 SPM and 53 sediment-trap samples together (Fig. 6.5E) indicate that brGDGT distributions were mainly divided by the relative abundance of 5- and 6-methyl brGDGTs (PC1 explains 48.6% of the total variance), and by a separation of brGDGTs Ia and IIb' from the six others (PC2 explains 22.4% of the total variance). As can be expected, the brGDGT distribution in settling particles is most similar to that in SPM from the upper water column, i.e. sampled at depths situated above the sediment trap (Fig. 6.5E).

6.3.4 BrGDGTs in catchment soils

BrGDGTs in the soils surrounding Lake Chala are predominantly tetra-methylated (fractional abundance 0.48-0.84, n = 7), followed by penta-methylated (0.15-0.44) and hexa-methylated (0.01-0.09) compounds (Fig. 6.4B). The tetra-methylated brGDGTs, as well as compounds IIa', IIb', and IIIa' were present in all analyzed soils. Penta- and hexa-methylated brGDGTs were below detection limit in two (IIa, IIIb), three (IIb), four (IIa', IIIb') or five (IIIa) soil samples, and the fractional abundance of IIc, IIc', IIIb and IIIb' was usually <0.02. BrGDGTs IIIc and IIIc' were always below detection limit (Fig. 6.4A). The ratio between 5- and 6-methyl brGDGTs (IR_{6ME}) ranges between 0.52 and 0.90, with a mean value of 0.73 (Fig. 6.6C). Variation in brGDGT distribution among soils is explained mainly by their location in- or outside of the crater basin (hinterland savanna, ravine, crater rim or lakeshore forest), in line with results of analyses which did not differentiate between 5- and 6-methyl brGDGTs (Buckles et al., 2014). The brGDGT distributions in soils differ from those in SPM and settling particles mainly by their higher fractional abundance of mainly Ia, Ib and IIa, and lower proportion of 6-methyl compounds (Fig. 6.4A). When added to the PCA of water-column brGDGTs (Fig. 6.5E) as passive samples, all soils plot in the third quadrant of positive PC1 and negative PC2 values.

6.3.5 BrGDGTs in lake sediments

All brGDGTs except IIIc and IIIc' were detected in the lake sediments (n = 3), although the fractional abundances of Ic, IIc, IIc', IIIb, IIIb' are always <0.02 (Fig. 6.4A). The brGDGT distribution in the three lake-sediment samples are also highly similar (Fig. 6.4B), with fractional

abundances of 0.47-0.48 for penta-methylated, 0.40-0.41 for tetra-methylated, and 0.12 for hexa-methylated brGDGTs, and Ia (0.31) and IIa' (0.27) being the dominant compounds. IR_{6ME} is ~0.67 (Fig. 6.6C). The brGDGT distribution in these lake sediments falls within the range of SPM and settling-particle distributions (Fig. 6.4B), however only with positive PC1 scores like the soil samples (Fig. 6.5E).

6.3.6 Microbial diversity and abundance in the water column of Lake Chala

The main groups of microbiota found in the water column of Lake Chala, over all successfully analyzed SPM samples independent of sampling months and depths (n = 216), were Acidobacteria, Actinobacteria, Chlorobi, Chloroflexi, Firmicutes, Bacteriodetes, Planctomycetes, Parcubacteria, Verrucomicrobia, and especially Proteobacteria (Table S6.5; S6.6). Among the Acidobacteria, sequences closely affiliated to Blastocatellia (subdivision SD 4), as well as those closely related to SD 21 and SD 6 dominated throughout the water column (Table S6.6).

The relationship between the distribution of 16S rRNA gene abundance estimates and absolute concentrations of the eight most common brGDGTs in the Lake Chala SPM is shown in Fig. 6.7. For Acidobacteria, the best correlation was found between brGDGTs Ib and IIb and Acidobacteria subdivision SD 21 (R^2 = 0.18 and 0.20, respectively; p <0.0001, n = 99). All other correlations between individual brGDGTs and Acidobacteria subdivisions (both SD 21 and others) are weaker (R^2 = 0.0 to 0.05; Fig. 6.7A). Outside of the Acidobacteria, modest positive correlations ($R^2 \geq 0.15$) were found between at least one of the eight major brGDGTs and the 16S rRNA gene abundance of 14 individual taxa of bacteria (Fig. 6.7B).

6.4 Discussion

6.4.1 Aquatic origin of Lake Chala brGDGTs

BrGDGTs in lakes can originate from terrestrial and aquatic sources, and hence a mixed signal is usually expected. There are several indications that the SPM of Lake Chala primarily contains brGDGTs produced within the water column rather than being washed in with eroding soils. Firstly, brGDGT concentrations show an order-of-magnitude increase with depth (Fig. 6.3). Based on data from a limited number of SPM profiles, it was previously thought that this pattern mainly originated because of favorable conditions for organic preservation in the anoxic lower water column of Lake Chala (Sinninghe Damsté et al., 2009; Buckles et al., 2014). Such a presumed stable brGDGT reservoir might be formed when slowly sinking organic particles become neutrally buoyant in the cooler hypolimnion and consequently accumulate over time, combined with a lack of processes (such as grazing and aggregation) to remove these particles from the water column (Sinninghe Damsté et al., 2009; Buckles et al., 2014). However, since our data show significant variation in brGDGT composition between different depth intervals within the anoxic lower water column (Fig. 6.3), the concept of a static hypolimnetic brGDGT reservoir is clearly untenable. Secondly, the total brGDGT concentration throughout the water column in SPM is lower at the end of the mixing season (and start of the ensuing stratification) than during peak stratification conditions (Fig. 6.3), arguing against the notion that upwelling during the mixing season merely disperses deep-water brGDGTs throughout the water column. Thirdly, the distribution and abundance of individual brGDGTs changes not only with depth but also through time (Fig. 6.3). Especially the changes in the lower water column are remarkable given the fact that the maximum mixing depth between September 2013 and January 2015 was limited to ~45 m (Fig. 6.2; van Bree et al.,

2018b). For example, the total brGDGT concentration at 80 m depth fluctuated between 0.98 ng L^{-1} (February 2014) and 15.5 ng L^{-1} (October 2014), and there are large fluctuations in the degrees of cyclization, methylation, and 5- or 6-methyl positioning within the brGDGTs (Fig. 6.3). Finally, the contrast in brGDGT distributions between SPM from the oxygenated and anoxic parts of the water column (largely corresponding with the zones above and below the sediment trap; Fig. 6.3), and soils (Fig. 6.4A-B) strongly suggests that high deep-water brGDGT concentrations do not result primarily from the accumulation of soil-derived brGDGTs preserved in anoxic conditions, but from *in situ* production, especially below the oxycline. Our combined evidence indicates that over the studied 17-month interval, (almost) all brGDGTs in the water column of Lake Chala have a solely aquatic source while terrestrial input is negligible. This result corroborates the findings of Buckles et al. (2014), and is also consistent with the general lack of terrestrial biomarkers, such as long-chain *n*-alkanes, in the SPM of Lake Chala during this same time interval (van Bree et al., 2018b).

6.4.2 Temporal variation in brGDGT distributions

Variation in the distributions and concentrations of individual brGDGTs over time is larger than the variation with depth. From November 2013 to August 2014, the anoxic lower water column is characterized by high concentrations and fractional abundances of brGDGTs Ib and IIb, both peaking at 50 m depth (Fig. 6.3). Although seemingly similar environmental conditions occur at the end of 2014 when deep mixing ends and stratification develops, Ib and IIb do not return. Instead, the concentrations of IIa' and IIIa' rapidly increase at this time. Hence, it appears that deep mixing promotes either the production of Ib-IIb (5-methyl with rings) brGDGTs or that of IIa'-IIIa' (branched 6-methyl) brGDGTs. Our PCA indeed indicates that most temporal variation in the brGDGT composition of SPM is explained by the dominance of either 5-methyl or 6-methyl brGDGTs (PC1 47.4%, Fig. 6.5A). Moreover, 5-methyl and 6-methyl brGDGTs with cyclopentyl moieties show distinct patterns both with depth and over time, reflected in their opposite scores on PC2 (Fig. 6.5A-B). The 5-methyl brGDGTs with cyclopentyl moieties are mainly restricted to the medium deep anoxic waters (centered at 50 m) during strong stratification when anoxia extends up to ~15 m water depth, while 6-methyl brGDGTs with cyclopentyl moieties are most prominent at 80 m depth, although the concentrations of IIb' in SPM is overall quite low. Incorporation of cyclopentyl moieties into 5-methyl and 6-methyl brGDGTs thus seems to be driven by different factors.

6.4.3 Membrane plasticity versus community changes in aquatic brGDGT producers

It is generally assumed that brGDGT producers adjust the molecular structure of their membrane lipids in response to environmental changes, and in fact, these membrane adaptations are at the heart of brGDGT-based paleoenvironmental proxies (e.g. Weijers et al., 2007b). However, a straightforward link between brGDGT signatures and seasonally changing environmental conditions seems to be lacking in Lake Chala, as illustrated by the distinct brGDGT distributions during the two stratification episodes in our 17-month study period, and the apparently different drivers of cyclization in 5-methyl versus 6-methyl brGDGTs (Section 6.4.2). The fact that temporal variation in the fractional abundance of brGDGTs is not easily linked to the seasonally recurring variation in either temperature, oxygen or pH indicates that the molecular composition of brGDGT membrane lipids is not primarily governed by membrane adaptation to changing abiotic conditions. Instead, they may result from changes in the composition of the microbial community, which consequently will produce different brGDGTs at different times. This is also seen in meromictic

Lake Lugano (Switzerland), where compositional changes in brGDGTs with depth are strongly related to bacterial community changes across the oxycline (Weber et al., 2018).

The producers of aquatic brGDGTs in Lake Chala can potentially be identified by comparing the depth distribution and temporal variation of individual brGDGTs with 16S rRNA gene data obtained from the same SPM samples. The only bacteria currently known to produce brGDGT Ia, as well as its precursor lipids 5- and 6-methyl *iso*-diabolic acid, are Acidobacteria (Sinninghe Damsté et al., 2018). However, this has only been demonstrated for certain Acidobacteria strains cultured from soils. Although some individual brGDGTs in Lake Lugano show strong empirical correlation (R^2 >0.56) with certain acidobacterial subdivisions (Weber et al., 2018), very little is known about the occurrence and diversity of Acidobacteria in lakes (e.g., Zimmermann et al., 2012; Parvenova et al., 2016; Preheim et al., 2016). In Lake Chala, only few correlations between individual brGDGTs and Acidobacteria subdivisions are at least moderately strong (Fig. 6.7A). However, whereas in Lake Chala the abundance of SD 21 is correlated to the concentration of brGDGTs Ib and IIb, in Lake Lugano this subdivision relates with brGDGTs IIa, IIIa and IIIa" (Weber et al., 2018). Given the overall low abundance of acidobacterial 16S rRNA sequences in Lake Chala SPM notwithstanding the omnipresence and high concentrations of brGDGTs, and the mostly weak correlation between them, it seems unlikely that Acidobacteria are main producers of brGDGTs in Lake Chala.

To investigate alternative sources for the Lake Chala brGDGTs, we correlated their distributions with all microbial taxa identified in the SPM (Fig. 6.7B). Although empirical co-occurrence of brGDGTs and microbial taxa alone does not suffice to reveal the exact source organism(s) of those

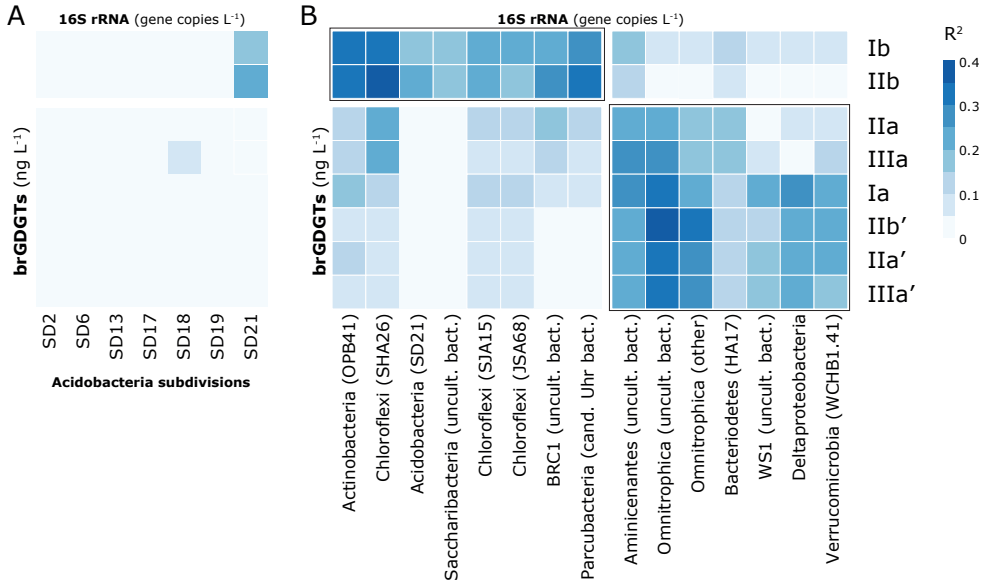

Figure 6.7 Correlation matrix (R^2; represented by shades of blue) between the absolute concentration of the eight major brGDGTs in Lake Chala SPM (ng L^{-1}) and estimated 16S rRNA gene abundances (copies L^{-1}, see details in text). A: Acidobacteria subdivisions (SD) 2, 6, 13, 17, 18, 19 and 21. B: The 15 taxa of microbiota displaying highest correlation with individual brGDGTs, divided in clusters of highest correlation with Ib and IIb or with the other brGDGTs.

brGDGTs, the detected phyla might either contain brGDGT-producing organisms or be associated with similar habitats. For example, the correlation of Ib and IIb with members of the Chloroflexi phylum can be indicative of the depth habitat or growth season of the organism producing these specific brGDGTs. Our broad brGDGT-DNA data comparison generates two clusters (Fig. 6.7B). One cluster of microorganisms correlates with brGDGTs Ib and IIb, whereas the other cluster correlates with non-cyclic and/or 6-methyl brGDGTs. This clustering is hence consistent with the spatiotemporal alternation of brGDGTs Ib+IIb and IIa'+IIIa' observed in the water column of Lake Chala (Fig. 6.3), and suggests that these different brGDGTs (i.e., 5-methyl *vs* 6-methyl, and cyclic *vs* non-cyclic brGDGTs) are produced by different (groups of) microbiota. Despite our extensive SPM dataset, it is at this stage not possible to determine exactly which aquatic microbiota produce the brGDGTs in Lake Chala.

6.4.4 Congruence between brGDGT distributions in settling particles and SPM

The 53-month record of brGDGTs in settling particles fully encompasses our 17-month SPM time series, enabling direct comparison of the depth-resolved but 'snapshot' brGDGT signatures in the water column with the depth- and time-integrated brGDGT signature from the upper water column being transferred to the lake floor and intercepted by the sediment trap. The near-absence of terrestrial biomarkers in Lake Chala SPM was noted previously (van Bree et al., 2018b), whereas its bottom sediments do contain such biomarkers in adequate concentrations (e.g., Sinninghe Damsté et al., 2011b). We therefore expected the settling particles to contain more terrestrial material and so bridge the gap between SPM and sediments (van Bree et al., 2018b) with a mixed soil – aquatic signature. However, brGDGT distribution in sediment-trap material is highly similar to that in the SPM, both in individual samples (Figs. 6.4B and 6.5E), and as expressed in the respective temporally-integrated weighted-average brGDGT fractional abundances (Figs. 6.4A and 6.6C-F). It thus appears that also the vast majority of brGDGTs in settling particles has an aquatic origin, and consequently can be expected to show the same temporal trends as the brGDGTs in SPM. Indeed, in the PCA including both SPM and settling particles (Fig. 6.5E), PC1 reflects the temporal separation of 5- and 6-methyl brGDGTs probably associated with different microbial communities (see Section 6.4.3), whereas PC2 separates the higher fractional abundance of Ia+IIb' in the warm and oxygenated upper water column versus all other common brGDGTs in the cooler, oxygen-depleted, low-pH lower water column. Although the concentration of IIb' is low in the upper water column, its fractional abundance is generally higher in the oxygenated water column compared to the anoxic water.

Despite their similarity, the sediment-trap and SPM time series are not fully equivalent. Settling particles represent brGDGTs produced in the upper 35 m of the water column, and indeed, the individual sediment-trap samples overlap mostly with the $SPM_{abovetrap}$ samples (Fig. 6.5E). In contrast, the time-integrated brGDGT distribution in sediment-trap material of the overlapping 17-month record seems to be more similar with the depth- and time-integrated (weighted average) brGDGT signal in SPM from the mostly anoxic water column below the sediment trap (>35 m) than that of the more oxic upper water column (<35 m; Fig. 6.4A-B) for various brGDGTs. For example, the proportion of tetra-, penta- and hexamethylated brGDGTs of the weighted-average settling particles is similar to that of the $SPM_{belowtrap}$ samples, as well as the abundance of Ib+IIb. In this study, the depth- and time-integrated value of $SPM_{abovetrap}$ is based on brGDGT fractional abundances from 0, 10 and 25 m depth, so that distributional differences between $SPM_{abovetrap}$, $SPM_{belowtrap}$ and the settling particles can also be caused by brGDGT production between 25 and 35 m. Indeed, brGDGTs in two SPM profiles analyzed at higher resolution (November 2013 and

August 2014) indicate a moderate to large increase in concentration between these depth intervals. The general agreement between the brGDGTs in the anoxic water column and the setting particles might also reflect the fact that the depth discrimination only develops during periods of water-column stratification. During mixing episodes (reaching down to ~40-45 m in the 2014/2015 monitoring period, and possibly to as much as 60 m in other time intervals; *cf.* Verschuren et al., 2009), the sediment trap can also include material upwelled from the deeper water layers, where brGDGT concentrations are much higher.

6.4.5 Multi-annual trends in brGDGT fluxes and composition

The substantial temporal variation in both the fluxes and fractional abundances of brGDGTs in Lake Chala was documented in a previous study covering settling particles collected in the period from November 2006 to August 2010 (Buckles et al., 2014), but appears to be even stronger with the separation of 5- and 6-methyl brGDGTs performed in this study. This contrasts with findings from sediment-trap studies in north-temperate lakes (e.g. Loomis et al., 2014b; Miller et al., 2018), where brGDGT distributions in settling particles remain relatively stable despite large seasonal changes in their flux.

Aside from the large temporal variation in brGDGT distributions, the whole of our 17-month SPM sampling period, and the period from September 2013 to September 2014 in particular, stand out in the 53-month sediment-trap record due to the relatively high flux of 5-methyl brGDGTs with rings (IIb), and a relatively low flux of 6-methyl brGDGTs (IIa', IIIa') (Fig. 6.6D-E). The relatively large contribution of 5-methyl brGDGTs during this period is reflected in a very low IR_{6ME} values, unprecedented in the entire 53-month time series (Fig. 6.6C). Notably, this 13-month period of low IR_{6ME} is also characterized by the near-absence of terrestrial biomarkers (van Bree et al., 2018b). As the bottom sediments of Lake Chala contain reasonably high concentrations of terrestrial biomarkers such as plant waxes (Sinninghe Damsté et al., 2009; van Bree et al., 2016), these should transfer through the water column at some point, and end up in the sediment trap. We surmise that some differences in brGDGT distributions between the said 13-month period and other years are due to an unusually low terrestrial input during this time interval, leaving aquatic production to dominate the brGDGTs pool. Generally speaking, Lake Chala catchment soils are characterized by the high fractional abundance of brGDGT Ia. In contrast, there is not much variation in the fractional abundance of Ia in the sediment-trap record (Fig. 6.6F). Moreover, its fractional abundance is much lower than that in soils (Figs. 6.4A and 6.6F), supporting the lack of soil input during the studied period.

The temporal variation in the brGDGT distributions of Lake Chala SPM seemed to vary mainly with the alternating episodes of stratification and mixing (Fig. 6.3). At first glance, the temporal variation in the sediment-trap record does not show a reoccurring brGDGT response to these alternating conditions on a longer timescale (Fig. 6.6). Nevertheless, alternation can be observed in the relative contributions of Ib+IIb and IIa'+IIIa' through time (Fig. 6.6D, E), in which the onset of stratification is marked by the relative increase of one of these two groups: the fractional abundance of IIa'+IIIa' increased sharply at the onset of stratification in 2010, 2012 and 2014, whereas those of Ib+IIb increased in 2011 and 2013. Although it is not clear which environmental variable controls the predominance of either group in any one year, this pattern supports our suggestion that changing brGDGT distributions in Lake Chala primarily reflect distinct microbial communities rather than a physiological response in a stable resident community, also on multi-annual timescales.

6.4.6 Implications for paleoclimate reconstruction

6.4.6.1 Temperature

As biomarker proxies based on brGDGT distributions are often used for paleoclimate reconstruction, it is important to understand whether variability on short time scales (seasonal, inter-annual) is recorded in the settling particles that eventually end up in the sediment record. An earlier study of brGDGTs in time series of settling particles from Lake Chala (Buckles et al., 2014) indicated that the mean annual air temperature (MAAT) was underestimated by ~11-13°C (values of 14.4±5.2°C and 12.5±5.5°C, using the calibrations of Tierney et al. (2010b) and Loomis et al. (2012), respectively). Also, maxima and minima in reconstructed temperatures based on settling particles lagged air temperature by 5-6 months, and upper water-column temperature by ~3 months. Buckles et al. (2014) attributed these offsets to either a shifted ratio of aquatic versus soil-derived brGDGTs and remarked that the brGDGTs in Lake Chala may have a different temperature relationship than accounted for in the East African lake surface-sediment calibrations. The newest East African lake (EAL) temperature calibration (Russell et al., 2018), which is based on improved chromatography separating the 5- and 6-methyl brGDGTs, substantially improves MAAT estimates from sediment-trap material in this study, yielding $MAAT_{SFS}$ values ranging between 18.5 and 25.2°C (22.1±1.7°C on average, and flux-weighted average 22.8°C), i.e. underestimating the true local MAAT of 25.1°C by ~2-3°C. Nevertheless, the brGDGT-based MAAT reconstruction are still underestimations, and also the seasonal variation in reconstructed temperature is not very systematic (Fig. 6.6G).

Although Lake Chala is not included in the Russell et al. (2018) EAL calibration dataset, the three Chala surface-sediment samples from this study do plot within the overall range of brGDGT distributions found in EAL sediment samples, at least with respect to the overall fractional abundances of type I, II and III brGDGTs (Fig. 6.4B). BrGDGT distributions in Chala SPM and sediment-trap samples, on the other hand, are different from those in EAL sediments (Fig. 6.4B), mainly due to a higher relative abundance of brGDGT IIa'. While in Lake Chala most of the variation in brGDGT production (PC1 48.6%; Fig. 6.5E) is explained by the division between Ib+IIb and IIa'+IIIa', this same division explains a more modest fraction of the variance in EAL sediments (18.8% along PC2; Russell et al., 2018). Conversely, a large part of brGDGT variation in EAL sediments is explained by the changing proportions of Ia and IIa+IIIa (PC1 56.6%; Russell et al., 2018), whereas this is less important in Lake Chala (22.4% along PC2; Fig. 6.5E). This suggests that although temperature appears to be an important driver of variation in brGDGT distributions among modern-day lakes spanning a wide temperature gradient, and by extension also changes in brGDGT distributions at any one location over long time scales, it does not explain short-term temporal changes in brGDGT distributions within a specific lake. Lake Chala is likely not exceptional in this regard, besides being the only equatorial lake that has been studied this extensively so far.

Short-term temporal variation in the brGDGT distributions in Lake Chala most likely reflect microbial community changes, which may be one reason why brGDGT signatures are not directly related to the corresponding MMAT (Fig. 6.6G). Considering that reconstructed MMAT systematically underestimates measured MMAT in almost all sediment-trap samples, it is remarkable that the flux-weighted and temporally-integrated brGDGT signature of the setting particles (22.8°C, n = 53) and especially the 17-month period (23.6°C, n = 17) matches the measured local MAAT within the model's calibration error (2.14°C; Russell et al., 2018). Also the most often higher temperature of the epilimnion compared to the lower water column (up to ~4°C, depending on the season) is reflected in a higher overall average $SPM_{abovetrap}$ temperature value

(23.2°C, n = 57) than the corresponding $SPM_{belowtrap}$ value (20.7°C, n = 44, p <0.01; Fig. 6.6G). Given these results, it is notable that both aquatic and soil-derived brGDGTs reconstruct a slightly higher MAAT than that is recorded in the sediment (21.9°C, n = 3; Fig. 6.6G). In theory, the lake sediments should integrate both aquatic and terrestrial brGDGTs, with more soil-derived brGDGTs leading to higher reconstructed temperatures, as brGDGTs in soils reflect on average 4-6°C higher temperatures than aquatic brGDGTs (e.g. based on the $MAAT_{SFS}$ of Russell et al., 2018; Fig. 6.6G). Thus, brGDGTs in Chala sediments (time-integrated mixtures of brGDGTs from terrestrial and aquatic sources) are expected to overestimate actual MAAT, and not underestimate MAAT as is recorded in Lake Chala. This might indicate additional brGDGT production within the sediments.

6.4.6.2 pH

In soils and peats, both the number of cyclopentyl moieties in brGDGTs and the relative abundance of 6-methyl brGDGTs relate with soil pH (Weijers et al., 2007b; Peterse et al., 2010; De Jonge et al., 2014a; Naafs et al., 2017b). Even though this relationship is much weaker in East African lakes (Russell et al., 2018), the EAL calibration dataset does indicate a possible influence of surface-water pH on the composition of aquatic brGDGTs. In our data from Lake Chala, reconstructed pH in settling particles varies between 6.5 and 8.9 (n = 53), with no consistent trend over time (Fig. 6.6H). Nevertheless, time-integrated reconstructed pH values from the different study materials suggest an influence of pH (or associated environmental factors) on brGDGT composition. The pH values in the water column decrease with depth (Wolff et al., 2014; van Bree et al., 2018b), a pattern which is reflected in the SPM pH reconstructions, where the average surface-water pH estimate at 0 m (8.5) is higher than that at 80 m (8.1, p <0.01). Also, pH reconstructed from brGDGTs in settling particles is higher, on average, during deep mixing (8.1, n = 16) when surface-water pH values can increase due to increased primary productivity, than during stratified conditions (7.7, n = 37; p <0.02). Nevertheless, the pH value based on flux-weighted temporally-integrated settling-particle data (7.3) underestimates Lake Chala's surface water (~8.1; Fig. 6.6H). This underestimation of pH based on the aquatic brGDGTs contrasts with overestimation when based on sediment samples (9.1; Fig. 6.6H), likely due to the influence of soil-derived brGDGTs with a relatively high fractional abundance of compound Ia (Fig. 6.4A).

6.4.6.3 Discrepancy between water-column and sedimentary brGDGT signatures

The brGDGT distribution in the surficial bottom sediments of Lake Chala clearly differs from those in the SPM and settling particles, even when the latter are integrated over time and weighted-averaged (Fig. 6.6C-F). The full range of IR_{6ME} values, for example, is very large in SPM and settling particles whereas the three sediment samples give near-identical values (Fig. 6.6C). The weighted-average values indicate that over 88% (n = 17) or 96.2% (n = 53) of brGDGTs II and III in settling particles belong to the 6-methyl variety (Fig. 6.6B), whereas this is only 67% in the sediment. It may be that brGDGTs accumulating in the sediments comprise more soil-derived brGDGTs with lower IR_{6ME} than aquatic brGDGTs, and that during accumulation of the analyzed sediments (the 3-5 cm depth interval represents a period of ~10-15 years during the late 20th-century; Blaauw et al., 2011) there was more soil input, on average, compared to the very low soil input in the studied time interval of the sediment trap. It is also possible that additional production of brGDGTs in the sediment is responsible for the offsets between proxy values in soils, the water column and the sediment. Thus, seasonal changes and inter-annual variability in aquatic brGDGT production in the water column (and/or sediments), as well as varying proportions of aquatic and terrestrial

brGDGTs over time may influence paleoenvironmental reconstructions based on brGDGTs in Lake Chala sediments.

6.5 Conclusions

BrGDGTs in the water column of Lake Chala are primarily produced *in situ*. The amounts and distributions of individual aquatic brGDGT compounds are highly variable with depth and over time, and do not consistently relate to ambient temperature, pH or oxygen but still appear to respond to the alternation of water-column mixing and stratification. The observed switch from a Ib+IIb dominated brGDGT signature to a IIa'+IIIa' signature can be linked to a coincident shift in the lake's microbial community unrelated to the Acidobacteria. Hence, the changes in brGDGTs in response to changing environmental conditions are likely due to the sequential occurrence of different groups of microbiota producing different brGDGTs, and not by membrane adaptation by the same resident microbiota. This detailed and long-term study on brGDGTs in Lake Chala highlights substantial inter-annual variation in the aquatic microbial community of this tropical lake, superimposed on seasonal variation. Although the brGDGT distributions in SPM and settling particles from Lake Chala cannot be linked directly to local variation in air or water temperature, temporally-integrated and flux-weighted brGDGT compositions do produce fairly accurate temperature and surface-water pH estimates when using the new EAL calibration of Russell et al. (2018). Thus, this study established an empirical link between aquatic brGDGT signatures and local environmental variables, when the former are integrated over a longer period of production. Regardless, it remains crucial to discover the producers of brGDGTs and general drivers of brGDGT production in lakes so that the uncertainties in lacustrine paleothermometry can be further constrained.

Data availability

All data presented in this study will be made available upon publication in a scientific journal.

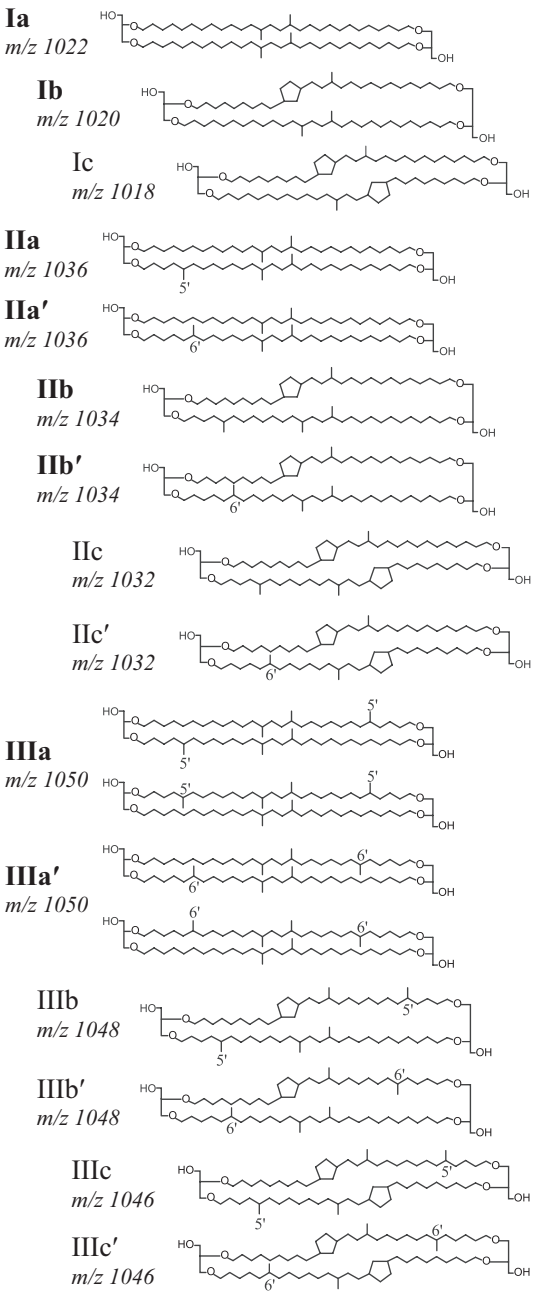

Figure S6.1 Structures of the 15 brGDGT compounds considered in this study, consisting of two ether-linked dialkyl chains with zero to two additional methyl branches (I, II and III) and zero to two cyclopentyl moieties (suffixes a, b and c). The 6-methyl isomers are denoted with a prime. Compounds indicated in bold are the eight most common brGDGTs encountered in this study.

Acknowledgements

We thank C.M. Oluseno for conducting the monthly lake sampling and monitoring. We thank A.M.D. Negash and P. de Regt for lipid extractions, J.W. de Leeuw and A. Baxter for feedback on the manuscript. We are grateful to A. van Dijk, D. Kasjaniuk, A. van Leeuwen-Tolboom and K. Nierop at Utrecht University; and M. Baas, D. Dorhout, E. Hopmans, A. Mets, J. Ossebaar, S. Vreugdenhil and M. Brouwer at the Royal NIOZ for technical and analytical support. We furthermore thank A. Roepert for help with R, and C. De Jonge for discussions on brGDGTs. Fieldwork with collection of the studied sample materials was carried out with permission from the government of Kenya through permit 13/001/11C to D.V. In accordance with National Environmental Management Authority regulations in the context of the Nagoya Protocol, DNA extracts of the analyzed suspended-particulate samples are archived at the National Museums of Kenya (NMK), under voucher numbers NMK:BCT:80001 to NMK:BCT:80221; we thank A. Mwaura and S.M. Rucina for facilitation. The raw data of the 16S rRNA gene amplicon reads were deposited in the NCBI Sequence Read Archive (SRA); BioProject number upon request. This research was supported by the NESSC Gravitation Grant (024.002.001) from the Dutch Ministry of Education, Culture and Science (OCW) to J.S.S.D.

A pregnant black rhinoceros is accompanied by her mate in the Kenyan Masai Mara National Reserve, 300 km north-west of Mt. Kilimanjaro.

7 Seasonal and multi-annual variation in isoGDGT membrane lipids and their producers in the water column of a meromictic equatorial crater lake (Lake Chala)

L.G.J. van Bree, F. Peterse, S. van Grinsven, L. Villanueva, D. Verschuren and J.S. Sinninghe Damsté

Abstract

Isoprenoid glycerol dialkyl glycerol tetraethers (isoGDGTs) are membrane lipids of archaea. These lipids and associated proxies, such as the TEX_{86} paleothermometer, are often used in paleoenvironmental reconstructions for the marine environment. The general applicability of isoGDGT-based proxies in lacustrine settings is hampered by a limited understanding of their biological sources and the environmental drivers influencing their production. To validate the use of isoGDGT-proxies in lakes, we studied the occurrence of isoGDGTs in Lake Chala, a permanently stratified (meromictic) crater lake in equatorial East Africa. We analyzed the abundance and distribution of isoGDGTs in 17 depth profiles of suspended particulate matter (SPM) collected monthly between September 2013 and January 2015, and compared the results with the abundance and composition of archaea based on 16S rRNA gene and quantitative PCR analysis in the same SPM samples. Subsequently we analyzed the flux and distribution of isoGDGTs in settling particles collected monthly between November 2006 and January 2015 from a sediment trap suspended at 35 m water depth to assess seasonal and inter-annual variability in isoGDGT production, and compared the results with the abundance of isoGDGTs deposited in the sediments. Both isoGDGT and archaeal abundance in the SPM were exceptionally low throughout the 17-month study period. Regardless, the composition of isoGDGTs and the archaeal community in the oxygenated upper water column clearly differ from that in the anoxic lower water column. In oxygenated waters, higher fractional abundances of crenarchaeol are matched by a predominance of the ammonia-oxidizing Thaumarchaeota I.1b that are known to produce it, whereas the deep water is characterized by the presence of isoGDGT-0, as well as anaerobic heterotrophic group C_3 MCG Bathyarchaea and specific euryarchaeotal methanogens. The multi-annual variation of isoGDGT distributions in settling particles confirms that the ambient oxygen level is an important driver of archaeal community composition through time. Episodes of high isoGDGT-0 concentrations relative to those of crenarchaeol in the settling particles can be linked to a very shallow depth of the oxic-anoxic boundary (i.e., well above sediment-trap depth) during episodes of strong water-column stratification in 2008 and 2014. These high isoGDGT-0/crenarchaeol values result from both increased isoGDGT-0 fluxes and very low crenarchaeol fluxes, indicating suppression of the thaumarchaeotal bloom at these times. TEX_{86} reconstructed paleotemperatures are not reliable when the thaumarchaeal bloom is suppressed during strong stratification, as isoGDGT input from

other archaeal sources then disproportionally influences TEX_{86} values. The amount of crenarchaeol isomer relative to total crenarchaeol gradually increases during prolonged stratification, and might prove a good marker for a high frequency of prolonged stratification in the sedimentary record. Most importantly, the associated near-absence of crenarchaeol results in high Branched and Isoprenoid Tetraether (BIT) index values. We propose that this suppression mechanism may be a principal driver of variation in the sedimentary BIT index record from Lake Chala, where strong stratification is linked to increased monsoonal precipitation.

7.1 Introduction

Lipid biomarkers in lake sediments are increasingly used to reconstruct paleoenvironmental changes, such as temperature, rainfall and vegetation dynamics in the lake's catchment (e.g., Castañeda and Schouten, 2011; Schouten et al., 2013; Berke, 2018). Sediments of meromictic lakes are especially suitable for biomarker studies due to their high preservation potential resulting from permanent water-column stratification and associated stable anoxic conditions at the sediment-water interface. Isoprenoid and branched glycerol dialkyl glycerol tetraethers (isoGDGTs and brGDGTs, respectively) represent an important groups of biomarkers in sediments. IsoGDGTs are membrane lipids of Archaea, which biosynthesize varying proportions of isoGDGTs with zero to eight cyclopentyl moieties (GDGT-0 to 8), as well as a compound with four cyclopentyl and one cyclohexyl moiety called crenarchaeol (de Rosa and Gambacorta, 1988; Sinninge Damsté et al., 2002; structures in Fig. S7.1). IsoGDGT-0 is the most common GDGT in archaea, and is found in chemolithotrophic, ammonia-oxidizing Thaumarchaeota (e.g., Sinninghe Damsté et al., 2012b; Schouten et al., 2013; Elling et al., 2017), anaerobic methane-oxidizing archaea (e.g., Pancost et al., 2001; Schouten et al., 2001) and methanogenic Eury- and Bathyarchaeota (Schouten et al., 2013, and references therein). IsoGDGT-1 to -3 are common lipids in eury-, cren- and thaumarchaeotal membranes (Schouten et al., 2013, and references therein), whereas crenarchaeol and its isomer have only been found in cultures of Thaumarchaeota (e.g., Sinninghe Damsté et al., 2002; Schouten et al., 2013; Elling et al., 2017).

The empirical correlation between the distribution of isoGDGTs in marine surface sediments and local sea surface temperature (SST) led to development of the TetraEther indeX of 86 carbon atoms (TEX_{86}; e.g., Schouten et al., 2002; Kim et al., 2012), that is now widely used as SST proxy in paleoclimate reconstructions. An initial study showed that the TEX_{86} for lake sediments also reflected lake surface temperature (LST; Powers et al., 2010), although this relation was based on a substantially smaller calibration set than that for the marine environment. However, the applicability of this proxy in lakes appeared complicated by various factors, such as potential input from soil-derived isoGDGTs, or contributions of isoGDGTs from methanotrophs, methanogens and other archaea (Blaga et al., 2009, 2011; Powers et al., 2010; Sinninghe Damsté et al., 2012a). The contribution of isoGDGTs from methanogens can be assessed by the isoGDGT-0/crenarchaeol ratio. A ratio of >2 indicates that methanogens, that also produce isoGDGT-0, contribute significantly to the total pool of isoGDGTs in the sediments (e.g., Blaga et al., 2009; Bechtel et al., 2010), so that the TEX_{86} proxy cannot be used. Despite these uncertainties, the TEX_{86} paleothermometer has resulted in several important records of past LST variation (e.g., Powers et al., 2005, 2011; Tierney et al., 2008; Woltering et al., 2011), although applicability seems mainly restricted to large lakes.

To assess the input of terrestrial material into an aquatic environment, the Branched and Isoprenoid Tetraether index (BIT index; Hopmans et al., 2004) was proposed, where the relative

abundance of soil-derived brGDGTs compared to that of the aquatic isoGDGT crenarchaeol represents the contribution of soil-derived material delivered to the system after erosion and runoff. It was also applied as such to the 25-kyr sediment core from Lake Chala, a permanently stratified crater lake in equatorial East Africa, where intervals with high BIT index values were linked to periods with increased precipitation (Verschuren et al., 2009). However, in following years several studies showed that brGDGTs are also produced within lakes (e.g., Sinninghe Damsté et al., 2009; Tierney et al., 2010a), challenging the initial interpretation of this proxy in lake settings. Therefore, Sinninghe Damsté et al. (2012a) proposed an alternative explanation for the (indirect) relationship between the BIT index and precipitation in Lake Chala, as strong wind and limited rainfall promotes mixing and thus stimulates primary production, including nitrifying Thaumarchaea that produce crenarchaeol, resulting in a lower BIT. These authors argued that on longer time scales, low lake levels in dry climate conditions would enhance the nitrogen recycling in the lake by improved water-column mixing, in turn promoting crenarchaeol production and resulting in a lower BIT index. Later, Buckles et al. (2016) posed that high BIT values can be linked to episodic high rainfall, during which extreme soil-erosion events increase nutrient availability to the extent that nitrifying Thaumarchaeota are outcompeted by a bloom of nitrifying bacteria. These two alternative mechanisms appear incongruent, however, in that higher aquatic primary production is either presumed to enhance Thaumarchaeota activity (Sinninghe Damsté et al., 2012a) or suppress it by enhancing other microbiota (Buckles et al., 2016). Moreover, these mechanisms do not explain the BIT values reflecting periods of low or normal aquatic productivity.

To better understand the production of isoGDGTs, and thus the functioning of isoGDGT-based proxies in Lake Chala, their occurrence and distribution were studied in one year of monthly collected settling particles (Sinninghe Damsté et al., 2009). This indicated that isoGDGTs were primarily produced in January and February, i.e. after the short rain season, and produced TEX_{86} values that generally reflected LST well but did not reflect the seasonal LST variation (Sinninghe Damsté et al., 2009). However, production of especially GDGT-2 below the depth of the sediment trap (35 m) appeared to alter the isoGDGT signature stored in the sediment record in such a way that the TEX_{86} proxy did not yield reliable results (Sinninghe Damsté et al., 2009, 2012a). Subsequently, the possible producers of isoGDGTs in Lake Chala were studied by comparing the distribution of isoGDGTs and archaeal 16S rRNA sequences in depth profiles of suspended particulate matter (SPM) during two months with contrasting conditions, namely deep mixing in September 2006 and more stratified conditions in February 2010 (Buckles et al., 2013). During mixing, isoGDGTs were most abundant between 50 and 90 m depth, whereas crenarchaeol also showed small increases at 15 and 30 m depth (Sinninghe Damsté et al., 2009). During stratified conditions, crenarchaeol concentrations in the lower water column were substantially lower than during mixing, and all isoGDGTs except isoGDGT-0 peaked at 40 m depth (Buckles et al., 2013). The production of crenarchaeol in the oxygenated upper water column of Lake Chala was attributed to group I.1a and I.1b of the class Thaumarchaeota (also known as the Thaumarchaeota Soil Crenarchaeotic Group), while the high concentrations of isoGDGT-0 in the anoxic deep water was linked to non-methanotrophic archaea of group C3 (Sinninghe Damsté et al., 2009; Buckles et al., 2013), formerly known as Crenarchaeota group 1.2 but currently classified as Miscellaneous Crenarchaeotic Group (MCG), a subgroup of the phylum Bathyarchaeota (Kubo et al., 2012; Lavergne et al., 2018). The presence of archaeal groups that can synthesize isoGDGTs other than Thaumarchaeota has obvious consequences for the reliability of isoGDGT-based proxies in this, and possibly all lakes (Buckles et al., 2013).

However, these initial findings are based on 'snapshot' analyses of the water column of Lake Chala, whereas sediment-trap and high-resolution sedimentary time series reveal that the isoGDGT flux and distribution show a large inter-annual variability (Sinninghe Damsté et al., 2009; Buckles et al., 2014, 2016), which may also hold for their archaeal sources. Here we aim to further investigate spatio-temporal patterns in the production and distribution of isoGDGTs and their producers in Lake Chala. This is accomplished by analyzing the distribution and abundance of isoGDGTs and archaeal 16S rRNA gene copies in SPM depth profiles over a 17-month period. Furthermore, we look for recurrent patterns in 8 years (98 consecutive months) of settling particles to link seasonal and multi-annual trends of isoGDGT production in the upper water column to potential environmental drivers, and to elucidate the interpretation of isoGDGT distributions and proxies such as the BIT index and TEX_{86} in the lake's sediment record.

7.2 Material and methods

7.2.1 Location

Lake Chala (locally known as "Challa", after a nearby village) is a small (4.2 km²), deep (~90 m) and permanently stratified (meromictic) crater lake, situated at ~880 m above sea level on the border of Kenya and Tanzania (3°19′S, 37°42′E) in the southeastern foothills of Mt. Kilimanjaro. Mean monthly air temperature (MMAT) is highest in January-February (25-27°C) during the southern hemisphere (SH) summer, and lowest in July-August (20-21°C). Part of the lake's water budget is maintained by rainfall on the lake surface and inside the steep-sloping crater basin; only occasionally after high rainfall a small creek is activated which breaches the north-western crater rim (Buckles et al., 2014). As lake-surface evaporation (1700 mm yr^{-1}) greatly exceeds annual rainfall (600 mm yr^{-1}), the lake's water budget must be maintained by a substantial subsurface inflow (Payne, 1970) of water which originates from percolation in or above the forest belt on Mt. Kilimanjaro (Hemp, 2006; Bodé et al., submitted). The tropical rain belt associated with latitudinal migration of the Inter-Tropical Convergence Zone (ITCZ) passes over the region twice yearly, resulting in two wet seasons and two dry seasons. "Short rains" occur from late October to December, and "long rains" from March to mid-May. The main dry season occurs during the SH

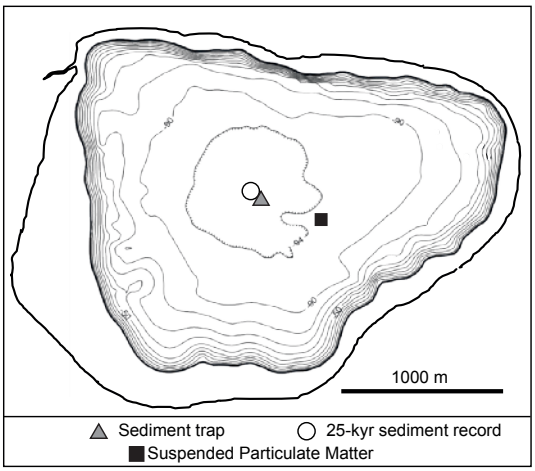

Figure 7.1 Bathymetry of Lake Chala relative to its 2003 shoreline with depth contours at 10-m intervals (modified after Moernaut et al., 2010) with sampling locations of suspended particulate matter (SPM; black square), settling particles (Sediment trap; gray triangle) and the 25-kyr sediment record (open circle). The outer bold line is the crater rim, confining the catchment area.

winter and is characterized by lower air temperature and higher wind speeds that drive deep mixing of the lake's water column down to 40-60 m depth, while the deeper water remains permanently stratified and anoxic (Wolff et al., 2011; van Bree et al., 2018b). Periods of deep mixing (DM) generally start at the end of April, and end in the first half of September (Chapter 6). During DM, oxygen is injected into progressively deeper water, and phytoplankton productivity increases as nutrient-rich deep water is slowly mixed upwards into the normally unproductive epilimnion (Wolff et al., 2014; van Bree et al., 2018b). Conditions of water-column stratification generally develop from September to April, and are strongest during the SH summer months (Wolff et al., 2014; van Bree et al., 2018b; Chapter 6). Superimposed on this long period of stratification, shallow mixing (SM; mixing limited to ~20-25 m depth) occurs in between the two rain seasons. Its timing is variable, but generally starts between the beginning of December and half January, and ends between half February and half March.

7.2.2 Field observations and sample collection

7.2.2.1 Water column sampling

Samples for CH_4 analysis were collected at a mid-lake position on 01-11-2016, using a WildCo® water sampler. Five liter was collected at the same depth intervals as SPM sampling, and brought up as quickly as possible to prevent possible outgassing. The sample from 90 m depth was brought up more slowly and therefore partly outgassed, this CH_4 measurement was dismissed. Two replicate samples were taken at 50 and 60 m depth. The water was transferred immediately to airtight 12 ml exetainer vials, and stored at room temperature prior to analysis. Simultaneous with the water sampling, profiles were collected of ambient physical conditions (temperature, dissolved oxygen and pH), at 2-m intervals throughout the upper 50 m of the water column, using a Hydrolab Quanta multiprobe.

7.2.2.2 SPM

The collection of suspended particulate matter (SPM) profiles used in this study was described in detail by van Bree et al. (2018b). In short, 5-10 L of lake water was collected at 13 discrete depths, monthly between September 2013 and January 2015 (n = 221). The date of collection was at or near the start of each month as discussed here, with samples collected on, for example, 07-09-2013 representing September 2013, and samples collected on 30-09-2013 representing October 2013 (see Table S7.1). The samples were filtered on pre-combusted glass fiber GF/F filters (142 mm diameter, Whatman), stored frozen and freeze-dried prior to analysis. For this study we analyzed lipids in the SPM from all depths for the months November 2013 and August 2014, as well as from 0, 10, 25, 50 and 80 m depth for all other months (n = 101).

7.2.2.3 Sediment trap

Sediment trap sample collection in Lake Chala has been described extensively before (Sinninghe Damsté et al., 2009; Buckles et al., 2014, 2016; Chapter 6). In short, in November 2006 a UWITEC double-funneled sediment trap of 86 mm diameter was installed at 35 m water depth in a mid-lake position (Fig. 7.1), and emptied and redeployed at approximately monthly intervals during the ensuing 8 years (Table S7.1). Collected material was allowed to settle for two days, and stored frozen after decantation of excess water. Prior to analysis, the samples were thawed, filtered over pre-weighed and pre-combusted (400°C, 5h) glass fiber GF/F filters (110 mm diameter, Whatman), frozen and freeze-dried. This study combines new analyses of GDGTs in settling particles representing the period September 2010 to January 2015 (n = 53; Table S7.2), with published data

covering the period November 2006 to August 2010 (Sinninghe Damsté et al., 2009; Buckles et al., 2014, 2016). The brGDGTs in these two sets of samples are discussed separately by Buckles et al. (2014, 2016) and in Chapter 6.

7.2.3 Sample preparation, extraction and analysis

7.2.3.1 Methane analysis

To measure the methane concentration, a 1 ml high purity nitrogen (N_2) headspace was generated in the exetainers, after which samples were left to equilibrate for at least 48 hours prior to measurement. They were injected by hand on a GC-FID, and measured as technical triplicates. The reported values are the average of triplicates and their standard deviation. The two pairs of replicate samples at 50 and 60 m yielded similar results.

7.2.3.2 Lipids

Sample preparation for SPM was described in detail by van Bree et al. (2018b; Chapter 6). In short, the freeze-dried SPM filters were cut in small pieces and extracted using a modified Bligh-Dyer method. Each Bligh-Dyer extract was acid-hydrolyzed with 1.5N hydrochloric acid (HCl) in methanol (MeOH). This hydrolyzed total lipid extract (TLE) was separated on an activated Al_2O_3 column into an apolar, neutral and polar fraction, using hexane:dichloromethane (DCM); 9:1, v:v), DCM, and DCM:MeOH (2:1, v:v) as eluents, respectively. Sample preparation for the sediment-trap samples has been described elsewhere (Chapter 6). In short, the freeze-dried filters with sediment-trap material were cut in small pieces and extracted directly by acid hydrolysis, and the obtained TLE was processed similar to the SPM TLE. A known amount of internal standard (99 ng $GDGT_{46}$) was added to the polar fractions of SPM and settling particles. These fractions were re-dissolved in hexane:isopropanol (99:1, v:v) and passed over a 0.45 µm PTFE filter prior to analysis.

The GDGT analysis was performed with Agilent 1260 Infinity ultrahigh performance liquid chromatography (UHPLC) coupled to an Agilent 6130 single quadrupole mass detector, either at Utrecht University (SPM) or at the Royal NIOZ (settling particles and SPM at 0 m, except SPM from November 2013 and September 2014) following the method of Hopmans et al. (2016). Separation was achieved by two silica Waters Acquity UPLC HEB Hilic (Ø1.7 µm) columns at 30°C, preceded by a guard column with similar packing. Isocratic elution was used for GDGT separation, starting with 82% A (hexane) and 18% B (hexane: isopropanol, 9:1, v:v) for 25 min at a flow rate of 0.2 mL min^{-1}, followed by a linear gradient to 70% A and 30% B for 25 min. Injection volume was 10 µL for settling particles, and 20 µL for SPM. Ionization of the GDGTs was achieved by atmospheric-pressure chemical ionization with as source conditions a gas temperature of 200°C, vaporizer temperature of 400°C, N_2 flow of 6 L min^{-1}, capillary voltage of 3500 V, nebulizer pressure of 25 psi and corona current of 5.0 µA. GDGTs were identified by detecting the $[M+H]^+$ ions in selected ion monitoring (SIM) mode for *m/z* 1018, 1020, 1022, 1032, 1034, 1036, 1046, 1048 and 1050 (brGDGTs), *m/z* 1292, 1294, 1296, 1298, 1300 and 1302 (isoGDGTs), and *m/z* 744 (internal standard). Peak area integration of the GDGTs was done with Chemstation (SPM) or Agilent Masshunter (settling particles, SPM at 0 m) software. Individual GDGTs were quantified by comparing their areas to that of the internal standard, assuming a comparable response of the mass spectrometer for all GDGTs. Selected sediment-trap samples were measured twice in different concentrations (n = 13), which yielded comparable fluxes, fractional abundances and index values. For example, the difference between duplicates was typically <8% for total isoGDGT flux, typically <0.07 for TEX_{86}, and always <0.013 for the BIT index.

7.2.3.3 DNA extraction, 16S rRNA gene sequencing and analysis, and quantitative PCR of 16S rRNA gene sequences

DNA extraction, 16S rRNA gene sequencing and analysis, and quantitative PCR of 16S rRNA gene sequences has been described in detail in Chapter 6. In short, DNA was extracted from a small section (1/32) of the SPM filters, using the PowerSoil DNA extraction kit (Mo Bio Laboratories, Carlsbad, CA, USA). The 16S rRNA gene amplicon sequencing and analysis was performed with the general 16S rRNA archaeal and bacteria primer pair 515F and 806RB targeting the V4 region (Caporaso et al., 2012), as described in Besseling et al. (2018). PCR products were gel-purified using the QIAquick Gel-Purification kit (Qiagen), pooled and diluted. Sequencing was performed by the Utrecht Sequencing Facility (Utrecht, the Netherlands), using an Illumina MiSeq 2x300 bp sequencing platform. The 16S rRNA gene amplicon sequences were analyzed by an in-house pipeline including quality assessment by FastQC (Andrews, 2010), assembly of the paired-end reads with PEAR (Zhang et al., 2013), and taxonomic assignment (including picking of a representative set of sequences with the 'longest' method; Caporaso et al., 2010) with BLAST (Altschul et al., 1990) by using the Silva 128 release as reference database (https://www.arb-silva.de/). 16S rRNA gene copies were quantified using quantitative PCR (qPCR) with the same primer pair as used for amplicon sequencing (515F, 806RB). The qPCR reaction mixture (25 µl) contained 1 U of Pico Maxx high fidelity DNA polymerase (Stratagene, Agilent Technologies, Santa Clara, CA), 2.5 µl of 10x Pico Maxx PCR buffer, 2.5 µl 2.5 mM of each dNTP, 0.5 µl BSA (20 mg ml^{-1}), 0.02 pmol μl^{-1} of primers, 10 000-fold diluted SYBR Green® (Invitrogen) (optimized concentration), 0.5 µl of $MgCl_2$ (50 mM), and ultrapure sterile water. Cycling conditions for the qPCR reaction were the following: initial denaturation at 98°C for 30 s, 45 cycles of 98°C for 10 s, 56°C for 20 s, followed by a plate read, 72°C of 30 s, 80°C for 25 s. Specificity of the reaction was tested with a gradient melting temperature assay, from 55°C to 95°C with a 0.5°C increment each five seconds. The qPCR reactions were performed in triplicate with standard curves from 100 to 107 molecules per microliter. qPCR efficiency for the 16S rRNA quantification was on average 95% (R^2 = 0.998).

7.2.4 Proxy calculation

The molecular structures of the GDGTs discussed in this study are shown in Figure S7.1. The BIT index (Hopmans et al., 2004) was modified by De Jonge et al. (2014a) to include 6-methyl brGDGT isomers.

$$BIT = (Ia + IIa + IIa' + IIIa + IIIa')/(Ia + IIa + IIa' + IIIa + IIIa' + crenarchaeol)$$

The fractional abundance of the crenarchaeol isomer (cren') is calculated as follows:

$$f[CREN'] = cren'/(cren' + crenarchaeol)$$

TEX_{86} is calculated using concentrations of the following isoGDGTs (Schouten et al., 2002):

$$TEX_{86} = (isoGDGT\text{-}2 + isoGDGT\text{-}3 + cren')/(isoGDGT\text{-}1 + isoGDGT\text{-}2 + isoGDGT\text{-}3 + cren')$$

7.2.5 Statistical analysis

The concentrations of isoGDGTs (ng L^{-1}) were correlated with the estimated abundance of archaeal groups to assign a possible source of the former. Archaeal abundance was expressed as 16S rRNA

gene copies L^{-1}, and calculated by multiplying their relative abundance obtained by 16S rRNA gene amplicon sequencing analysis with the absolute abundance of microorganisms in a given sample based on qPCR, under the simplifying assumption that each microbe contains a single 16S rRNA copy in its genome.

7.3 Results

7.3.1 Physical and chemical properties of the water column

Periods of deep mixing and stratification during SPM and sediment trap sampling were determined based on *in situ* temperature monitoring (Buckles et al., 2014, 2016; van Bree et al., 2018b; Chapter 6). The depth of deep mixing varies between years (down to 40-60 m depth), and the deeper water remains permanently stratified and anoxic. Additional physical and chemical water column properties were determined on 1 November 2016 (Fig. 7.2). These measurements indicate stratified conditions, including a shallow oxycline (~20 m depth) and a strong methane gradient (Fig. 7.2A). Methane concentrations in the water column of Lake Chala increased sharply with depth from 0.44-0.77 μmol L^{-1} between 0 and 30 m, and below detection at 35 m depth, to 1.8-49.4 μmol L^{-1} between 40 and 50 m, and are highest between 60 and 80 m depth (2379.8 to 8761.7 μmol L^{-1}).This strong methane gradient must be permanent due to the strong chemical and physical stratification of the water column (Fig. 7.2B-E). Although this methane profile is taken outside our SPM and sediment trap period (1 November 2016, stratified conditions), it is expected to be representative for the methane gradient during our sampling period, due to the permanent stratification.

7.3.2 IsoGDGTs in suspended particulate matter

All targeted isoGDGTs were detected in the SPM of Lake Chala. Generally, the isoGDGT concentration increased with depth (Fig. 7.3A), both in stratified (September 2013 to April 2014; and from September 2014 onwards) and deep mixing (May-August 2014) conditions. IsoGDGT-0 was the dominant compound with especially high concentrations in the lower water column below 50 m depth (up to 112 ng L^{-1} at 80 m in November 2014 and 9.2±21.7 ng L^{-1} on average; Fig. 7.3B), and was the only isoGDGT present above the reliable detection limit in every SPM sample analyzed (n = 101). IsoGDGTs-1, -2, -3 and crenarchaeol occurred less frequently and in much lower concentrations and relative abundance than isoGDGT-0, except in December 2014, when the fractional abundance of isoGDGT-0 was 0.32 at 25 m depth as opposed to a fractional abundance over 0.65 in 90% of all SPM samples. Crenarchaeol was present in ~60% of all samples (max. 3.2 ng L^{-1}; 0.10±0.35 ng L^{-1} on average), followed by isoGDGT-1 (43%, max. 0.5 ng L^{-1}), isoGDGT-2 (26%, max. 0.4 ng L^{-1}), cren' (16%, max. 0.2 ng L^{-1}) and isoGDGT-3 (9%, max. 0.05 ng L^{-1}). The spatio-temporal distribution of crenarchaeol, isoGDGT-1, isoGDGT-2 and isoGDGT-3 showed mostly similar patterns (Fig. 7.3C-D), and had the highest concentrations at 60 m depth in August 2014. IsoGDGT-1 showed an additional increase around 50 m depth during deep mixing between May and September 2014. The concentrations of isoGDGT-0 and crenarchaeol are not correlated (r = -0.002, p = 0.99, n = 60). We did not correlate the other isoGDGTs due to the high number of samples where these compounds were below the reliable detection limit. For clarity, isoGDGT-0, crenarchaeol (including cren') and the rest (isoGDGT-1 to isoGDGT-3) are discussed separately below.

Although the concentration of crenarchaeol in the SPM of Lake Chala was low overall, its fractional abundance was generally highest in the upper water column (max. 0.53, at 25 m in

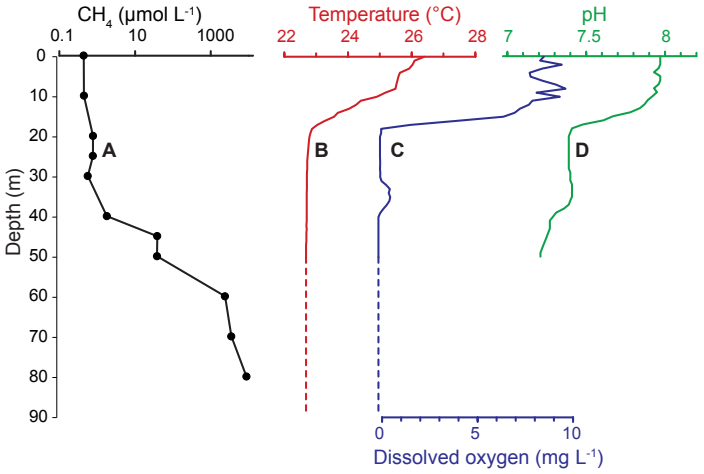

Figure 7.2 Physical properties of the water column of Lake Chala on 1 November 2016, showing a strong methane gradient (A) compared to the physical water column properties (B-E), with A: methane (µmol L^{-1}, note the logarithmic scale), error bars of the duplicate or triplicate measurements at each depth are within the size of each dot; B: temperature (in °C); C: dissolved oxygen (mg L^{-1}) and D: pH.

December 2014), mostly due to the comparatively low concentration of isoGDGT-0. Peaks in crenarchaeol abundance were few, and restricted to narrow depth ranges that varied over the seasons. For example, in the well-resolved depth profile of 2 November 2013 a modest crenarchaeol peak occurred at 25 m depth (1.4 ng L^{-1}), and two smaller ones at 50 (0.5 ng L^{-1}) and 80 m (0.4 ng L^{-1}), whereas in the profile from 31 July 2014 (= August 2014) the main peak in crenarchaeol was located at 60 m (3.2 ng L^{-1}), with smaller peaks at 20 (0.6 ng L^{-1}) and 80 m (0.3 ng L^{-1}). The BIT index was 1 and the isoGDGT-0/crenarchaeol ratio limitless in ~40% of the SPM samples, due to the absence or presence of crenarchaeol below or around the reliable detection limit. The BIT index in this SPM dataset ranges from 0.56 to 1. The accuracy of the high BIT values depends on whether crenarchaeol was reliably quantified, although whether the BIT index is 0.99 or 1 hardly matters for interpretation. On average, reliable isoGDGT-0/crenarchaeol values were lowest at the lake surface (0 m: range 1.66-5.54; mean = 3.12), and increased with depth (e.g., 80 m: range 86-1495; mean = 740). About 15% of the SPM samples had values <2, and ~30% values >15. Concentrations of cren' in SPM were mostly too low for quantification, therefore f[CREN'] and TEX_{86} proxies in SPM samples are not discussed.

7.3.3 Composition and abundance of Archaea in SPM

Archaeal abundance displayed maximum values in the order of 10^4 archaeal cells or archaeal 16S rRNA gene copies L^{-1}. Those peak values were usually restricted to the anoxic lower water column (with the exception of the surface-water sample in September 2014), and are highest between 70 and 90 m depth (especially in December 2013, and in February to October 2014), but also peaked around the oxic-anoxic boundary during deep mixing in 2014 (Fig. 7.4). The maximum values are close to the detection limit, and interpretations are therefore tentative. Certain taxa have higher concentrations of 16S rRNA gene copies in the oxic water column (Thaumarchaea), and others in the anoxic water column (Bathyarchaea, Woesearchaea). Archaeal 16S rRNA gene reads were mostly classified as closely related to the classes Methanomicrobia and Methanobacteria within the Euryarchaeota (Fig. 7.4D). Reads affiliated to the Euryarchaeota class Thermoplasmata were also detected in the deepest samples from September 2013, February to April 2014, and July

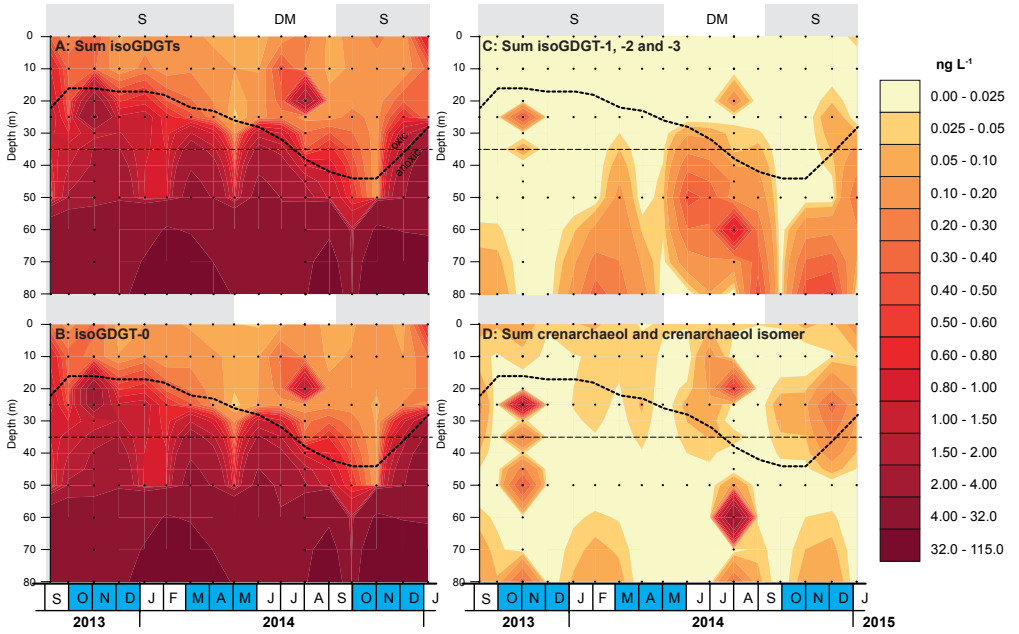

Figure 7.3 Interpolated concentrations (in ng L^{-1}) of all and selected isoGDGTs in SPM from between 0 and 80 m water depth in Lake Chala, at approximately monthly intervals between September 2013 and January 2015. A: Total isoGDGTs. B: IsoGDGT-0. C: Sum of isoGDGT-1, -2, and -3. D: Sum of crenarchaeol and its isomer. Also indicated is the varying position of the oxic-anoxic boundary (thick black stippled line: depth to anoxia; see Chapter 6), the static position of the sediment trap (thin dashed line at 35 m depth) and the grid of SPM samples analyzed in this study (black dots). The grey background shading indicates the periods of seasonal water-column stratification (S) relative to those of deep mixing (DM), and blue shading in the calendar bars shows the typical timing of local rain seasons.

to September 2014. Archaeal 16S rRNA gene copies affiliated to group C3 of the MCG (itself part of the phylum Bathyarchaeota; Fig. 7.4C) were a substantial part (15-30%) of total archaeal 16S rRNA gene reads in deep-water (70-90 m) SPM samples in September 2013, February and April 2014 and even a dominant part (40-80%) in June, July and October 2014. Other groups of Archaea such as the Thaumarchaeota group I.1b (Fig. 7.4B) were generally present in high proportions (60-100% of the total archaeal 16S rRNA gene reads) above the oxic-anoxic boundary, and sometimes make up all of the archaeal 16S rRNA gene reads from these samples.

7.3.4 IsoGDGTs in settling particles

All targeted isoGDGTs were detected in the settling particles from Lake Chala, in both stratified (generally from September to April) and deep mixing (generally from the end of April to mid-September) conditions (Fig. 7.5). In contrast to the SPM, the full suite of isoGDGTs was present in most sediment-trap samples (n = 98). Here, crenarchaeol was the dominant compound with fluxes ranging from 0.002 to 9.16 ng m^{-2} day^{-1} (Fig. 7.5E) although occasionally isoGDGT-0 amounts to 99% of all isoGDGTs (0.009 to 5.30 ng m^{-2} day^{-1}; Fig. 7.5D). Temporal variations in the fluxes of all isoGDGTs, except isoGDGT-0, are highly similar throughout the study period and strongly

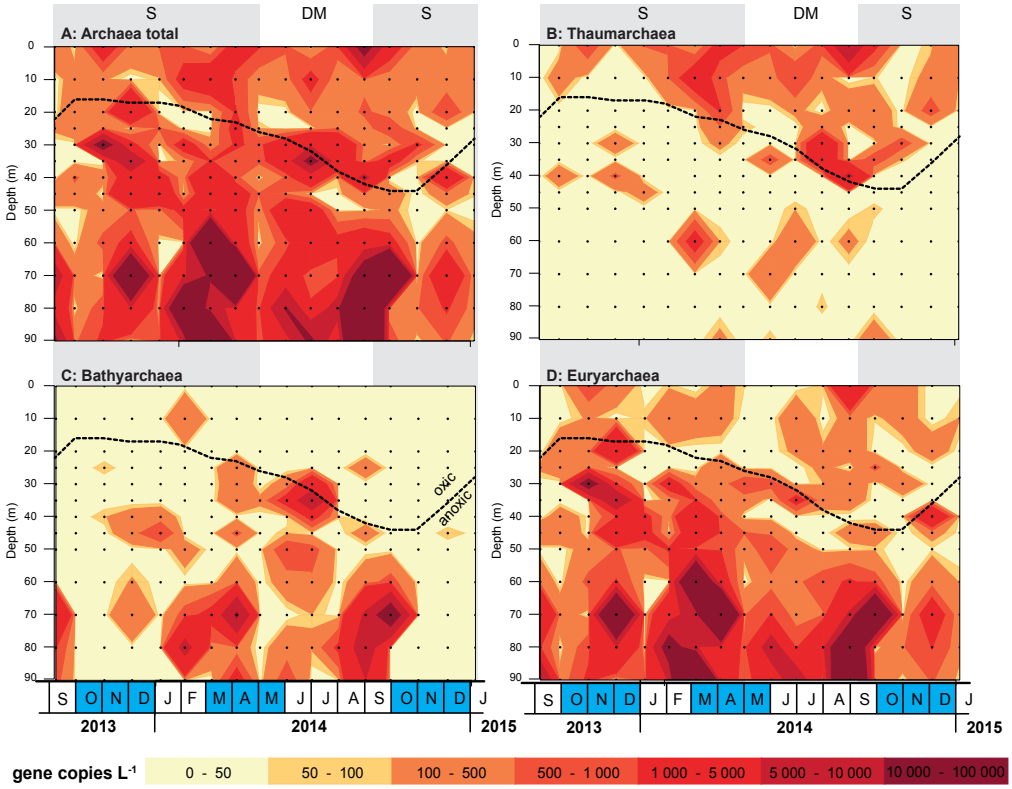

Figure 7.4 Interpolated concentrations (in gene copies L^{-1}) of archaeal 16S rRNA in SPM from between 0 and 90 m water depth in Lake Chala, at approximately monthly intervals between September 2013 and January 2015. A: Sum of all archaea; B: Thaumarchaeota, comprised of Thaumarchaea group I.1b. C: Bathyarchaeota, almost only comprised of Bathyarchaeota group C3. D: Euryarchaea, dominated by methanogenic Methanomicrobia and Methanobacteria. Also indicated are the varying position of the oxic-anoxic boundary (thick black stippled line: depth to anoxia; see Chapter 6) and the grid of SPM samples analyzed for archaeal 16S rRNA gene diversity in this study (black dots). The grey background shading indicates the periods of seasonal water-column stratification (S) relative to those of deep mixing (DM), and blue shading in the calendar bars shows the typical timing of local rain seasons.

correlated (R^2 between 0.77 and 0.98, p <0.001). Fluxes of isoGDGT-1, -2, -3 and cren' are minor (fractional abundances typically <0.1). The flux of isoGDGT-0 is very weakly correlated to that of crenarchaeol between September 2010 and January 2015 (R^2 = 0.11, p = 0.02, n = 53), but not when data from November 2006 to August 2010 (Sinninghe Damsté et al., 2009; Buckles et al., 2014, 2016) are included (R^2 = 0.01, p = 0.27, n = 98). Crenarchaeol often peaks during the annual period of water-column stratification, especially in January-February 2007, February-May 2010 and January-April 2012 (Fig. 7.5E). The BIT index is low (<0.50) during these same periods (Fig. 7.5F), but consistently high (>0.9) from August 2008 to November 2009 and from September 2013 to January 2015. The total range in BIT varies from 0.09 to 1.0 (on average 0.72±0.29). The isoGDGT-0/crenarchaeol ratio ranges from 0.06 to 273.6 (on average 26.7±51.6), its maximum value being five

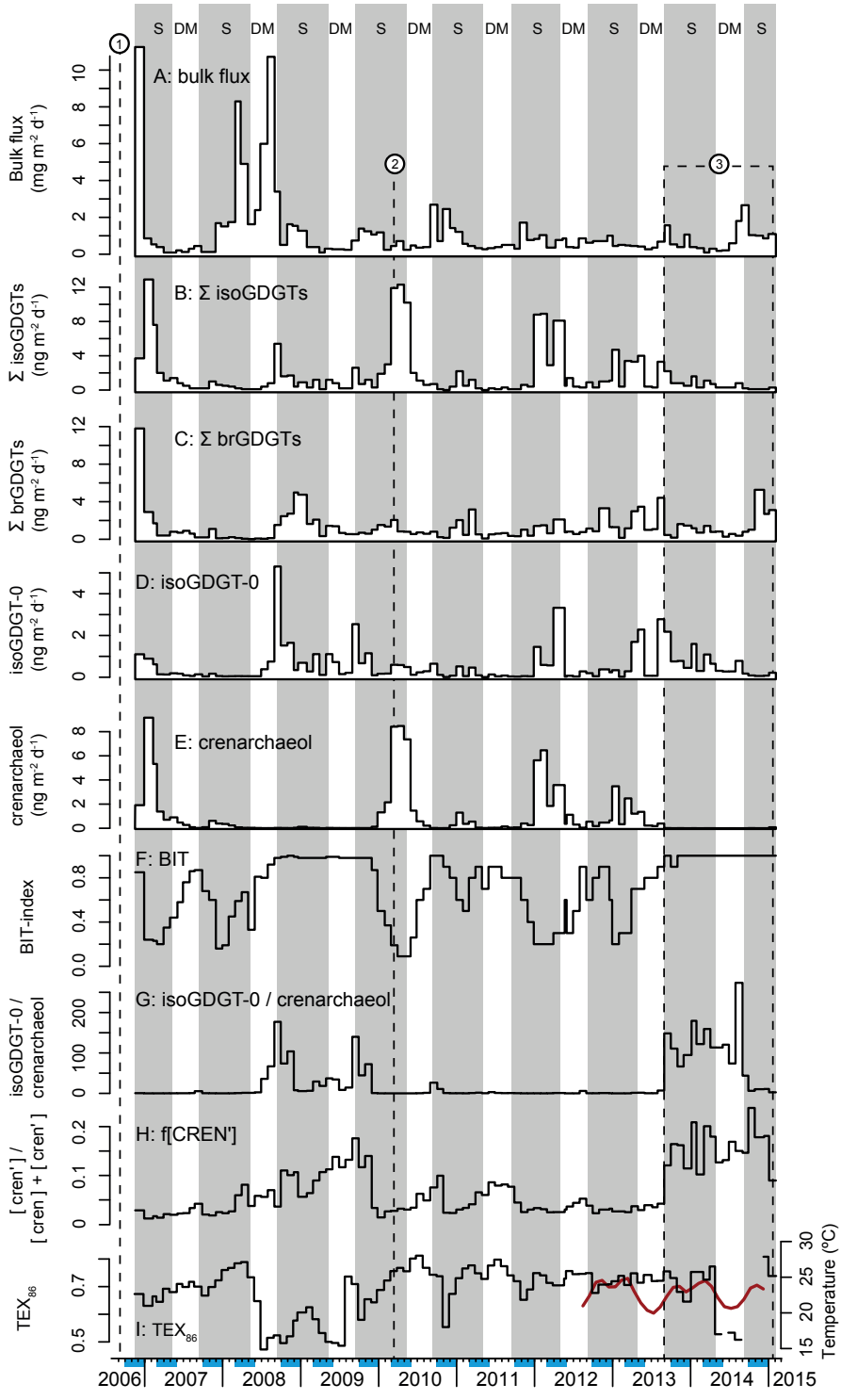
S DM S DM S DM S DM S DM S DM S DM S DM S
A: bulk flux
Bulk flux (mg m-2 d-1)
B: Σ isoGDGTs
Σ isoGDGTs (ng m-2 d-1)
C: Σ brGDGTs
Σ brGDGTs (ng m-2 d-1)
D: isoGDGT-0
isoGDGT-0 (ng m-2 d-1)
E: crenarchaeol
crenarchaeol (ng m-2 d-1)
F: BIT
BIT-index
G: isoGDGT-0 / crenarchaeol
isoGDGT-0 / crenarchaeol
H: f[CREN']
[cren'] / [cren] + [cren']
I: TEX86
TEX86
Temperature (°C)
2006 2007 2008 2009 2010 2011 2012 2013 2014 2015

Figure 7.5 (left) A-E: Temporal variation in the daily flux (ng m^{-2} day^{-1}) of isoGDGTs in settling particles from Lake Chala, trapped at 35 m depth during 98 approximately monthly intervals between November 2006 and January 2015 (A-E) and derived biomarker proxies (F-H). A: Bulk flux (mg m^{-2} day^{-1}). B: Total isoGDGTs. C: Total brGDGTs. D: IsoGDGT-0. E: Crenarchaeol. F: BIT index. G: IsoGDGT-0/crenarchaeol ratio. H: f[CREN']. I: TEX_{86} values, with the Tierney et al. (2010a) calibration. Red line is measured near-surface (2 m) temperature (Chapter 6). The timing of SPM sampling is indicated with stippled lines, where (1) September 2006 (Sinninghe Damsté et al., 2009), (2) February 2010 (Buckles et al., 2013) and (3) this study. The background shading indicates the seasonal periods of water-column stratification (S; gray bands) and deep mixing (DM). Blue shading in the calendar bars indicates the typical timing of local rain seasons. Data from November 2006 to December 2007 were previously reported by Sinninghe Damsté et al. (2009); data from January 2008 to August 2010 by Buckles et al. (2014, 2016).

times smaller than that found in SPM. Periods with elevated isoGDGT-0/crenarchaeol values occur from July to November 2008, August to November 2009, in September 2010, and continuously from September 2013 until September 2014 (Fig. 7.5G), i.e. generally coinciding with periods of high BIT values. High isoGDGT-0/crenarchaeol values are a result of both very low crenarchaeol fluxes and high levels of isoGDGT-0. The f[CREN'] ranged between 0.01 and 0.24 (on average 0.06±0.06), and is highest when isoGDGT-0/crenarchaeol and BIT values are high (Fig. 7.5H). TEX_{86} values range from 0.47 to 0.86 (0.69±0.09 on average, n = 94; Fig. 7.5I).

7.4 Discussion

7.4.1 Spatio-temporal distribution of isoGDGTs in the water column of Lake Chala

Overall, isoGDGT concentrations were substantially higher in the anoxic lower water column than in the oxygenated upper water column of Lake Chala (Fig. 7.3). They were particularly high below 45-50 m depth, typically the greatest depth of seasonal mixing (Buckles et al., 2014). However, even though environmental conditions in the lower water column can be assumed stable year-round, the generally high concentrations of isoGDGT-0 at 60-90 m varied over time, and were somewhat higher during stratification than during the mixing season. These high isoGDGT-0 concentrations are also reflected in the exceedingly high values of the isoGDGT-0/crenarchaeol ratio in this part of the water column throughout our monitoring period (up to 1495 at 80 m in November 2014), which are most often one or two orders of magnitude higher than the previously reported highest values of 32 and 38 recorded respectively at 80 m in January 2010 (Buckles et al., 2013) and at 90 m in September 2006 (Sinninghe Damsté et al., 2009).

The concentration of crenarchaeol in the water column of Lake Chala was generally very low during our monitoring period, but at least present in most SPM above the oxic-anoxic boundary. The crenarchaeol concentrations found in this study are in the same order of magnitude as those recorded during previous sampling campaigns. However, during deep mixing in September 2006, crenarchaeol concentrations increased with depth from 0.06 ng L^{-1} near the surface to 1.8 ng L^{-1} at 80 m depth (Sinninghe Damsté et al., 2009); during stratified conditions in February 2010 core lipid crenarchaeol concentrations were generally absent or low, with a peak (3.5 ng L^{-1}) at 39 m (Buckles et al., 2013). In our data, distinct crenarchaeol peaks are restricted to narrow depth ranges within the lower water column that vary over time, but do not show clear patterns between stratified and mixing periods as could be expected based on the previous sampling campaigns. The potentially narrow depth niches of crenarchaeol production at any one time suggest that either the crenarchaeol

production between September 2013 and January 2015 was exceptionally low, or that the peak of crenarchaeol was missed in most months due to this erratic occurrence.

7.4.2 Spatio-temporal distribution of archaeal groups in the water column of Lake Chala

In line with Buckles et al. (2013), the composition of archaeal communities in Lake Chala differed substantially between the oxic and anoxic parts of the water column, and displayed substantial temporal variability (Fig. 7.4). Overall, however, archaeal gene abundances were very low with maximum abundances on the order of 10^4 cells L^{-1}, i.e. close to the limit of detection. This is much lower than found previously in February 2010 (Buckles et al., 2013), where total archaeal 16S rRNA gene abundances ranged between $4{\cdot}10^3$ and $2{\cdot}10^7$ copies L^{-1} (Parch519F-Arc915R primer pair; maximum at 24 m depth) and $7{\cdot}10^4$ to $8{\cdot}10^7$ copies L^{-1} (Arc344F-Arc915R primer pair; maximum between 69 and 82 m). This is unexpected, especially as we used a higher-resolution method than Buckles et al. (2013), and should yield higher archaeal abundances. These major differences suggest that the abundance of Archaea in Lake Chala is highly variable between different years. Together with our data on isoGDGT concentrations in SPM and settling particles, it appears that the 17-month monitoring period of this study is characterized by an exceptionally low amount of archaea as well as archaeal biomarkers.

Notwithstanding these low archaeal abundances, there are several interesting patterns in the composition and distribution of archaea in the water column of Lake Chala. Thaumarchaeota group I.1b were mainly restricted to the upper water column, in agreement with Buckles et al. (2013). The lower limit of their depth distribution closely follows the oxic-anoxic boundary (Fig. 7.4B), indicating a close association of these ammonia-oxidizing archaea with the abiotic conditions in this specific aquatic habitat. They were also continuously present between March and October 2014, with higher concentrations in the dry period between July and September 2014, arguing against a close association with rain-induced runoff from catchment soils. Members of Thaumarchaeota group I.1a were not detected in this study, although they were a substantial part of the thaumarchaeotal community in February 2010 when they bloomed at ~40 m depth (Buckles et al., 2013).

Group C3 archaea, a subgroup of MCG Bathyarchaeota (MCG-15) closely related to the Thaumarchaeota (Kubo et al., 2012; Lavergne et al., 2018; Zhou et al., 2018) were mainly restricted to anoxic waters in Lake Chala (Fig. 7.4C). During our monitoring period they occurred most prominently in the deepest waters (60-90 m), comparable to their depth distribution in February 2010 (Buckles et al., 2013). Although water-column mixing, and thus oxygen penetration, remained shallower than 45 m between September 2013 and January 2015, and therefore water-column conditions below that depth can be expected to have been relatively constant, there are large temporal variations of these Bathyarchaeota. Bathyarchaeota are a highly diverse group of archaea (Kubo et al., 2012), but because they have not been cultured, their metabolism is at present unclear. It has been suggested (e.g., Zhou et al., 2018) that they are metabolic generalists, specialized in degrading recalcitrant organic matter under anoxic conditions. It is therefore possible that seasonal variation in their occurrence may reflect the variable input of complex organic matter.

Methanobacteria and methanomicrobia are relatively dominant in the deep, anoxic water column of Chala (Fig. 7.4D), although in very low absolute abundances between September 2013 and January 2015. The methane profile of November 2016 indicates the presence of methane at depth, with highest concentrations between 50 and 90 m depth. It is therefore possible that these archaeal taxa are involved in methanogenesis in the deep water column of Lake Chala. In February

2010, the only methanogens detected were Methanosarcinales (Buckles et al., 2013), which were not detected in this study.

Taking the generally very low abundances of archaeal 16S rRNA gene reads into account, the composition of the archaeal community in Lake Chala and the depth distribution of the various groups suggests that i) Thaumarchaeota I.1b mainly occurred in the surface waters, ii) anaerobic heterotrophs of (group C3) MCG Bathyarchaeota mainly occurred in the anoxic lower water column, and iii) at depth, specific euryarchaeotal taxa occurred that might be involved with methanogenesis.

7.4.3 Archaeal sources of Lake Chala isoGDGTs

The similar fluxes of isoGDGTs in settling particles in Lake Chala (R^2 = 0.77 to 0.98, p <0.001, n = 98) suggest that they are produced by the same group of microbiota, except isoGDGT-0, which is not correlated to any of the other isoGDGTs (R^2 <0.02) and is thus likely produced by different archaeal group(s). In SPM, although concentrations of isoGDGTs are generally low, it is clear that isoGDGT-0 has a different distribution over time and with depth than other isoGDGTs. However, note that this record may be impacted by the low abundance of Archaea, therefore, comparisons of archaeal 16S rRNA gene reads and isoGDGT concentrations must be interpreted with caution.

Crenarchaeol occurrence is more often in oxic water column, and more 'patchy' in the anoxic water column. Thaumarchaeota are the only known producers of crenarchaeol so far, and the general occurrence in the oxic water column of thaumarchaeotal gene copies (Fig. 7.4B) is in agreement with general spatio-temporal distribution of crenarchaeol concentrations in SPM. Previously, production of crenarchaeol in the epilimnion of Lake Chala was attributed to Thaumarchaeota of both group 1.1a and 1.1b (Sinninghe Damsté et al., 2009; Buckles et al., 2013). In this study, Thaumarchaeota of group I.1a were not detected, suggesting that group I.1b was responsible for crenarchaeol production during the studied interval. However, local peaks of crenarchaeol in our well-resolved depth profiles from November 2013 and August 2014 do not fully match those of the 16S rRNA gene copy profiles of Thaumarchaeota Group I.1b (compare Fig. 7.3 and Fig. 7.4). Also in February 2010, the depth of crenarchaeol (39 m) and thaumarchaeotal 16S rRNA gene (24 m) peaks did not exactly match (Buckles et al., 2013). Instead, the remarkably low number of archaeal 16S rRNA gene copies and low concentrations of crenarchaeol and total isoGDGTs in both SPM and settling particles of this study indicate that no thaumarchaeotal, or archaeal bloom in general, has occurred between September 2013 and January 2015. This intermittent (near-)absence of Thaumarchaeota in Lake Chala was previously noted by Buckles et al. (2014, 2016), on the basis of low or non-existent crenarchaeol flux in settling particles during large parts of 2008 and 2009 (Fig. 7.5E).

In the deep water column isoGDGT-0 predominates, especially during periods of stratification (Fig. 7.3). Overall, the spatio-temporal distribution of isoGDGT-0 is most similar to Euryarchaea (dominated by Methanomicrobia and Methanobacteria) and Bathyarchaeota (dominated by Group C3), all displaying the highest numbers of 16S rRNA gene copies in the deep anoxic water column (compare Fig. 7.3 and Fig. 7.4). IsoGDGT-0 has previously been linked to Bathyarchaeota group C3 in Lake Chala (Sinninghe Damsté et al., 2009; Buckles et al., 2013). Although the highest isoGDGT-0 concentration during stratification (112 ng L^{-1}) was comparable to that reported in previous studies (sum of CL and IPL is 99 ng L^{-1} at 85 m depth in February 2010; Buckles et al., 2013), the highest isoGDGT-0 concentration during mixing (31 ng L^{-1}) was somewhat lower than previously reported for similar conditions (51 ng L^{-1} at 80 m depth; September 2006; Sinninghe Damsté et al., 2009). The overall low isoGDGT-0 concentrations in SPM during the here studied

interval compared to previous studied may be attributed to the generally low archaeal activity from September 2013 to January 2015.

7.4.4 Long-term isoGDGT trends in settling particles: how the Chala BIT index works

The 98-month sediment-trap record of isoGDGTs in Lake Chala shows large variability in isoGDGT composition and fluxes over time that cannot easily be linked to the seasonal succession of stratification and deep mixing (Fig. 7.5). Nevertheless, the flux of crenarchaeol appears to influence both the BIT index and the isoGDGT-0/crenarchaeol ratio, as has been noted before based on concentration profiles of brGDGTs and isoGDGTs in SPM (Sinninghe Damsté et al., 2012a; Buckles et al., 2014, 2016). Extensive water-column monitoring during the period of SPM sampling indicates that low concentrations (or absence) of crenarchaeol coincide with a persistently shallow (~15 m depth) oxic-anoxic boundary during the stratification period followed by a still relatively shallow position (<40 m) during the subsequent deep mixing period (Fig. 7.3D). Furthermore, the spatio-temporal distribution of isoGDGT-0 in SPM indicates that it is mainly produced under anoxic conditions, so that a high relative abundance of isoGDGT-0 in the sediment trap material would imply that the oxycline position must have been well above 35 m. Hence, periods with a shallow oxycline can be recognized by a high ratio of isoGDGT-0/crenarchaeol in settling particles. Thus, the two main periods of sustained high values for isoGDGT-0/crenarchaeol and the BIT index in the sediment trap record indicate shallow oxycline conditions from June 2008 to November 2009, and from August 2013 to January 2015 (Fig. 7.5F-G). Rather than linking high BIT values to an increased input of soil-derived brGDGTs as a result from precipitation-induced runoff (Verschuren et al., 2009), nutrient-induced Thaumarchaeota enhancement (Sinninghe Damsté et al., 2012a) or bloom suppression (Buckles et al., 2016) we here explain variations in BIT by the impact of the position of the oxycline on the archaeal community composition in Lake Chala. In this lake, the duration of water-column stratification is linked to the strength of the monsoon (Wolff et al., 2011). Higher wind speeds are connected to dry conditions and more extensive water-column mixing potential, cutting stratification short. On the other hand, lower wind speeds are connected to wet conditions, where a prolonged wet season will lead to an increasingly strong temperature stratification of the water column. This results in an ongoing shallowing of the oxycline, expanding the anoxic habitat of isoGDGT-0 producers relative to that of the crenarchaeol producers. Hence, the shallower the oxycline, the further the potential habitat of Thaumarchaea is decreased. Moreover, the limited oxygen availability can also increase the competition with nitrifying bacteria under elevated ammonium levels upon the degradation of large algal blooms (Buckles et al., 2016).

During stratified conditions and high BIT values, f[CREN'] in settling particles tends to gradually increase over time (Fig. 7.5H). Notably, f[CREN'] reaches up to 0.24 during the inferred periods with a prolonged shallow oxycline in 2008-2009 and 2013-2014, substantially higher values than those attained in the sediment record of Lake Chala (~0.03 over the past 2.2 kyr; Buckles et al., 2016; and ~0.02 over the past 25 kyr, with intermittent peaks up to 0.15, Sinninghe Damsté et al., 2012a). As aquatic Thaumarchaeota typically have <5% of the crenarchaeol isomer, much less than soil Thaumarchaeota (e.g., Pitcher et al., 2010; Kim et al., 2012; Sinninghe Damsté et al., 2012b; Elling et al., 2017), Sinninghe Damsté et al. (2012a) interpreted the high f[CREN'] present at certain periods as Lake Chala experiencing a higher input of soil-derived Thaumarchaeota during those periods. However, it is not likely that the high f[CREN'] between September 2013 and January 2015 are due to increased soil-derived isoGDGTs, as we have very little evidence of terrestrial organic matter input at this time (van Bree et al., 2018b; Chapter 6). Thus, our data suggest that it is a valuable indicator of prolonged water-column stratification.

The isoGDGTs in settling particles between November 2006 and December 2007 translated into TEX_{86} values that reflected average LST generally well, although the seasonal variability in LST was not reflected (Sinninghe Damsté et al., 2009). Our multi-year sediment trap record now indicates that periods with low crenarchaeol concentrations, high BIT, high isoGDGT-0/crenarchaeol and high f[CREN'] values (i.e., shallow oxycline conditions and thaumarchaeotal bloom suppression) coincide with low TEX_{86} values that underestimate LST (Fig. 7.5). This suggests that the TEX_{86} index does not reliably reflect the LST when the thaumarchaeotal bloom is suppressed. As we can recognize shallow oxycline conditions and associated thaumarchaeotal bloom suppression by high isoGDGT-0/crenarchaeol, high BIT and high f[CREN'] values, we are now able to identify those intervals during which the LST is truly recorded by the isoGDGTs in Lake Chala (*cf.* Sinninghe Damsté et al., 2012a).

7.4.5 Implications for the sedimentary GDGT biomarker record

The large seasonal and inter-annual variability in isoGDGT content of settling particles begs the question what their longer-term variations in the 25 kyr sediment record actually represent. Overall, the occurrence of strong stratification appears to be key in understanding isoGDGT production in Lake Chala. It exerts a large influence on isoGDGT signatures in the settling particles, and therefore also on the isoGDGTs accumulating in the sediments.

The mechanism of a shallow oxycline inhibiting the development of seasonal thaumarchaeotal blooms as here proposed allows use of the BIT index as an indirect proxy for rainfall over longer time intervals, as was done by Verschuren et al. (2009), Sinninghe Damsté et al. (2009, 2012a) and Buckles et al. (2014, 2016). In fact, our shallow oxycline mechanism may also explain some of the remaining discrepancies between the Chala BIT record and other hydroclimate proxies. For example, the BIT record does follow the first-order lake-level reconstruction inferred from seismic stratigraphy (Moernaut et al., 2010) at the start of the Heinrich-1 event ca. 16.8 kyr ago (Fig. 7.6). Where the seismic record indicates a short-lived (ca. 500 years) but extreme low-stand, implying arid conditions during this time, the BIT index does not decrease during the extreme low-stand, is always higher than ~0.3 and in fact increases slightly during the event, inferred to reflect the post-glacial reinvigoration of monsoon rainfall (Verschuren et al., 2009). We propose that the very low water levels during this time interval resulted in a well-mixed water column with a deep oxycline, enabling Thaumarchaeota to regularly bloom. This would explain the lack of response in the BIT index. Our mechanism also explains the high BIT values between 11.6 and 9.0 kyr BP. The high BIT values are accompanied by a high isoGDGT-0/crenarchaeol, indicating a shallow oxycline as a result of increased rainfall (Fig. 7.6), presumably due to an intensified southeastern monsoon feeding the 'long rains' at Lake Chala (Verschuren et al., 2009). In addition, the simultaneous increase in f[CREN'] confirms that prolonged stratified conditions occurred more often at this time. These shallow oxycline conditions can also be linked to the period between 24.7 and 22.3 kyr BP, albeit some variability in BIT, isoGDGT-0/crenarchaeol and f[CREN'] values indicate that the climate was generally wet, but relatively unstable. These wetter conditions have been attributed to the intensification of the northeast monsoon that mainly feeds the precipitation during the 'short rains' (Verschuren et al., 2009).

In an attempt to reconstruct a LST record for Lake Chala, Sinninghe Damste et al. (2012) noticed that sediment horizons with unrealistically low TEX_{86} values also contain a high proportion of isoGDGT-0, indicating that methanogens and archaea other than Thaumarchaeota must have contributed to the isoGDGT pool. A value >2 for the ratio of isoGDGT-0/crenarchaeol is commonly used as a cutoff for the application of the TEX_{86} index, based on the fact that in pure

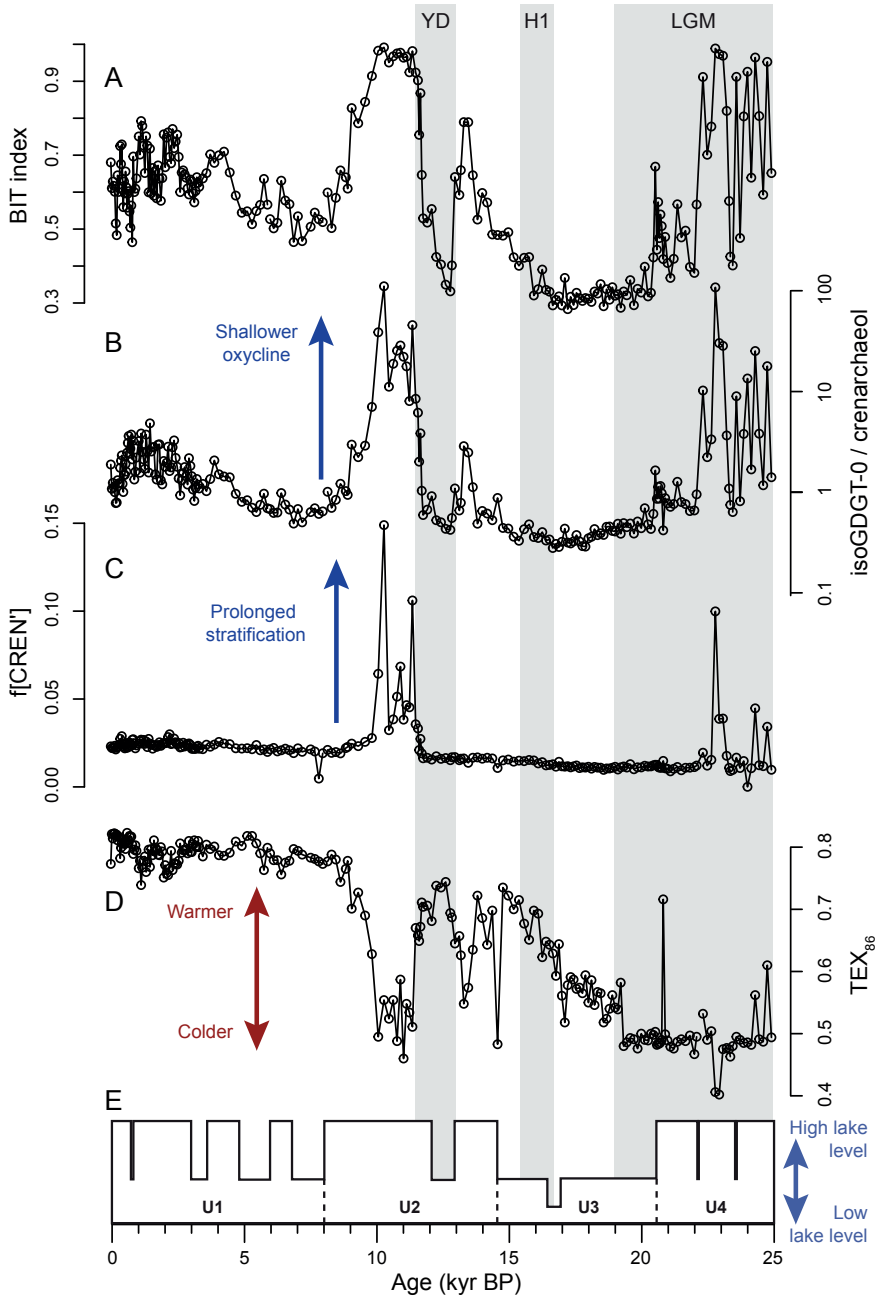

Figure 7.6 Lake Chala's 25,000-year (25-kyr) sediment record of A: the BIT index (Verschuren et al., 2009); B: isoGDGT-0/crenarchaeol; C: f[CREN']; D: Raw data series of TEX_{86}, all modified after Sinninghe Damsté et al. (2012a); E: Succession of lake high- and lowstands based on seismic-reflection stratigraphy (Moernaut et al., 2010). Shaded areas represent the Last Glacial Maximum (LGM; 26.5-19 kyr BP), Heinrich event (H1; 16.8-15.4 kyr BP) and the Younger Dryas period (YD; 13-11.5 kyr BP).

Thaumarchaeota cultures this ratio is always <2 (Blaga et al., 2009; Sinninghe Damsté et al., 2012b). Yet high isoGDGT-0 concentrations should not necessarily disqualify the use of TEX_{86} in cases where isoGDGT-0 is mainly produced by non-methanotrophic archaea (Buckles et al., 2013). The concentration and flux of isoGDGT-0 in Lake Chala is not correlated to that of other isoGDGTs, implying that the main archaeal isoGDGT-0 source contains no or limited amounts of other isoGDGTs. As isoGDGT-0 is not considered in the TEX_{86} index, there is no reason to exclude samples based on high isoGDGT-0/crenarchaeol values in Lake Chala. However, the same sediment horizons with unrealistically low TEX_{86} values that were excluded from the 25 kyr record of Sinninghe Damsté et al. (2012a) also have high BIT and high f[CREN'] values (Fig. 7.6), which are all indicators of shallow oxycline conditions and a suppression of the thaumarchaeotal community in the lake. This leads to a substantial contribution of non-thaumarchaeotal isoGDGT producers to the TEX_{86}–based temperature signal and therefore unreliable reconstructed LSTs. Thus, the here identified indicators of shallow oxycline conditions should be taken into account when selecting samples for paleotemperature reconstructions based on the TEX_{86} index.

7.5 Conclusions

The main isoGDGTs in the water column of Lake Chala are isoGDGT-0 and crenarchaeol, and are produced by different archaeal communities. Thaumarchaeota are the main producers of the isoGDGTs (except isoGDGT-0), and generally occur in the oxic water column. IsoGDGT-0 production is high in the anoxic deeper water column, and seasonally variable even though conditions at depth do not change over time. Although crenarchaeol production is only indirectly affected by rainfall, the BIT index may work as precipitation proxy in the sedimentary record of Lake Chala because shallowing of the oxycline during prolonged stratification during the wet season severely limits the space for Thaumarchaeota to bloom, leading to low crenarchaeol fluxes and high BIT values. Overall, strong stratification and shallow oxycline depth are key in understanding the archaeal ecology and production of isoGDGTs in Lake Chala, and aids in the interpretation of sedimentary isoGDGT-proxy records. Strong stratification can be recognized by high BIT, high isoGDGT-0/crenarchaeol values, as well as a high proportion of the crenarchaeol isomer. Furthermore, TEX_{86}–based LST estimates are not reliable when strong stratification suppresses the thaumarchaeotal bloom.

Data availability

All data presented in this study will be made available upon publication in a scientific journal.

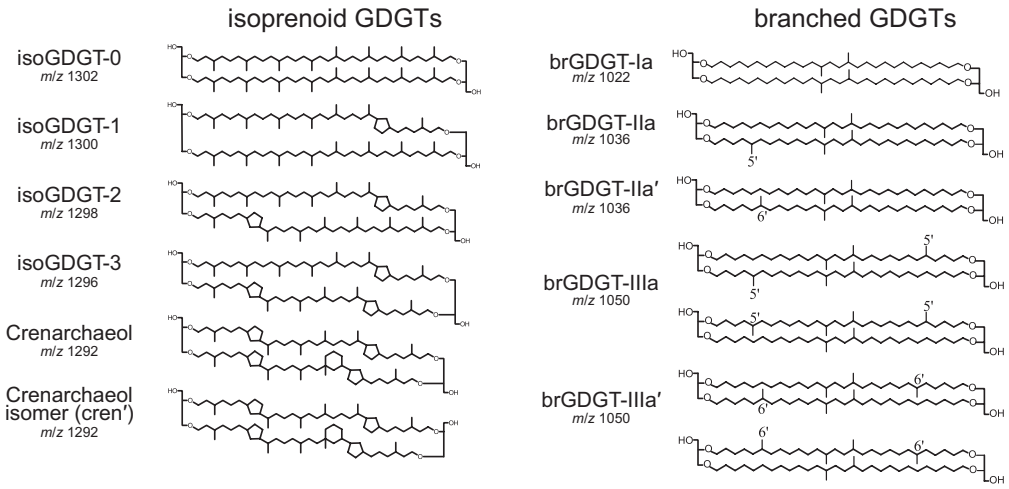

Figure S7.1 IsoGDGT and brGDGT structures and their mass-to-charge ratio (*m/z*).

Acknowledgements

We thank C.M. Oluseno for conducting the monthly sampling and other field assistance in Kenya, A.M.D. Negash and P. de Regt for lipid extractions, A. Baxter and especially J.W. de Leeuw for extensive feedback on the manuscript. W. De Crop is thanked for compiling the physical water column data. We are grateful to A. van Dijk, D. Kasjaniuk, A. van Leeuwen-Tolboom, T. Claessen, K. Nierop and N. van Helmond at Utrecht University, and M. Baas, D. Dorhout, E. Hopmans, A. Mets, J. Ossebaar, S. Vreugdenhil and M. Brouwer at the Royal NIOZ for technical and analytical support. We furthermore thank A. Roepert for help with R. Sample collection was carried out with permission of the Permanent Secretary of the Ministry of Education, Science and Technology of Kenya, research permit 13/001/11C to D.V. DNA extracts are deposited in the National Museum of Kenya (NMK), Kenya, in accordance with National Environmental Management Authority (NEMA) regulations in the context of the Nagoya protocol under voucher numbers NMK:BCT:80001 to NMK:BCT:80221. The raw data of the 16S rRNA gene amplicon reads have been deposited in the NCBI Sequence Read Archive (SRA), BioProject number upon request. This research was supported by the NESSC Gravitation Grant (024.002.001) from the Dutch Ministry of Education, Culture and Science (OCW) to J.S.S.D.

On our way to retrieve and redeploy the sediment trap in Lake Chala with local Kenyan field assistant Caxton in September 2014.

8 Large seasonal and inter-annual variability in lipid biomarker fluxes: 4.5 years of monthly sediment-trap data from East African Lake Chala

L.G.J. van Bree, P. de Regt, F. Peterse, D. Verschuren, C. Cocquyt, J.W. de Leeuw and J.S. Sinninghe Damsté

Abstract

We studied the distribution and stable carbon-isotopic ($\delta^{13}C$) composition of lipid biomarkers in settling particles collected monthly in a sediment trap at 35 m water depth between September 2010 and January 2015 in Lake Chala, a permanently stratified crater lake in equatorial East Africa. Variations in phytoplankton, bacterial and archaeal biomarker fluxes indicate that water-column mixing and stratification strongly influenced microbial communities during the studied interval. High fluxes of biomarkers for chlorophytes (long-chain *n*-alk-1-enes, C_{21} and C_{23} *n*-alkanes) and diatoms (loliolide and isololiolide) show that these taxa were seasonally dominant, although they did not regularly respond to each deep mixing period. The flux of the C_{28} fatty acid, often used as a plant wax biomarker, was similar to the chlorophyte biomarkers and chlorophyte biovolume estimates, indicating an aquatic source for this compound. *Tetraedron minimum* is suggested as a likely source of chlorophyte biomarkers in the studied period. Moreover, large fluctuations over time in the $\delta^{13}C$ values of C_{28} fatty acid indicate that chemically enhanced fractionation at a high pH occurred regularly throughout this interval. The flux of the cyanobacterial biomarker $C_{19:1}$ *n*-alkene was highest when the position of the oxic-anoxic boundary was well above the sediment-trap depth. These periods with shallow anoxic conditions coincide with an enhanced flux of 5-methyl branched glycerol dialkyl glycerol tetraethers (brGDGTs), and an increased isoprenoid GDGT-0/crenarchaeol ratio. Taken together, it appears that the competition between microbial taxa in the upper water column is primarily controlled by the depth of seasonal water column mixing and the balance between oxygenated and anoxic habitats. The large inter-annual variability of aquatic lipid biomarkers in the settling particles of Lake Chala indicates that small environmental differences can cause large changes in the microbial communities that prevent a microbial succession pattern to annually recur. Moreover, input of terrestrial biomarkers is low and irregular. This large variability implies that monitoring programs organized to capture the natural variability of a lake system have to run for many years to fully reveal the relationship between biomarkers in the modern lake system and the interpretation of biomarker proxies in the sedimentary record for the purpose of paleoenvironmental reconstruction.

8.1 Introduction

Sediments accumulating in lakes are natural archives of past environmental conditions. Such archives can be explored microscopically and chemically at a high temporal resolution. On the molecular level, lipid biomarkers are increasingly used to reconstruct past ecological and climatic variability, based on the principle that these lipids in a sedimentary archive reflect the response of their producer(s) to (past) environmental changes. To better link the presence and relative abundances of these biomarkers in lake sediments with the (environmental) processes that drive their production or input over time, long-term monitoring of the modern water column is required. However, such extensive lake monitoring is not often implemented. Available studies either cover relatively short time intervals, i.e. up to one full year (e.g., Meyers et al., 1984), and / or focus only on specific biomarker groups, such as long-chain diols (e.g., Villanueva et al., 2014), long-chain alkenones (e.g., Longo et al., 2018) or bacterial and archaeal membrane lipids (Woltering et al., 2012; Buckles et al., 2014; Loomis et al., 2014b; Chapter 6 and 7). In particular long-term lake monitoring studies in combination with high-resolution studies of sedimentary biomarkers are scarce, especially in the tropics, whereas these regions are already underrepresented in terms of continental paleoclimate reconstructions.

One notable exception is Lake Chala, a meromictic crater lake bridging the border of Kenya and Tanzania in equatorial East Africa. The permanently anoxic bottom water ensures excellent organic-matter preservation. Lipid biomarkers have been studied extensively in a 25,000 year (25 kyr) sediment core from the lake, where they have been used to for example infer past changes in rainfall and monsoon intensity, vegetation type, and phytoplankton productivity (e.g., Verschuren et al., 2009; Sinninghe Damsté et al., 2011b; Tierney et al., 2011; Buckles et al., 2014, 2016; van Bree et al., 2014, 2016, 2018a). A recent study aimed at verifying the use of lipid biomarkers as paleoclimate proxies in this lake, and focused on the same biomarkers associated with suspended particulate matter (SPM) in the modern water column of Lake Chala. However, biomarker analysis of SPM collected at 5 depths over 17 consecutive months revealed unexpected sources and processes driving the presence of these biomarkers in the water column (van Bree et al., 2018b). Firstly, terrestrial biomarkers were nearly absent in the water column during the studied interval, while plant leaf-wax biomarkers such as long-chain *n*-alkanes and *des*-A-lupane are clearly present in the sedimentary record (Sinninghe Damsté et al., 2011b; van Bree et al., 2016). Secondly, the C_{28} fatty acid, normally considered as a higher plant wax biomarker, appeared to have a primary aquatic origin (van Bree et al., 2018b). This is noteworthy since the C_{28} fatty acid is generally abundant in East African lake sediments, and its stable isotopic composition is often used in paleovegetation ($\delta^{13}C$) or paleohydrological (δD) reconstructions (e.g., Eglinton and Eglinton, 2008; Tierney et al., 2010a; Castañeda and Schouten, 2011; Freeman and Pancost, 2014; Hemingway et al., 2016). The aquatic rather than higher plant source of this fatty acid has large implications for the straightforward interpretation of these records. Thirdly, an atypical stable carbon-isotope fractionation process occurred in the water column during periods with high epilimnetic pH and increased production of aquatic biomarkers. Chemically enhanced diffusion of atmospheric CO_2 into the lake resulted in a strong fractionation of the carbon isotopes and exceptionally depleted aquatic biomarker $\delta^{13}C$ signatures. The occurrence and extent of this process over longer time scales is unfortunately still unknown, but it is imperative to understand its importance as this process may affect the $\delta^{13}C$ values of aquatic biomarkers and therefore that of the bulk organic matter stored in the sediments.

Given the potentially large influence of these modern day processes on the interpretation of biomarker proxy records it is important to assess whether the trends observed over the 17-month

SPM interval are also present on longer time scales. To this end, we studied the occurrence and distributions of various biomarkers in settling particles collected in a sediment trap at 35 m water depth in Lake Chala over a period of 53 consecutive months between September 2010 and January 2015, overlapping the SPM interval studied by van Bree et al. (2018b). The multi-year time period covered by our sediment trap material and the overlap with the SPM interval enables us for the first time to assess both inter- and intra-annual variation in biomarker distributions in settling particles in a tropical lake. Furthermore, biomarker fluxes will be compared to phytoplankton biovolume estimates from the same sediment-trap samples to evaluate possible sources. The settling particles are an important link between the input or production of biomarkers in the water column and those that end up in the sediment record. Hence, this study may provide the crucial information to reveal the (environmental) parameters that drive the temporal dynamics of biomarkers and their producers in lakes, and thus the significance of their occurrence and composition in lacustrine sediments for paleoclimate reconstruction.

8.2 Material and methods

8.2.1 Study site

Lake Chala (locally "Challa", after a nearby village) is a crater lake located on the border of Kenya and Tanzania in the foothills of Mt. Kilimanjaro (3°19'S, 37°42'E). The lake is situated at ~880 m above sea level, has a surface area of ~4.5 km² and is ~90 m deep. As evaporation (~1700 mm yr^{-1}) exceeds local precipitation (~600 mm yr^{-1}; Payne, 1970), lake level is maintained by subsurface groundwater input, most likely originating from the forest belt and adjacent subalpine zone on Mt. Kilimanjaro (Hemp, 2006; Bodé et al., submitted). The Inter-Tropical Convergence Zone (ITCZ) passes over the Lake Chala region twice yearly, resulting in two distinct rain seasons, with relatively heavy 'short rains' from October to December and 'long rains' from March to May (Nicholson, 2000; Verschuren et al., 2009). High temperature and low wind speeds in the rainy seasons lead to stratified water-column conditions, while higher wind speeds in January-February and especially during the colder southern hemisphere winter (June-September) lead to deeper water-column mixing. Depending on wind speed and air temperature the deep mixing (DM) of the water column extends down to 40-60 m during this main dry season, while shallower mixing (SM) during the short dry season extends to only 25-30 m and daily wind-driven mixing extends to 10-20 m

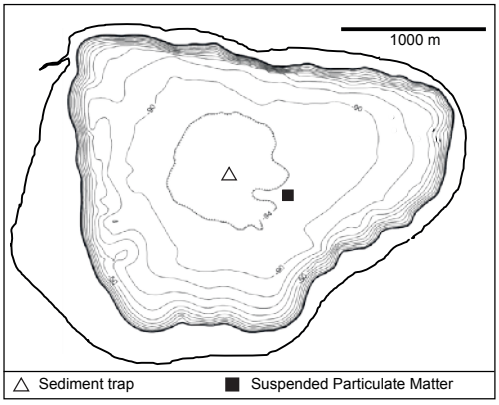

Figure 8.1 The mid-lake position of the sediment trap (triangle) and previously published SPM sampling (van Bree et al., 2018b) in Lake Chala. Crater-basin map and bathymetry are adapted from Moernaut et al. (2010).

(Wolff et al., 2011; van Bree et al., 2018b) throughout the year. The convective upwelling during deep mixing brings nutrients to the surface waters which initiate a seasonal phytoplankton bloom. Variation in air temperature and wind speed is important for the seasonal cycle of stratification and mixing of the lake, and therefore the timing and duration of the shallow mixing (SM) and deep mixing (DM) varies slightly over time (Chapter 6).

8.2.2 Sample collection

The sediment-trap deployment and sample collection has been described previously (e.g., Sinninghe Damsté et al., 2009; Buckles et al., 2014, 2016; Chapter 6). In short, a sediment trap (UWITEC, double-funneled, 86 mm diameter) was installed in November 2006, at 35 m water depth in a mid-lake position (Fig. 8.1), and emptied and redeployed at approximately monthly intervals. Collected material was allowed to settle for two days before excess water was decanted and the remaining material was stored frozen. The sediment-trap samples were thawed to allow subsampling for quantitative analysis of phytoplankton remains, and again stored frozen. The phytoplankton subsamples were kept in a fridge until microscopic analysis. The remaining sediment-trap material was thawed again, filtered over pre-weighed and pre-combusted (400°C, 5h) glass fiber GF/F filters (110 mm diameter, Whatmann), frozen and freeze-dried. This study focuses on the 53 monthly samples collected between September 2010 and January 2015.

8.2.3 Sample preparation, extraction and instrumental analysis of lipid biomarkers

Sample preparation and lipid extraction of the sediment-trap samples was described in detail in Chapters 6 and 7. In short, the freeze-dried filters with sediment-trap material were cut into small pieces and directly acid hydrolyzed with 1.5N hydrochloric acid (HCl) in methanol (MeOH) with a known carbon isotopic composition. After 2h reflux at 80°C, the pH was adjusted to 4-5 with potassium hydroxide (KOH)/MeOH, prior to liquid-liquid extraction (three times) with dichloromethane (DCM). The combined supernatant was dried under N_2, water was removed with a Na_2SO_4 column and again dried under a stream of N_2. This total lipid extract was separated on an activated Al_2O_3 column into an apolar, neutral and polar fraction, using hexane/DCM (9:1, v/v), DCM, and DCM/MeOH (2:1, v/v) as eluents, respectively. A known amount of pristane (apolar fractions) or 5α-cholestane (other fractions) was added as internal standard.

The lipid biomarkers in all fractions were analyzed on a gas chromatograph (GC) coupled to a flame ionization detector (GC-FID; Hewlett Packard 6890 series). All fatty acids were measured as their methyl-ester derivatives, and polar fractions were silylated using N,O-bis-trimethylsilyl-trifluoroacetamide (BSTFA). The samples (in hexane or EtOAc as solvent) were injected on-column at 70°C, with helium as carrier gas with a flow rate of 2 ml min^{-1}. The oven was programmed to 130°C at 20°C min^{-1}, and then at 4°C min^{-1} to 320°C, and held isothermal for 10 min. Selected samples were analyzed on a GC-mass spectrometer (GC-MS; Finnigan Trace GC Ultra, DSQ MS) for compound identification, with similar column properties and temperature program as the GC analysis. The mass spectral identification of biomarkers was based on retention times, comparison with a NIST library and interpretation of mass fragmentation patterns.

Samples selected for compound-specific $\delta^{13}C$ analysis were measured with GC combustion isotope-ratio-monitoring MS (GC-C-irMS; ThermoFinnigan Delta Plus XP) using similar column properties and temperature program as GC-FID measurements. GC-C-irMS performance was checked daily by injection of a Schimmelmann alkane standard. The $\delta^{13}C$ values are expressed in ‰ versus the VPDB standard. Fatty-acid $\delta^{13}C$ values were corrected for the carbon atom added to the fatty acid molecule during acid hydrolysis. The reported values are based on at least duplicate

analyses, with results averaged to obtain a mean value and standard deviation. Reproducibility is typically better than 0.7‰ for fatty acids and *n*-alk-1-enes, and <0.2‰ for *n*-alkanes.

Biomarker fluxes were calculated for each month by taking the GC-based biomarker quantification, number of days of collection, and the surface area of the sediment trap (58 cm^2) into account; fluxes are expressed in ng m^{-2} day^{-1}. The average chain length (ACL) and carbon preference index (CPI) of the *n*-alkanes were calculated as:

$$CPI = 0.5 \cdot [(\Sigma C_{25\text{-}33\text{-}odd} / \Sigma C_{26\text{-}34\text{-}even}) + (\Sigma C_{25\text{-}33\text{-}odd} / \Sigma C_{24\text{-}32\text{-}even})]$$

$$ACL = \Sigma(C_n \cdot n) / \Sigma C_n, \text{ where } C_n \text{ is the abundance of each } n\text{-alkane with n carbon atoms (23 to 35)}$$

8.2.4 Phytoplankton abundance

Phytoplankton biovolume estimates from the sediment-trap material were determined as reported in van Bree et al. (2018b). In short, the major groups of pelagic phytoplankton (chlorophytes, diatoms, dinophytes, euglenophytes, chrysophytes, cryptophytes and cyanobacteria) were identified and counted with an inverted Olympus CKX41 microscope equipped with an Olympus UC30 digital camera, following the Utermöhl method (Utermöhl 1931, 1958) using sedimentation chambers of 10 ml. At least 500 solitary phytoplankton cells (≥3 µm) or colonies were counted per sample, as well as the number of cells per colony. The total biovolume of each taxon present was calculated based on mean cell dimensions of the phytoplankton species, and expressed in μm^3 L^{-1}.

8.3 Results and discussion

In order to link biomarkers with environmental or climatic processes, we studied sediment-trap material throughout four full annual cycles of stratification and mixing. To better understand the seasonal and inter-annual variability in lipid biomarker fluxes and biovolume estimates in the settling particles, we need to compare them with those in the SPM interval (van Bree et al., 2018b), for which the characteristics of the different samples and methods used need to be discussed (Section 8.3.1). We can then focus on the 'big picture' of the large annual variability of total phytoplankton fluxes, mainly comprised of Bacillariophyta (diatoms) and Chlorophyta (green algae) (Section 8.3.2), after which we can zoom in and discuss several 'inside stories' that help with the identification of possible biological sources of biomarkers, the microbial responses to water-column changes (Section 8.3.3), and of the processes influencing the $\delta^{13}C$ signatures of aquatic biomarkers (Section 8.3.4). Finally, all these findings combined should lead to the identification of the physical processes important for phytoplankton productivity and succession in Lake Chala, and how changes in these processes are reflected by the lipid biomarker content of the settling particles (Section 8.3.5).

8.3.1 Comparability of biomarkers and biomass estimates in suspended versus settling particles

As the sediment trap captures settling particles continuously, the biomass and lipid biomarkers captured are a reflection of the total organic-matter content which has settled through the water column from the surface to 35 m water depth for every one of the 53 trap samples collected approximately monthly between September 2010 and January 2015. This is different from the

biomarkers in SPM and the water-column biomass estimates (as published by van Bree et al., 2018b), which represent a temporal 'snapshot' of biomarker-producing organisms present at that particular time and depth. As we are ultimately interested in understanding the changes in biomarker contents in the sediments and their link to (paleo)environmental and (paleo) climatic changes, the settling particles give the best indication of the signal that is transferred to the sediments of Lake Chala. Nevertheless, the content of the sediment traps depends on the mechanisms by which microorganisms and biomarkers move through the water column and how that flux is influenced by degradation during transfer.

In order to compare biomarker concentrations in SPM to the fluxes in the sediment trap, the SPM data are reported as average lipid content between 0 and 25 m (at 0-10-25 m; van Bree et al., 2018b). When linking biomarker data to biomass estimates of the possible source organisms (as expressed in biovolume), we need to take into account that biomarkers associated with SPM and settling particles include lipids of both living and decaying organisms, whereas biovolume estimates represent phytoplankton ≥3 µm that was alive at the time of water-column sampling between 0 and 20 m water depth (the average of values at 0-5-10-15-20 m; van Bree et al., 2018b) in each month between September 2013 and January 2015, or all phytoplankton ≥3 µm that accumulated in the sediment trap samples. The lower size threshold of microscopy-based biovolume estimates may have serious consequences for the total biomass estimates, since potentially large pools of photosynthetic picoplankton (mainly cyanobacteria and chlorophytes) are not taken into account. Other oligotrophic lakes in East Africa are reported to have relatively large proportions of photosynthetic picoplankton (e.g., Lake Tanganyika: Vuorio et al., 2003; Descy et al., 2006; Lake Kivu: Sarmento et al., 2008). Although microscopy-based methods such as epifluorescence microscopy or flow cytometry are able to assess the amount of picoplankton, these methods were not conducted in this study of Lake Chala. However, during phytoplankton analyses for this study solitary cells <3 µm were detected only incidentally, and certainly not in the large quantities as is customary in Lake Tanganyika (Descy et al., 2006; C. Cocquyt, personal observations from both lakes). This indicates that the biovolume estimates of the picoplankton, if present, is negligible and falls within the error of biovolume calculations.

8.3.2 The big picture: annual variability in diatom and chlorophyte primary production in Lake Chala

Total aquatic primary productivity in Lake Chala is reflected by the concentration of phytadienes (van Bree et al., 2018b), which are transformation products of chlorophyll-derived phytol produced by acid hydrolysis of the lipid extracts (Grossi et al., 1996). High phytadiene fluxes in the settling particles correlate to those of total phytoplankton biomass (Fig. 8.2A-B). Therefore, phytadienes in settling particles seem to be a useful proxy for primary productivity. Although the amount of primary production shows large seasonal and inter-annual variation, it is usually highest at the end of deep mixing and the start of subsequent stratifying water conditions, especially in September 2010, 2013 and 2014 (Fig. 8.2).

Diatoms are the dominant primary producers in modern-day Lake Chala and are also abundant throughout its sedimentary record, suggesting they were also major contributors to primary production in the past (e.g., Barker et al., 2011; Wolff et al., 2014). They constitute between 5.8 and 100% (62.8±29.5% on average, n = 53) of the total biovolume over the period of sediment-trap deployment. Loliolide and isololiolide are degradation products of the diatom pigment fucoxanthin and therefore often used as biomarkers for diatoms (e.g., Castañeda and Schouten, 2011; van Bree et al., 2018b), although some Haptophyta and Dinophyta species have also been reported to contain

fucoxanthin (Klok et al., 1984; Jeffrey and Vesk, 1997). High (iso-)loliolide concentrations in the SPM and fluxes in settling particles correspond reasonably well with peaks in diatom biomass (Fig. 8.2C-D). There are a few instances where high (iso-)loliolide fluxes occur (in March to April 2011, December 2013, and March 2014; Fig. 8.2C-D) while diatom biomass estimates are low, which possibly indicates a secondary, non-diatom source of (iso-)loliolide. For example, a dinophyte bloom in March and April 2014 (van Bree et al., 2018b) may be responsible for the small peak in (iso-)loliolide in March 2014, although (iso-)loliolide generally seems to represent diatoms best (Fig. 8.2). Generally speaking, the highest diatom production occurs at the end of deep mixing, when elevated nutrient levels are able to sustain diatom blooms. However, the flux and duration of diatom biomarkers in the settling particles varies substantially over time, and the diatom bloom does not systematically recur every year.

After diatoms, chlorophytes appear the most important phytoplankton group in Lake Chala, and constitute between 0 and 91.8% (29.5±27.9% on average, n = 53) of total biomass in the settling particles (Fig. 8.2E). The green microalga *Tetraedron minimum* is usually the dominant species, constituting up to 99.8% of total Chlorophyta biomass (67.0±30.4% on average, n = 53). Previous studies have indicated that both $C_{23:1}$, $C_{25:1}$ and $C_{27:1}$ *n*-alk-1-enes (Castañeda et al., 2009b; van Bree et al., 2014), and C_{21} and C_{23} *n*-alkanes are biomarkers for chlorophytes, and *T. minimum* in particular (van Bree et al., 2018b). Although long-chain fatty acids ($\geq C_{24}$) are major constituents of terrestrial higher plant leaf waxes, and therefore often used as biomarkers for vascular plants in paleoclimate reconstruction (e.g., Feakins et al., 2005; Tierney et al., 2010a, 2011; Holland et al., 2013), it was shown that the C_{28} fatty acids in SPM of Lake Chala are predominantly of aquatic origin (van Bree et al., 2018b), possibly produced by chlorophytes. The $\delta^{13}C$ values of these biomarkers in the settling particles also support an aquatic origin. The flux-weighted average $\delta^{13}C$ values of C_{21} and C_{23} *n*-alkanes (-40.1‰ and -38.7‰, respectively) is similar to that of C_{28} fatty acid (-39.2‰), and even more depleted than the flux-weighted average $\delta^{13}C$ values of $C_{25:1}$ and $C_{27:1}$ *n*-alk-1-enes (-37.1‰ and -37.4‰, respectively). This is comparable to the $\delta^{13}C$ values found in SPM (van Bree et al., 2018b). The trends of these chlorophyte biomarkers in the settling particles are comparable to those in the SPM (Fig. 8.2F-H), and are characterized by a large peak in abundance from July to November 2014. Interestingly, the peak in chlorophytes is not recurring annually, and although not absent, only low concentrations of Chlorophyta biomarkers and biovolume were found between September 2010 and June 2014. Overall similarity of the $\delta^{13}C$ values and trends of these chlorophyte biomarkers in the sediment trap and SPM support the hypothesis that they are mainly produced by *T. minimum*. Although the C_{28} fatty acid has been found in cultures of *T. minimum* and is part of its algaenan (Blokker et al., 1998), van Bree et al. (2018b) hesitated to assign the main source of C_{28} fatty acid to *T. minimum* since the occurrence of the C_{28} fatty acid in SPM peaked slightly later than the living *T. minimum* biomass. However, it is clear that the flux of *T. minimum* in the settling particles is sustained well into November 2014, consistent with the SPM data, rendering *T. minimum* as the most likely source organism for the C_{28} fatty acid in Lake Chala. Discrepancies in biomass estimates for the SPM and the sediment trap material may be caused by the contribution of decaying phytoplankton to the biomass in the trap material.

Together, diatoms and chlorophytes constitute on average 92.3±14.0% (n = 53) of the total phytoplankton biomass that accumulated in the sediment trap. Both phytoplankton groups behave differently over time and show large inter-annual variability. The total biomass (mainly diatoms) shows a rather systematic seasonal response to deep mixing initiating increased nutrient availability, with increases of diatom biomass and (iso-) loliolide fluxes at the end of the deep mixing in 2010, 2012, 2013 and 2014 (Fig. 8.2C-D). The highly variable flux with generally lower diatom (and

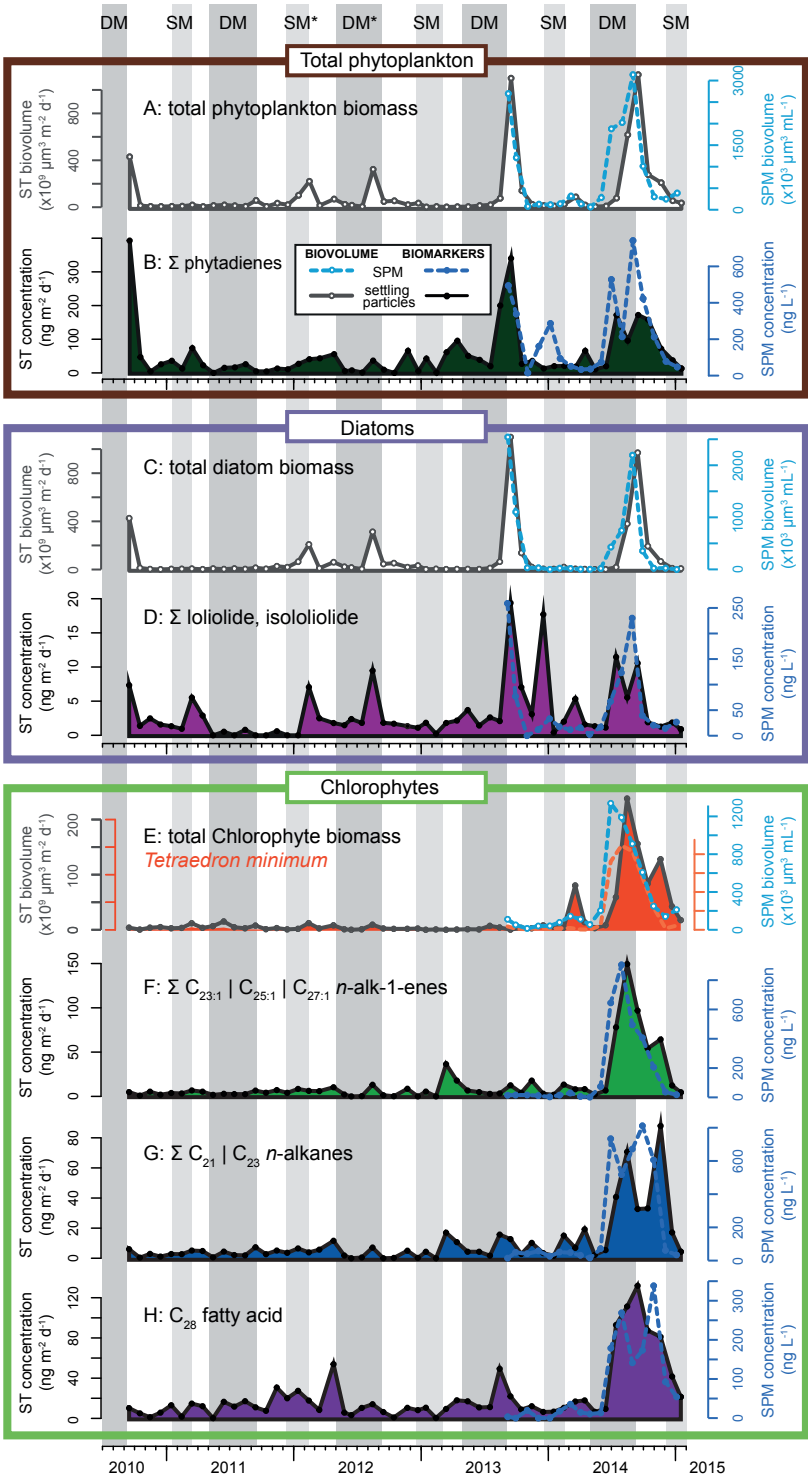
DM
SM
DM
SM*
DM*
SM
DM
SM
DM
SM
Total phytoplankton
A: total phytoplankton biomass
B: Σ phytadienes
BIOVOLUME
BIOMARKERS
SPM
settling particles
ST biovolume (x10⁶ µm³ m⁻² d⁻¹)
SPM biovolume (x10⁶ µm³ mL⁻¹)
ST concentration (ng m⁻² d⁻¹)
SPM concentration (ng L⁻¹)
Diatoms
C: total diatom biomass
D: Σ loliolide, isololiolide
Chlorophytes
E: total Chlorophyte biomass
Tetraedron minimum
F: Σ C23:1 | C25:1 | C27:1 n-alk-1-enes
G: Σ C21 | C23 n-alkanes
H: C28 fatty acid
2010
2011
2012
2013
2014
2015

Figure 8.2 (left) Total phytoplankton (A-B), diatom (C-D) and chlorophyte (E-H) biomarkers and biomass in Lake Chala between September 2010 and January 2015. A: total phytoplankton biomass in settling particles (biovolume in 10^9 µm^3 m^{-2} d^{-1}; solid gray line) and the average biomass of total phytoplankton between 0 and 20 m water depth (in 10^3 µm^3 mL^{-1}; dashed light blue line; excluding heterotrophic dinoflagellates; van Bree et al., 2018b). B: flux of phytadienes in settling particles (in ng m^{-2} d^{-1}; dark green) and concentration of phytadienes in SPM (in ng L^{-1}; dashed blue line; average of 0-10-25 m depth; van Bree et al., 2018b). C: total diatom biomass in settling particles (biovolume in 10^9 µm^3 m^{-2} d^{-1}; solid gray line) and the average biomass of diatoms between 0 and 20 m water depth (in 10^3 µm^3 mL^{-1}; dashed light blue line; van Bree et al., 2018b). D: flux of loliolide and isololiolide in settling particles (in ng m^{-2} d^{-1}; purple) and concentration of loliolide and isololiolide in SPM (in ng L^{-1}; dashed blue line; average of 0-10-25 m depth; van Bree et al., 2018b). E: total chlorophyte biomass in settling particles (biovolume in 10^9 µm^3 m^{-2} d^{-1}; solid black line), and specifically *Tetraedron minimum* (orange), compared to the average biomass of Chlorophytes (and *T. minimum*) between 0 and 20 m water depth (in 10^3 µm^3 mL^{-1}; dashed blue (orange) line; van Bree et al., 2018b). F: flux of $\Sigma C_{23:1}$, $C_{25:1}$ and $C_{27:1}$ *n*-alk-1-enes in settling particles (in ng m^{-2} d^{-1}; green) and concentration of these *n*-alk-1-enes in SPM (in ng L^{-1}; dashed blue line; average of 0-10-25 m depth; van Bree et al., 2018b). G: ΣC_{21} and C_{23} *n*-alkanes flux in settling particles (in ng m^{-2} d^{-1}; blue) and concentration in SPM (in ng L^{-1}; dashed blue line; average of 0-10-25 m depth; van Bree et al., 2018b). H: C_{28} fatty acid flux in settling particles (in ng m^{-2} d^{-1}; purple) and concentration in SPM (in ng L^{-1}; dashed blue line; average of 0-10-25 m depth; van Bree et al., 2018b). Samples of the settling particles are plotted on the median day of the approximately monthly sediment trap deployment, while SPM is plotted at the day of sampling. Gray bands indicate deep (DM) and shallow (SM) mixing periods as estimated from the temperature gradients in the water, where an asterisk (*) indicate that the specific start or end dates of these periods are approximated.

Chlorophyta) blooms between October 2010 and July 2013, spanning almost three full cycles of mixing and stratification, indicates that nutrient availability in the photic zone has changed over time. The chlorophyte biomarkers ($C_{23:1}$, $C_{25:1}$ and $C_{27:1}$ *n*-alk-1-enes, C_{21} and C_{23} *n*-alkanes, and C_{28} fatty acid) are highest between July and November 2014. Based on the currently available sediment-trap record it seems not possible to predict if and when a bloom of chlorophytes will develop in a specific year. It is noted that the fluxes of both diatoms and green algae were highest during the time of SPM sampling (September 2013 to January 2015). This interval is characterized by a relatively shallow oxycline (ranging from ~15 m in November 2013, to ~40 m depth in September 2014; van Bree et al., 2018b), and the subsequent deep mixing was at the lower end of reported mixing depths (45-60 m; Wolff et al., 2011). Although this relatively shallow mixing should result in lower nutrient upwelling and therefore less potential for intensive phytoplankton blooms (and especially diatoms), compared to the other studied years, 2014 appeared a relatively productive year.

8.3.3 Inside stories: abundance trends and $\delta^{13}C$ signature of specific biomarkers

8.3.3.1 The $C_{19:1}$ *n*-alkene as biomarker for cyanobacteria

The $C_{19:1}$ *n*-alkene was identified as a potential biomarker for cyanobacteria in Lake Chala (van Bree et al., 2018b), mainly based on its joint peak abundance in the SPM and living biomass during episodes of shallow mixing. In the longer time series of settling particles, there are two periods with increased $C_{19:1}$ *n*-alkene flux: from December 2010 to January 2011, and from August 2013 to March 2014, including the highest recorded flux of 26.9 ng m^{-2} d^{-1} in December 2013 (Fig. 8.3A). The timing of seasonal variation in $C_{19:1}$ *n*-alkene flux differs from that of any other biomarker in the settling particles, and is to some extent comparable to that of $C_{19:1}$ *n*-alkene

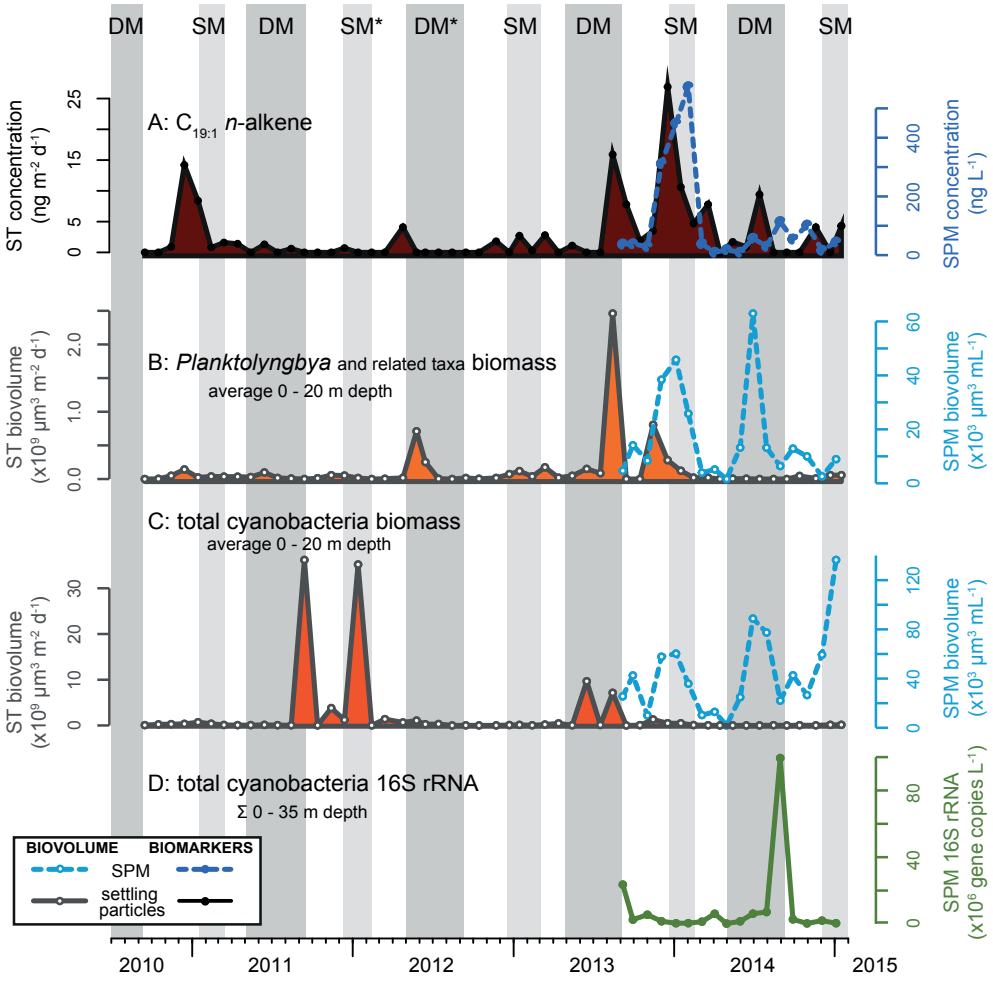

Figure 8.3 Cyanobacterial biomarker (A), biomass (B-C), 16S rRNA (D) in Lake Chala between September 2010 and January 2015. A: flux of $C_{19:1}$ *n*-alkene in settling particles (in ng m^{-2} d^{-1}; brown) and concentration in SPM (in ng L^{-1}; dashed blue line; average of 0-10-25 m depth; van Bree et al., 2018b). B: *Planktolyngbya* and related taxa biomass in settling particles (biovolume in 10^9 µm^3 m^{-2} d^{-1}; orange) and its average biomass in the water column between 0 and 20 m water depth (in 10^3 µm^3 mL^{-1}; dashed light blue line; van Bree et al., 2018b). C: total cyanobacterial biomass in settling particles (biovolume in 10^9 µm^3 m^{-2} d^{-1}; red), compared to the average biomass of cyanobacteria between 0 and 20 m water depth (in 10^3 µm^3 mL^{-1}; dashed light blue line; van Bree et al., 2018b). D: summed estimated cyanobacterial 16S rRNA gene abundance (in 10^3 gene copies L^{-1}) between 0 and 35 m depth (Σ 0, 10, 20, 25, 30 and 35 m; Table S6.6). Samples of the settling particles are plotted on the median day of the approximately monthly sediment trap deployment, while SPM is plotted at the day of sampling. Gray bands indicate deep (DM) and shallow (SM) mixing periods as estimated from the temperature gradients in the water, where an asterisk (*) indicate that the specific start or end dates of these periods are approximated.

concentrations in SPM during the overlapping period (van Bree et al., 2018b). The main difference between the sediment-trap and SPM time series is the increased $C_{19:1}$ *n*-alkene fluxes at the transition period from deep mixing to stratified water conditions in September 2013, and the high flux of $C_{19:1}$ *n*-alkene in July 2014, neither of which is reflected in the SPM (Fig. 8.3A). Based on its similarity with the temporal variation in $C_{19:1}$ *n*-alkene concentrations in SPM, *Planktolyngbya* (including related taxa) was identified as the most likely cyanobacterial source of the $C_{19:1}$ *n*-alkene in Lake Chala (van Bree et al., 2018b). *Planktolyngbya* was one of the dominant groups of cyanobacteria during the SPM study, and is related to *Leptolyngbya* of which some species are known to produce $C_{19:1}$ *n*-alkenes (Coates et al., 2014). The flux of $C_{19:1}$ *n*-alkene is however only modestly correlated with *Planktolyngbya* biovolume ($R^2 = 0.16$, $p < 0.01$, $n = 53$) for the sediment-trap series, and does not correlate at all with total cyanobacterial biovolume ($R^2 = 0.005$, $p = 0.63$, $n = 53$). The cyanobacterial biovolume estimates in this study are limited to the size fraction ≥3 µm, which does not influence the filamentous taxa (including *Planktolyngbya* and related taxa) much, but could influence the total biovolume estimates of small coccoid cyanobacteria. Even though picoplanktonic cyanobacteria are not expected to represent a large proportion of all cyanobacteria in Lake Chala (Section 8.3.1), 16S rRNA analysis of the SPM may paint a more comprehensive picture of total cyanobacterial abundance. Notably, the temporal distribution of total cyanobacterial 16S rRNA (Table S6.6) does not correspond to the biovolume estimates of either total (Fig. 8.3C) or specific (Fig. 8.3B) cyanobacterial species. This mismatch is interesting, and will require further study. The 16S rRNA pattern of the cyanobacterial taxon that best corresponds to the $C_{19:1}$ *n*-alkene concentrations in the SPM is that of the class Melainabacteria, which peak between November 2013 and April 2014 (Fig. S8.1), similar to the largest concentrations of $C_{19:1}$ *n*-alkenes. However, the Melainabacteria are not a likely the source of $C_{19:1}$ *n*-alkenes as they mainly have an anaerobic and non-phototrophic nature and mostly occur in the anoxic water column, whereas $C_{19:1}$ *n*-alkene concentrations are highest in the surface waters (at 0 and 10 m depth; van Bree et al., 2018b). Therefore, the similar timing of high $C_{19:1}$ *n*-alkenes fluxes and Melainabacteria 16S rRNA concentrations are likely a reflection of similar environmental conditions favoring these two groups of cyanobacteria at different depths. Thus, the $C_{19:1}$ *n*-alkene record in settling particles represents cyanobacteria that bloom at low nutrient levels in the surface waters during shallow mixing within the long seasonal period of stratification, while Melainabacteria mainly reside in the anoxic water below the associated shallow oxycline during the same stratification period.

To conclude, a cyanobacterial origin of $C_{19:1}$ *n*-alkene is more likely than other microbial source. Of all cyanobacteria, *Planktolyngbya* and/or related taxa are the most likely candidate(s) for $C_{19:1}$ *n*-alkene synthesis. More research on the specific lipid content of these taxa would help narrow down this possible biomarker origin. During the 2013/2014 stratification period the oxycline was relatively shallow, with dissolved oxygen profiles indicating anoxic conditions to as little as ~15 m below the surface. It is likely that the higher flux of $C_{19:1}$ *n*-alkenes in the sediment trap series is indicative of shallow mixing during strongly stratified conditions, and may be a good indicator of these conditions when found in the sedimentary record.

8.3.3.2 Bacterial biomarkers

The *ai*-C_{15}, *i*-C_{15}, *i*-C_{16} and *i*-C_{17} fatty acids are generally considered as non-specific bacterial biomarkers (e.g., Kaneda, 1991; Boschker and Middelburg, 2002). The presence of these bacterial biomarkers in settling particles is to some extent comparable to that in SPM (Fig. 8.4A), with the highest values in August-September 2013 (up to 243.4 ng m^{-2} d^{-1}). The fluxes of these *iso* and *anteiso* fatty acids correlate well with those of the C_{20} and C_{22} fatty acids ($R^2 = 0.61$, $p < 0.001$,

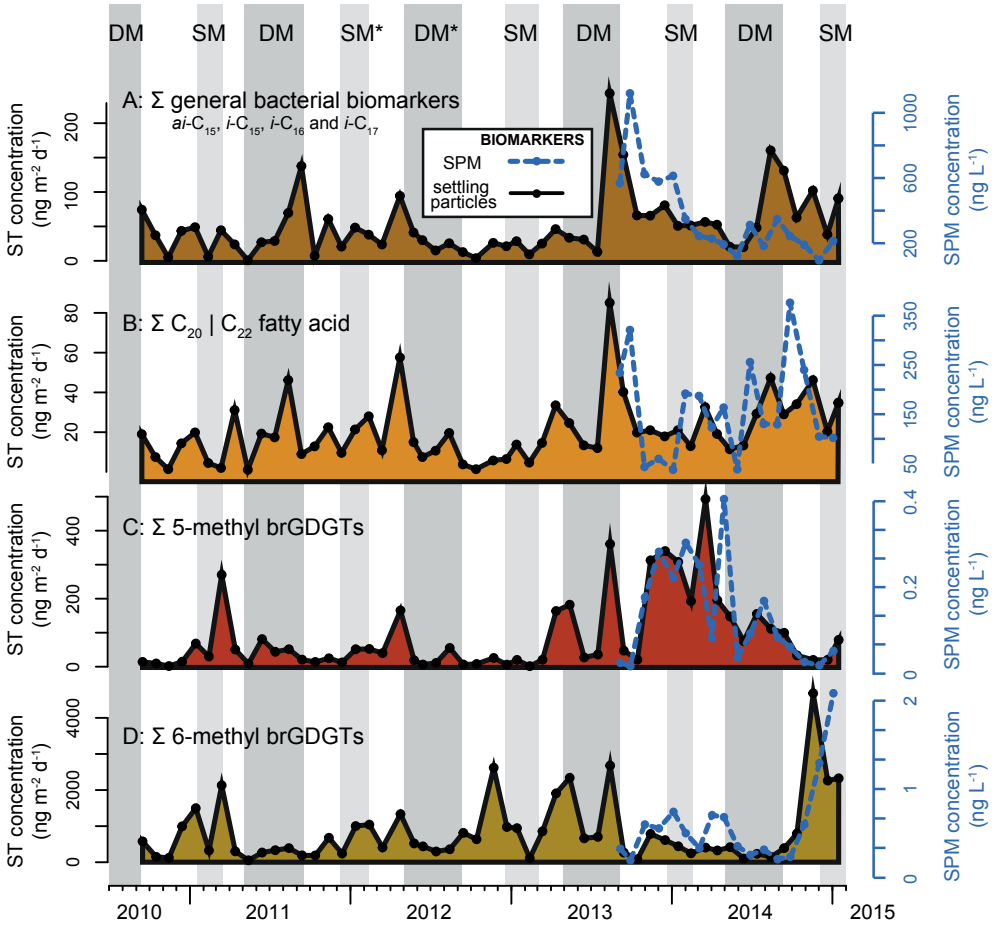

Figure 8.4 Bacterial biomarkers. A: summed flux of *ai*-C_{15}, *i*-C_{15}, *i*-C_{16} and *i*-C_{17} fatty acids in settling particles (in ng m^{-2} d^{-1}; dark brown) and concentration of these fatty acids in SPM (in ng L^{-1}; dashed blue line; van Bree et al., 2018b). B: ΣC_{20} and C_{22} fatty acid flux in settling particles (in ng m^{-2} d^{-1}; orangebrown) and concentration in SPM (in ng L^{-1}; dashed blue line; van Bree et al., 2018b). C: summed flux of 5-methyl brGDGTs (in ng m^{-2} d^{-1}; magenta) and concentrations of these brGDGTs in SPM (in ng L^{-1}; dashed blue line; Chapter 6). D: summed flux of 6-methyl brGDGTs (in ng m^{-2} d^{-1}; taupe) and concentrations of these brGDGTs in SPM (in ng L^{-1}; dashed blue line; Chapter 6). SPM represents the average biomarker concentrations of 0, 10 and 25 m water depth. Samples of the settling particles are plotted on the median day of the approximately monthly sediment trap deployment, while SPM is plotted at the day of sampling. Gray bands indicate deep (DM) and shallow (SM) mixing periods as estimated from the temperature gradients in the water column, where an asterisk (*) indicate that these periods are approximated.

n = 53; Fig. 8.4B), indicating a joint bacterial source. The fluxes of both types of bacterial biomarkers mainly increase during periods of shallow (January to May 2012, February to April 2014) or deeper mixing (July to September 2011, April to October 2013, July to December 2014). Higher fluxes of bacterial biomarkers are expected to occur during and after phytoplankton blooms, as those

blooms contribute to the pool of decaying organic matter that heterotrophic bacteria remineralize. Nevertheless, although the timing of increased bacterial biomarkers during mixing is consistent with the expected timing of phytoplankton blooms, the succession of bacterial biomarkers following phytoplankton blooms is not as clear-cut as expected, and not all phytoplankton blooms coincide with or are followed by high bacterial biomarker fluxes. For example, peak fluxes of the fatty-acid bacterial biomarkers occur in August 2014, coinciding with high levels of chlorophytes, but high fluxes in September 2010 do not correspond with increases in any biomarker, and the peak flux of fatty-acid bacterial biomarkers in August 2013 (Fig. 8.4A) precedes the peak diatom flux (Fig. 8.2C).

Other bacterial biomarkers are branched dialkyl glycerol tetraethers (brGDGTs), which are membrane lipids of unknown bacterial origin (Fig. 8.4C-D; Chapter 6). These lipids have a methyl group on either the 5-methyl or 6-methyl position, which are likely produced by different bacterial communities (Chapter 6). There is only a weak correlation between the fluxes of 5- and 6-methyl brGDGTs on the one hand and those of bacterial fatty acids on the other ($R^2 = 0.16$, $p < 0.01$, and $R^2 = 0.10$, $p < 0.05$, respectively). This indicates that brGDGTs are biosynthesized by different bacteria and under different environmental conditions than the fatty-acid bacterial biomarkers, with the brGDGT producers likely thriving under stratified and anoxic conditions (Chapter 6) while the fatty-acid bacterial biomarkers are more generic.

8.3.3.3 Isoarborinol and stratification

Isoarborinol and its degradation products are typically found in crater lakes and tropical lacustrine settings with permanently anoxic bottom waters and sediments (e.g., Jaffé and Hausmann, 1995; Hanisch et al., 2003; van Bree et al., 2018a). A suite of isoarborinol degradation products was found in the sediments of Lake Chala, where their concentrations were higher during inferred wetter periods, and during stratified conditions in the modern lake (van Bree et al., 2018a). The concentration of isoarborinol in the settling particles studied here was generally below detection limit, except during periods with a stratified water column, in October-November 2010, February-March 2012, September to December 2012, March-April 2013, February to May 2014 and November-December 2014, when isoarborinol is present in small amounts. Due to the low concentrations and co-elution with other compounds, isoarborinol was not quantified, but its presence/absence is indicated in Fig. 8.5. The specific aerobic microbial source organism of isoarborinol is unknown (see van Bree et al., 2018a), but the occurrence of isoarborinol indicates that it prefers stratified water-column conditions, and thus supports the use of isoarborinol and its degradation products as a proxy for stratification.

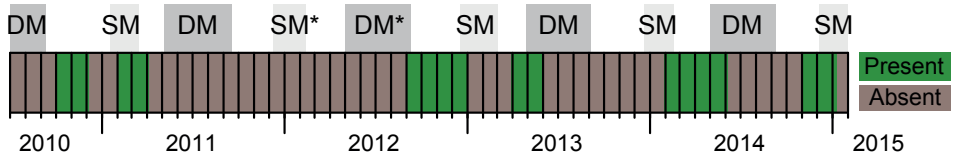

Figure 8.5 The presence of isoarborinol (traces) in the sediment trap samples is indicated with green bars. Gray bands indicate deep (DM) and shallow (SM) mixing periods as estimated from the temperature gradients in the water column, where an asterisk (*) indicate that these periods are approximated.

8.3.3.4 Eustigmatophytes and stratification

C_{30} and C_{32} 1,15 *n*-alkyl diols are known Eustigmatophyte biomarkers (e.g., Rampen et al., 2014). In the SPM of Lake Chala they were most abundant during periods of strong water-column stratification (Villanueva et al., 2014; van Bree et al., 2018b). In the settling-particle record, long-chain diols mainly peak between February and May 2012 and in April-May 2013 (up to 48.6 ng m^{-2} d^{-1} in May 2012; Fig. 8.6; Lattaud et al., unpublished data). This seems to suggest that the conditions during stratified periods in 2012 and 2013 were more favorable for Eustigmatophyte proliferation than during the stratification periods between September 2013 and January 2015. Apparently, the remarkably shallow oxycline (~15 m) that we know occurred during the latter stratified periods provided conditions that allowed other biota to bloom and to compete with the Eustigmatophytes. Due to their small size and the long sample storage prior to analysis in combination with their already fragile nature, microscopic biomass estimates of Eustigmatophytes are unfortunately not available to confirm these trends.

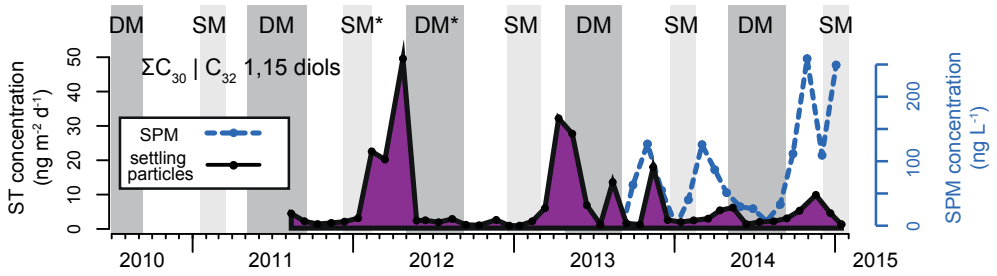

Figure 8.6 Eustigmatophyte biomarkers. Summed C_{30} and C_{32} 1,15 *n*-alkyl diols flux in settling particles (in ng m^{-2} d^{-1}; purple; Lattaud et al., unpublished data) and concentration in SPM (in ng L^{-1}; dashed blue line; average of 0-10-25 m depth; van Bree et al., 2018b). Samples of the settling particles are plotted on the median day of the approximately monthly sediment trap deployment, while SPM is plotted at the day of sampling. Gray bands indicate deep (DM) and shallow (SM) mixing periods as estimated from the temperature gradients in the water column, where an asterisk (*) indicate that these periods are approximated.

8.3.3.5 Archaeal biomarkers and stratification

The isoprenoid GDGTs (isoGDGTs) crenarchaeol and its isomer, isoGDGT-0, isoGDGT-1, isoGDGT-2 and isoGDGT-3 are archaeal membrane lipids of Thaumarchaeotal origin, although isoGDGT-0 is also produced by species of Eury- and Bathyarchaea (Schouten et al., 2013, and references therein). The inter-annual and seasonal variations in isoGDGTs in Lake Chala settling particles and SPM are reported in Chapter 7. In short, their flux is highest during stratified conditions, especially between January and April 2012 (Fig. 8.7B), reaching fluxes up to ~8000 ng m^{-2} day^{-1} (Fig. 8.7C). Although the flux of isoGDGT-0 is at times similar to that of the other isoGDGTs, it is clear that isoGDGT-0 partly reflects a different archaeal origin (Fig. 8.7D), with the highest concentrations in the deep anoxic water column (Chapter 7). A non-Thaumarchaeotal production of isoGDGT-0 is reflected by the ratio of isoGDGT-0/crenarchaeol (Fig. 8.7A), where high values represent a large contribution of non-Thaumarchaeotal isoGDGT-0 in the deeper anoxic water layer. Given that the sediment trap is suspended at 35 m, high isoGDGT-0/crenarchaeol values in the settling particles indicate periods with a very shallow

oxycline. The highest isoGDGT-0/crenarchaeol values are recorded between September 2013 to September 2014, when physical water-column data confirm the presence of a very shallow oxycline (van Bree et al., 2018b; Chapter 7). A study on isoGDGTs in settling particles between November 2006 and August 2010 indicated that similarly high isoGDGT-0/crenarchaeol values also occurred in the period between July 2008 and November 2009 (Buckles et al., 2016), which suggests that these shallow oxycline conditions are recurring at least more than once per decade.

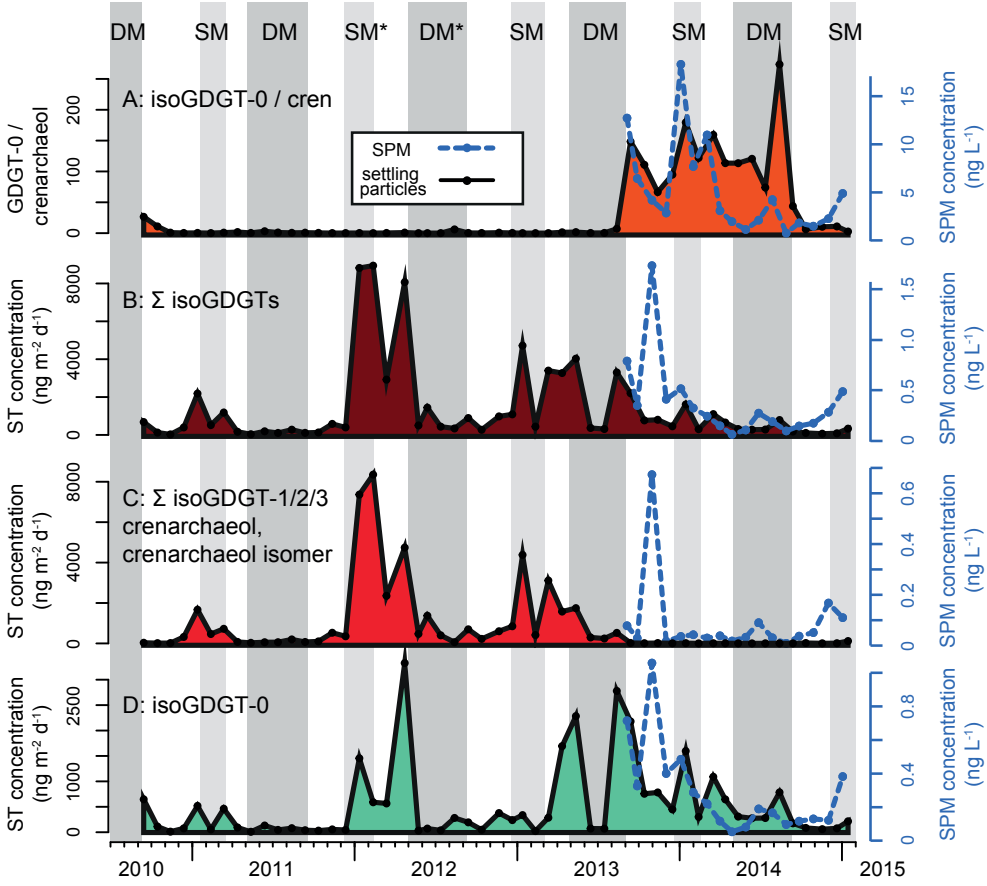

Figure 8.7 Archaeal membrane lipids. A: GDGT-0/crenarchaeol, in settling particles (darkorange) and SPM (dashed blue line; average of 0-10-25 m depth). B: sum of the flux of all isoGDGTs in settling particles (in ng m^{-2} d^{-1}; maroon; Chapter 7) and concentration in SPM (in ng L^{-1}; dashed blue line; average of 0-10-25 m depth; Chapter 7). C: Thaumarchaeotal isoGDGTs (sum of GDGT-1, GDGT-2, GDGT-3, crenarchaeol and its isomer) in settling particles (in ng m^{-2} d^{-1}; crimson; Chapter 7) and concentration in SPM (in ng L^{-1}; dashed blue line; average of 0-10-25 m depth; Chapter 7). D: GDGT-0 flux in settling particles (in ng m^{-2} d^{-1}; jade; Chapter 7) and concentration in SPM (in ng L^{-1}; dashed blue line; average of 0-10-25 m depth; Chapter 7). Samples of the settling particles are plotted on the median day of the approximately monthly sediment trap deployment, while SPM is plotted at the day of sampling. Gray bands indicate deep (DM) and shallow (SM) mixing periods.

8.3.3.6 Limited terrestrial input

C_{29} to C_{35} long-chain *n*-alkanes are well-established leaf-wax biomarkers. Sinninghe Damsté et al. (2011b) used *n*-alkanes with chain lengths ≥31 in Lake Chala sediments as true plant waxes based on the correlations and $\delta^{13}C$ values of the *n*-alkane homologues. C_{29} to C_{35} *n*-alkanes show similar fluxes over the sediment trap interval (R^2 between 0.55 and 0.85, p <0.001, n = 53), implying that all *n*-alkanes ranging from C_{29} to C_{35} can be considered as terrestrial plant wax biomarkers here. As expected, variations in the fluxes of these terrestrial long-chain *n*-alkanes (Fig. 8.8B) is clearly different than those of the aquatic chlorophyte biomarkers C_{21} and C_{23} *n*-alkanes (Fig. 8.2G), and at times similar to the C_{25} and C_{27} *n*-alkanes (Fig. 8.8A), which in Lake Chala are considered a mix of terrestrial and aquatic *n*-alkanes (Sinninghe Damsté et al., 2011b; van Bree et al., 2018b). Van Bree et al. (2018b) previously reported that biomarkers for terrestrial vegetation are nearly absent in SPM, while they are clearly present in the sediments of Lake Chala. These authors explained this mismatch by the 'snapshot' nature of SPM, which mainly represents biomarkers that are present in the water column at the time of sampling, and not necessarily reflects those that are transferred to the sediments. Indeed, terrestrial biomarkers (C_{29} to C_{35} *n*-alkanes) were more abundant in settling particles, although the flux of summed plant wax *n*-alkanes (up to 60.3 ng m^{-2} d^{-1} in March 2013) is still low compared to the aquatic biomarkers (an order of magnitude lower than summed diatom and chlorophyte biomarkers). A markedly higher flux of summed plant wax *n*-alkanes than during the period of SPM monitoring occurred in March-April 2013, and also during 2011-2012 it regularly exceeded 10 ng m^{-2} d^{-1} (Fig. 8.8A). Hence, it seems that the main reason for the low (trace) amounts of these biomarkers in the SPM interval is an unusually long period with very low input of C_{29} to C_{35} long-chain *n*-alkanes into the lake.

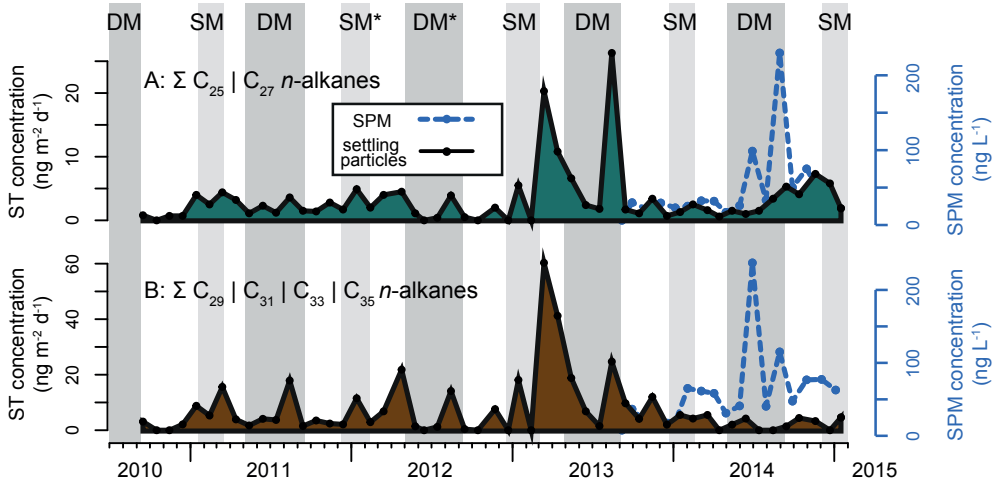

Figure 8.8 A: Summed C_{25} and C_{27} *n*-alkanes flux in settling particles (in ng m^{-2} d^{-1}; navy) and concentration in SPM (in ng L^{-1}; dashed blue line; average of 0-10-25 m depth; van Bree et al., 2018b), compared to B: Summed C_{29} to C_{35} *n*-alkanes flux in settling particles (in ng m^{-2} d^{-1}; chocolatebrown) and concentration in SPM (in ng L^{-1}; dashed blue line; average of 0-10-25 m depth; van Bree et al., 2018b). Samples of the settling particles are plotted on the median day of the approximately monthly sediment trap deployment, while SPM is plotted at the day of sampling. Gray bands indicate deep (DM) and shallow (SM) mixing periods as estimated from the temperature gradients in the water column, where an asterisk (*) indicate that these periods are approximated.

Several proxies based on *n*-alkanes are used to reconstruct aspects of paleovegetation. The carbon preference index (CPI) is used as a measure of *n*-alkane origin, where high CPI values are indicative of a plant wax origin and represent the strong odd-over-even *n*-alkane distribution of vascular plants, while bacterial or algal sources have CPI values ~1 (Gelpi et al., 1970; Cranwell et al., 1987). The CPI values in settling particles range from 0.4 to 14 (3.3±2.8, $n = 43$), indicating the presence of both aquatic and terrestrial sourced *n*-alkanes in the lake. Furthermore, the average chain length (ACL) is often used as a vegetation indicator, where higher ACL values indicate relatively higher amounts of C_3 savannah vegetation (C_{31} dominated) and C_4 grasses (C_{31} dominated, relatively high contribution of C_{33}) compared to trees and shrubs that are thought to produce more shorter (C_{27}/C_{29}) *n*-alkanes (e.g., Vogts et al., 2012; Freeman and Pancost, 2014; Garcin et al., 2014; Diefendorf and Freimuth, 2017). In Lake Chala settling particles, ACL values range from 23.0 to 29.6 (27.2±2.0, $n = 51$). As the ACL also includes the aquatic C_{23} to C_{27} *n*-alkanes, it is not possible to reconstruct the (paleo)vegetation type using this proxy. Instead, ACL values in Lake Chala are indicative of a predominantly aquatic versus a plant wax origin of *n*-alkanes.

In addition to the long-chain *n*-alkanes, also long-chain fatty acids ($\geq C_{26}$) are considered as biomarkers for higher plants. As mentioned above (Section 8.3.2), C_{28} fatty acids have a predominantly aquatic source in Lake Chala. The C_{26} fatty acid is also likely primarily aquatic in Lake Chala, as the flux trends (Fig. 8.9A-B; $R^2 = 0.34$, $p < 0.001$, $n = 53$) and $\delta^{13}C$ variation of C_{26} and C_{28} fatty acids (Fig. 8.9C; $R^2 = 0.24$, $p < 0.01$, $n = 31$) are correlated and fairly similar most of the time. Although fluxes of the C_{26} fatty acid are on average threefold lower than those of the C_{28} fatty acid, there are periods when the flux of C_{26} fatty acids is much larger than that of C_{28} fatty acids, coinciding with a relative enrichment of the $\delta^{13}C$ values of the C_{26} fatty acids, such as in September 2010 and September-October 2013 (when $\delta^{13}C$ of C_{26} fatty acids is -26.6±0.6‰, -26.5±0.5‰, and -29.3±0.1‰, respectively). These dissimilarities are indicative of periods with input of an additional, isotopically less depleted source of C_{26} fatty acids. If this reflects a vascular plant contribution, it is most likely a C_4 or CAM plant, which have on average $\delta^{13}C$ values of –22.9‰ around Lake Chala, while C_3 plants are more depleted with average $\delta^{13}C$ values of –35.0‰ (van Bree et al., 2018b). Although the C_{26} fatty acid has similar general features as its C_{28} homologue, this second, ^{13}C-enriched source suggests that C_{26} fatty acids should not be used as either an aquatic biomarker or as a biomarker for terrestrial input in the sedimentary record of Lake Chala.

8.3.4 Chemically enhanced fractionation in Lake Chala

Aquatic biomarkers in Lake Chala are generally more depleted in ^{13}C than expected. This has been reported for various aquatic biomarkers in the sedimentary record, e.g. for mid-chain *n*-alkanes (Sinninghe Damsté et al., 2011b), green algal *n*-alk-1-enes (van Bree et al., 2014) and microbial *des*-A-arborenes (van Bree et al., 2018a), and also for aquatic biomarkers in SPM (van Bree et al., 2018b). Furthermore, the $\delta^{13}C$ signature of biomarkers in SPM showed a remarkable trend and large variation throughout the studied interval, which indicated that processes of chemically enhanced diffusion and fractionation were taking place (van Bree et al., 2018b). Chemically enhanced diffusion is characterized by a strong stable carbon-isotopic fractionation (Mook et al., 1974) due to the reaction of CO_2 with OH^- instead of H_2O to form HCO_3^- when lake water pH is high (Herczeg and Fairbanks, 1987; Bade and Cole, 2006). The pH in Lake Chala is elevated at times of high primary productivity, which indeed fits with the occurrence of increased fractionation (Fig. 8.9C). The $\delta^{13}C$ of algal biomarkers in settling particles reach values as low as -43.1‰ ($C_{27:1}$ *n*-alk-1-ene), -43.2 ‰ (C_{21} *n*-alkane), and -43.7‰ (C_{28} fatty acid), and compare well with

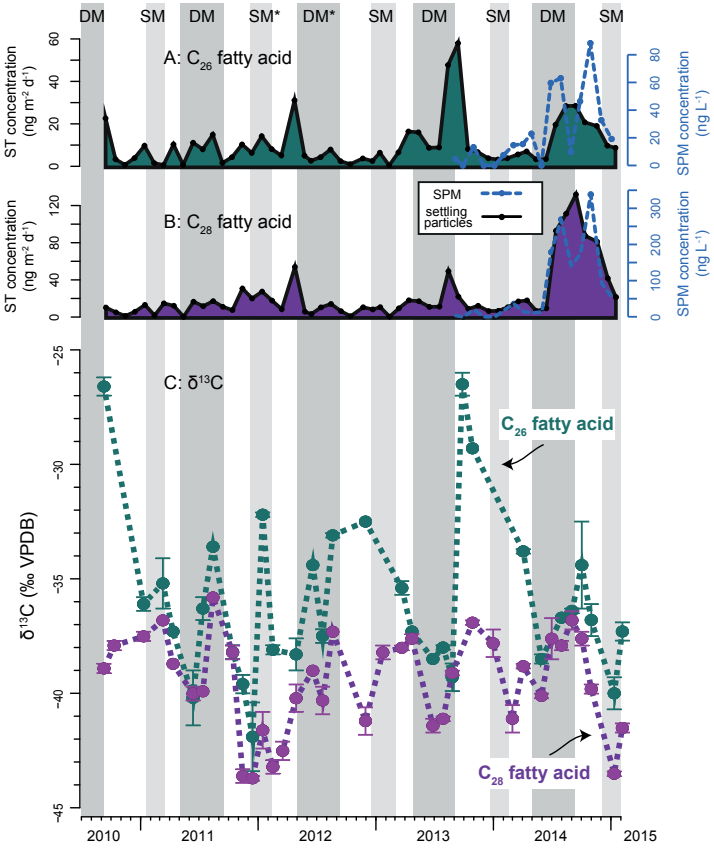

Figure 8.9 C_{26} fatty acid (A) and C_{28} fatty acid (B) flux in settling particles (in ng m^{-2} d^{-1}) and concentration in SPM (in ng L^{-1}; dashed blue line; average of 0-10-25 m depth; van Bree et al., 2018b). C: $\delta^{13}C$ values of C_{26} fatty acid (green) and C_{28} fatty acid (purple) in the settling particles. Gray bands indicate deep (DM) and shallow (SM) mixing periods.

the $\delta^{13}C$ values and ranges of the biomarkers in the SPM (van Bree et al., 2018b), i.e., up to 8.0‰ variation in $\delta^{13}C$ values over time for the C_{28} fatty acid (Fig. 8.9C), 8.4‰ (C_{21} *n*-alkane), 7.8‰ (C_{23} *n*-alkane), 6.3‰ ($C_{25:1}$ *n*-alk-1-ene) and 5.2‰ ($C_{27:1}$ *n*-alk-1-ene). The trends in $\delta^{13}C$ of these biomarkers indicate that chemically enhanced fractionation occurred regularly between September 2010 and January 2015 (Fig. 8.9C). For example, the C_{28} fatty acid $\delta^{13}C$ record shows two periods with strong ^{13}C depletion (November 2011 to March 2012, and October 2014 to January 2015), as well as shorter or less intense periods of depletion (e.g. June-July 2011, July and November 2012, June-July 2013, and February 2014). Hence, chemically enhanced fractionation is a regular feature in the water column of Lake Chala, and thus exerts an important influence on the $\delta^{13}C$ signature of aquatic biomarkers (and consequently that of bulk organic matter) stored in the sediments.

8.3.5 Influence of physical water-column conditions on biomarker distribution

The occurrence and distribution of biomarkers in Lake Chala varies throughout the year. The largest variation is linked to changes in physical properties of the lake, mainly governed by mixing and stratification of the water column. For instance, the nutrients that are released during deeper mixing drive the phytoplankton proliferation of diatoms and chlorophytes (Figs 8.2, 8.10A-C). The low-nutrient conditions during stratification subsequently create opportunities for other autotrophs. For example, Eustigmatophytes profit from the more stagnant conditions during and at the end

of stratification (Figs. 8.6 and 8.10G). Also, cyanobacteria can outcompete other phytoplankton under low nutrient conditions, as is reflected by the high concentrations of $C_{19:1}$ *n*-alkene during shallow mixing during strong stratification periods (Figs. 8.3A and 8.10D). Furthermore, mixing and stratification also influences the heterotrophic bacterial community of Lake Chala. Bacterial biomarkers are much more prevalent under oxygen-depleted conditions, although there is a large seasonal and inter-annual variability in the bacterial communities (Figs. 8.4, 8.10E, 8.10H-I). The high flux of biomarkers from anoxic archaea (that are mainly prevalent in the deepest water column) in the settling particles from September 2013 to August 2014 (Figs. 8.7D and 8.10F) indicates that the oxycline was exceptionally shallow during this time.

At first glance, the period between September 2013 and January 2015, which coincides with the period of extensive SPM and water-column monitoring, seems to be different from the other years covered by the sediment-trap series (Fig. 8.10). The flux of phytoplankton cells and biomarkers is much lower during the three years prior to this period (Fig. 8.10A-D). Moreover, there is very little terrestrial input during the extensive monitoring period (Fig. 8.10J). Water-column monitoring data indicate that the oxycline was very shallow during the 2013-2014 stratification, which is reflected in high isoGDGT-0/crenarchaeol values (Fig. 8.10F) and an increase in the concentration of the crenarchaeol isomer (Chapter 7). Although the period from September 2013 to January 2015 seems to stand out in this time-series, the occurrence of a period with similarly high isoGDGT-0/crenarchaeol values between July 2008 and November 2009 (Sinninghe Damsté et al., 2009; Buckles et al., 2014, 2016) suggests that certain water-column conditions and their associated biomarker distributions occur on multi-annual rather than seasonal or annual timescales. Hence, the order of appearance and trends in the terrestrial and aquatic microbial biomarkers observed in this study do not necessarily indicate that any microbial succession is annually recurring or predictable (Fig. 8.10).

The low-frequency changes in the biomarker-inferred microbial community structure indicate that threshold effects may be important in this lake system. This is illustrated by the binary behavior of certain biomarkers. For example, chlorophytes are a major constituent of the primary producers, or they are not (Fig. 8.2A and E; van Bree et al., 2018b). The diatom bloom is dominated by either *Afrocymbella* or *Nitzschia* taxa (van Bree et al., 2018b). Thaumarchaeotal blooms develop under stratified conditions with a relatively deep oxycline, or they do not occur at all (Chapter 7). BrGDGTs generally thrive under the expanded anoxia during stratification, but are dominated by either 5-methyl brGDGT-Ib and IIb or 6-methyl brGDGT-IIa' (Chapter 6). This threshold behavior of the microbial community in Lake Chala appears quite drastic considering that climatic conditions are relatively similar between years. The minor inter-annual variation in rainfall, wind speed and temperature over the course of sediment-trap sampling indicates that small physical and/or chemical disturbances of the water column can obviously trigger large changes in the microbial community. It has been proposed that changes in the metabolism of oligotrophic lakes seem to be subtle and sensitive to short-term changes in physical parameters, such as precipitation, wind and thermal stratification (e.g. Richardson et al., 2017). Indeed, our biomarker records from Lake Chala confirm this large and dynamic variability in primary productivity, as well as bacterial and archaeal activity with depth (van Bree et al., 2018b, Chapter 6 and 7) and over time.

8.3.6 Implications for modern system monitoring and the sedimentary record

The observed threshold behavior of microbial populations in modern-day Lake Chala indicates that subtle environmental variability can have a large impact on aquatic microbial biomarkers, and thus on those stored in the sedimentary record. This sensitivity to subtle changes is a treasure trove for

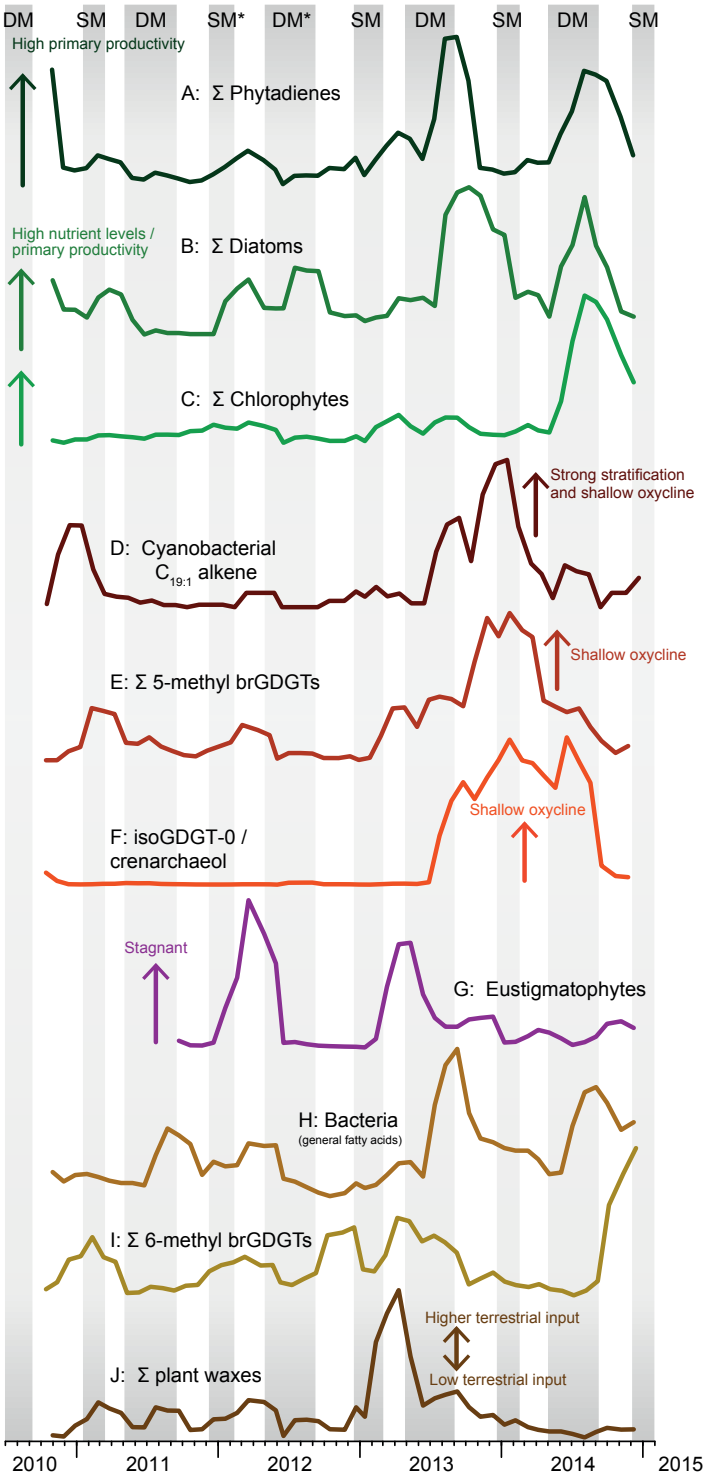

Figure 8.10 The 3-month running average of biomarker fluxes indicating periods of high primary productivity (A-C), stratification and shallow oxycline (D-F), stagnant water conditions (G), bacterial activity (H-I) and vegetation input (J) between August 2010 and January 2015, each normalized to the highest flux measured for the given biomarker (absolute monthly fluxes are plotted in Figs. 8.2 to 8.8). Primary productivity is represented by A: sum phytadienes for total productivity, B: loliolide and isoloriolide represent diatoms productivity and C: Sum of $C_{23:1}$, $C_{25:1}$ and $C_{27:1}$ *n*-alk-1-enes, C_{21} and C_{23} *n*-alkanes, and C_{28} fatty acid are Chlorophyte biomarkers. Periods of stratification and shallow oxycline is indicated by D: Cyanobacterial $C_{19:1}$ *n*-alkene, E: 5-methyl brGDGTs (Chapter 6), F: isoGDGT-0/crenarchaeol (Chapter 7). G: Stagnant water conditions are indicated by Eustigmatophyte C_{30} and C_{32} 1,15 *n*-alkyl diols (Lattaud et al., unpublished data). Two different bacterial groups are represented in H: summed *ai*-C_{15}, *i*-C_{15}, *i*-C_{16}, *i*-C_{17}, C_{20} and C_{22} fatty acids, and I: 6-methyl brGDGTs (Chapter 6). J: summed C_{29}-C_{35} *n*-alkanes are a measure of input of terrestrial material.

sedimentary proxy applications and paleoclimate reconstructions, as it allows to reconstruct past environmental parameters, including monsoon intensity, temperature, primary productivity and nutrient availability. It is clear, however, that 53 months of sediment trap data, or 17 months of SPM depth profiles, is not nearly long enough to capture the full range of inter-annual variability of the lake's microbial community, and to identify the (climatic) drivers of threshold systems such as Lake Chala. This supports the earlier suggestions (Buckles et al., 2016; Chapter 6 and 7) that monitoring programs of modern lake systems need to be carried out over long time scales (>5 years) to fully unravel the dynamics of the system.

8.4 Conclusion

Large seasonal and inter-annual variations in aquatic biomarker fluxes in Lake Chala are observed for a large variety of microbiota such as diatoms, chlorophytes, eustigmatophytes, bacteria and archaea. Based on the sediment-trap data obtained, the occurrence of certain biomarkers can be linked to seasonally and inter-annually recurring periods of mixing and stratification of the water column, although large variations exist between consecutive years. Notably, seemingly similar open-water conditions can trigger different microbial communities to flourish. At this stage it is not certain what drives this threshold behavior and how this impacts the microbial community over longer time periods.

Data availability

All data presented in this study will be made available upon publication in a scientific journal.

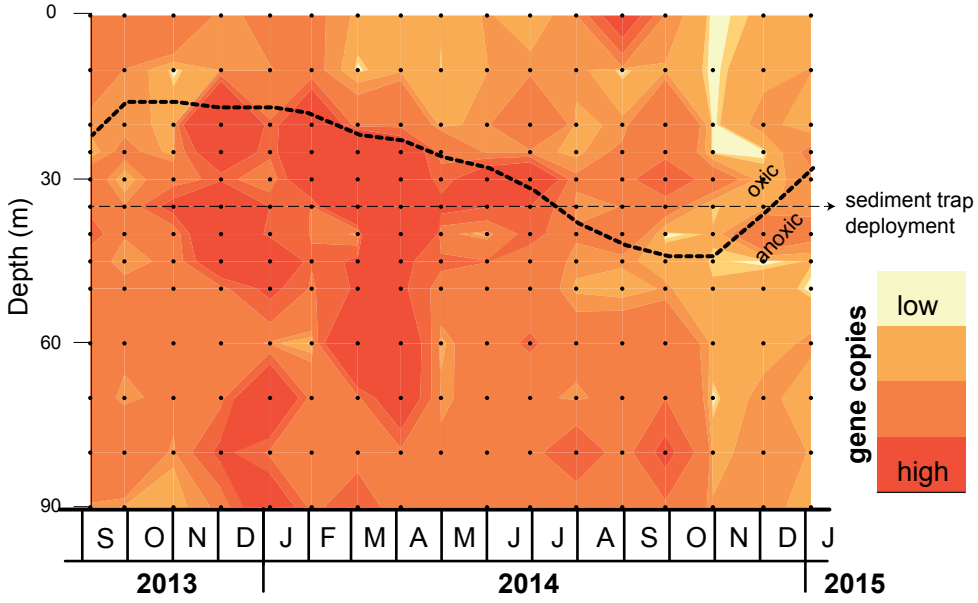

Figure S8.1 Interpolated concentrations (in gene copies L^{-1}) of Melainabacterial 16S rRNA in SPM from between 0 and 90 m water depth in Lake Chala, at approximately monthly intervals between September 2013 and January 2015. The varying position of the oxic-anoxic boundary is indicated (thick black stippled line; depth to anoxia; from Chapter 6), as well as the grid of SPM samples analyzed for archaeal 16S rRNA gene diversity in this study (black dots).

Acknowledgements

We thank C.M. Oluseno for conducting extensive monthly sampling and field assistance in Kenya. Sample collection was carried out with permission of the Permanent Secretary of the Ministry of Education, Science and Technology of Kenya, research permit 13/001/11C to D.V. We thank A.M.D. Negash and P. de Regt for lipid extractions. We are grateful to A. van Dijk, D. Kasjaniuk, A. van Leeuwen-Tolboom and K. Nierop at Utrecht University for technical and analytical support. This research was supported by the NESSC Gravitation Grant (024.002.001) from the Dutch Ministry of Education, Culture and Science (OCW) to J.S.S.D. Phytoplankton investigation was done in the frame of the Brain-be project BR/121/A2 PAMEXEA (Patterns and mechanisms of climate extremes in East Africa) financed by the Belgium Science Policy (BELSPO).

A lilac-breasted roller in Masai Mara National Reserve.

References

Abell GC (1985) Empirical chemical pseudopotential theory of molecular and metallic bonding. Phys. Rev. B 31, 6184–6196.

Afi L, Metzger P, Largeau C, Connan J, Berkaloff C and Rousseau B (1996) Bacterial degradation of green microalgae: incubation of *Chlorella emersonii* and *Chlorella vulgaris* with *Pseudomonas oleovorans* and *Flavobacterium aquatile*. Org. Geochem. 25, 117-130.

Albrecht P and Ourisson G (1969) Triterpene alcohol isolation from oil shale. Science 163, 1192-1193.

Altschul SF, Gish W, Miller W, Myers EW and Lipman DJ (1990) Basic local alignment search tool. J. Mol. Biol. 215, 403–410.

Andrews S (2010) A quality control tool for high throughput sequence data. http://www.bioinformatics.babraham.ac.uk/projects/fastqc/.

Arpino P, Albrecht P, and Ourisson G (1971) Studies on the organic constituents of lacustrine Eocene sediments. Possible mechanisms for the formation of some geolipids related to biologically occurring terpenoids, In: von Gaertner HR and Wehner H (Eds.), Advances in Organic Geochemistry, Pergamon Press, Oxford, pp. 173-187.

Baas WJ (1985) Naturally occurring seco-ring-A-triterpenoids and their possible biological significance. Phytochemistry 24, 1875-1889.

Bade DL and Cole JJ (2006) Impact of chemically enhanced diffusion on dissolved inorganic carbon stable isotopes in a fertilized lake. J. Geophys. Res. 111, C01014.

Bade DL, Carpenter SR, Cole JJ, Hanson PC and Hesslein RH (2004) Controls of δ^{13}C-DIC in lakes: Geochemistry, lake metabolism, and morphometry. Limnol. Oceanogr. 49, 1160-1172.

Banta AB, Wei JH, Gill CCC, Giner J-L and Welander PV (2017) Synthesis of arborane triterpenols by a bacterial oxidosqualene cyclase. PNAS 114, 245-250.

Barker PA, Leng MJ, Gasse G and Huang Y (2007) Century-to-millennial scale climatic variability in Lake Malawi revealed by isotope records. Earth Planet. Sci. Lett. 261, 93-103.

Barker PA, Hurrell ER, Leng MJ, Wolff C, Cocquyt C, Sloane HJ and Verschuren D (2011) Seasonality in equatorial climate over the past 25 k.y. revealed by oxygen isotope records from Mount Kilimanjaro. Geology 39, 1111-1114.

Barker PA, Hurrell ER, Leng MJ, Plessen B, Wolff C, Conley DJ, Keppens E, Milne I, Cumming BF, Laird KR and Kendrick CP (2013) Carbon cycling within an East African lake revealed by the carbon isotope composition of diatom silica: a 25-ka record from Lake Challa, Mt. Kilimanjaro. Quat. Sci. Rev. 66, 55-63.

Bechtel A and Püttmann W (1992) Combined isotopic and biomarker investigations of temperature-and facies-dependent variations in the Kupferschiefer of the Lower Rhine Basin, northwestern Germany. Chem. Geol. 102, 23-40.

Bechtel A, Smittenberg RH, Bernasconi SM and Schubert CJ (2010) Distribution of branched and isoprenoid tetraether lipids in an oligotrophic and a eutrophic Swiss lake: insights into sources and GDGT-based proxies. Org. Geochem. 41, 822-832.

Becke AD (1988) Density-functional exchange-energy approximation with correct asymptotic behavior. Phys. Rev. A 38, 3098.

Berke MA (2018) Reconstructing terrestrial paleoenvironments using sedimentary organic biomarkers. In: Methods in Paleoecology, Springer Cham., 121-149.

Berke MA, Johnson TC, Werne JP, Grice K, Schouten S and Sinninghe Damsté JS (2012a) Molecular records of climate variability and vegetation response since the Late Pleistocene in the Lake Victoria basin, East Africa. Quat. Sci. Rev. 55, 59-74.

Berke MA, Johnson TC, Werne JP, Schouten S and Sinninghe Damsté JS (2012b) A mid-Holocene thermal maximum at the end of the African Humid Period. Earth Planet. Sci. Lett. 351-352, 95-104.

Besseling MA, Hopmans EC, Boschman RC, Sinninghe Damsté JS and Villanueva L (2018) Benthic archaea as potential sources of tetraether membrane lipids in sediments across an oxygen minimum zone. Biogeosciences 15, 4047-4064.

Blaauw M, van Geel B, Kristen I, Plessen B, Lyaruu A, Engstrom DR, van der Plicht J and Verschuren D (2011) High-resolution ^{14}C dating of a 25,000-year lake-sediment record from equatorial East Africa. Quat. Sci. Rev. 30, 3043-3059.

Black E, Slingo J and Sperber KR (2003) An observational study of the relationship between excessively strong short rains in coastal East Africa and Indian Ocean SST. Mon. Weather Rev. 131, 74-94.

Blaga CI, Reichart G-J, Vissers EW, Lotter AF, Anselmetti FS and Sinninghe Damsté JS (2011) Seasonal changes in glycerol dialkyl glycerol tetraether concentrations and fluxes in a perialpine lake: implications for the use of the TEX_{86} and BIT proxies. Geochim. Cosmochim. Acta 75, 6416–6428.

Blaga CI, Reichart G-J, Heiri O and Sinninghe Damsté JS (2009) Tetraether membrane lipid distributions in lake particulate matter and sediments: a study of 47 European lakes along a North–South transect. J. Paleolimnol. 41, 523–540.

Blokker P, Schouten S, van den Ende H, de Leeuw JW, Hatcher PG and Sinninghe Damsté JS (1998) Chemical structure of algaenans from the fresh water algae *Tetraedron minimum*, *Scenedesmus communis* and *Pediastrum boryanum*. Org. Geochem. 29, 1453-1468.

Blomquist GJ and Jackson LL (1979) Chemistry and biochemistry of insect waxes. Prog. Lipid Res. 17, 319-345.

Bodé S, De Wispelaere L, Hemp A, Verschuren D and Boeckx P (submitted) Implications of isotope ecohydrology on Mt. Kilimanjaro for paleohydrological studies.

Bontes BM, Pel R, Ibelings BW, Boschker HTS, Middelburg JJ and van Donk E (2006) The effects of biomanipulation on the biogeochemistry, carbon isotopic composition and pelagic food web relations of a shallow lake. Biogeosciences 3, 69-83.

Boon JJ, Rijpstra WIC, de Lange F, de Leeuw JW, Yoshioka M and Shimizu Y (1979) Black Sea sterol - a molecular fossil for dinoflagellate blooms. Nature 277, 125-127.

Boreham CJ, Summons RE, Roksandic Z, Dowling LM, Hutton AC (1994) Chemical, molecular and isotopic differentiation of organic facies in the Tertiary lacustrine Duaringa oil shale deposit, Queensland, Australia. Org. Geochem. 21, 685-712.

Borrego AG, Blanco CG and Püttmann W (1997) Geochemical significance of the aromatic hydrocarbon distribution in the bitumens of the Puertollano oil shales, Spain. Org. Geochem. 26, 219-228.

Borrel G, Adam PS and Gribald S (2016) Methanogenesis and the Wood–Ljungdahl pathway: an ancient, versatile, and fragile association. Genome Biol. Evol. 8, 1706-1711.

Boschker HTS and Middelburg JJ (2002) Stable isotopes and biomarkers in microbial ecology. FEMS Microbiol. Ecol. 40, 85-95.

Bossard N, Jacob J, Le Milbeau C, Sauze J, Terwilliger V, Poissonnier B and Vergès E (2013) Distribution of miliacin (olean-18-en-3β-ol methyl ether) and related compounds in broomcorn millet (*Panicum miliaceum*) and other reputed sources: Implications for the use of sedimentary miliacin as a tracer of millet. Org. Geochem. 63, 48-55.

Bottari F, Marsili A, Morelli I and Pacchiani M (1972) Aliphatic and triterpenoid hydrocarbons from ferns. Phytochemistry 11, 2519-2523.

Boudou JP, Trichet J, Robinson N and Brassell SC (1986a) Lipid composition of a recent Polynesian microbial mat sequence. Org. Geochem. 10, 705-709.

Boudou JP, Trichet J, Robinson N and Brassell SC (1986b) Profile of aliphatic hydrocarbons in a recent Polynesian microbial mat. Int. J. Environ. Anal. Chem. 26, 137-155.

Brenner DW (1990) Empirical potential for hydrocarbons for use in simulating the chemical vapor deposition of diamond films. Phys. Rev. B 42, 9458–9471.

Buckles LK, Verschuren D, Weijers JWH, Cocquyt C, Blaauw M and Sinninghe Damsté JS (2016) Interannual and (multi-) decadal variability in the sedimentary BIT index of Lake Challa, East Africa, over the past 2200 years: assessment of the precipitation proxy. Clim. Past. 12, 1243-1262.

Buckles LK, Weijers JWH, Verschuren D and Sinninghe Damsté JS (2014) Sources of core and intact branched tetraether membrane lipids in the lacustrine environment: anatomy of Lake Challa and its catchment, equatorial East Africa. Geochim. Cosmochim. Acta 140, 106-126.

Buckles LK, Villanueva L, Weijers JWH, Verschuren D and Sinninghe Damsté JS (2013) Linking isoprenoidal GDGT membrane lipid distributions with gene abundances of ammonia-oxidizing Thaumarchaeota and uncultured crenarchaeotal groups in the water column of a tropical lake (Lake Challa, East Africa). Environ. Microbiol. 15, 2445–2462.

Caporaso JG, Kuczynski J, Stombaugh J, Bittinger K, Bushman FD, Costello EK, Fierer N, Pena AG, Goodrich JK, Gordon JI, Huttley GA, Kelley ST, Knights D, Koenig JE, Ley RE, Lozupone CA, McDonald D, Muegge BD, Pirrung M, Reeder J, Sevinsky JR, Turnbaugh PJ, Walters WA, Widmann J, Yatsunenko T, Zaneveld J and Knight R (2010) QIIME allows analysis of high-throughput community sequencing data. Nature Methods 7, 335–336.

Caporaso JG, Lauber CL, Walters WA, Berg-Lyons D, Huntley J, Fierer N, Owens SM, Betley J, Fraser L, Bauer M and Gormley N (2012) Ultra-high-throughput microbial community analysis on the Illumina HiSeq and MiSeq platforms. ISME J. 6, 1621.

Cardoso JN, Gaskell SJ, Quirk MM and Eglinton G (1983) Hydrocarbon and fatty acid distributions in Rostherne lake sediment (England). Chem. Geol. 38, 107-128.

Castañeda IS and Schouten S (2011) A review of molecular organic proxies for examining modern and ancient lacustrine environments. Quat. Sci. Rev. 30, 2851-2891.

Castañeda IS, Werne JP and Johnson TC (2007) Wet and arid phases in the southeast African tropics since the Last Glacial Maximum. Geology 35, 823-826.

Castañeda IS, Mulitza S, Schefuß E, Lopes dos Santos RA, Sinninghe Damsté JS and Schouten S (2009a) Wet phases in the Sahara/Sahel region and human migration patterns in North Africa. PNAS 106, 20159–20163.

Castañeda IS, Werne JP and Johnson TC (2009b) Influence of climate change on algal community structure and primary productivity of Lake Malawi (East Africa) from the Last Glacial Maximum to present. Limnol. Oceanogr. 54, 2431-2447.

Castañeda IS, Werne JP, Johnson TC and Powers LA (2011) Organic geochemical records from Lake Malawi (East Africa) of the last 700 years, part II: Biomarker evidence for recent changes in primary productivity. Palaeogeogr. Palaeoclimatol. Palaeoecol. 303, 140-154.

Cheng H, Spötl C, Breitenbach SF, Sinha A, Wassenburg JA, Jochum KP, Scholz D, Li X, Yi L, Peng Y, Lv Y, Zhang P, Votintseva A, Loginov V, Ning Y, Kathayat G and Edwards RL (2016) Climate variations of Central Asia on orbital to millennial timescales. Sci. Rep. 6, 36975.

Chenoweth K, van Duin ACT, Dasgupta S and Goddard WA (2009) Initiation Mechanisms and Kinetics of Pyrolysis and Combustion of JP-10 Hydrocarbon Jet Fuel. J. Phys. Chem. A 113, 1740–1746.

Chenoweth K, van Duin ACT and Goddard WA (2008) ReaxFF Reactive Force Field for Molecular Dynamics Simulations of Hydrocarbon Oxidation. J. Phys. Chem. A 112, 1040–1053.

Chikaraishi Y, Kaneko M and Ohkouchi N (2012) Stable hydrogen and carbon isotopic compositions of long-chain (C_{21}-C_{33}) *n*-alkanes and *n*-alkenes in insects. Geochim. Cosmochim. Acta 95, 53-62.

Coates RC, Podell S, Korobeynikov A, Lapidus A, Pevzner P, Sherman DH, Allen EE, Gerwick L and Gerwick WH (2014) Characterization of cyanobacterial hydrocarbon composition and distribution of biosynthetic pathways. PloS one 9, e85140.

Cocquyt C and Ryken E (2016) *Afrocymbella barkeri* spec. nov. (Bacillariophyta), a common phytoplankton component of Lake Challa, a deep crater lake in East Africa. Eur. J. Phycol. 51, 217-225.

Cocquyt C and Ryken E (2017) Two new needle-shaped Nitzschia taxa from a deep East African crater lake. Diatom Res. 32, 465-475.

Colcord DE, Cadieux SB, Brassell SC, Castañeda IS, Pratt LM and White JR (2015) Assessment of branched GDGTs as temperature proxies in sedimentary records from several small lakes in southwestern Greenland. Org. Geochem. 82, 33–41.

Colcord DE, Pearson A and Brassell SC (2017) Carbon isotopic composition of intact branched GDGT core lipids in Greenland lake sediments and soils. Org. Geochem. 110, 25-32.

Collister JW, Rieley G, Stern B, Eglinton G and Fry B (1994) Compound-specific $\delta^{13}C$ analyses of leaf lipids from plants with differing carbon dioxide metabolisms. Org. Geochem. 21, 619–627.

Corbet B (1980) Origine et transformation des triterpènes dans les sédiments récents. Ph.D. thesis, Université Louis Pasteur, Strasbourg, France, 106 p.

Costa K, Russell JM, Konecky B and Lamb H (2014) Isotopic reconstruction of the African Humid Period and Congo air boundary migration at Lake Tana, Ethiopia. Quat. Sci. Rev., 83, 58-67.

Cranwell PA, Eglinton G and Robinson N (1987) Lipids of aquatic organisms as potential contributors to lacustrine sediments II. Org. Geochem. 11, 513-527.

Cranwell PA, Jaworski GHM and Bickley HM (1990) Hydrocarbons, sterols, esters and fatty acids in six freshwater chlorophytes. Phytochemistry 29, 145-151.

Damon PE and Jirikowic JL (1992) The sun as a low-frequency harmonic oscillator. Radiocarbon 34, 199-205.

D'Anjou RM, Wei JH, Castañeda IS, Brigham-Grette J, Petsch ST and Finkelstein DB (2013) High-latitude environmental change during MIS 9 and 11: biogeochemical evidence from Lake El'gygytgyn, Far East Russia. Clim. Past 9, 567-581.

de Garidel-Thoron T, Beaufort L, Linsley BK and Dannenmann S (2001) Millenial-scale dynamics of the East Asian winter monsoon during the last 200,000 years. Paleoceanography 16, 491-502.

De Jonge C, Hopmans EC, Stadnitskaia A, Rijpstra WIC, Hofland R, Tegelaar EW and Sinninghe Damsté JS (2013) Identification of novel penta- and hexamethylated branched glycerol dialkyl glycerol tetraethers in peat using HPLC–MS, GC–MS, and GC–SMB-MS. Org. Geochem. 54, 78–82.

De Jonge C, Hopmans EC, Zell CI, Kim J-H, Schouten S and Sinninghe Damsté JS (2014a) Occurrence and abundance of 6-methyl branched glycerol dialkyl glycerol tetraethers in soils: implications for paleoclimate reconstruction. Geochim. Cosmochim. Acta 141, 97–112.

De Jonge C, Stadnitskaia A, Hopmans EC, Cherkashov G., Fedotov A and Sinninghe Damsté JS (2014b) *In situ* produced branched glycerol dialkyl glycerol tetraethers in suspended particulate matter from the Yenisei River, Eastern Sibera. Geochim. Cosmochim. Acta 125, 476–491.

de Leeuw JW, Cox HC, van Graas G, van de Meer FW, Peakman TM, Baas JMA and van de Graaf B (1989) Limited double bond isomerisation and selective hydrogenation of sterenes during early diagenesis. Geochim. Cosmochim. Acta 53, 903-909.

de Mesmay R, Grossi V, Williamson D, Kajula S and Derenne S. (2007) Novel mono-, di- and tri-unsaturated very long chain (C_{37}-C_{43}) *n*-alkenes in alkenone-free lacustrine sediments (Lake Masoko, Tanzania). Org. Geochem. 38, 323-333.

De Rosa M and Gambacorta A (1988) The lipids of archaebacteria. Prog. Lip. Res. 27, 153-175.

Descy J-P, Plisnier P-D, Leporcq B, Sténuite S, Pirlot S, Stimart J, Gosselain V, André L, Alleman L, Langlet D, Vyverman W, Cocquyt C, De Wever A, Stoyneva MP, Deleersnijder E, Naithani J, Chitamwebwa D, Chande A, Kimirei I, Sekadende B, Mwaitega S, Muhoza S, Sinyenza D, Makasa L, Lukwessa C, Zulu I and Phiri H (2006) Climate variability as recorded in Lake Tanganyika (CLIMLAKE). Final report EV/02. Scientific Support Plan for a Sustainable Development Policy (SPSD II). Belgian Science Policy, Brussels.

Diefendorf AF and Freimuth EJ (2017) Extracting the most from terrestrial plant-derived *n*-alkyl lipids and their carbon isotopes from the sedimentary record: A review. Org. Geochem. 103, 1-21.

Diefendorf AF, Mueller KE, Wing SL, Koch PL and Freeman KH (2010) Global patterns in leaf ^{13}C discrimination and implications for studies of past and future climate. PNAS 103, 5738-5743.

Diefendorf AF, Freeman KH, Wing SL and Graham HV (2011) Production of *n*-alkyl lipids in living plants and implications for the geological past. Geochim. Cosmochim. Acta 75, 7472-7485.

Diefendorf AF, Freeman KH and Wing SL (2012) Distribution and carbon isotope patterns of diterpenoids and triterpenoids in modern temperate C_3 trees and their geochemical significance. Geochim. Cosmochim. Acta 85, 342-356.

Ding J, Zhang L, Zhang Y, Han K-L (2013) A Reactive Molecular Dynamics Study of *n*-Heptane Pyrolysis at High Temperature. J. Phys. Chem. A 117, 3266–3278.

Duan Y and Ma L (2001) Lipid geochemistry in a sediment core from Ruoergai Marsh deposit (Eastern Qinghai-Tibet plateau, China). Org. Geochem. 32, 1429-1442.

Eggermont H and Verschuren D (2004) Sub-fossil Chironomidae from East Africa. 1. Tanypodinae and Orthocladiinae. J. Paleolimnol. 32, 383-412.

Eggermont H, De Deyne P and Verschuren D (2007) Spatial variability of chironomid death assemblages in the surface sediments of a fluctuating tropical lake (Lake Naivasha, Kenya). J. Paleolimnol. 38, 309-328.

Eglinton G and Hamilton RJ (1967) Leaf epicuticular waxes. Science 156, 1322-1335.

Eglinton TI and Eglinton G (2008) Molecular proxies for paleoclimatology. Earth Planet. Sci. Lett. 275, 1-16.

Elling FJ, Könneke M, Nicol GW, Stieglmeier M, Bayer B, Spieck E, de la Torre JR, Becker KW, Thomm M, Prosser JI and Herndl GJ (2017) Chemotaxonomic characterisation of the thaumarchaeal lipidome. Environ. Microbiol. 19, 2681-2700.

Evans PN, Parks DH, Chadwick GL, Robbins SJ, Orphan VJ, Golding SD and Tyson GW (2015) Methane metabolism in the archaeal phylum Bathyarchaeota revealed by genome-centric metagenomics. Science 350, 434-438.

Fan F, Huang S, Yang H, Raju M, Datta D, Shenoy VB, van Duin ACT, Zhang S and Zhu T (2013) Mechanical properties of amorphous LixSi alloys: a reactive force field study. Model. Simul. Mater. Sci. Eng. 21, 74002.

Feakins SJ and Eglinton TI (2005) Biomarker records of late Neogene changes in northeast African vegetation. Geology 33, 977-980.

Feakins SJ, Levin NE, Liddy HM, Sieracki A, Eglinton TI and Bonnefille R (2013) Northeast African vegetation change over 12 my. Geology 41, 295-298.

Feakins SJ, Eglinton TI and deMenocal PB (2007) A comparison of biomarker records of northeast African vegetation from lacustrine and marine sediments (ca. 3.40 Ma). Org. Geochem. 38, 1607-1624.

Ficken KJ, Li B, Swain DL and Eglinton G (2000) An *n*-alkane proxy for the sedimentary input of submerged/floating freshwater aquatic macrophytes. Org. Geochem. 31, 745-749.

Fischer WW and Pearson A (2007) Hypotheses for the origin and early evolution of triterpenoid cyclases. Geobiology 5, 19–34.

Fleitmann D, Burns SJ, Mangini A, Mudelsee M, Kramers J, Villa I, Neff U, Al-Subary AA, Buettner A, Hippler D and Matter A (2007) Holocene ITCZ and Indian monsoon dynamics recorded in stalagmites from Oman and Yemen (Socotra). Quat. Sci. Rev. 26, 170-188.

Francis GW (1981) Alkylthiolation for the determination of double-bond position in unsaturated fatty acid esters. Chem. Phys. Lipids. 29, 369-374.

Freeman KH and Pancost RD (2014) Biomarkers for terrestrial plants and climate. Falkowski P and Freeman K, Treatise on Geochemistry, Elsevier, Amsterdam, 12, 395-416.

Freeman KH, Boreham CJ, Summons RE and Hayes JM (1994) The effect of aromatization on the isotopic compositions of hydrocarbons during early diagenesis. Org. Geochem. 21, 1037-1049.

Garcin Y, Schefuß E, Schwab VF, Garreta V, Gleixner G, Vincens A, Todou G, Séné O, Onana JM, Achoundong G and Sachse D (2014) Reconstructing C_3 and C_4 vegetation cover using *n*-alkane carbon isotope ratios in recent lake sediments from Cameroon, Western Central Africa. Geochim. Cosmochim. Acta 142, 482-500.

Gasse F, Charlié F, Vincens A, Williams MAJ and Williamson D (2008) Climatic patterns in equatorial and southern Africa from 30,000 to 10,000 years ago reconstructed from terrestrial and near-shore proxy data. Quat. Sci. Rev. 27, 2316-2340.

Gelin F, Boogers I, Noordeloos AM, Sinninghe Damsté JS, Riegman R and de Leeuw JW (1997) Resistant biomacromolecules in marine microalgae of the classes Eustigmatophyceae and Chlorophyceae: Geochemical implications. Org. Geochem. 26, 659-675.

Gelpi E, Oró J, Schneider HJ and Bennett EO (1968) Olefins of high molecular weight in two microscopic algae. Science 161, 700-702.

Gelpi E, Schneider HJ, Mann J and Oró J (1970) Hydrocarbons of geochemical significance in microscopic algae. Phytochemistry 9, 603-612.

Giger W, Schaffner C and Wakeham SG (1980) Aliphatic and olefinic hydrocarbons in recent sediments of Greifensee, Switzerland. Geochim. Cosmochim. Acta 44, 119-129.

Golkaram M and van Duin ACT (2015) Revealing graphene oxide toxicity mechanisms: A reactive molecular dynamics study. Materials Discovery 1, 54–62.

González AG, Bermejo J, Rodríguez Pérez EM and Hernández Padró CE (1991) Chemical constituents of the lichen *Cladina macaronesica*. Z. Naturforsch. 46, 12-18.

Grossi V, Baas M, Schogt N, Klein Breteler WCM, de Leeuw JW and Rontani J-F (1996) Formation of phytadienes in the water column: myth or reality? Org. Geochem. 24, 833-839.

Gupta AK, Anderson DM and Overpeck JT (2003) Abrupt changes in the Asian southwest monsoon during the Holocene and their links to the North Atlantic Ocean. Nature 421, 354-357.

Hammer Ø, Harper DAT and Ryan PD (2001) PAST: Paleontological statistics software package for education and data analysis. Palaeontol. Electron. 4.

Hanisch S, Ariztegui D and Püttmann W (2003) The biomarker record of Lake Albano, central Italy - implications for Holocene aquatic system response to environmental change. Org. Geochem. 34, 1223-1235.

Harvey HR and Mcmanus GB (1991) Marine ciliates as a widespread source of tetrahymanol and hopan-3β-ol in sediments. Geochim. Cosmochim. Acta 55, 3387-3390.

Hauke V, Graff R, Wehrung P, Trendel JM and Albrecht P (1992a) Novel triterpene-derived hydrocarbons of arborane/fernane series in sediments. Part I. Tetrahedron 48, 3915-3924.

Hauke V, Graff R, Wehrung P, Trendel JM and Albrecht P, Riva A, Hopfgartner G, Gülaçar FO, Buchs A and Eakin PA (1992b) Novel triterpene-derived hydrocarbons of arborane/fernane series in sediments. Part II. Geochim. Cosmochim. Acta 56, 3595-3602.

Hauke V, Adam P, Trendel JM, Albrecht P, Schwark L, Vliex M, Hagemann H, Püttmann W (1995) Isoarborinol through geological times: evidence for its presence in the Permian and Triassic. Org. Geochem. 23, 91-93.

Hausmann S, Pienitz R, St-Onge G, Larocque I and Richard PJH (2006) Lake circulation influenced by solar activity? Geol. Soc. Am. Abst. with Programs 38, 264.

Heiri O and Lotter AF (2005) Holocene and Lateglacial summer temperature reconstruction in the Swiss Alps based on fossil assemblages of aquatic organisms: a review. Boreas 34, 506-516.

Hemingway JD, Schefuß E, Dinga BJ, Pryer H and Galy VV (2016) Multiple plant-wax compounds record differential sources and ecosystem structure in large river catchments. Geochim. Cosmochim. Acta 184, 20-40.

Hemmers H, Gülz PG, Marner FJ and Wray V (1989) Pentacyclic triterpenoids in epicuticular waxes from *Euphorbia lathyris* L., Euphorbiaceae. Z. Naturforsch. C 44, 193-201.

Hemp A. (2006) Continuum or zonation? Altitudinal gradients in the forest vegetation of Mt. Kilimanjaro. Plant Ecol. 184, 27-42.

Herczeg AL and Fairbanks RG (1987) Anomalous carbon isotope fractionation between atmospheric CO_2 and dissolved inorganic carbon induced by intense photosynthesis. Geochim. Cosmochim. Acta 51, 895-899.

Hobbie EA and Werner RA (2004) Intramolecular, compound-specific, and bulk carbon isotope patterns in C_3 and C_4 plants: a review and synthesis. New Phytol. 161, 371–385.

Holland AR, Petsch ST, Castañeda IS, Wilkie KM, Burns SJ and Brigham-Grette J (2013) A biomarker record of Lake El'gygytgyn, far east Russian Arctic: investigating sources of organic matter and carbon cycling during marine isotope stages 1-3. Clim. Past Discuss. 9, 243-260.

Hopmans EC, Schouten S and Sinninghe Damsté JS (2016) The effect of improved chromatography on GDGT-based palaeoproxies. Org. Geochem. 93, 1-6.

Hopmans EC, Weijers JWH, Schefuß E, Herfort L, Sinninghe Damsté JS and Schouten S (2004) A novel proxy for terrestrial organic matter in sediments based on branched and isoprenoid tetraether lipids. Earth Planet. Sci. Lett. 224, 107-116.

Howard DL, Simoneit BRT and Chapman DJ (1984) Triterpenoids from lipids of *Rhodomicrobium vanniellii*. Arch. Microbiol. 137, 200-204.

Huang Y, Lockheart MJ, Collister JW and Eglinton G (1995) Molecular and isotopic biogeochemistry of the Miocene Clarkia Formation: hydrocarbons and alcohols. Org. Geochem. 23, 785-801.

Huang Y, Street-Perrott FA, Perrott RA, Metzger P and Eglinton G (1999) Glacial–interglacial environmental changes inferred from molecular and compound-specific $\delta^{13}C$ analyses of sediments from Sacred Lake, Mt. Kenya. Geochim. Cosmochim. Acta 63, 1383-1404.

Huang X, Xie S, Zhang CL, Jiao D, Huang J, Yu J, Jin F and Gu Y (2008) Distribution of aliphatic *des*-A-triterpenoids in the Dajiuhu peat deposit, southern China. Org. Geochem. 39, 1765-1771.

Hui WH and Lam CN (1965) An examination of the Rubiaceae of Hong Kong – II. Phytochemistry 4, 333-335.

IPCC (2013) Climate Change 2013: The Physical Science Basis. Contribution of Working Group I to the Fifth Assessment Report of the Intergovernmental Panel on Climate Change. [Stocker TF, Qin D, Plattner GK, Tignor M, Allen SK, Boschung J, Nauels A, Xia Y, Bex V and Midgley PM (eds)]. Cambridge University Press, Cambridge, United Kingdom and New York, NY, USA. 1535 pp.

Islam MM, Bryantsev VS, van Duin ACT (2014) ReaxFF Reactive Force Field Simulations on the Influence of Teflon on Electrolyte Decomposition during Li/SWCNT Anode Discharge in Lithium-Sulfur Batteries. J. Electrochem. Soc. 161, E3009–E3014.

Jacob J, Disnar JR, Boussafir M, Albuquerque ALS, Sifeddine A and Turcq B (2005) Pentacyclic triterpene methyl ethers in recent lacustrine sediments (Lagoa do Caçó, Brazil). Org. Geochem. 36, 449-461.

Jacob J, Disnar JR, Boussafir M, Albuquerque ALS, Sifeddine A and Turcq B (2007) Contrasted distributions of triterpene derivatives in the sediments of Lake Caçó reflect paleoenvironmental changes during the last 20,000 yrs in NE Brazil. Org. Geochem. 38, 180-197.

Jaffé R and Hausmann KB (1995) Origin and early diagenesis of arborinone/isoarborinol in sediments of a highly productive freshwater lake. Org. Geochem. 22, 231-235.

Jaffé R, Cabrera A, Najje N and Carvajal-Chitty H (1996) Organic biogeochemistry of a hypereutrophic tropical, freshwater lake - Part 1: particle associated and dissolved lipids. Org. Geochem. 25, 227-240.

Jaguar, version 7.5, Schrödinger, LLC: New York, 2008.

Jeffrey SW and Vesk M (1997) Introduction to marine phytoplankton and their pigment signatures. In: Phytoplankton Pigments in Oceanography: Guidelines to Modern Methods. UNESCO, Paris, pp. 37-84.

Kaneda T (1991) Iso- and anteiso-fatty acids in bacteria: biosynthesis, function, and taxonomic significance. Microbiol. Rev. 55, 288-302.

Kim JG, Jung MY, Park SJ, Rijpstra WIC, Sinninghe Damsté JS, Madsen EL, Min D, Kim JS, Kim GJ and Rhee SK (2012) Cultivation of a highly enriched ammonia-oxidizing archaeon of thaumarchaeotal group I.1b from an agricultural soil. Environ. Microbiol. 14, 1528-1543

Kimble BJ, Maxwell JR, Philp RP, Eglinton G, Albrecht P, Ensminger A, Arpino P and Ourisson G (1974) Tri-and tetraterpenoid hydrocarbons in the Messel oil shale. Geochim. Cosmochim. Acta 38, 1165-1181.

Klok J, Baas M, Cox HC, de Leeuw JW and Schenck PA (1984) Loliolides and dihydroactinidiolide in a recent marine sediment probably indicate a major transformation pathway of carotenoids. Tetrahedron Lett. 25, 5577-5580.

Kohn MJ (2016) Carbon isotope discrimination in C_3 land plants is independent of natural variations in pCO_2. Geochem. Perspect. Lett. 2, 35-43.

Kolattukudy P (1976) Chemistry and Biochemistry of Natural Waxes, Amsterdam: Elsevier, 459 pp.

Kubo K, Lloy KG, Biddl JF, Amann R, Teske A, and Knittel K (2012) Archaea of the Miscellaneous Crenarchaeotal Group are abundant, diverse and widespread in marine sediments, ISME J. 6, 1949–1965.

Kusch S, Rethemeyer J, Schefuß E and Mollenhauer G (2010) Controls on the age of vascular plant biomarkers in Black Sea sediments. Geochim. Cosmochim. Acta, 74, 7031-7047.

Lammers JM, Reichart G-J and Middelburg JJ (2017) Seasonal variability in phytoplankton stable carbon isotope ratios and bacterial carbon sources in a shallow Dutch lake. Limnol. Oceanogr. 62, 2773-2787.

Langenheim JH (1994) Higher plant terpenoids: A phytocentric overview of their ecological roles. J. Chem. Ecol. 20, 1223-1280.

Lattaud J, van Bree LGJ, Balzano S, Peterse F, van der Meer MTJ, Villanueva L, Hopmans EC, Sinninghe Damsté JS and Schouten S (unpublished) Sources and seasonality of long-chain diols in a temperate and a tropical lake.

Lavergne C, Hugoni M, Dupuy C and Agogué H (2018) First evidence of the presence and activity of archaeal C_3 group members in an Atlantic intertidal mudflat. Sci. Rep. 8, 11790.

Lavrieux M, Jacob J, LeMilbeau C, Zocatelli R, Masuda K, Bréheret JG and Disnar JR (2011) Occurrence of triterpenyl acetates in soil and their potential as chemotaxonomical markers of Asteraceae. Org. Geochem. 42, 1315-1323.

Lê S, Josse J and Husson F (2008) FactoMineR: An R Package for Multivariate Analysis. J. Stat. Softw. 25, 1-18.

Lee C, Yang W and Parr RG (1988) Development of the Colle-Salvetti correlation-energy formula into a functional of the electron density. Phys. Rev. B 37, 785–789.

Leng MJ and Henderson AC (2013) Recent advances in isotopes as palaeolimnological proxies. J. Paleolimnol. 49, 481-496.

Li J, Pancost RD, Naafs BDA, Huan Y, Cheng Z and Xie S (2016) Distribution of glycerol dialkyl glycerol tetraether (GDGT) lipids in a hypersaline lake system. Org. Geochem. 99, 113–124.

Liang T, Shin YK, Cheng Y-T, Yilmaz DE, Vishnu KG, Verners O, Zou C, Phillpot SR, Sinnott, SB and van Duin ACT (2013) Reactive Potentials for Advanced Atomistic Simulations. Annu. Rev. Mater. Sci. 43, 109–129.

Liu HY, Lin ZS, Qi XZ, Li YX, Yu MT, Yang H and Shen J (2012) Possible link between Holocene East Asian monsoon and solar activity obtained from the EMD method. Nonlinear Proc. Geoph. 19, 421-430.

Liu XL, Lipp JS, Birgel D, Summons RE and Hinrichs KU (2018) Predominance of parallel glycerol arrangement in archaeal tetraethers from marine sediments: Structural features revealed from degradation products. Org. Geochem. 115, 12-23.

Logan GA and Eglinton G (1994) Biogeochemistry of the Miocene lacustrine deposit, at Clarkia, northern Idaho, U.S.A. Org. Geochem. 21, 857-870.

Lohmann F, Trendel JM, Hetru C and Albrecht P (1990) C-29 tritiated β-amyrin: chemical synthesis aiming at the study of aromatization processes in sediments. J. Labelled Compd. Radiopharm. 28, 377-386.

Longo WM, Huang Y, Yao Y, Zhao J, Giblin AE, Wang X, Zech R, Haberzettl T, Jardillier L, Toney J and Liu Z (2018) Widespread occurrence of distinct alkenones from Group I haptophytes in freshwater lakes: Implications for paleotemperature and paleoenvironmental reconstructions. Earth Planet. Sci. Lett. 492, 239-250.

Loomis SE, Russell JM and Sinninghe Damsté JS (2011) Distributions of branched GDGTs in soils and lake sediments from western Uganda: Implications for a lacustrine paleothermometer. Org. Geochem. 42, 739–751.

Loomis SE, Russell JM, Ladd B, Street-Perrott FA and Sinninghe Damsté JS (2012) Calibration and application of the branched GDGT temperature proxy on East African lake sediments. Earth Planet. Sci. Lett. 357-358, 277-288.

Loomis SE, Russell JM, Eggermont H, Verschuren D and Sinninghe Damsté JS (2014a) Effects of temperature, pH, and nutrient concentration on branched GDGT distributions in East African lakes: implications for paleoenvironmental reconstruction. Org. Geochem. 66, 25–37.

Loomis S. E., Russell JM, Heureux A. M., D'Andrea W. J. and Sinninghe Damsté JS (2014b) Seasonal variability of branched glycerol dialkyl glycerol tetraethers (brGDGTs) in a temperate lake system. Geochim. Cosmochim. Acta 144, 173–187.

Macías-Rubalcava ML, Hernández-Bautista BE, Jiménez-Estrada M, Cruz-Ortega R, Anaya AL (2007) Pentacyclic triterpenes with selective bioactivity from *Sebastiania adenophora* leaves, Euphorbiaceae. J. Chem. Ecol. 33, 147-156.

Maier MS, Rosso ML, Fazio AT, Adler MT and Bertoni MD (2009) Fernene triterpenoids from the lichen *Pyxine berteriana*. J. Nat. Prod. 72, 1902-1904.

Matsumoto GI, Akiyama M, Watanuki K and Torii T (1990) Unusual distributions of long-chain *n*-alkanes and *n*-alkenes in Antarctic soil. Org. Geochem. 15, 403-412.

McGowan HA, Marx SK, Soderholm J and Denholm J (2010) Evidence of solar and tropical-ocean forcing of hydroclimate cycles in southeastern Australia for the past 6500 years. Geophys. Res. Lett. 37, L10705.

Mendez-Perez D, Herman NA and Pfleger BF (2014) A desaturase gene involved in the formation of 1,14-nonadecadiene in *Synechococcus* sp. Strain PCC 7002. Appl. Environ. Microbiol. 80, 6073-6079.

Meyers PA (1997) Organic geochemical proxies of paleoceanographic, paleolimnologic, and paleoclimatic processes. Org. Geochem. 27, 213-250.

Meyers PA (2003) Applications of organic geochemistry to paleolimnological reconstructions: a summary of examples from the Laurentian Great Lakes. Org. Geochem. 34, 261-289.

Meyers PA, Leenheer MJ, Eaoie BJ and Maule SJ (1984) Organic geochemistry of suspended and settling particulate matter in Lake Michigan. Geochim. Cosmochim. Acta 48, 443-452.

Miller DR, Habicht MH, Keisling BA, Castañeda IS and Bradley RS (2018) A 900-year New England temperature reconstruction from *in situ* seasonally produced branched glycerol dialkyl glycerol tetraethers (brGDGTs), Clim. Past Discuss. 14, 1653-1667.

Misra S, Choudhury A, Chattopadhyay S and Ghosh A (1988) Lipid composition of Porteresia coarctata from two different mangrove habitats in India. Phytochemistry 27, 361-364.

Moernaut J, Verschuren D, Charlet F, Kristen I, Fagot M and De Batist M (2010) The seismic-stratigraphic record of lake level fluctuations in Lake Challa: hydrological stability and change in equatorial East Africa over the last 140 kyr. Earth Planet. Sci. Lett. 290, 214–223.

Mölg T, Renold M, Vuille M, Cullen NJ, Stocker TF and Kaser G (2006) Indian Ocean zonal mode activity in a multicentury integration of a coupled AOGCM consistent with climate proxy data. Geophys. Res. Lett. 33, L18710.

Monti S, Corozzi A, Fristrup P, Joshi KL, Shin YK, Oelschlaeger P, van Duin ACT and Barone V (2013) Exploring the conformational and reactive dynamics of biomolecules in solution using an extended version of the glycine reactive force field. PCCP 15, 15062–15077.

Mook WG, Bommerson JC and Staverman WH (1974) Carbon isotope fractionation between dissolved bicarbonate and gaseous carbon dioxide. Earth Planet. Sci. Lett. 22, 169-176.

Mordvinov AV and Kramynin AP (2010) Long-term changes in sunspot activity, occurrences of grand minima, and their future tendencies. Sol. Phys. 264, 269-278.

Morrissey A (2014) Stratigraphic framework and quaternary paleolimnology of the Lake Turkana rift, Kenya (Doctoral dissertation, Syracuse University).

Murray J and Thomson A (1977) Hydrocarbon production in *Anacystis montana* and *Botryococcus braunii*. Phytochemistry 16, 465-468.

Myrbo A and Shapley MD (2006) Seasonal water-column dynamics of dissolved inorganic carbon stable isotopic compositions (δ^{13}C DIC) in small hardwater lakes in Minnesota and Montana. Geochim. Cosmochim. Acta 70, 2699-2714.

Naafs BDA, Inglis GN, Zheng Y, Amesbury MJ, Biester H, Bindler R, Blewett J, Burrows MA, Castillo Torres DD, Chambers FM, Cohen AD, Evershed P and Feakins SJ (2017a) Introducing global peat-specific temperature and pH calibrations based upon brGDGT bacterial lipids. Geochim. Cosmochim. Acta 208, 285–301.

Naafs BDA, Gallego-Sala AV, Inglis GN and Pancost RD (2017b) Refining the global branched glycerol dialkyl glycerol tetraether (brGDGT) soil temperature calibration. Org. Geochem. 106, 48-56.

Naidu PD and Malmgren BA (1995) A 2,200 years periodicity in the Asian monsoon system. Geophys. Res. Lett. 22, 2361-2364.

Nederbragt AJ and Thurow J (2005) Geographic coherence of millennial-scale climate cycles during the Holocene. Palaeogeogr. Palaeoclimatol. Palaeoecol. 221, 313-324.

Nelson DM, Verschuren D, Urban MA and Hu FS (2012) Long-term variability and rainfall control of savanna fire regimes in equatorial East Africa. Glob. Chang. Biol. 18, 3160-3170.

Nichols PD, Guckert JB and White DC (1986) Determination of monounsaturated fatty acid double-bond position and geometry for microbial monocultures and complex consortia by capillary GC-MS of their dimethyl disulphide adducts. J. Microbiol. Methods 5, 49-55.

Nicholson SE, Nash DJ, Chase BM, Grab SW, Shanahan TM, Verschuren D, Asrat A, Lézine AM and Umer M (2013) Temperature variability over Africa during the last 2000 years. The Holocene 23, 1085-1094.

Nicholson SE (2000) The nature of rainfall variability over Africa on time scales of decades to millenia. Glob. Planet. Change 26, 137-158.

Nicholson SE and Selato JC (2000) The influence of La Niña on African rainfall. Int. J. Climatol. 20, 1761–1776.

Nielson KD, van Duin ACT, Oxgaard J, Deng W-Q and Goddard WA (2005) Development of the ReaxFF reactive force field for describing transition metal catalyzed reactions, with application to the initial stages of the catalytic formation of carbon nanotubes. J. Phys. Chem. A 109, 493–499.

Ohmoto T, Ikuse M and Natori S (1970) Triterpenoids of the Gramineae. Phytochemistry 9, 2137-2148.

Oppermann BI, Michaelis W, Blumenberg M, Frerichs J, Schulz HM, Schippers A, Beaubien SE and Krüger M (2010) Soil microbial community changes as a result of long-term exposure to a natural CO_2 vent. Geochim. Cosmochim. Acta 74, 2697-2716.

Oudejans RCHM and Zandee DI (1973) The biosynthesis of the hydrocarbons in males and females of the milipede *Graphidostreptus tumuliporus*. J. Insect Physiol. 19, 2245-2253.

Ourisson G, Albrecht P and Rohmer M (1982) Predictive microbial biochemistry - from molecular fossils to procaryotic membranes. Trends Biochem. Sci. 7, 236-239.

Paillard D, Labeyrie L and Yiou P (1996) Macintosh program performs time-series analysis. Eos, Trans. Amer. Geophys. Union 77, 379-379.

Pancost RD and Sinninghe Damsté JS (2003) Carbon isotopic compositions of prokaryotic lipids as tracers of carbon cycling in diverse settings. Chem. Geol. 195, 29-58.

Pancost RD, Hopmans EC and Sinninghe Damsté JS (2001) Archaeal lipids in Mediterranean cold seeps: molecular proxies for anaerobic methane oxidation. Geochim Cosmochim Acta 65, 1611–1627.

Paoletti C, Pushparaj B, Florenzano G, Capella P and Lercker G (1976) Unsaponifiable matter of green and blue-green algal lipids as a factor of biochemical differentiation of their biomasses: I. Total unsaponifiable and hydrocarbon fraction. Lipids 11, 258-265.

Parfenova VV, Gladkikh AS and Belykh OI (2013) Comparative analysis of biodiversity in the planktonic and biofilm bacterial communities in Lake Baikal. Microbiology 82, 91–101.

Patterson GW (1967) The effect of culture conditions on the hydrocarbon content of *Chlorella vulgaris*. J. Phycol. 3, 22-23.

Paull R, Michaelsen BH, McKirdy DM (1998) Fernenes and other triterpenoid hydrocarbons in Dicroidium-bearing Triassic mudstones and coals from South Australia. Org. Geochem. 29, 1331-1343.

Payne BR (1970) Water balance of Lake Chala and its relation to groundwater from tritium and stable isotope data. J. Hydrol. 11, 47-58.

Pearson EJ, Juggins S, Talbot HM, Weckstrom J, Rosen P, Ryves DB, Roberts SJ and Schmidt R (2011) A lacustrine GDGT-temperature calibration from the Scandinavian Arctic to Antarctic: renewed potential for the application of GDGT paleothermometry in lakes. Geochim. Cosmochim. Acta 75, 6225-6238.

Peterse F, Hopmans EC, Schouten S, Mets A, Rijpstra WIC and Sinninghe Damsté JS (2011) Identification and distribution of intact polar branched tetraether lipids in peat and soil. Org. Geochem. 42, 1007–1015.

Peterse F, Kim JH, Schouten S, Klitgaard Kristensen D, Koc N and Sinninghe Damsté JS (2009) Constraints on the application of the MBT/CBT palaeothermometer at high latitude environments (Svalbard, Norway). Org. Geochem. 40, 692–699.

Peterse F, van der Meer MTJ, Schouten S, Weijers JWH, Fierer N, Jackson RB, Kim JH and Sinninghe Damsté JS (2012) Revised calibration of the MBT-CBT paleotemperature proxy based on branched tetraether membrane lipids in surface soils. Geochim. Cosmochim. Acta 96, 215-229.

Pitcher A, Rychlik N, Hopmans EC, Spieck E, Rijpstra WIC, Ossebaar J, Schouten S, Wagner M and Sinninghe Damsté JS (2010) Crenarchaeol dominates the membrane lipids of Candidatus *Nitrososphaera gargensis*, a thermophilic Group I.1b Archaeon. The ISME Journal 4, 542.

Pitcher A, Hopmans EC, Mosier AC, Park SJ, Rhee SK, Francis CA, Schouten S and Sinninghe Damsté JS (2011) Core and intact polar glycerol dibiphytanyl glycerol tetraether lipids of ammonia-oxidizing archaea enriched from marine and estuarine sediments. Appl. Environ. Microbiol. 77, 3468–3477.

Portielje R and Lijkema L (1995) Carbon dioxide fluxes across the air-water interface and its impact on carbon availability in aquatic systems. Limnol. Oceanogr. 40, 690-699.

Powers LA, Johnson TC, Werne JP, Castañeda IS, Hopmans EC, Sinninghe Damsté JS and Schouten S (2005) Large temperature variability in the southern African tropics since the Last Glacial Maximum. Geophys. Res. Lett. 32, L08706.

Powers LA, Werne JP, Vanderwoude AJ, Sinninghe Damsté JS, Hopmans EC and Schouten S (2010) Applicability and calibration of the TEX_{86} paleothermometer in lakes. Org. Geochem. 41, 404-413.

Powers LA, Johnson TC, Werne JP, Castañeda IS, Hopmans EC, Sinninghe Damsté JS and Schouten S (2011) Organic geochemical records of environmental variability in Lake Malawi during the last 700 years, Part I: The TEX_{86} temperature record. Palaeogeogr. Palaeoclimatol. Palaeoecol. 303, 133-139.

Preheim SP, Olesen SW, Spencer SJ, Materna A, Varadharajan C, Blackburn M, Friedman J, Rodríguez J, Hemond H and Alm EJ (2016) Surveys, simulation and single-cell assays relate function and phylogeny in a lake ecosystem. Nat. Microbiol. 1, 16130.

Raju M, Kim S-Y, van Duin ACT, Fichthorn KA (2013) ReaxFF Reactive Force Field Study of the Dissociation of Water on Titania Surfaces. J. Phys. Chem. C 117, 10558–10572.

Rampen SW, Abbas BA, Schouten S and Sinninghe Damsté JS (2010) A comprehensive study of sterols in marine diatoms (Bacillariophyta): implications for their use as tracers for diatom productivity. Limnol. Oceanogr. 55, 91-105.

Rampen SW, Datema M, Rodrigo-Gámiz M, Schouten S, Reichart G-J and Sinninghe Damsté JS (2014) Sources and proxy potential of long chain alkyl diols in lacustrine environments. Geochim. Cosmochim. Acta 144, 59-71.

Rasmussen SO, Bigler M, Blockley SP, Blunier T, Buchardt SL, Clausen HB, Cvijanovic I, Dahl-Jensen D, Johnsen SJ, Fischer H and Gkinis V (2014) A stratigraphic framework for abrupt climatic changes during the Last Glacial period based on three synchronized Greenland ice-core records: refining and extending the INTIMATE event stratigraphy. Quat. Sci. Rev. 106, 14-28.

Regnery J, Püttmann W, Koutsodendris A, Mulch A and Pross J (2013) Comparison of the paleoclimatic significance of higher land plant biomarker concentrations and pollen data: A case study of lake sediments from the Holsteinian interglacial. Org. Geochem. 61, 73-84.

Repeta DJ (1989) Carotenoid diagenesis in recent marine sediments: II. Degradation of fucoxanthin to loliolide. Geochim. Cosmochim. Acta 53, 699-707.

Řezanka T, Zahradník J and Podojil M (1982) Hydrocarbons in green and blue-green algae. Folia Microbiol. 27, 450-454.

Řezanka T and Podojil M (1986) Identification of wax esters of the fresh-water green alga *Chlorella kessleri* by gas chromatography-mass spectrometry. J. Chromatogr. 362, 399-406.

Richardson DC, Carey CC, Bruesewitz DA and Weathers KC (2017) Intra- and inter-annual variability in metabolism in an oligotrophic lake. Aquatic Sciences 79, 319-333.

Riettie-Shati M, Shemesh A and Karlen W (1998) A 3000-year climatic record from biogenic silica oxygen isotopes in an equatorial high-altitude lake. Science 281, 980-982.

Rimbu N, Lohmann G, Lorenz SJ, Kim JH and Schneider RR (2004) Holocene climate variability as derived from alkenone sea surface temperature and coupled ocean-atmosphere model experiments. Climate Dyn. 23, 215-227.

Robinson N, Cranwell PA, Finlay BJ, Eglinton G (1986) Lipids of aquatic organisms as potential contributors to lacustrine sediments. Org. Geochem. 6, 143-152.

Rommerskirchen F, Plader A, Eglinton G, Chikaraishi Y and Rullkötter J (2006) Chemotaxonomic significance of distribution and stable carbon isotopic composition of long-chain alkanes and alkan-1-ols in C_4 grass waxes. Org. Geochem. 37, 1303-1332.

Rontani JF and Volkman JK (2003) Phytol degradation products as biogeochemical tracers in aquatic environments. Org. Geochem. 34, 1-35.

Rullkötter J, Leythaeuser D and Wendisch D (1982) Novel 23,28-bisnorlupanes in Tertiary sediments. Widespread occurrence of nuclear demethylated triterpanes. Geochim. Cosmochim. Acta 46, 2501-2509.

Russell JM, Hopmans EC, Loomis SE, Liang J and Sinninghe Damsté JS (2018) Distributions of 5- and 6-methyl branched glycerol dialkyl glycerol tetraethers (brGDGTs) in East African lake sediment: Effects of temperature, pH, and new lacustrine paleotemperature calibrations. Org. Geochem. 117, 56–69.

Sabel M, Bechtel A, Püttmann W and Hoernes S (2005) Palaeoenvironment of the Eocene Eckfeld Maar lake (Germany): implications from geochemical analysis of the oil shale sequence. Org. Geochem. 36, 873-891.

Sachse D, Billault I, Bowen GJ, Chikaraishi Y, Dawson TE, Feakins SJ, Freeman KH, Magill CR, McInerney FA, van der Meer MTJ, Polissar P, Robins RJ, Sachs JP, Schmidt H-L, Sessions AL, White JWC, West JB and Kahmen A (2012) Molecular paleohydrology: interpreting the hydrogen-isotopic composition of lipid biomarkers from photosynthesizing organisms. Annu. Rev. Earth Planet. Sci. 40, 221-249.

Saleem M (2009) Lupeol. A novel anti-inflammatory and anti-cancer dietary triterpene. Cancer Letters 285, 109-115.

Salmon E, van Duin ACT, Lorant F, Marquaire P-M and Goddard WA (2009a) Thermal decomposition process in algaenan of *Botryococcus braunii* race L. Part 2: Molecular dynamics simulations using the ReaxFF reactive force field. Org. Geochem. 40, 416–427.

Salmon E, van Duin ACT, Lorant F, Marquaire P-M and Goddard WA (2009b) Early maturation processes in coal. Part 2: Reactive dynamics simulations using the ReaxFF reactive force field on Morwell Brown coal structures. Org. Geochem. 40, 1195–1209.

Sarmento H, Unrein F, Isumbisho M, Stenuite S, Gasol JM and Descy JP (2008) Abundance and distribution of picoplankton in tropical, oligotrophic Lake Kivu, eastern Africa. Freshwater Biology 53, 756-771.

Schefuß E., Schouten S and Schneider RR (2005) Climatic controls on central African hydrology during the past 20,000 years. Nature 437, 1003.

Schmitter JM, Arpino PJ and Guiochon G (1981) Isolation of degraded pentacyclic triterpenoid acids in a Nigerian crude oil and their identification as tetracyclic carboxylic acids resulting from ring A cleavage. Geochim. Cosmochim. Acta 45, 1951-1955.

Schnell G, Schaeffer P, Tardivon H, Motsch E, Connan J, Ertlen D, Schwartz D, Schneider N and Adam P (2014) Contrasting diagenetic pathways of higher plant triterpenoids in buried wood as a function of tree species. Org. Geochem. 66, 107-124.

Schoell M, Simoneit BRT and Wang TG (1994) Organic geochemistry and coal petrology of Tertiary brown coal in the Zhoujing mine, Baise Basin, South China – 4. Biomarker sources inferred from stable carbon isotope compositions of individual compounds. Org. Geochem. 21, 713–719.

Schoon PL, de Kluijver A, Middelburg JJ, Downing JA, Sinninghe Damsté JS and Schouten S (2013) Influence of lake water pH and alkalinity on the distribution of core and intact polar branched glycerol dialkyl glycerol tetraethers (GDGTs) in lakes. Org. Geochem. 60, 72–82.

Schouten S, Breteler WCK, Blokker P, Schogt N, Rijpstra WIC, Grice K, Baas M. and Sinninghe Damsté J.S (1998) Biosynthetic effects on the stable carbon isotopic compositions of algal lipids: Implications for deciphering the carbon isotopic biomarker record. Geochim. Cosmochim. Acta 62, 1397-1406.

Schouten S, Wakeham SG and Sinninghe Damsté JS (2001) Anaerobic methane oxidation in euxinic waters of the Black Sea is mediated by Archaea. Org. Geochem. 32, 1277–1281.

Schouten S, Hopmans EC, Schefuß E and Sinninghe Damsté JS (2002) Distributional variations in marine crenarchaeotal membrane lipids: a new tool for reconstructing ancient sea water temperatures? Earth Planet. Sci. Lett. 204, 265-274.

Schouten S, Rijpstra WIC, Durisch-Kaiser E, Schubert CJ and Sinninghe Damsté JS (2012) Distribution of glycerol dialkyl glycerol tetraether lipids in the water column of Lake Tanganyika. Org. Geochem. 53, 34–37.

Schouten S, Hopmans EC and Sinninghe Damsté JS (2013) The organic geochemistry of glycerol dialkyl glycerol tetraether lipids: a review. Org. Geochem. 54, 19-61.

Schwark L and Püttmann W (1990) Aromatic hydrocarbon composition of the Permian Kupferschiefer in the Lower Rhine basin, NW Germany. Org. Geochem. 16, 749-761.

Senftle TP, Hong S, Islam MM, Kylasa SB, Zheng Y, Shin YK, Junkermeier C, Engel-Herbert R, Janik MJ, Aktulga HM, Verstraelen T, Grama A, van Duin ACT (2016) The ReaxFF reactive force-field: development, applications and future directions. Nature Computational Materials 2, 15011.

Sheppard PR (2010) Dendroclimatology: extracting climate from trees. Wiley Interdiscip. Rev. Clim. Change 1, 343-352.

Shiojima K and Ageta H (1990) Fern constituents: Two new triterpenoid hydrocarbons, hop-16-ene and isohop-22(29)-ene, isolated from *Davallia mariesii*. Chem. Pharm. Bull. 38, 347-349.

Shiojima K, Arai Y, Masuda K, Takase Y, Ageta T and Ageta H (1992) Mass spectra of pentacyclic triterpenoids. Chem. Pharm. Bull. 40, 1683-1690.

Singariya P, Kumar P and Mourya KK (2012) Isolation of some new steroids and evaluation of bio-activity of Cenchrus ciliaris. Int. J. Res. Pharm. Sci. 3, 678-684.

Singariya P, Kumar P and Mourya KK (2014) Isolation of new steroids of Kala Dhaman grass (*Cenchrus setigerus*) and evaluation of their bioactivity. Braz. Arch. Biol. Technol. 57, 62-69.

Sinninghe Damsté JS (2016) Spatial heterogeneity of sources of branched tetraethers in shelf systems: the geochemistry of tetraethers in the Berau River delta (Kalimantan, Indonesia). Geochim. Cosmochim. Acta 186, 13–31.

Sinninghe Damsté JS, Schouten S, Hopmans EC, van Duin ACT and Geenevasen JA (2002) Crenarchaeol: the characteristic core glycerol dibiphytanyl glycerol tetraether membrane lipid of cosmopolitan pelagic crenarchaeota. J. Lip. Res. 43, 1641-1651.

Sinninghe Damsté JS, Ossebaar J, Abbas B, Schouten S and Verschuren D (2009) Fluxes and distribution of tetraether lipids in an equatorial African lake: constraints on the application of the TEX_{86} palaeothermometer and BIT index in lacustrine settings. Geochim. Cosmochim. Acta 73, 4232–4249.

Sinninghe Damsté JS, Rijpstra WIC, Hopmans EC, Weijers JWH, Foesel BU, Overman J and Dedysh SN (2011a) 13,16-Dimethyl octacosanedionic acid (iso-diabolic acid): a common membrane-spanning lipid of Acidobacteria subdivisions 1 and 3. Appl. Environ. Microbiol. 77, 4147-4154.

Sinninghe Damsté JS, Verschuren D, Ossebaar J, Blokker J, van Houten R, van der Meer MTJ, Plessen B and Schouten S (2011b) A 25,000-year record of climate-induced changes in lowland vegetation of eastern equatorial Africa revealed by the stable carbon-isotopic composition of fossil plant leaf waxes. Earth Planet. Sci. Lett. 302, 236-246.

Sinninghe Damsté JS, Ossebaar J, Schouten S and Verschuren D (2012a) Distribution of tetraether lipids in the 25-ka sedimentary record of Lake Challa: extracting reliable TEX_{86} and MBT/CBT palaeotemperatures from an equatorial African lake. Quat. Sci. Rev. 50, 43-54.

Sinninghe Damsté JS, Rijpstra WIC, Hopmans EC, Jung M-Y, Kim J-G, Rhee SK, Stieglmeier M and Schleper C (2012b) Intact polar and core dibiphytanyl glycerol tetraether lipids of Group I.1a and I.1b Thaumarchaeota in soil. Appl. Environ. Microbiol. 78, 6866–6874.

Sinninghe Damsté JS, Rijpstra WIC, Foesel BU, Huber K, Overmann J, Nakagawa S, Kim JJ, Dunfield P, Dedysh S and Villanueva L (2018) An overview of the occurrence of ether- and ester-linked isodiabolic acid membrane lipids in microbial cultures of the Acidobacteria: Implications for brGDGT paleoproxies for temperature and pH. Org. Geochem. 124, 63-76.

Smetanina OF, Kuznetzova TA, Denisenko VA, Pivkin MV, Khudyakova YV, Gerasimenko AV, Popov DY, Il'in SG and Elyakov GB (2001) 3β-methoxyolean-18-ene (miliacin) from the marine fungus *Chaetomium olivaceum*. Russ. Chem. Bull. 50, 2463-2465.

Steinhilber F, Beer J and Fröhlich C (2009) Total solar irradiance during the Holocene. Geophys. Res. Lett. 36.

Striegl RG, Kortelainen P, Chanton JP, Wickland KP, Bugna GC and Rantakari M (2001) Carbon dioxide partial pressure and ^{13}C content of north temperate and boreal lakes at spring ice melt. Limnol. Oceanogr. 46, 941-945.

Summons RE, Bradley AS, Jahnke LL and Waldbauer JR (2006) Steroids, triterpenoids and molecular oxygen. Philos. Trans. R. Soc. London [Biol] 361, 951-968.

Sun Q, Chu G, Liu M, Xie M, Li S, Ling Y, Wang X, Shi L, Jia G and Lu H (2011) Distributions and temperature dependence of branched glycerol dialkyl glycerol tetraethers in recent lacustrine sediments from China and Nepal. J. Geophys. Res. 116, G01008.

ten Haven HL and Rullkötter J (1988) The diagenetic fate of taraxer-14-ene and oleanene isomers. Geochim. Cosmochim. Acta 10, 2543-2548.

Tersoff J (1988) Empirical Interatomic Potential for Carbon, with Applications to Amorphous Carbon. Phys. Rev. Lett. 61, 2879–2882.

Theissen KM, Zinniker DA, Moldowan JM, Dunbar RB and Rowe HD (2005) Pronounced occurrence of long-chain alkenones and dinosterol in a 25,000-year lipid molecular fossil record from Lake Titicaca, South America. Geochim. Cosmochim. Acta 69, 623-636.

Tierney JE and Russell JM (2009) Distributions of branched GDGTs in a tropical lake system: implications for lacustrine application of the MBT/CBT paleoproxy. Org. Geochem. 40, 1032-1036.

Tierney JE, Russell JM, Huang Y, Sinninghe Damsté JS, Hopmans EC and Cohen AS (2008) Northern Hemisphere controls on tropical Southeast African climate during the past 60,000 years. Science 322, 252-255.

Tierney JE, Mayes MT, Meyer N, Johnson C, Swarzenski PW, Cohen AS and Russell JM (2010a) Late-twentieth-century warming in Lake Tanganyika unprecedented since AD 500. Nat. Geosci. 3, 422-425.

Tierney JE, Russell JM, Eggermont H, Hopmans EC, Verschuren D and Sinninghe Damsté JS (2010b) Environmental controls on branched tetraether lipid distributions in tropical East African lake sediments. Geochim. Cosmochim. Acta 74, 4902–4918.

Tierney JE, Russell JM, Sinninghe Damsté JS, Huang Y and Verschuren D (2011) Late Quaternary behavior of the East African monsoon and the importance of the Congo Air Boundary. Quat. Sci. Rev. 30, 798-807.

Tierney JE, Schouten S, Pitcher A, Hopmans EC and Sinninghe Damsté JS (2012) Core and intact polar glycerol dialkyl glycerol tetraethers (GDGTs) in Sand Pond, Warwick, Rhode Island (USA): insights into the origin of lacustrine GDGTs. Geochim. Cosmochim. Acta 77, 561–581.

Trendel JM, Lohmann F, Kintzinger JP, Albrecht P, Chiarone A, Riche C, Cesario M, Guilhem J and Pascard C (1989) Identification of *des*-A-triterpenoid hydrocarbons occurring in surface sediments. Tetrahedron 6, 4457-4470.

Utermöhl H (1931) Neue Wege in der quantitativen Erfassung des Planktons. Verh. int. Ver. theor. angew. Limnnol. 5, 567-596.

Utermöhl H (1958) Zur vervollkommnung der quantitativen phytoplankton methodik. Mitt. Int. Ver. Theor. Angew. Limnol. 9, 1-38.

van Bree LGJ, Rijpstra WIC, Cocquyt C, Al-Dhabi NA, Verschuren D, Sinninghe Damsté JS and de Leeuw JW (2014) Origin and palaeo-environmental significance of C_{25} and C_{27} *n*-alk-1-enes in a 25,000-year lake-sedimentary record from equatorial East Africa. Geochim. Cosmochim. Acta 145, 89-102.

van Bree LGJ, Rijpstra WIC, Al-Dhabi NA, Verschuren D, Sinninghe Damsté JS and de Leeuw JW (2016) *Des*-A-lupane in an East African lake sedimentary record as a new proxy for the stable carbon isotopic composition of C_3 plants. Org. Geochem. 101, 132-139.

van Bree LGJ, Islam MM, Rijpstra WIC, Verschuren D, van Duin ACT, Sinninghe Damsté JS and de Leeuw JW (2018a) Origin, formation and environmental significance of *des*-A-arborenes in the sediments of an East African crater lake. Org. Geochem. 125, 95-108.

van Bree LGJ, Peterse F, van der Meer MTJ, Middelburg JJ, Negash AMD, De Crop W, Cocquyt C, Wieringa JJ, Verschuren D and Sinninghe Damsté JS (2018b) Seasonal variability in the abundance and stable carbon-isotopic composition of lipid biomarkers in suspended particulate matter from a stratified equatorial lake (Lake Chala, Kenya/Tanzania): Implications for the sedimentary record. Quat. Sci. Rev. 192, 208-224.

van Duin ACT, Dasgupta S, Lorant F and Goddard WA (2001) ReaxFF: a reactive force field for hydrocarbons. J. Phys. Chem. A 105, 9396–9409.

van Duin ACT, Strachan A, Stewman S, Zhang Q, Xu X and Goddard WA (2003) ReaxFFSiO reactive force field for silicon and silicon oxide systems. J. Phys. Chem. A 107, 3803–3811.

van Duin ACT and Sinninghe Damsté J.S (2003) Computational chemical investigation into isorenieratene cyclisation. Org. Geochem. 34, 515–526.

van Duin ACT, Sinninghe Damsté JS, Koopmans MP, van de Graaf B and de Leeuw JW (1997) A kinetic calculation method of homohopanoid maturation: Applications in the reconstruction of burial histories of sedimentary basins. Geochim. Cosmochim. Acta 61, 2409-2429.

van Geel B, Gelorini V, Lyaruu A, Aptroot A, Rucina S, Marchant R, Sinninghe Damsté JS and Verschuren D (2011) Diversity and ecology of tropical African fungal spores from a 25,000-year palaeoenvironmental record in southeastern Kenya. Rev. Palaeobot. Palynol. 164, 174-190.

Vasiliev SS and Dergachev VA (2002) The ~2400-year cycle in atmospheric radiocarbon concentration: bispectrum of ^{14}C data over the last 8000 years. Ann. Geophys. 20, 115-120.

Verlackt CCW, Neyts EC, Jacob T, Fantauzzi D, Golkaram M, Shin Y-K, van Duin ACT and Bogaerts A (2015) Atomic-scale insight into the interactions between hydroxyl radicals and DNA in solution using the ReaxFF reactive force field. New J. Phys. 17, 103005.

Verschuren D, Sinninghe Damsté JS, Moernaut J, Kristen I, Blaauw M, Fagot M, Haug GH and CHALLACEA project members (2009) Half-processional dynamics of monsoon rainfall near the East African Equator. Nature 462, 637-641.

Verschuren D and Russell JM (2009) Paleolimnology of African lakes: beyond the exploration phase. Pages News 17, 112-114.

Verschuren D (2003) Lake-based climate reconstruction in Africa: progress and challenges. In: Aquatic Biodiversity, Springer, Dordrecht, 315-330.

Versteegh GJM, Bosch H-J and de Leeuw JW (1997) Potential palaeoenvironmental information of C_{24} to C_{36} mid-chain diols, keto-ols and mid-chain hydroxy fatty acids; a critical review. Org. Geochem. 27, 1-13.

Villanueva L, Besseling M, Rodrigo-Gámiz M, Rampen S, Verschuren D and Sinninghe Damsté JS (2014) Potential biological sources of long chain alkyl diols in a lacustrine system. Org. Geochem. 68, 27-30.

Vliex M, Hagemann W and Püttmann W (1994) Aromatized arborane/fernane hydrocarbons as molecular indicators of floral changes in Upper Carboniferous/Lower Permian strata of the Saar-Nahe Basin, southwestern Germany. Geochim. Cosmochim. Acta 58, 4689-4702.

Volkman JK (2003) Sterols in microorganisms. Appl. Microbiol. Biotechnol. 60, 495-506.

Volkman JK (2005) Sterols and other triterpenoids: source specificity and evolution of biosynthetic pathways. Org. Geochem. 36, 139-159.

Volkman JK, Johns RB, Gillan FT, Perry GJ and Bavor HJJr (1980) Microbial lipids of an intertidal sediment - I. Fatty acids and hydrocarbons. Geochim. Cosmochim. Acta 44, 1133-1143.

Volkman JK, Jeffrey SW, Nichols PD, Rogers GI and Garland CD (1989) Fatty acid and lipid composition of 10 species of microalgae used in mariculture. J. Exp. Mar. Biol. Ecol. 128, 219-240.

Volkman JK, Barrett SM, Dunstan GA and Jeffrey SW (1992) C_{30}-C_{32} alkyl diols and unsaturated alcohols in microalgae of the class Eustigmatophyceae. Org. Geochem. 18, 131–138

Volkman JK, Barrett SM, Blackburn SI, Mansour MP, Sikes EL and Gelin F (1998) Microalgal biomarkers: a review of recent research developments. Org. Geochem. 29, 1163-1179.

Volkman JK, Barrett SM, and Blackburn SI (1999) Eustigmatophyte microalgae are potential sources of C_{29} sterols, C_{22}-C_{28} *n*-alcohols and C_{28}-C_{32} *n*-alkyl diols in freshwater environments. Org. Geochem. 30, 307-318.

Vorbrüggen H, Pakrashi SC and Djerassi C (1963) Arborinol, ein neuer Triterpen-Typus. Liebigs Ann. 668, 57-76.

Vuorio K, Nuottajärvi M, Salonen K and Sarvala J (2003) Spatial distribution of phytoplankton and picocyanobacteria in Lake Tanganyika in March and April 1998. Aquat. Ecosyst. Health. 6, 263-278.

Wakeham SG, Schaffner C and Giger W (1980) Polycyclic aromatic hydrocarbons in recent lake sediments – II. Compounds derived from biogenic precursors during early diagenesis. Geochim. Cosmochim. Acta 44, 415-429.

Wang HY, Liu WG, Zhang CLL, Wang Z, Wang JX, Liu ZH and Dong HL (2012) Distribution of glycerol dialkyl glycerol tetraethers in surface sediments of Lake Qinghai and surrounding soil. Org. Geochem. 47, 78–87.

Wang Y, Cheng H, Edwards RL, Kong X, Shao X, Chen S, Wu J, Jiang X, Wang X and An Z (2008) Millennial- and orbital-scale changes in the East Asian monsoon over the past 224,000 years. Nature 451, 1090-1093.

Wang YJ, Cheng H, Edwards RL, An ZS, Wu JY, Shen CC and Dorale JA (2001) A high-resolution absolute-dated late Pleistocene monsoon record from Hulu Cave, China. Science 294, 2345-2348.

Wanninkhof R and Knox M (1997) Chemical enhancement of CO_2 exchange in natural waters. Limnol. Oceanogr. 41, 689-697.

Weber Y, De Jonge C, Rijpstra WIC, Hopmans EC, Stadnitskaia A, Schubert CJ, Lehmann MF, Sinninghe Damsté JS and Niemann H (2015) Identification and carbon isotope composition of a novel GDGT isomer in lake sediments: evidence for lacustrine brGDGT production? Geochim. Cosmochim. Acta 154, 118–129.

Weber Y, Sinninghe Damsté JS, Zopfi J, De Jonge C, Gili A, Schubert CJ, Lepori F, Lehmann MF and Niemann H (2018) Redox-dependent niche differentiation provides evidence for multiple bacterial sources of glycerol tetraether lipids in lakes. PNAS, 201805186.

Weijers JWH, Schouten S, Hopmans EC, Geenevasen JAJ, David ORP, Coleman JM, Pancost RD and Sinninghe Damsté JS (2006) Membrane lipids of mesophilic anaerobic bacteria thriving in peats have typical archaeal traits. Environ. Microbiol. 8, 648–657.

Weijers JWH, Schefuß E, Schouten S and Sinninghe Damsté JS (2007a) Coupled thermal and hydrological evolution of tropical Africa over the last deglaciation. Science 315, 1701–1704.

Weijers JWH, Schouten S, van den Donker JC, Hopmans EC and Sinninghe Damsté JS (2007b) Environmental controls on bacterial tetraether membrane lipid distribution in soils. Geochim. Cosmochim. Acta 71, 703-713.

Weijers JWH, Panoto E, van Bleijswijk J, Schouten S, Rijpstra WIC, Balk M, Stams AJM and Sinninghe Damsté JS (2009) Constraints on the biological source(s) of the orphan branched tetraether membrane lipids. Geomicrobiol. J. 26, 402–414.

Weijers JWH, Wisenberg GLB, Bol R, Hopmans EC and Pancost RD (2010) Carbon isotopic composition of branched tetraether membrane lipids in soils suggest a rapid turnover and a heterotrophic life style of their source organism(s). Biogeosciences 7, 2959–2973.

Weijers JWH, Bernhardt B, Peterse F, Werne JP, Dungait JAJ, Schouten S and Sinninghe Damsté JS (2011) Absence of seasonal patterns in MBT–CBT mid-latitude soils. Geochim. Cosmochim. Acta 75, 3179–3190.

Winters K, Parker PL and van Baalen C (1969) Hydrocarbons of blue-green algae: geochemical significance. Science 163, 467-468.

Wolff C, Haug GH, Timmermann A, Sinninghe Damsté JS, Brauer A, Sigman DM, Cane MA and Verschuren D (2011) Reduced interannual rainfall variability in East Africa during the Last Ice Age. Science 333, 743-747.

Wolff C, Kristen-Jenny I, Schettler G, Plessen B, Meyer H, Dulski P, Naumann R, Brauer A, Verschuren D and Haug GH (2014) Modern seasonality in Lake Challa (Kenya/Tanzania) and its sedimentary documentation in recent lake sediments. Limnol. Oceanogr. 59, 1621-1636.

Woltering M, Johnson TC, Werne JP, Schouten S and Sinninghe Damsté JS (2011) Late Pleistocene temperature history of Southeast Africa: a TEX_{86} temperature record from Lake Malawi. Palaeogeogr. Palaeoclimatol. Palaeoecol. 303, 93-102.

Woltering M, Werne JP, Kish JL, Hicks R, Sinninghe Damsté JS and Schouten S (2012) Vertical and temporal variability in concentration and distribution of thaumarchaeotal tetraether lipids in Lake Superior and the implications for the application of the TEX_{86} temperature proxy. Geochim. Cosmochim. Acta 87, 136-153.

Xu Y and Jaffé R (2008) Biomarker-based paleo-record of environmental change for an eutrophic, tropical freshwater lake, Lake Valencia, Venezuela. J. Paleolimnol. 40, 179-194.

Xu Y and Jaffé R. (2009) Geochemical record of anthropogenic impacts on Lake Valencia, Venezuela. Appl. Geochem. 24, 411-418.

Zhang J, Kobert K, Flouri T and Stamatakis A (2013) PEAR: a fast and accurate Illumina Paired-End reAd mergeR. Bioinformatics 30, 614-620.

Zhang Z, Zhao M, Yang X, Wang S, Jiang X, Oldfield F and Eglinton G (2004) A hydrocarbon biomarker record for the last 40 kyr of plant input to Lake Heqing, southwestern China. Org. Geochem. 35, 595-613.

Zhang Z, Metzger P and Sachs JP (2011) Co-occurrence of long chain diols, keto-ols, hydroxy acids in keto acids in recent sediments of Lake El Junco, Galápagos Islands. Org. Geochem. 42, 823-837.

Zheng Y, Pancost RD, Liu X, Wang Z, Naafs BDA, Xie X, Liu Z, Yu X and Yang H (2017) Atmospheric connections with the North Atlantic enhanced the deglacial warming in northeast China. Geology 45, 1031-1034.

Zhou Z, Pan J, Wang F, Gu JD and Li M (2018) Bathyarchaeota: globally distributed metabolic generalists in anoxic environments. FEMS Microbial. Rev. 42, 639-655

Zimmermann J, Portillo MC, Serrano L, Ludwig W and Gonzalez JM (2012) Acidobacteria in freshwater ponds at Doñana National Park, Spain. Microb. Ecol. 63, 844–55.

Zink KG, Leythaeuser D, Melkonian M and Schwark L (2001) Temperature dependency of long-chain alkenone distributions in recent to fossil limnic sediments and lake waters. Geochim. Cosmochim. Acta 65, 253–265.

Majestic lion in Masai Mara National Reserve, 300 km north-west of Mt. Kilimanjaro.

Acknowledgements (dankwoord)

Allereerst wil ik al mijn promotoren en copromotor bedanken. Francien, super bedankt voor al je hulp tijdens mijn PhD en bij het veldwerk naar Kenia dat we samen hebben gedaan. Geen domme vraag was je te gek, en we hebben heel wat uren/dagen/jaren naar alle biomarkerdata gekeken zonder er veel wijzer uit te worden. We hebben goed geprobeerd alle successen te vieren. Ook heb ik alle gekkigheid over de jaren heen erg gewaardeerd, van Bob Ross groepsuitjes, bierviltjes in je mond, en je Oxford komma, tot het ontwerpen van het groepslogo van de Organische Geochemische vakgroep en uitspraken zoals "nou heb ik poep tussen mijn tenen". Jaap, bedankt voor de kans om onderzoek met jou te doen, ook al was het dan in een meertje en ook al deed ik in den beginne niets met jouw favoriete biomarkers. Onze wetenschappelijke discussies over de biomarkers van Lake Chala (en uiteindelijk toch ook maar die GDGTs) hebben veel bijgedragen aan de kwaliteit van dit boek. Dirk, ook jou wil ik bedanken voor al je hulp en wetenschappelijke discussies over de afgelopen jaren. Zonder jouw immer gedetailleerde feedback en enorme kennis van Lake Chala was dit boek een stuk minder leesbaar (en de titels veel te kort). En tenslotte Stefan, bedankt voor het bijspringen in tijden van nood. Jouw kalmte en pragmatische efficiëntie waren erg welkom tijdens de stressvolle afrondfase. And of course, I would like to thank my committee for taking the time to read this thesis.

Naast deze officiële begeleiding heb ik veel te danken aan enkele sleutelfiguren in mijn wetenschappelijke carrière. De eerste woorden van deze thesis dateren namelijk al uit november 2012, toen ik vrij snel na het afronden van al mijn studies als onderzoeker startte bij Jan de Leeuw op Texel. Van een achteraf gezien ietswat ambitieus project om in een paar maanden enkele papers te schrijven over Lake Chala (toen nog Lake Challa) is dit uitgegroeid tot een PhD in Utrecht met dit proefschrift als eindproduct. Jan, zonder jou was ik nooit aan dit onderzoek begonnen, en was het ook nooit op deze manier tot dit boek verworden. Ik wil je enorm bedanken voor de tijd die je altijd voor mij en de moleculen uit Lake Chala maakte, zowel op Texel als in de jaren erna, en meer nog voor je immer positieve en nieuwsgierigheidsgedreven kijk op de wetenschap en de wereld. Gert-Jan, zonder jouw enthousiasme was ik waarschijnlijk nooit in de wereld van organische geochemie gerold, en daar wil ik je graag voor bedanken. Je bent een oneindige put van ideeën en hebt veel invloed gehad op mijn loopbaan (en snoepreisjes vermomd als veldwerk), inclusief mijn masteronderzoek (in Florida), KNAW onderzoek met Su en Marieke (in Zwitserland), en stiekem heb ke zelfs deze PhD mogelijk gemaakt door me aan te bevelen bij Jan. Ik weet niet of we ons paper over de Surfplas ooit echt afmaken, maar het was wel altijd gezellig om te schrijven.

Ook wil ik graag mijn twee masterstudenten en de rest van mijn samenwerkingspartners bedanken, zonder jullie hulp was dit onderzoek nooit zo uitgebreid en interessant geworden. Araya en Pauline, bedankt voor al jullie harde en zelfstandige werk in het lab, en ik ben blij dat jullie beiden niet gek zijn geworden van alle vragen die jullie masteronderzoek hebben opgeworpen in plaats van hebben beantwoord. Araya, bedankt voor je enthousiasme en nieuwsgierigheid, en ik vond het super leuk dat je je kleine onderzoek ook nog wilde besteden aan Lake Chala. En Pauline, bedankt en super goed gedaan, ondanks dat ik een groot deel van de tijd niet in Nederland was om je te helpen. Irene, bedankt voor al je hulp in het lab, op de machines en met de vele massaspectra, en zeker voor alle discussies over de beste opwerkmethodes, zonder jou hadden we zeker niet zoveel verschillende informatie uit de monsters geëxtraheerd. Christine Cocquyt, bedankt voor alle overleg en samenwerking, zonder jouw algenkennis en –tellingen was dit onderzoek veel minder

interessant geweest. Jack, bedankt voor alle discussies over het koolstofsysteem en 'elementjes', en zonder jouw briljante ingeving waren we nu nóg aan het nadenken over de rare koolstofisotopen. Marcel, bedankt voor je hulp bij het meten van die rare koolstofisotopen en het vervangen van de vele voorkolommen die ik ermee heb vervuild. Wannes, bedankt voor je hulp met de waterkolom van Lake Chala, ondanks dat je het zelf behoorlijk druk had. Jan Wieringa, bedankt voor je hulp bij het identificeren van de planten van Lake Chala ook al waren ze gevriesdroogd, gebroken en incompleet, en tijdens ons bezoek aan het herbarium zag ik hoe leuk het eigenlijk kon zijn om planten te determineren. Laura Villanueva, thanks for your help and for the enormous undertaking analyzing the DNA from SPM, just to find out our sampling year was super unproductive. Sigrid, ook jij bedankt voor jouw aandeel in die enorme onderneming van de DNA analyses en andere metingen van Lake Chala (en het chillen op Hawaii). Ellen, bedankt dat we altijd bij jou mochten meten. Adri and Mahbub, thanks for the (discussions on the) molecular mechanics calculations.

Research on Lake Chala is an enormous group effort. The research in this thesis would not have been possible without your help Caxton, thanks for all the hard work hauling jerry cans of water from the lake all the way to your lab-room in Taveta. And thanks to the other locals who helped you carry almost 1700 liter of lake water. Furthermore, I'd like to thank all my international colleagues that made the DeepCHALLA fieldwork and sampling party a huge success and lots of fun, and a few in particular. Chris, thanks for your help, data and knowledge of Lake Chala, and for making the fieldwork night-shift, sampling party and Honolulu much more fun. Cheers! Nick, thanks for the good conversations, beers and the beautiful picture that is now the cover of this thesis. And of course, for the 'Kilimanjaro' theme song of DeepCHALLA that will be in my head forever. Lien, bedankt voor het gezellige en super snelle zakjes vullen met modder die we beiden gelukkig nooit meer hoeven te analyseren. Heidi, thanks for letting me check out your pigment data. En Daan, super bedankt dat ik je foto's mocht lenen voor in dit boekje en voor alle gezelligheid.

Ook mijn oude en nieuwe collega's van Organische Geochemie wil ik graag bedanken, het was een klein maar fijn groepje. Frédérique en Emily, bedankt voor jullie gezelschap en discussies over biomarkers in het Aardwetenschappengebouw, het Unnik en uiteindelijk in het VMA. Al waren we er bijna nooit allemaal tegelijk, onze besneeuwde bergketens zullen voor altijd de muur versieren. Laura Buckles, during my PhD I read your thesis many times with pleasure (and confusion, because I still have no clue what all these biomarkers mean), thanks for all your virtual help sorting out samples and the previous work you did on Lake Chala. And Allix, thanks for taking over Lake Chala! I'm sure those almost one thousand Lake Chala sediment samples are in good hands, and hopefully after your PhD we will finally understand the story these biomarkers tell (although I kinda doubt it). Marieke, bedankt voor al je hulp en gezelligheid in het lab tijdens onze metingen samen, en de eer om je paranimf te mogen zijn. Els, bedankt voor je hulp tijdens en na mijn masteronderzoek, en daarnaast ook dat je me zo goed getraind hebt in het lab. Lottie, thanks for making working during the weekend such a pleasure! Johan Weijers, bedankt voor je hulp over de jaren heen, met de GRS en je enthousiasme voor moleculen. Paul, bedankt voor je plantenverpoederaar en alle ballonnen en gezelligheid in Zwitserland. Jiefei, I enjoyed all our dinners, trips and adventures (and maybe jumping off a boat frantically searching for whale sharks in the Philippines most of all), and thanks for the honor of being your paranymf. Su, thanks for all the good times in the lab in Utrecht, "sharing" a tandembike on Terschelling and for showing us around in China.

Zonder de ondersteuning in het lab van vele mensen was dit onderzoek ook niet tot wasdom gekomen. Klaas, bedankt voor al je hulp met moleculen, mensen en machines, altijd gezellig op de 5e. Coen, bedankt voor je blije en behulpzame aanwezigheid in het lab (konden we je maar

klonen). Anita, bedankt voor al je hulp in het lab. Ook wil ik graag Arnold, Natasja, Ton, Thom, Dineke, Dominika, John, Desmond, Michiel, Giovanni, Ramon, Jan, Linda, Hans, Bernadette en Katja in Utrecht; en Jort, Marianne, Anchelique, Monique, Denise, Irene, Piet, Sanne en Maartje op Texel bedanken voor alle hulp en technische ondersteuning in het lab. Veerle en Pieter (UVA), bedankt voor de nutrientenmetingen toen het in Utrecht niet lukte. En J.F. Veldkamp (Naturalis), bedankt voor de grasdeterminaties. Margot Stoete, bedankt voor de hulp met het opmaken van mijn boekje, en Ton, bedankt voor de last-minute aanpassingen. Karin, bedankt voor je feedback en hulp met de samenvattingen. En Tjitske, Pien, Marjolein en Jan-Willem, bedankt voor jullie praktische ondersteuning. Verder wil ik de vele (oud)collega's, labbezoekers en studenten uit Utrecht bedanken (in willekeurige volgorde en vast niet helemaal compleet): Angie, Appy, Tjerk, Johan, Karin, Nynke, Evelangelos, David, Paul, Margot, Carolien, Caroline, Anne v.d. Meer, Laurianne, Rolande, Julia, Bastiaan, Philip, Sander, Marie, Anna, Niels, Alwina, Rick, Arjen, Joost, Mirja, Frieda, Peter Kraal, Peter Bijl, Ilja, Huub, Christine, Jorien, Marie-Louise, Mathilde, Lottie, Mohammed, Tom, Fati, Chris, Emmy, Franci, Timme, Wytse, Martin, Annique, Bas, Luc, Fabian, Iris en vele anderen. Ook mijn oud-collega's op Texel wil ik bedanken, zowel van toen ik op het NIOZ begon aan Lake Chala, maar ook tijdens de vele PhD metingen: Sandra, Els, Lisa, Sabine, Darci, Nicole, Ellen, Dave, Eli, Sebastian, Martina, Yvonne, Yuki, Willemijn, Laura, Marijke, Marc, Eveline, Esmee, Gabriella, Cait, Julie, Sophie, Nadine, Linda and many others. Saara, thanks for the pleasure of sharing Hawaiian sushi, and all the nights you let me crash at your place in Den Helder. Cindy, bedankt voor alle discussies over brGDGTs en de gezelligheid tijdens de vele congressen en koffies op Antwerpen Centraal.

Naast deze meer directe collega's, zijn er natuurlijk ook veel anderen die ik graag wil bedanken. Allereerst de NESSCwork-board en natuurlijk iedereen in het NESSCwork zelf. Thanks Cait, Bregje, Anne, Robin, Shaun, Itzel, Emily, Josh, Els, Michiel, Luke, Carolien, Matthias, Nadine, André, Anniek, Olivia en vele anderen, ik heb genoten van al onze borrels, activiteiten, workshops, vergaderingen, koffie- en pizzameetings. Cindy, Anne, Anne, Carolien en Julian, bedankt dat jullie zo gek waren om eens of zelfs vaker mee te gaan op schrijfweek! En vanuit het NESSC zelf, bedankt Bjinze, Rineke, Marjolein, Lisa en Mirjam (extra bedankt voor je hulp en aanmoediging bij het opzetten van het NESSCwork, workshops en solliciteren). Zonder de coaching van Berry, Koos en Amber was dit boek er ook nog lang niet geweest, bedankt voor jullie steun en aanmoediging. Babysteps are also progress! De FEST-commissie (in verschillende samenstellingen) was erg gezellig. Ook heb ik vele internationale congressen mogen bezoeken, die naast wetenschappelijk prikkelend ook gewoon erg gezellig waren door de vele mensen die ik er heb ontmoet, teveel om allemaal los te noemen. Een kleine greep uit de hoogtepunten zijn Urbino 2015 (en de roadtrip vooraf), Plant Wax 2015 ('Annie, I'm not your daddy'), ASLO 2017 op Hawaii (en een fantastische trip met Anniek en Olivia), IMOG in 2015 en 2017, Gordon in 2014, 2016 en 2018, met als persoonlijk hoogtepunt het organiseren van de GRS (thanks Lloyd, Rich, and everybode else who made this seminar a success), de vele NESSCdagen en NACs (inclusief de beste first biannual post-NAC trip ever).

De gezelligheid en afleiding van mijn niet-wetenschappelijke vrienden was ook heel belangrijk tijdens deze bij tijden lastige periode, bedankt dat jullie er waren ook al had ik niet veel ruimte en tijd voor jullie. Lein, ik ben super blij dat we nu beiden 'verlost' zijn van onze PhD, en weer alleen maar leuke dingen kunnen doen. Bedankt voor alle jaren van vriendschap, kamperen, sabreren, thee, logeren, fietsen en gezelligheid, en ben vereerd dat ik zowel je paranimf als de suikertante van Koen en Tom mag zijn. De WdZ-dames, bedankt voor de ongelooflijke hoeveelheid thee die we verdronken hebben de afgelopen jaren, en Tessa en Tamara, bedankt voor alle goede zorgen voor (mij en) mijn plantjes als ik weer eens een week of maand op congres, veldwerk of

reis was. Lau, thanks voor alle gezelligheid, reisjes, series en schuimblokken van de afgelopen jaren! Tik 'm aan, Linda! Groovy chick Taliet, thanks voor je enthousiasme, theetjes, pizzabisli en vriendschap. Rie, soms uit het oog maar altijd dichtbij. Jann, bedankt voor alle gezelligheid de afgelopen jaren, ik ben blij dat je die ene bevrijdingsdag naar Utrecht bent gekomen en nooit meer bent weggegaan. Ann, bedankt voor je steun in gekke tijden en voor alle rupsen! En natuurlijk vergeet ik jullie niet: Linda Schol (met de vele ontspannen fietskampeertripjes), de musical-dames Anna, Linda en Marijke, Leonie, Marjolein (de kraan!), Merel, Kimmie en de oud-IBBers. En een extra speciaal bedankje voor Linda en Anne, ik vind het super fijn dat jullie aan mijn zijde staan op de heugelijke dag van mijn promotie, zoals jullie er ook waren tijdens alle ups en downs de afgelopen jaren. Linda, wat hebben we veel mooie reizen (en kaasfondues) gemaakt de afgelopen jaren, niet erg duurzaam maar wel gezellig. Gelukkig hebben we jouw fotoboeken nog. En Anne, tijdens onze PhD hebben we behoorlijk veel koffie, gezelligheid, veel te hard werken, bijzondere kampeerplekken en leed gedeeld. Ik leerde je de Nederlandse krul en taalsubtiliteiten, en jij leerde me überhaupt nog steeds geen Duits (ein Gluhwein bitte! Genau! Bromberen!).

Ik wil ook graag mijn familie bedanken. Allereerst, bedankt papa en mama! Jullie hebben me mijn eigen keuzes laten maken en steunden me altijd, bijvoorbeeld als ik een jaar naar Australië wilde, voor de derde keer in een jaar ging verhuizen of nóg een studie wilde doen. En thanks Hanneke! Ook al woon je nog zo ver weg, je blijft altijd mijn grote zussie en ik ben blij dat we al die jaren toch nog zoveel hebben beleefd samen, van samen in cafeetjes koffie drinken (en soms ook zelfs werken) tot nachtenlang kletsen over niks. En natuurlijk samen hard lachen om de gekkigheid van mijn liefste neefjes, zowel onverschrokken Liam die het liefst de hele dag met mij knuffelt, als opgewekte grond- en dierenvriend Noam (die natuurlijk ook het liefst de hele dag met mij knuffelt). Thanks Nimrod, and also thank you Itzhak and Ahuva for your hospitality every time I visit. Bedankt ook Wil en Elly, en de rest van de Timmermansen, voor jullie gastvrijheid en interesse. Marja en Alie, bedankt voor al jullie gezelligheid, advies en levenswijsheid. Oma, bedankt voor de eindeloze telefoongesprekken die we hadden als ik weer eens op de boot van Texel naar het vasteland zat. Ik vind het verdrietig dat je het einde van mijn wetenschappelijke reis niet meer hebt kunnen meemaken. En last but not least... Holymoly Rufus, het is eindelijk af! En je hebt nog steeds geen flauw idee wat archaea zijn. Bedankt dat je er voor me was de afgelopen drie stressvolle en niet-zo-sociale jaren aan de verkeerde kant van de work-life balance. Nu hebben we eindelijk tijd voor de life kant.

A leisurely walk at an 'elephant safari' at Lake Jipe.
Photo credit: D. van der Velden

Sampling the local vegetation around Lake Chala.
Photo credit: F. Peterse

Lake Chala on a rainy day.
Photo credit: F. Peterse

Looking out for stray elephants near Lake Jipe.
Photo credit: F. Peterse

Young lion devouring an African buffalo.

List of publications

First author publications

L.G.J. van Bree, M.M. Islam, W.I.C. Rijpstra, D. Verschuren, A.C.T. van Duin, J.S. Sinninghe Damsté and J.W. de Leeuw (2018) Origin, formation and environmental significance of *des*-A-arborenes in the sediments of an East African crater lake. *Organic Geochemistry* 125, 95-108.

L.G.J. van Bree, F. Peterse, M.T.J. van der Meer, J.J. Middelburg, A.M.D. Negash, W. De Crop, C. Cocquyt, J.J. Wieringa, D. Verschuren and J.S. Sinninghe Damsté (2018) Seasonal variability in the abundance and stable carbon-isotopic composition of lipid biomarkers in suspended particulate matter from a stratified equatorial lake (Lake Chala, Kenya/Tanzania) - Implications for the sedimentary record. *Quaternary Science Reviews* 192, 208-224.

L.G.J. van Bree, W.I.C. Rijpstra, N.A. Al-Dhabi, D. Verschuren, J.S. Sinninghe Damsté and J.W. de Leeuw (2016) *Des*-A-lupane in an East African lake sedimentary record as a new proxy for the stable carbon isotopic composition of C3 plants. *Organic Geochemistry* 101, 132-139.

L.G.J. van Bree, W.I.C. Rijpstra, C. Cocquyt, N.A. Al-Dhabi, D. Verschuren, J.S. Sinninghe Damsté and J.W. de Leeuw (2014) Origin and palaeo-environmental significance of C25 and C27 *n*-alk-1-enes in a 25,000-year lake-sedimentary record from equatorial East Africa. *Geochimica et Cosmochimica Acta* 145, 89-102.

Co-authored publications

Y. Su, J.M. Lammers, Y. Zhang, **L.G.J. van Bree,** Z. Liu, G.J. Reichart and J.J. Middelburg (2017) Sources of organic matter for bacteria in sediments of Lake Rotsee, Switzerland. *Journal of Paleolimnology* 58, 391-402.

A.S. von der Heydt, H.A. Dijkstra, R.S.W. van de Wal, R. Caballero, M. Crucifix, G.L. Foster, M. Huber, P. Köhler, E. Rohling, P.J. Valdes, P. Ashwin, S. Bathiany, T. Berends, **L.G.J. van Bree** et al. (2016) Lessons on climate sensitivity from past climate changes. *Current Climate Change Reports* 2, 148-158.

African bush elephants escape Tsavo West National Park regularly to hang out with the local goats at Lake Jipe, 30 km south of Lake Chala.

About the Author

Loes van Bree was born on the 20th of June 1987 in Heemskerk, The Netherlands. From an early age, Loes had many different interests, mostly revolving around nature and understanding how and why things have happened in the past. After secondary education at the Jac. P. Thijsse College in Castricum (1999-2005), Loes went off to study Liberal Arts & Sciences at Utrecht University (2005-2009). This program enabled taking a wide range of courses in just as many topics, although in the end, Loes mainly focused on biogeology and history. She spent one year in Australia, which included studying one semester at Deakin University in Melbourne, and conducting her bachelor thesis research at the University of Melbourne. Loes continued at Utrecht University with a master in Biogeology (2009-2012) which she finished cum laude. She mainly focused on reconstructing relatively modern climate changes, usually with organic geochemical approaches. This included a research traineeship funded by the Royal Netherlands Academy of Arts and Sciences (KNAW), an internship at the Netherlands Organization for Applied Scientific Research (TNO), and master thesis research in Florida. Out of sheer curiosity she also studied for a second bachelor degree (2009-2012), this time in History. After graduation, she worked for nine months as a researcher at the Royal Netherlands Institute for Sea Research (NIOZ) on Texel (2012-2013). She was offered the opportunity to continue this biomarker research on an East African lake as a PhD researcher at Utrecht University (2014-2018). Loes went to her study site Lake Chala twice for fieldwork, which included participation in the ICDP DeepCHALLA coring expedition. Next to spending countless hours in the organic geochemistry lab, she presented her research at many international conferences and published various peer-reviewed papers. Loes also conducted many non-research related activities during her time as PhD researcher. She was the founder and chair of the early career network NESSCwork, organized workshops and informal meetings, and was active in the committee for the departmental Friday Earth Science Talks. Furthermore, Loes organized and chaired the 2018 Gordon Research Seminar on Organic Geochemistry in the USA. Loes will start as program officer at the Netherlands Organization for Scientific Research (NWO).

Allememaggies
- Clown Bassie

A vulture looking out over the Kenyan savannah.

Utrecht University
Faculty of Geosciences
Department of Earth Sciences

ISSN 2211-4335